Amphotericin B Nano-Formulations: Development, characterisation and suitability for oral administration

Dissertation

zur Erlangung des Grades

"Doktor der Naturwissenschaften"

im Promotionsfach Pharmazie

am Fachbereich Chemie, Pharmazie und Geowissenschaften

der Johannes Gutenberg-Universität

in Mainz

Raphael Johnson

geb. in Obuasi, Ghana

Mainz, 2015

DEKAN:

1. **Gutachter:**
2. **Gutachter:**

Tag der mündlichen Prüfung: 11/12/2015

Dedication

ACKNOWLEDGEMENT

TABLE OF CONTENTS

Table of Contents

Table of Contents

Table of Contents

Table of Contents

LIST OF ABBREVIATIONS

AmB	Amphotericin B
ATR	Attenuated total reflectance
BCS	Biopharmaceutic classification system
BHT	Butylhydroxytoluene
BSA	Bovine serum albumin
CD	Cyclodextrin
DLS	Dynamic light scattering
DMEM	Dulbecco's modified Eagle medium
DMSO	dimethyl sulfoxide
DMPC	1, 2-Dimyristoyl-sn-glycerol-3-phosphocholine
DOPC	1, 2-Dioleolyl-sn-glycerol-3-phosphocholine
DPPC	1, 2-Dipalmitoyl-sn-glycerol-3-phosphocholine
DSC	Differential scanning calorimetry
DSPC	Distearoyl-sn-glycerol-3-phosphocholine
EDTA	Ethylenediaminetetraacetic acid
FBS	fetal bovine serum
FRM2	Forschungs-Neutronenquelle of the Heinz Maier-Leibnitz center
FTIR	Fourier transform infrared
GIT	Gastrointestinal tract
GRAS	Generally regarded as safe
GUV	Giant unilamellar vesicles
HBSS	Hank's balanced salt solution
HEPES	4-(2-hydroxyethyl)-1-piperazineethanesulfonic acid
HLB	Hydrophile-lipophile balance
HPβCD	Hydroxypropyl-beta-cyclodextrin
HPMC	Hydroxypropylmethylcellulose

List of Abbreviations

HST	Hydrophilic solubilisation technology
JCNS	Jülich center of neutron scattering
LD	Lethal dose
LCT	Long chain triglycerides
LFCS	Lipid formulation classification system
MCT	Medium chain triglycerides
MLV	Multilamellar vesicles
MTT	3-(4, 5-dimethylthiazol-2-yl)-2, 5-diphenyltetrazolium bromide
MVV	Multivesicular vesicles
MWCO	Molecular weight cutoff
NCE	New chemical entity
NEAA	nonessential amino acids
O/W	Oil-in-water
PBS	Phosphate buffered saline
PDI	Polydispersity index
PEG	Polyethylene glycol
PG	Propylene glycol
Ppt	Precipitate
SANS	Small angle neutron scattering
SDMT	Sedimentation
SDS	Sodium dodecyl sulphate
SEDDS	Self-emulsifying drug delivery system
SLD	Scattering length density
SMEDDS	Self-microemulsifying drug delivery system
SNEDDS	Self-nanoemulsifying drug delivery system
SUV	Small unilamellar vesicles
TEER	Transepithelial electrical resistance

List of Abbreviations

TDOC	Taurodeoxycholate
TM	Transport medium for intestinal model fluid studies
TPGS	Tocopheryl polyethylene glycol 1000 succinate
USFDA	United States Food and drug administration
UV-Vis	Ultra violet and visible
W/O	Water-in-oil

1. INTRODUCTION

1.1 Oral drug absorption

The majority of the drugs that are available on the global pharmaceutical market are administered by the oral route which is a convenient, safe and cost effective route of administration (Lipinski 1995; Lipinski 2000; Lipinski et al. 2001; Lipinski 2004; Abrahamsson and Lennernas 2005). Therefore, oral bioavailability is one of the key considerations for drug discovery and development. Bioavailability is influenced by several factors which can be identified broadly as physiological, physicochemical and biopharmaceutical (Horter and Dressman, 2001; Pouton 2006).

1.2 Factors affecting oral drug absorption

1.2.1 Physiological factors

Prominent among the physiological factors which impact oral drug absorption are the anatomy and physiology of the gastrointestinal tract (GIT), pH, influence of bile and pancreatic secretions, transit times of the various sections of the tract, lymphatic absorption, drug transporters and bacterial microflora. Anatomically, The GIT consists of the stomach, the small intestine (duodenum, jejunum and ileum) and the large intestine (cecum, colon and rectum). Each of these regions has a specific pH, length, function and morphology. The most important section to this thesis is the small intestine since Amphotericin B is acid labile and its absorption not suitable for formulations depicting disintegration or dissolution in the stomach.

The small intestine is the largest absorptive site for nutrients, water, electrolytes and most drugs administered orally (DeSesso et al, 2001). The mucosa of the absorptive sites exhibits a variety of modifications that increase the surface area including plicae (Kerckring's folds), crypts and finger-like projections called villi which is also covered by microvilli. This increased surface area is convenient for the transport of drugs from the lumen to the vascular system. The dense supply of blood and lymphatic capillaries also aid in efficient absorption.

Motility and transit time also affect drug absorption and hence a drug's bioavailability. Ingested materials upon reaching the stomach experience different transit times depending on the nature of their content (Vander et al, 1985). The gastric emptying time for a meal is about 4 hours, chyme traverses the human small intestine on average of 3-4 hours and transit time through the large intestine in healthy humans is 2-4 days depending on the amount of fiber or insoluble materials in the diet (Granger et al., 1985; DeSesso et al, 2001).

The pH at the site of absorption is critical in facilitating or inhibiting the dissolution and absorption of various ionizable drugs. Therefore, the extent of ionization plays an important role in the bioavailability of drugs. The pH of the luminal content is modified by the pH of the various secretions and ion pumps. The secretion of acid by the gastric mucosa results in the pH of 1-2 in the stomach. When the chyme enters the duodenum, it is quickly neutralized by the alkaline secretions from the Brunner's glands, gall bladder and the pancreas. This pH shift

in addition to the release of bile which contains bile salts such as taurocholic acid and deoxycholic acid derivatives and pancreatic enzymes affects the digestion and absorption of nutrients and drugs especially of the BCS classes II and IV. Structure and dynamics of the colloids and nanoparticles that result, which help in solubilization, intestinal permeability and/or lymphatic uptake of drugs have been the focus of current research (Nawroth et al., 2011; Khoshakhlagh et al., 2015). The biopharmaceutics classification system (BCS) group drugs into four classes based on their solubility and permeability. Class I drugs have high solubility and permeability. Class II drugs are those with low solubility and high permeability while class III drugs have high solubility but low permeability. Class IV drugs exhibit both low solubility and low permeability.

1.2.2 Physicochemical factors

Ionization state, molecular weight and lipophilicity of a drug influence its bioavailability. Molecular weight trends suggest that increasing the size above 400g/mol lead to a steady decrease in bioavailability (El-Kattan et al., 2012). Trends in lipophilicity (cLog P and cLog D) reveal that very hydrophilic compounds tend to have reduced intestinal absorption. These factors are clearly explained by the Lipinski's rule of 5 which is a widely used concept used to qualitatively predict oral drug absorption. Results from analysis of 2245 compounds from the World Drug Index (WDI) database indicate that good oral absorption is more likely with compounds that have less than 5 hydrogen bond donors (defined as NH or OH groups), not more than 10 hydrogen bond acceptors (defined as oxygen or nitrogen atoms, including those that are part of the hydrogen-bond donors), a molecular weight less than 500, and lipophilicity (Log P) of less than 5 (Lipinski et al., 1995; 2000; 2001). Poor bioavailability is more likely when the compound violates two or more this rule.

1.2.3 Biopharmaceutical factors

Factors considered to affect bioavailability in this category include particle size, salt form of the drug molecule, polymorphism, complexation, solubility, permeability and intestinal metabolism. Particle properties such as size, shape and surface area have far-reaching impact on bioavailability of dosage forms. The rate of drug dissolution is proportional to its surface area exposed to the dissolution medium. Therefore, particle size reduction which leads to increased surface area has long been used to enhance the dissolution rate and bioavailability of poorly soluble drugs.

Polymorphism has a profound implication on formulation development, because polymorphs may exhibit significantly different solubility, dissolution rate, compactibility, hygroscopicity, physical stability, and chemical stability (Bryn et al., 1999). Although use of a faster dissolving polymorph may have clinical benefit, it is important to keep in mind that a polymorph with a higher solubility or faster dissolution rate is also metastable (i.e., a higher energy form) and tends to convert to a thermodynamically more stable form over time. Conversion from a metastable form to a stable form could lower a drug's oral bioavailability, and lead to inconsistent product quality. Therefore, it is paramount that one selects thermodynamically the most stable polymorph for development.

Interest in complexation technologies has grown considerably due to increased applications of cyclodextrins (CDs), which are cyclic oligosaccharides obtained from enzymatic conversion

of starch. The parent or natural cyclodextrins that are of pharmaceutical relevance are α -, β , and γ -CDs, which contain 6, 7, or 8 glucopyranose units joined through 1–4 bonds, respectively (Hersey et al., 1986). Cyclodextrins can be used to solubilize, stabilize, taste mask, and reduce the irritancy and toxicity of drug molecules in solid oral dosage forms. It is well demonstrated in the literature that complexation with CD can significantly enhance oral bioavailability of poorly soluble compounds, such as cinnarizine (Järvinen et al.,1999), carbamazepine (Betlach et al., 1993), itraconazole (Hostetler et al., 1993) and insulin (Shao et al., 1994) in animals and humans. The enhanced bioavailability is in part attributed to increased rate of drug dissolution from the drug–CD complex, and in part may be attributed to the effect of CD as a potential penetration enhancer. Studies showed that CD might complex with membrane components, such as cholesterol, thereby modifying the transport properties of the membrane and facilitating drug absorption (Nakanishi et al., 1992).

1.3 Oral drug delivery systems of poorly water soluble drugs

Advances in combinatorial chemistry have led to the generation of a large number of new chemical entities (NCE) in addition to the existing ones. Many of these compounds show poor solubilization properties which lead to poor oral bioavailability resulting in a wide intra- and inter- subject variation (Talegaonkar et al., 2008). This presents a huge technical challenge to formulators. Thus, the selection of an appropriate dosage form for a drug with poor aqueous solubility is very crucial as this can render a useful drug worthless. Many approaches that have been explored for BCS II and IV drugs are as shown in figure 1 below:

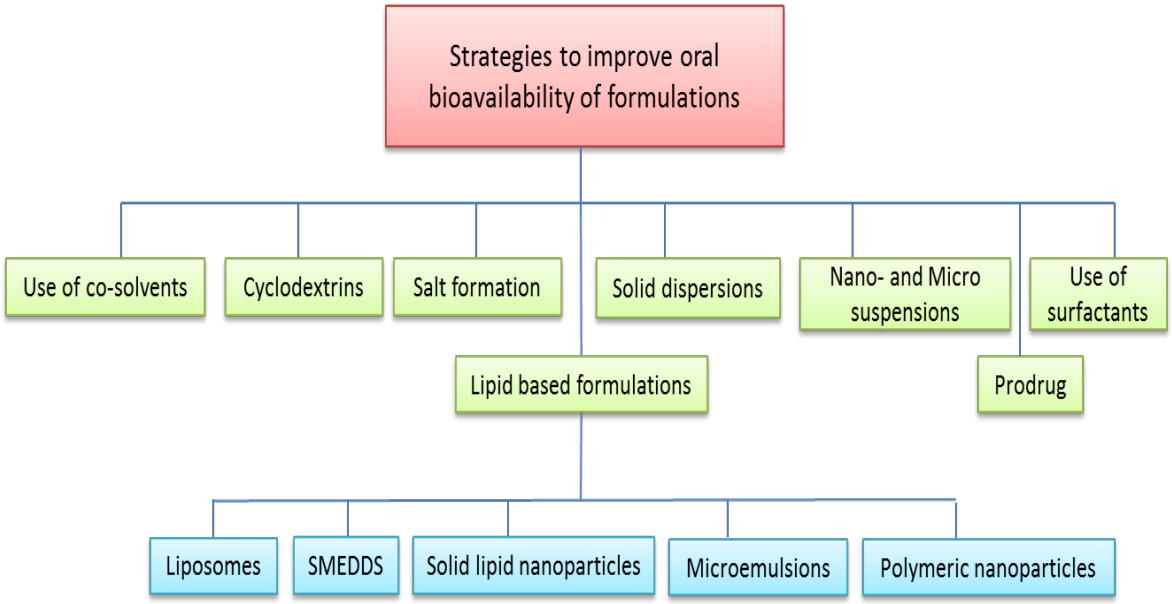

Figure 1.1: Formulation approaches to improve the oral bioavailability of poor aqueous soluble drugs (diagram adapted from Talegaonkar et al).

Chemical modification of the molecule (prodrug) of Amphotericin B was successful but majority of them caused a reduction in its fungal activity (Tevyashova et al., 2013). Complexation with cyclodextrins and other conventional polymers have also been investigated. These improved the solubility of the drug but most of the investigations were for its intravenous application (Lavasanifar et al., 2002; Vandermeulen et al., 2006; Abeer et al., 2012; Adams et al., 2003; Charvalos et al., 2006). Of interest to this thesis is the lipid based

formulations specifically liposomes and self-emulsifying drug delivery system (SEDDS) since these two drug delivery systems were investigated for their potential oral application of Amphotericin B.

1.3.1 Liposomes

Liposomes are nano to micro-particulate or colloidal carriers, usually 50 – 5,000 nm in diameter which forms spontaneously when certain lipids are hydrated in aqueous media (Bangham and Horne, 1964). As indicated in figure 1.2, they are composed of biocompatible and biodegradable material, and consist of an aqueous volume entrapped by one or more bilayers of natural and /or synthetic lipids. They occur in native material transport in tissues and intracellular.

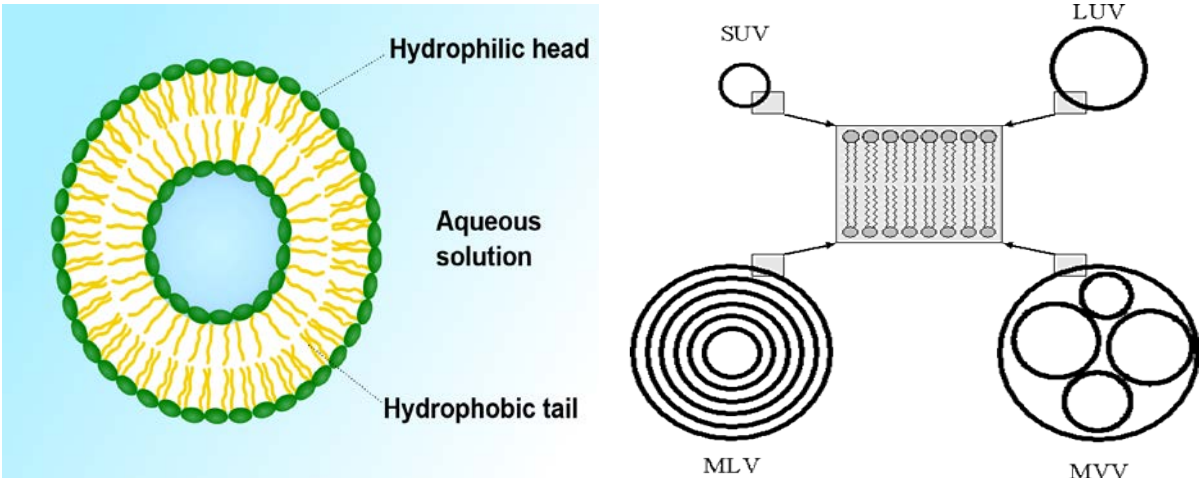

Figure 1.2: Structure of a liposome formed by a phospholipid bilayer (adapted from Liposome scheme-en.svg).

1.3.1.1 Classification of liposomes

Liposomes are classified on the basis of size, number of bilayers and composition. On the basis of composition, they are composed of natural and/or synthetic lipids (phosphor- and sphingo-lipids), and may also contain other bilayer constituents such as cholesterol and hydrophilic polymer conjugated lipids (Sharma, 1997). The liposome size can vary from very small (0.025 µm) to large (2.5µm) vesicles. Thus, on the basis of size and bilayers, they are classified as either unilamellar or multilamellar. Below is a description of the classification.

Table 1: Classification of liposomes based on size and lamellar

Liposome type	Size	Number of bilayers
Small Unilamellar Vesicles (SUV)	20 nm – 100 nm	Single
Large Unilamellar Vesicles (LUV)	100 nm – 400 nm	Single
Giant Unilamellar Vesicles (GUV)	1 µm and larger	Single
Large Multilamellar Vesicles (MLV)	200 nm - ~ 3 µm	Multiple
Multivesicular Vesicles (MVV)	200 nm - ~ 3 µm	Multiple

1.3.1.2 Methods of liposome preparation

All methods of preparing liposomes involve four basic stages: (a) drying down lipids from organic solvent. (b) dispersing the lipid in aqueous media. (c) purifying the resultant liposome and (d) analyzing the final product (Akbarzadeh et al., 2013).

1.3.1.3 Multilamellar vesicles (MLV)

The most simple and widely used method of preparing MLV is the thin-film hydration procedure. In this method, a thin film of lipids is hydrated spontaneously with an aqueous buffer at a temperature above the transition temperature of lipids (Sharma et al., 1997). The drug to be encapsulated is added either in the aqueous hydrating buffer (for hydrophilic drugs) or the lipid film (for lipophilic drugs). Heterogenous mixtures and low encapsulation efficiency of hydrophilic drugs are the main disadvantages of many MLV production protocols. Ohsawa et al. reported that the encapsulation efficiency of MLV could be improved by freeze-drying preformed small unilamellar vesicles (SUV) dispersion in an aqueous solution of the drug to be encapsulated. Hydration of lipids in the presence of organic solvents has also been investigated to improve entrapment efficiency (Papahajopoulos and Watkins, 1967; Gruner et al., 1985).

1.3.1.4 Unilamellar vesicles (SUV and LUV)

Methods developed for the preparation of large unilamellar vesicles (LUV) include solvent injection (ethanol or ether), calcium induced infusion, detergent dialysis and reverse-phase evaporation. Small unilamellar vesicles (SUV) are prepared from either MLV or LUV by sonication (probe or bath) or extrusion through polycarbonate filters under high pressure. The exposure of the encapsulating materials to organic solvents, ultrasound and the production of heterogenous mixtures are disadvantages of these processes.

1.3.1.5 Applications of liposomes in drug delivery

Liposomes, as a result of being composed of relatively non-toxic, non-immunogenic, biocompatible and biodegradable lipids, are used as delivery system for a number of drugs for diagnostic and therapeutic purposes. Liposomes have been successful with potent drugs with narrow therapeutic window by reducing toxicity and improving therapeutic efficacy. They have been effective in treating diseases that affect the phagocytes of the immune system because they tend to accumulate in the phagocytes, which act as mediators in the process to recognize them as foreign invaders. The best reported so far in human therapy are liposomes as carriers for amphotericin B in antifungal therapy (Lopez-Berstein et al., 1985). This however, has only parenteral application.

Liposomes containing Paclitaxel were able to deliver the drug systemically and increase the therapeutic index of the drug in human ovarian tumor models (Sharma et al., 1995, 1997). The success story of the anticancer drug, Doxorubicin, has been its liposomal formulation. Liposomes are taken up poorly by tissues such as heart and kidney which are major sites for toxic side-effects of a variety of neoplastic drugs. Thus, the formulation improved the

therapeutic index by altering the bio-distribution of the drug away from the heart tissues and hence reduced its cardiac toxicity (Ahmad et al., 1993).

Diptherin toxins (DT) have been encapsulated in immunoliposomes and have been shown to provide protection against non-specific toxicity of DT during cancer chemotherapy (Vingerhoeds et al., 1996).

1.3.1.6 Limitations of liposome technology

Despite the broad range of pharmaceutical applications and clinical acceptance, liposomes have challenges in development and manufacture. Stability issues, sterilization methods, batch to batch reproducibility, low entrapment, particle size control, production on a large scale and short circulation half-life of vesicles are some of the major limitations of the technology. However, stability is improved by lyophilisation.

1.4 Self-emulsifying drug delivery systems (SEDDS)

Self-emulsifying drug delivery systems are mixtures of oil and surfactants, ideally isotropic, sometimes including co-solvent or co-emulsifiers, which emulsify under conditions of gentle agitation, similar to those which would be encountered in the gastrointestinal tract (Fricker et al., 2010). Several names are given to these drug delivery systems based on their droplet size. SEDDS is considered to be the broad term referring to emulsions producing a droplet size ranging from a few nanometers to several microns. Self-microemulsifying drug delivery systems (SMEDDS) are those that produce transparent microemulsions with droplet size between 100 and 250 nm. The most recent terminology is self-nanoemulsifying drug delivery systems (SNEDDS) which refers to formulations with droplet size below 100 nm (Kanchan et al., 2012). They are considered to belong to type II and III formulations in the Lipid Formulation Classification System (LFCS) postulated by Pouton in 2000 and updated in 2006. This classification is based on the type of excipients and concentrations used in the formulation as shown in the table 2 below.

Table 2: Lipid Formulation Classification system according to Pouton 2006

Excipients in formulation	**Content of formulation (% w/w)**				
	Type I	**Type II**	**Type IIIA**	**Type IIIB**	**Type IV**
Oils: triglycerides or mixed mono and diglycerides	100	40–80	40–80	< 20	-
Water-insoluble surfactants (HLB<12)	-	20–60	-	-	0-20
Water-soluble surfactants (HLB>12)	-	-	20–40	20-50	30-80
Hydrophilic cosolvents (e.g. PEG, propylene glycol, transcutol)	-	-	0-40	20-50	0-50

*HLB – Hydrophile Lipophile Balance; PEG – Polyethylene glycol

The general characteristics, advantages, disadvantages and example of each type of lipid formulation are shown in Table 3.

Table 3: Characteristic features, advantages, disadvantages and examples of LCFS (Pouton, 2006)

LFCS type	Characteristics	Advantages	Disadvantages	Examples
I	Non-dispersing; requires digestion	GRAS status; simple; excellent capsule compatibility	Formulation has poor solvent capacity unless drug is highly lipophilic	Progesterone dissolved in peanut oil (Prometrium®); Testosterone in oleic acid (Restandol®/ Merck Sharp& Dohme)
II	SEDDS without water soluble components	Unlikely to lose solvent capacity on dispersion	Turbid oil-in-water dispersion (0.25-2 µm)	
IIIA	SEDDS/SMEDDS with water soluble components	Clear or almost clear dispersion; drug absorption without digestion	Possible loss of solvent capacity on dispersion; less easily digested	Cyclosporine (Neoral®/ Novartis); Ritonavir/Lopinavir (Kaletra®/ Abbot)
IIIB	SMEDDS with water soluble components and low oil content	Clear dispersion; drug absorption without digestion	Likely loss of solvent capacity on dispersion	
IV	Oil-free formulation, only surfactants and cosolvents	Good solvent capacity for many drugs; disperses to micellar solution	Loss of solvent capacity on dispersion; may not be digestible	Amprenavir (Agenerase®, GSK)

1.4.1 Components of SEDDS formulation

There are a large number of oils, surfactants and co-surfactants available for use in the preparation of self-emulsifying systems. The emphasis is on the use of excipients that are generally regarded as safe (GRAS) in terms of toxicity, irritancy, biocompatibility and clinical acceptability. The right concentration of the above excipients determines the self-emulsification and droplet size of the emulsion.

1.4.1.1 Oil phase

The oil is an important component of SEDDS formulations which influences the curvature of the droplets formed. It solubilizes large amounts of lipophilic drugs, aid in emulsification and enhances lymphatic transport of lipophilic drugs through the intestinal lymphatic system. The lipids utilized include Long Chain (LCT) and Medium Chain (MCT) triacylglycerides, diacylglycerides and fatty acid esters as well as protonated long-chain fatty acids. They are commonly ingested as food, fully digested and absorbed (Pouton et al, 2008). The

triglycerides are highly lipophilic and their solvent capacity for drugs is commonly a function of the effective concentration of the ester groups. Cao et al. thus reported on a weight basis that MCT has a higher solvent capacity than LCT and are subject to oxidation (Anderson, 1999; Cao et al., 2004). Modified long chain and medium chain triglyceride oils with varying degrees of saturation and hydrolysis are also available for use in SEDDS preparations. These semisynthetic derivatives form good emulsification systems in combination with approved solubility enhancing surfactants (Kimura et al., 1994, Hauss et al., 1998). The solubility of the drug in the oil phase is the main criterion for selecting the type of oil. This reduces the volume of the formulation required to deliver the therapeutic dose of the drug.

1.4.1.2 Surfactants

Surfactants are compounds that lower the surface tension between two liquids or between a liquid and a solid and form micelles when applied above the critical micelle concentration (CMC). Surfactants contain both hydrophilic (their heads) and hydrophobic (their tails) domains. Hence, they are considered amphiphilic. They are classified according to their polar head group as ionic, non-ionic and zwitterionic. A non-ionic surfactant has no charge groups in its head whiles the zwitterionic contains a head with two oppositely charged groups. The ionic surfactants are either positively or negatively charged. The surfactant chosen for SEEDS formulation must be able to lower the interfacial tension to facilitate dispersion, provide the correct curvature at the interfacial region and must be safe. The Hydrophile-Lipophile Balance (HLB) and the desired type of emulsion (either O/W or W/O) are guiding criteria for selecting surfactants. It is generally accepted that low HLB surfactants favours water-in-oil (W/O) emulsions whilst high HLB (> 12) ones are preferred for oil-in-water (O/W) emulsions.

Non-ionic surfactants are mostly used in the formulation of SEDDS because they are less toxic; possess good emulsion stability over a wide range of ionic strength and pH changes (Tenjarla, 1999). They may also cause changes in intestinal permeability (Swenson et al., 1994). Examples of such surfactants are polyethoxylated sorbitan esters (Tweens), polyethoxylated glycerides (Cremophors and Labrasol) and polyethoxylated fatty acid ester (Myrj and Solutol HS 15).

1.4.1.3 Co-surfactants/Co-solvents

Co-solvents are added to SEDDS formulations to:

1. Enforce the dissolution of the drug during manufacture.
2. Promote dispersion of systems which contain a high proportion of water-soluble surfactants.
3. Increase the solvent capacity of the formulation for drugs that dissolve freely in co-solvents (Pouton and Porter, 2008).

There is a limit of concentration to which these co-solvents could be used since they loose their solvent capacity upon dispersion in water leading to a higher risk of drug precipitation. Miscibility with oils, incompatibilities with capsule shells and toxicity should also be considered. The most popularly used materials include polyethylene glycol 400 (PEG 400), glycerol, ethanol and propylene glycol.

1.5 Amphotericin B

'Amphotericin B' is the international non-proprietary name. Its chemical (IUPAC) name is (1R,3S,5R,6R,9R,11R,15S,16R,17R,18S,19E,21E,23E,25E,27E,29E,31E,33R,35S,36R,37S)-33-[(3-amino-3,6-dideoxy-β-D-mannopyranosyl)oxy]-1,3,5,6,9,11,17,37-octahydroxy-15,16,18-trimethyl-13-oxo- 14,39-dioxabicyclo [33.3.1] nonatriaconta- 19,21,23,25,27,29,31-heptaene-36-carboxylic acid. Its molecular weight and melting point are 924.08 and 170^{o}C, respectively with CAS number 1397-89-3. Its structure is shown in figure 1.

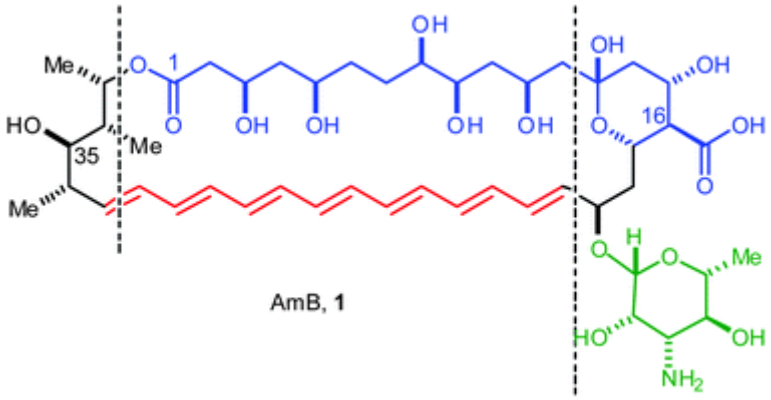

Figure 1.3: Schematic representation of Amphotericin B (AmB, 1). The structural features are depicted in colours. Blue is the polyol, red is the heptaene and green is the mycosamine (adapted from carreira et al.2010).

1.5.1 Therapeutic indication, therapeutic index and toxicity

Amphotericin B is an antifungal antibiotic used in treating progressive and potentially life-threatening fungal infections such as Aspergillosis, Candidiasis, Blastomycosis, Coccidioidomycosis, Cryptococosis and Histoplasmosis. It is currently being used to treat certain protozoan infections such as Leishmaniasis. The drug is administered intravenously and dosage varies depending on whether the drug is administered as conventional Amphotericin B (deoxycholate) or as Amphotericin B cholesteryl sulfate complex, Amphotericin B lipid complex, or Amphotericin B liposomal and the type of infection being treated. Thus, dosage recommendations for the specific formulation being administered should be followed. Depending on patient's cardio-renal status, the dosage may range from 0.25 to 5 mg/kg per day (Moore et al, 2002). A study quoted the LD_{50} of Amphotericin B-deoxycholate as 5.1mg/kg (rabbit) (Patterson et al, 1989). Toxicological information showing acute toxicity in different species and route of administration of Amphocin ® injection is given in Table 4.

Table 4: Toxicological studies of Amphotericin B in different animals (Amphocin® data sheet, Pfizer)

Species	Route of administration	LD_{50}
Rat	Oral	> 5000 mg/kg
Rat	Intravenous	1.6 mg/kg
Rat	Intraperitoneal	> 5000 mg/kg
Mouse	Intravenous	1.2 mg/kg
Mouse	Intraperitoneal	27.7 mg/kg

The drug is known for its severe and potentially lethal side effects which are dose-dependent. The common ones are nephrotoxicity, blood dyscrasias (leukopenia, thrombocytopenia) and hypotension (Garcia et al., 2000, Wasan et al., 2009). Nephrotoxicity measured by Blood Urea Nitrogen and Plasma creatinine levels is the main research tool for assessing the toxicity of the drug. Wingard et al conducted a study in 239 immunocompromised patients with suspected or proven aspergillosis. Amphotericin B (Fungizone) was administered for a mean of 20 days and the rate of nephrotoxicity (defined as creatinine doubling) was 53%. About 14.5% of these patients had to go on renal dialysis and 60% died (Wingard et al.2000).

Due to its lipophilic properties and its affinity to biological membranes and lipoproteins, Amphotericin B accumulates in the liver, sometimes leading to hepatic and bile disorders (Garcia et al., 2000). The drug however is not teratogenic.

1.5.2 Chemical properties

Amphotericin B belongs to the class of polyene antibiotics. It is a yellow/orange-coloured natural product that is extracted from cultures of *Streptomyces nodosus* on a large industrial scale (Lemka et al., 2005). Production yields both Amphotericin B and a low yield of unwanted Amphotericin A. As Amphotericin A shows less antifungal activity, its concentration must be below 5% (Liu et al., 1984, Monji et al., 1976). Amphotericin B has two physicochemical properties: amphiphilic, due to the apolar and polar sides of the lactone ring and amphoteric, due to the presence of ionisable carboxylic and amine groups.

1.5.3 Solubility

All polyene antibiotics are characterised by a very low solubility of less than 1 mg/L in water or water-free alcohols at physiological pH (pH 6-7) (Lemke et al., 2005). The drug is

sparingly soluble in different organic solvents, as shown in table 5. This very low general solubility is the main reason why there is almost no gastrointestinal absorption and thus only minimal oral bioavailability (Bennett 1995; Plumb 1999). Bennett and Windholz et al reported that Amphotericin B is water soluble at a pH below 2 or above 11 and at this pH the value is about 0.1 mg/ml (Bennett.1995; Windholz et al.1983). Under these extreme conditions the molecule is not stable. The molecule may form salts which would show better solubility. However, Plumb et al. reported these molecules have less antimycotic activity than the basic compound.

Table 5: Solubility of Amphotericin B in different solvents (Lemke et al 2005)

Solvent	**Solubility (mg/L)**
Water	< 1 (at pH 6-7)
Methanol	2000
Ethanol	500
Chloroform	100
Petroleum ether	10
Dimethyl formamide	2
Propylene glycol	1
Cyclohexane	20
Dimethylsulfoxide	30,000 – 40,000

Its low aqueous solubility has been the subject of a lot of research. Table 6 shows some experimental data.

Table 6: Experimental aqueous solubility data

Sample	Solubility	Author
AmpB complexed with poly (α-glutamic acid)	1.5 – 3.0 mg/ml	Abeer et al. (2013)
AmpB-Arabinogalactan conjugates	> 1,000 mg/ml	Polacheck et al. (1999)
AmpB encapsulated in PEG-block-poly(ε-caprolactone-co-trimethylenecarbonate)	5% - 85 µg/ml 10% - 104 µg/ml 20% - 122 µg/ml	Vandermeulen et al. (2006)
Micelles of AmpB with PEG-block-poly(N-hexyl stearate L-aspartamide)	250 µg/ml	Lavasanifar et al. (2002)
AmpB with Peceol/DSPE-PEG	100 – 500 µg/ml	Wasan et al. (2009)
Micelles of AmpB with PEO-block-poly(β benzyl-L-aspartate)	57 – 141 µg/ml	Yu et al. (1998)

- Temperature of determination is not stated

1.5.4 Aggregation

Owing to its amphipathic nature, Milhaud et al. reported Amphotericin B aggregates in water at concentrations around 2 x 10^{-7} M (Milhaud et al.2002). They are formed well below the critical micellar concentration (about 3 µM) by interaction between neighbouring polyene chains. The aggregation state can be easily assayed by spectrophotometry and should be assessed in formulations. The aggregation state of the molecule is related to its activity and toxicity. Torrado et al. have reported that although all aqueous Amphotericin B formulations are yellowish they have different appearance depending on their aggregation state (Torrado et al., 2013). The prevalence of a monomeric conformation supposes a transparent complete dissolution; oligomers (water-soluble aggregates) give translucent colloidal dispersion and larger aggregation of oligomers (water-insoluble aggregates or super aggregates) produce an opaque suspension. It is therefore possible to have different aggregation states present in the same formulation. Absorption spectra can be used to study the relative aggregation state. Adams et al. have used the ratio between the first peak and the last absorption peak to monitor

the aggregation state of Amphotericin B (Adams et al., 2003). The degree of aggregation depends on the concentration of the drug (Gruda et al., 1991; Brajtburg et al., 1996; Legrand et al., 1997; Aramwit et al., 2000), the medium in which the drug is dispersed (Lavasanifar et al., 2002; Vakil et al., 2005; Adams et al. 2003), the action of surfactants, the method of preparation of the dispersions (Vandermuelen et al., 2006) and the temperature of exposure (Gaboriau et al., 1997).

1.5.5 pKa

The pKa of the drug is quoted as 5.5 and 10.0 representing the two ionisable groups in the molecule (Sigmaaldrich.com). Another source also quotes the pKa as 5.7 and 10 (druginfosys.com). However, temperatures of determination were not stated.

1.5.6 Partition coefficient

The experimentally determined log P is reported to be 0.8. The predicted log P using ALOGPS is -0.66 and -2.3 using ChemAxon.

1.5.7 Pharmacokinetic properties

1.5.7.1 Absorption and permeability

Amphotericin B has poor gastrointestinal absorption and negligible bioavailability when administered orally due to its hydrophobicity. Its current usage is solely parenteral which requires attendance at a hospital, well trained personnel and infusion equipment. Oral bioavailability improvement is a major topic of research. Various research works have been carried out in this direction. Majority of the tests done to evaluate these formulations are in vitro which assesses haemolysis and toxicity to various organs and tissues using animal models.

1.5.7.2 Distribution

The drug is extensively bound to plasma proteins (≈95%) by β-lipoproteins, albumin and α_1 acid glycoprotein. High concentrations are usually found in liver and lungs (Barlett et al., 2004). It is also reported that the drug distribution depends on the drug carrier of the formulation (Bolard et al, 1980; Veerareddy et al., 2004).

1.5.7.3 Metabolism and excretion

Most of the drug is removed unchanged from the blood in the liver and excreted with the bile through faeces (Bekersky et al., 2002). The plasma half-life ranges between 14 and 48 hours with an elimination half-life of approximately 15 days (Daneshmend et al., 1983).

1.5.7.4 Commercial formulations

The conventional Amphotericin B formulation used deoxycholate, a detergent to solubilise the drug in micelles for intravenous administration (Fungizone®). Unfortunately, the activity of the drug is not exclusive to fungal cells but also to the tissues of the recipient with the kidney being the major target organ. It is believed that association of Amphotericin B with lipid carriers reduces the interaction of the drug with cholesterol found in the host membrane.

Introduction

The development of lipid-based formulations has been successful in reducing the nephrotoxicity associated with Fungizone. These formulations are a lipid complex (Abelcet®, Enzon Pharmaceuticals), and a liposomal Amphotericin B (Ambisome®, Gilead Sciences). Investigations into the physical properties of Abelcet® showed that it was heterogenous, containing both liposomes which incorporates less than 5 % of Amphotericin B and a lipid complex with a higher proportion of the drug (Janoff et al., 1988). Ambisome® on the other hand employed saturated phospholipids with cholesterol. Table 7 summarises the type of formulation, composition, size and pharmacokinetic properties of the commercially available Amphotericin B administered parenterally.

Table 7: Comparison of commercial Amphotericin B formulations

	Fungizone	**Abelcet**	**Ambisome**
Composition	Sodium deoxycholate	Dimyristoylphosphatidylcholine, dismyristoylphosphatidylglycerol 7:3 (molar ratio)	Hydrogenated soy phosphatidylcholine, distearoylphosphatidylglycerol, cholesterol, α-tocopherol
AmpB/lipid ratio	NA	1:1 (molar ratio)	1:9 (molar ratio)
Charge	None	Negative	Negative
Class	Colloidal system	Lipid complex	Liposome
Structure	Micellar	Ribbon-like complexes	Small unilamellar vesicles
Size (nm)	100	1,600-11,000	60 – 80
Recommended dose (mg/kg/day)	0.75	1 – 5	3 – 5
Half-life (hr)	24 – 48	19.7 – 23.5	8.7 – 11.2
C_{max} (ug/ml)	1.5 - 2.9	1.7	83
Clearance (ml/hr/kg)	40.6	17.8	9.4

Pharmacokinetic data for commercial formulations (Bekersky et al. 2002; Walsh et al. 2001)

1.6 Scattering techniques for structural investigations

1.6.1 Dynamic light scattering

Dynamic light scattering (DLS), also referred to as photon correlation spectroscopy (PCS), is a non-invasive, well-established technique for measuring the size and size distribution of molecules and particles typically in the submicron region which have been dispersed or dissolved in a liquid.

1.6.1.1 Theory of DLS

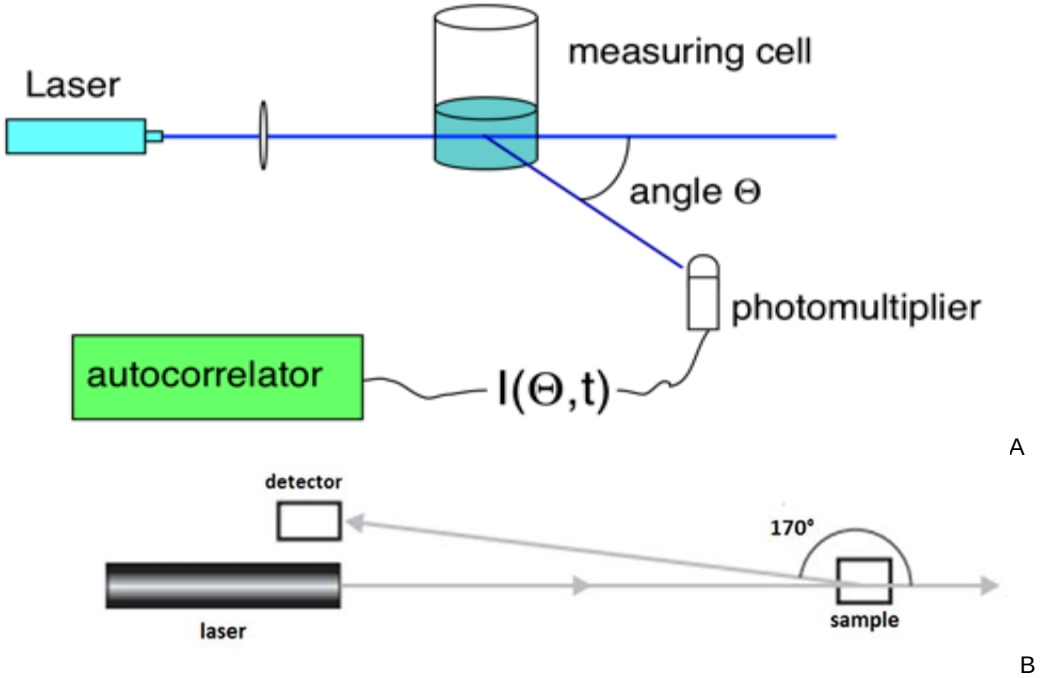

Figure 1.4: Example of a typical dynamic light scattering setup A (according to Jörg Langowski) with (B) showing backscattering mode of detection

A monochromatic light source (laser beam) is incident through a polarizer and into a sample. The scattered light including interferences of contribution from different particles then goes through a second polarizer where it is collected by a photomultiplier and the resulting image is projected onto a screen.

Dynamic light scattering makes use of two common properties of samples namely Tyndall effect (scattering) and Brownian motion (Hassan et al, 2015). In this technique, the time of interference fluctuations in the scattered intensity (speckles) obtained from a small sample volume containing a limited number of particles (10 to 1000), is measured and it depends on the diffusion coefficient of the particles undergoing Brownian motion. The time scale of these fluctuations is analysed by auto correlation, as the fluctuations of the light have the same kinetics as the motion of the particles.

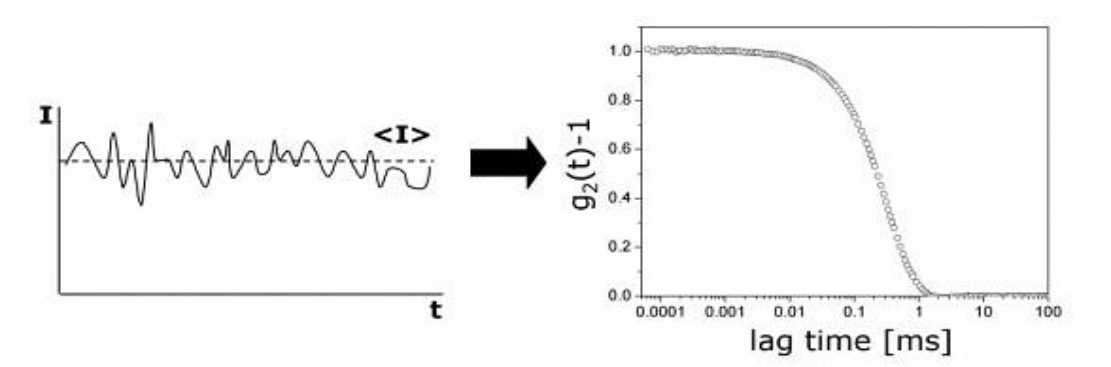

Figure 1.5: The time scale of intensity fluctuations (adapted from LS instrument_ www.lsinstruments.ch)

The dynamic information of the particles is derived from the autocorrelation of the intensity trace recorded by the equation below, that is, by multiplication of the original and a time-shifted signal I(t + τ)

$$g^2(q;\tau) = \frac{\langle I(t) * I(t+\tau) \rangle}{\langle I(t) \rangle^2} \qquad \text{(eqn.1)}$$

where $g^2(q;\tau)$ is the autocorrelation function at a particular wave vector, q, and τ is the delay time. I is the intensity.

Small particles diffuse in the medium relatively faster resulting in a rapidly fluctuating intensity signal as compared to large particles which diffuse slowly.

For spherical particles, the hydrodynamic radius, R, is calculated from the diffusion coefficient (D) using Stokes-Einstein equation

$$D = \frac{KT}{6\pi\eta R} \qquad \text{(eqn.2)}$$

where k is the Boltzmann's constant, η is the solvent viscosity and T is the absolute temperature.

1.6.1.2 Small Angle Scattering (Neutrons, X-rays, Light)

In any small angle scattering experiment, a beam of collimated monochromatic radiation is directed at a sample, illuminating a small volume, V, typically < 0.5 cm^3 for solvated systems. Some of the incident radiation is transmitted by the sample, some is absorbed and some is scattered. A detector, or detector element, of dimensions dx x dy positioned at some distance, L , and scattering angle, θ , from the sample then records the flux of radiation scattered into a solid angle element, ΔΩ (= dx dy / L^2). This flux, I (λ, θ), may be expressed in general terms in the following way

$$I(\lambda, \theta) = I_o(\lambda)\, \Delta\Omega\, \eta(\lambda)\, T\, V\, \partial\sigma / \partial\Omega\, (q) \qquad \text{(eqn.3)}$$

where I_0 is the incident flux, η is the detector efficiency (sometimes called the response), T is the sample transmission and $(\partial\sigma/\partial\Omega)(q)$ is a function known as the (microscopic) differential scattering cross-section. The first three terms of equation 3 are instrument-specific whilst the last three terms are sample-dependent.

The objective of a small angle scattering experiment is to determine the differential scattering cross-section, since it is this which contains all the information on the shape, size and interactions of the scattering bodies (assemblies of scattering centres) in the sample. The differential cross-section is given by

$$\partial\sigma/\partial\Omega\,(q) = N_p\, V_p^{\,2}\, (\Delta\delta)^{\,2}\, P(q)\;\; S(q) + B_i \qquad \text{(eqn.4)}$$

where N_p is the number concentration of scattering bodies (given the subscript "p" for "particles"), V_p is the volume of one scattering body, $(\Delta\delta)^2$ is the square of the difference in neutron scattering length density (contrast), P(q) is a function known as the form or shape factor, S(q) is the interparticle structure factor, q is the modulus of the scattering vector and B_i is the (isotropic) incoherent background signal. $(\partial\sigma/\partial\Omega)(q)$ has dimensions of $(\text{length})^{-1}$ and is normally expressed in units of cm^{-1}.

1.6.1.3 The scattering vector

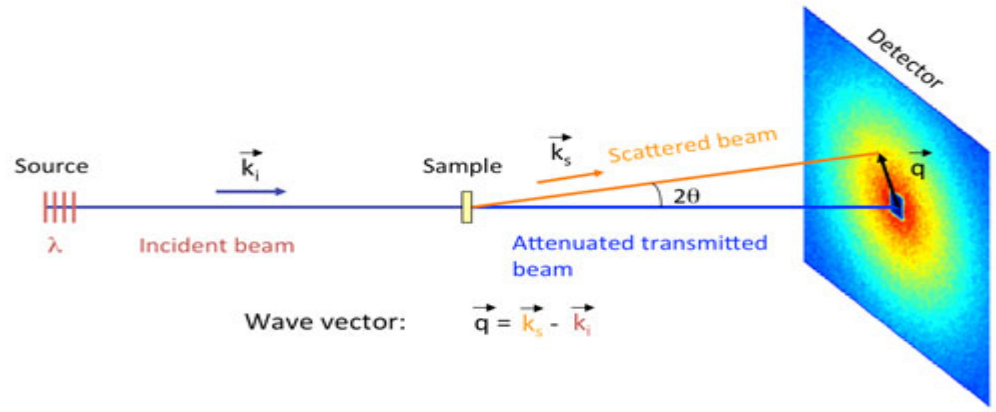

Figure 1.6: Schematic representation of a small angle scattering experiment (Image courtesy of ILL-Grenoble).

The quantity colloquially referred to as "the scattering vector" (given the symbol q) is the modulus of the resultant between the incident, k_i, and scattered, k_s, wave vectors, as shown in Figure 1.6, and is given by

$$q = /q/ = /k_s - k_i/ = \frac{4\pi * Sin\ \theta}{\lambda} \qquad \text{(eqn.5)}$$

q has dimensions of $(\text{length})^{-1}$; normally quoted in nm^{-1} or $Å^{-1}$ and θ is the half scattering angle.

Substituting Equation 5 into Bragg's Law of Diffraction

$$\lambda = 2d^{*}\mathrm{Sin}(\theta) \qquad \text{(eqn.6)}$$

yields a very useful expression

$$d = \frac{2\pi}{q} \qquad \text{(eqn.7)}$$

where d is a distance. Equations 5 and 7 are central to SANS experiments because through their combined use it is possible to both configure an instrument (i.e., ensure that its "q-range" allows you to see what you expect) and to quickly and rapidly "size" the scattering bodies in a sample from the position of any diffraction peak in q-space. In a typical scattering experiment, the scattered intensity I(q) is reported as a function of the scattering vector q which is related to the wavelength of the incident radiation by equation 5. This measured I(q) includes both coherent and incoherent elastic scattering. The coherent scattering provides information about the structure of the scatteres. The incoherent scattered intensity is q-independent and therefore manifests as a flat background noise.

1.6.1.4 The contrast term

The scattering length density,δ, of a molecule of i atoms is given by the formula;

$$\delta = \Sigma_i\, b_i \times \rho N_A / M_w \qquad \text{(eqn.8)}$$

where ρ is the bulk density of the scattering body and M_w is its molecular weight. δ has units of $(\text{length})^{-2}$ and can also be negative. Equation 8 is the same for X-rays and neutrons but the nature of b_i is different.

The contrast is simply the difference in δ values between that part of the sample , δp , and the surrounding medium or matrix, δm, all squared; i.e., $(\Delta\delta)^2 = (\delta_p - \delta_m)^2$. Therefore, if $(\Delta\delta)^2$ is zero then equations 3 and 4 are also zero and there is no small angle scattering. When this condition is met the scattering bodies are said to be at contrast match. Since the small angle scattering from a multi-component sample is essentially a contrast-weighted summation of the small angle scattering from each individual component, the technique of contrast matching has been used to dramatically simplify the scattering pattern.

In small angle X-ray scattering (SAXS), the photons interact with the electrons of the atom and thus the scattering power varies regularly with atomic number. The neutrons interact with the nucleus of the atoms. Therefore, the neutron scattering power of a given element does not depend on its proton (electron) number but is isotope dependent. The X-ray and neutron scattering lengths of some elements are indicated in table 8

Table 8: X-ray and neutron scattering length of some atoms

Atom	H	D	C	O	N
Atomic mass	1	2	12	16	14
Number of electrons	1	1	6	8	7
f_X, 10^{-12} cm	0.282	0.282	1.69	2.16	1.97
f_N, 10^{-12} cm	-0.374	0.667	0.665	0.580	0.940

f_X – X-ray scattering length f_N – neutron scattering length

Table 8 highlights the large difference in scattering length of hydrogen (^{1}H) and deuterium (^{2}D). This difference in scattering length makes neutrons very useful for structural studies especially for hydrogen-rich organic materials. Hence components of biomolecules can be highlighted in neutron experiments by either preparation in deuterium solvent or by selective isotopic labelling of the desired component. Neutrons do not cause damage to biological samples and therefore very suitable for the structural investigation of the Amphotericin B formulations since Amphotericin B is light sensitive and fluoresces.

2. AIM OF THESIS

Amphotericin B is the drug of choice for the treatment of systemic fungal infections and leishmaniasis. It is classified under class IV of the Biopharmaceutics Classification System (BCS). Due to its poor solubility and permeability characteristics, the drug till date is given parenterally. This work attempts to solubilize the drug with solubilizing and permeation enhancing agents to explore its potential use by the oral route. Three different drug delivery systems would therefore be developed and evaluated for the suitable delivery of Amphotericin B.

The Hydrophilic Solubilisation Technology (HST) was employed in the successful formulation of simvastatin, a BCS class II drug, to improve its solubility. In this technology, lecithin and gelatin was used as solubility enhancing excipients to coat the particles of simvastatin. Although pharmaceutical studies quoted the solubilizing power of HST formulations, no structural investigation was done to elucidate the number of layers and thickness of the coat. This thesis sought to use Amphotericin B as prototype drug with solubility problem (as well as high molecular weight, 924.08) by employing lecithin and gelatin to coat the particles of the drug to yield a well-structured construct. The structure of this construct would be investigated by microscopy, dynamic light scattering (DLS) and small angle neutron scattering (SANS). Suitability for oral administration would be explored.

Multilamellar liposomes are easy to prepare and are reported to have greater encapsulation of lipophilic drugs. They are mechanically stable upon long term storage. Amphotericin B would therefore by encapsulated in multilamellar liposomes and evaluated for possible oral administration using neutral lipids with different chain lengths of fatty acids and degree of saturation, and cholesterol.

Drugs with low lipid solubility may have considerable high solubility in surfactants and co-solvents as well as mixtures of such excipients. In this regard, a self-nanoemulsifying drug delivery system (SNEDDS) of Amphotericin B would be developed as the third drug delivery system and characterized. Emphasis would be placed on the amount of drug solubilized since it is the cardinal parameter for Amphotericin B oral delivery.

3. MATERIALS AND METHODS

3.1 Materials

3.1.1 Materials for HST preparation

Gelatin (Type B, 160 Bloom)	Caelo GmbH, Hilden, Germany
Soybean lecithin	Caelo GmbH, Hilden, Germany
Mannitol	Merck KGaA, Darmstadt, Germany
Sucrose	Merck KGaA, Darmstadt, Germany
Amphotericin B (Oral grade)	Hangzhou Dawn Ray Co. Ltd, China
Glucose	Carl Roth GmbH & Co. KG, Karlsruhe, Germany

3.1.2 Materials for liposome preparation

1, 2-Dioleolyl-sn-glycerol-3-phosphocholine	Sigma Aldrich Co., St. Louis, Missouri, USA
1, 2-Dimyristoyl-sn-glycerol-3-phosphocholine	Sigma Aldrich Co., St. Louis, Missouri, USA
1, 2- Distearoyl-sn-glycerol-3-phosphocholine	Sigma Aldrich Co., St. Louis, Missouri, USA
1, 2-Dipalmitoyl-sn-glycerol-3-phosphocholine	Sigma Aldrich Co., St. Louis, Missouri, USA
Trehalose (> 99%)	Sigma-Aldrich, Steinheim, Germany
Cholesterol	Fagron GmbH, Barsbüttel, Germany
Taurodeoxycholate (TDOC) (>95%)	FerroMed Biomedical Nanotechnology, Nanovel Ltd. & Co. KG, Langenlonsheim, Germany

3.1.3 Materials for self-emulsifying system (SEDDS)

The following excipients were free gift samples from Gattefosse', France.

Peceol® (Glyceryl monooleate: Code 3088BA2, Batch 141261)

Labrafil® M2125CS (Linoleoyl macrogol-6 glycerides EP: Code 3066BA2, Batch 140997)

Labrafac Lipophile® WL1349 (Medium chain Triglycerides NF: Code 3139JVI, Batch 140806)

Labrasol® (Caprylocaproylmacrogol-8 glycerides EP: Code 3074JVI, Batch 142605)

Labrafac® PG (Propylene glycol dicaprylate NF: Code 3230BA2, Batch 132068)

Transcutol® P (Highly purified diethylene glycol monoethyl ether EP/NF: Code 3260JVI, Batch 142448)

Labrafil® M1944CS (Oleoyl macrogol-6 glycerides EP: Code 3063BA2, Batch 141405)

Maisine™ 35-1 (Glycerol monolinoleate EP: Code 134565, Batch 134565)

Olive oil	Edeka Zentrale, AG & Co. KG-Hamburg, Germany
Sesame oil	Sigma-Aldrich, Steinheim, Germany
Cottonseed oil	Sigma Aldrich, Steinheim, Germany
Sunflower oil	Thomy-Nestle, 41415 Neuss, Germany
Avocado oil	Vandemoortele GmbH, Dresden, Germany
Soybean oil	Vandemoortele GmbH, Dresden, Germany
Peanut oil	Biozentral GmbH, Ulbering, Germany
Castor oil	Biozentral GmbH, Ulbering, Germany
Safflower oil	Biozentral GmbH, Ulbering, Germany
Polyoxyethylene 20 sorbitan monoleate (Tween 80)	Caelo GmbH, Hilden, Germany
Polyoxyethylene 20 sorbitan monolaurate (Tween 20)	Caelo GmbH, Hilden, Germany
Propylene glycol	Caelo GmbH, Hilden, Germany
Polyethylene glycol 400	Caelo GmbH, Hilden, Germany

3.1.4 Cell culture

Cell culture media and supplements were purchased from Life Technologies, Darmstadt, Germany.

Caco-2 cell line	American Type Culture Collection, Rockville, MD.

Growth medium	Dulbecco's modified eagle medium: GlutaMax-I, 4.5 g/l glucose, without Na-pyruvate, supplemented with 10% FBS and 1% PenStrep.
Fetal bovine serum (FBS)	Fetal bovine serum standard, qualified, E.U.approved, South America origin
Buffer	Dulbecco's phosphate-buffered saline without Ca^{2+} and Mg^{2+} (PBS)
Trypsin	0.25% trypsin and 0.25%-EDTA (1mM), with phenol red
Antibiotics	PenStrep, 10000 U/ml penicillin/ 10000 µg/ml streptomycin

Non-essential amino acids (NEAA, Gibco 11140-035)

3-(4, 5-dimethylthiazol-2-yl)-2, 5-diphenyl-2H-tetrazolium bromide (MTT-reagent)	Carl Roth GmbH & Co. KG, Karlsruhe, Germany

3.1.5 Chemicals and solvents

All chemicals and solvents were of analytical grade or higher.

4-(2-hydroxyethyl)-1-piperazineethanesulfonic acid, HEPES	Carl Roth GmbH & Co. KG, Karlsruhe, Germany
Bovine serum albumin (fatty acid free)	Sigma-Aldrich, Steinheim, Germany
Butylhdroxytoluene (BHT)	Fagron GmbH, Barsbüttel, Germany
Deuterium oxide (D_2O)	Merck KGaA, Darmstadt, Germany
Ethanol (96%)	Carl Roth GmbH & Co. KG, Karlsruhe, Germany
Hank's balanced salt solution	Life Technologies GmbH, Darmstadt, Germany
Dimethylsulfoxide	Carl Roth GmbH & Co. KG, Karlsruhe, Germany
Chloroform	Carl Roth GmbH & Co. KG, Karlsruhe, Germany

Sodium lauryl sulphate	Carl Roth GmbH & Co. KG, Karlsruhe, Germany

3.1.6 General equipment and disposables

Double-distillation apparatus	Destamat Bi-Destillierapparat Bi 18E, Heraeus Quartzglas GmbH, Klein Ostheim, Germany
Centrifuge	Centrifuge 5804R, Eppendorf, Hamburg, Germany
Microplate reader	Tecan infinite™ F200, Tecan Group Ltd., Männedorf, Switzerland
Rotary evaporator	Rotavapor R-3 with vaccuum pump V-700, Büchi Labortechnik, Flawil, Switzerland
Size measurement	Zetasizer Nano ZS, Malvern Instruments, Malvern, England Custom-made DLS, Nanovel, Langenlonsheim, Germany
Ultrasound bath	RK 510, Brandelin, Berlin, Germany
Vortex	Agitateur Top-Mix 11118, Bioblock Scientific, Frenkendorf, Switzerland
Water Bath	SV 15, Gerhardt, Bonn, Germany
FTIR spectrophotometer	8400S, Shimadzu, Duisburg, Germany
UV-Visible spectrophotometer	Lambda 30, Perkin Elmer, Waltham, MA, USA
Fluorescence spectrophotometer	Perkin Elmer 650-40, Überlingen, Germany
Differential Scanning Calorimeter	DSC 1 Star system, Mettler-Toledo AG, Schwerzenbach, Switzerland
Freeze dryer	Christ alpha 1-4, Martin Christ GmbH, Osterode, Germany
Microplate reader	FLUOstar® Omega, BMG Labtech, Ortenberg, Germany

Materials and methods

Ultracentrifuge	SW 40 T1 Beckman Coulter, California, USA
Microscope	Wilovert®203147, Hund Wetzlar, Wetzlar, Germany
Microscope	IPBLa-Zeiss, Leica DMIL, Portugal
Hemocytometer	Thoma, Marienfeld, Germany
Laminar Flow	Herasafe HSP12, Heraeus, Germany
Incubator	Incubator MCO-17AI, Sanyo Electric, Co., Japan
Ultrasound tip	UP 200S, dr. hielscher GmbH, Germany
Microplates	96 well microplates clear, Greiner Bio One, Frickenhausen, Germany 6 well microplates clear, Greiner Bio One, Frickenhausen, Germany
Cell culture flasks	Cell culture flasks with filter cap, surface area 25 and 75 cm², Greiner Bio One, Frickenhausen, Germany
Petri dishes	100 x 20 mm, Greiner Bio One, Frickenhausen, Germany
Glass vials	Carl Roth GmbH & Co. KG, Karlsruhe, Germany
Amber glass vials	Carl Roth GmbH & Co. KG, Karlsruhe, Germany
Cuvettes for DLS	Carl Roth GmbH & Co. KG, Karlsruhe, Germany
Hot plate	IKAMAG®_IKA Labortechnik, Staufen, Germany
Slide-A-Lyzer® Dialysis Cassette MWCO 10,000	Thermo scientific, Rockford, IL, USA
Nanorelease chamber	Custom-made, Nanovel, Langenlonsheim, Germany

Haake Rheostress 1 viscometer	Thermo Fisher Scientific, Karlsruhe, Germany
Weighing balance	Sartorius AG, Germany
Shaking water bath	Köttermann 3047, Bensheim, Germany
Centrifuge	HF-130 TOMY KOGYO, Fokushima, Japan

3.1.7 Data processing

Excel	Microsoft Corporation, Redmont, Washington, US
Origin 7	Microcal, Northampton, MA
Zetasizer Software	Malvern Instruments, Malvern, England
ALV-7004 Software V3.0	ALV-GmbH, Langen, Germany

3.2 Methods

3.2.1 Formulation of AmB-HST

The method developed by Hilfinger et al. (US patent 2005/0220876 A1) was used with slight modification. About 100 mg of gelatin was dissolved in bi-distilled water at a temperature between 40 and 50^{o}C under magnetic stirring at 300rpm on a hot plate. 100 mg soybean lecithin was added (mass ratio of 1:1 with gelatin) and stirred for about 30 minutes. The mixture was allowed to cool to room temperature under moderate stirring and butylhydroxytoluene solution (3.044% in 96% ethanol) was added (1:1 mass ratio with gelatin, lecithin and amphotericin B). Amphotericin B was added gradually and stirred for 24 hours (1:1 mass ratio with gelatin and lecithin). Mannitol was then added and freeze-dried. Sample was passed through No. 4 preparative sieve and weight determined.

3.2.2 Solubility of Amphotericin B in intestinal model media FaSSIF-C

The solubility of Amphotericin B was determined in simulated fasted state intestinal fluid (FaSSIF) containing different concentrations of cholesterol (0, 7, 10 and 13 mole %).

Excess amount of Amphotericin B was added to the intestinal model media (3 ml) in glass stoppered tubes and incubated in a shaking water-bath (35% speed, 60 min^{-1}) at 37^{o}C for 24 hours. After this time period, the samples were centrifuged for 10 minutes at 800g (HF-130 centrifuge). 2ml of the supernatant was transferred into new tubes and centrifuged again for 5

minutes. The absorbance of the drug in the second supernatant was determined using the UV-Visible spectrophotometer at a wavelength maximum of 412 nm with the respective media as blank. The amount of drug was estimated via standard calibration curves of the drug in the different media. The particle size of the supernatant was determined by dynamic light scattering.

3.2.3 Manufacture of liposomes

3.2.3.1 Preparation of multilamellar liposomes

Different concentrations (mole %) of Lipid, Cholesterol and Amphotericin B were used as shown in Table 9.

Table 9: Different concentrations of Lipid, Cholesterol and Amphotericin B used for the formulations

Sample	Lipid (Mole %)	Cholesterol (Mole %)	Amphotericin B (Mole %)
A	85	10	5
B	80	15	5
C	70	20	10

The lipid, cholesterol and Amphotericin B were dissolved in chloroform: methanol (1:3) at 100 mg/ml, 40 mg/ml and 0.5 mg/ml respectively. The respective volumes according to the mole percent were pipetted with the aid of Hamilton syringe into test tubes and the solvent evaporated using the rotary evaporator at 150 mbar for the first 30 minutes and subsequently at 100 mbar to form the film. The films were hydrated with 0.2M trehalose and 10mM taurodeoxycholate (TDOC) in Hanks balanced salt solution and vortexed to form multilamellar liposomes. In the case of DMPC, DPPC and DSPC the films were hydrated above the lipids transition temperatures at 30^{o}C, 50^{o}C and 60^{o}C respectively. Drug free (blank) liposomes were prepared using the same volume of solvent as in the drug containing liposomes. The samples were freeze dried with mannitol as a lyoprotectant.

3.2.3.2 Preparation of small unilamellar liposomes for contrast variation experiment

Small unilamellar vesicles (SUV) of DOPC and Amphotericin B with (76:5:19 mole %) and without (95:5 mole %) cholesterol as well as blanks were prepared by the film hydration method. 100 mg/ml of DOPC and cholesterol were prepared with chloroform. A concentrated solution of the Amphotericin B was prepared in methanol. The respective amount of each excipient was measured with a Hamilton syringe into a test tube and the procedure as stated for the multilamellar liposomes was followed. To obtain the SUV, the multilamellar liposomes were sonicated with ultrasonic tip (40% amplitude) for 20 minutes. The sample was centrifuged at 800g rpm for 1 minute to remove the titanium grains. Blank DOPC liposomes with and without cholesterol were also prepared by the same procedure.

3.2.4 Preparation of self-emulsifying drug delivery system

3.2.4.1 Solubility of Amphotericin B in excipients

The solubility of Amphotericin B was determined by adding excess amount of the drug to various oils, surfactants and co-surfactants in screw capped vials. The mixture was vortexed for one minute and then incubated in a water bath at 37^{o}C for 48 hours. After 48 hours, the sample was centrifuged at 4000 rpm, 37^{o}C for 10 minutes to remove undissolved drug. The supernatant was taken and appropriately diluted with methanol and the amount of Amphotericin B quantified by UV spectroscopy at 407 nm.

3.2.4.2 Preparation of ternary phase diagram

Based on the Lipid formulation classification system (LFCS) a type IIIB formulation was aimed at to solubilize Amphotericin B since it is not readily lipid soluble (Pouton, 2006). Blank formulations were prepared by setting out the following excipient compositions:

Oil: 5 to 60 % w/w

Surfactant: 30 to 90 % w/w

Co-surfactant: 0 to 50 % w/w

Different concentrations of oil, surfactant and co-surfactant (total = 1g) were weighed into screw-capped vials and vortexed for one minute and allowed to stabilize. The samples were subjected to particle size analysis and emulsification. Ternary phase diagrams were then constructed.

3.2.4.3 Preparation of drug containing pre-concentrate

10 mg of Amphotericin B was weighed into a glass vial and the co-surfactant (either propylene glycol or Transcutol®) added. The surfactant (Tween 80) and oil (Peceol®) were added and magnetic stirred for 5 minutes to mix (Total of oil, surfactant and co-surfactant = 2g). The mixture was bath sonicated for 20 minutes. The mixture was transferred into eppendorf tubes and centrifuged at 6000 rpm, 25^{o}C for 10 minutes. The supernatant was kept in glass vials protected from light. The mixture was allowed to equilibrate at ambient temperature for 24 hours and examined for signs of phase separation prior to drug content, droplet size and emulsification analysis

3.2.5 Freeze drying of samples

The AmB-HST and liposome samples were frozen at -84^{o}C for one hour with the rate of cooling not controlled. The sample was freeze-dried at -21^{o}C (condenser temperature of -54^{o}C, chamber pressure 0.120 mbar) for 36 to 48 hours. Afterwards, the temperature was raised gradually to 0^{o}C with continued applied vacuum.

3.2.6 Characterization of formulations

3.2.6.1 Drug content

- Liposomes**:** An amount of formulation equivalent to 0.2 mg of Amphotericin B was accurately weighed and dissolved in 10 ml methanol. 100ul of this solution was diluted to 1 ml with methanol and absorbance determined at 407nm.

- Nanoemulsion: 0.2g of the mixture was weighed into a volumetric flask and methanol added to 10 ml mark. The mixture was appropriately diluted and the absorbance measured at a maximum wavelength of 407 nm

3.2.6.2 Drug entrapment in liposomes

An amount of formulation equivalent to 0.2 mg of Amphotericin B was dispersed in 1 ml of HBSS. The resulting suspension was centrifuged at 4^{o}C, 14,000 rpm for 30 minutes. 900ul of the supernatant was diluted to 5 ml with methanol in a volumetric flask. The absorbance of this solution was measured to represent the amount of the unentrapped drug. The pellets were dissolved in 10 ml methanol. 100ul of the solution was diluted ten times with methanol and absorbance measured at 407nm. The amount of Amphotericin B entrapped was determined and efficiency calculated.

3.2.6.3 Size measurements

The size measurements were conducted by dynamic light scattering using the Malvern zetasizer, Nano-ZS and data analyzed with Zetasizer software V 6.20. Some measurements were done in triplicate. The Z-average and polydispersity index (PDI) were recorded.

- AmB-HST: The particle size of the formulation was assessed after the addition of the Amphotericin B at pre-determined time intervals (0.5, 1, 2, 4, 8 and 24 hours). In the determination, 20 µl of the mixture was diluted to 1ml with Hank's balanced Salt Solution (HBSS).

- Liposomes: 20 µl of the mixture after suspension of the film was diluted to 1ml with Hank's balanced Salt Solution.
  After freeze drying, about 1 mg of sample was suspended with 1ml of HBSS and size of the resulting mixture measured.

- Nanoemulsion: 100µl of the mixture (blanks) was added in drops to 100ml of distilled water under moderate magnetic stirring for 5 minutes. 1ml of the mixture was taken and measured (Jeoung et al., 2010). The same procedure was used for the pre-concentrates (drug containing samples).

3.2.6.4 Emulsification properties of nanoemulsion

200µl of the mixture (blank or drug containing) was added in drops with moderate magnetic stirring to 300ml of distilled water at 37^{o}C in a glass beaker (Kommuru et al., 2001, Jeoung et al., 2010). The tendency to emulsify spontaneously and the progress of emulsion droplets were visually observed. The resultant emulsion was graded according to the five grading systems shown in Table 10 (Shen et al, 2006; Pouton et al, 1985; Khoo et al, 1998; Heshmati, et al, 2013). All experiments were done in triplicate.

Table 10: Visual Assessment of Self-Emulsification (adapted from Heshmati et al., 2013)

Grade	Dispersibility and Appearance	Time of Self-Emulsification
I	Rapidly forming nanoemulsion, which is clear or slightly bluish in appearance	< 1 min
II	Rapidly forming, slightly less clear emulsion, which has a bluish white appearance	< 2 mins
III	Bright white emulsion (similar to milk in appearance)	< 3 mins
IV	Dull, greyish white emulsion with a slightly oily appearance that is slow to emulsify	> 3 mins
V	Exhibits poor or minimal emulsification with large oil droplets present on the surface	> 3 mins

3.2.6.5 Precipitation study of nanoemulsion

The mixture used for the evaluation of emulsification properties was kept for 24 hours to observe for any visible precipitation. Some were also observed for 72 hours.

3.2.6.6 Microscopy

- AmB-HST: Samples of pure Amphotericin B and formulated powders were placed on a glass slide and covered with a cover slip without any treatment. This was observed under a Phase-contrast microscope using a 40 X objective and a digital camera. The virtual magnification is given as a bar (10 µm) in the images.

- Liposomes: Microscopic observation was performed with 20 X objective using the IPBLa-Zeiss microscope. A drop of the dispersion was placed on a glass slide and covered with a cover slip without any treatment.

3.2.6.7 UV-Visible spectrum

Spectra of pure Amphotericin B in methanol and in water, the gelatin-lecithin formulated Amphotericin B (in water) and liposome formulated Amphotericin B were obtained by absorbance scanning in the range 300 – 500 nm wavelength at a concentration of 0.2-1 µM.
The mixture used for the particle size determination of the nanoemulsion was used for the spectrum. This was to investigate the effect of the formulation process on the drug.

3.2.6.8 Fluorescence spectrum of Amphotericin B

Different concentrations of pure Amphotericin B were prepared in methanol and the fluorescence spectrum measured with the fluorescence spectrometer at an excitation and emission wavelengths of 333 nm and 475 nm respectively. The Tecan microplate reader was also used to assess the possibility of analysing the drug formulations with fluorescence spectroscopy at an excitation of 340 nm and background of 560 nm.

3.2.7 Differential scanning calorimetry (DSC)

Thermograms of the freeze-dried liposome formulations (powder) with weight between 3 to 6 mg (sealed in 40 µl aluminium crucible pans) were generated using the DSC apparatus at a scan rate of 5^oC per minute under a nitrogen purge from 20^oC to 250^oC. Blank liposomes were also investigated to deduce the influence of the drug on the matrix. Duplicate measurements were made.

3.2.8 Fourier transform infrared spectroscopy (ATR-FTIR)

Spectra of the formulated liposomes and their physical mixtures were recorded using FTIR spectrophotometer equipped with ATR at wave numbers ranging from 600 cm^{-1} to 4000 cm^{-1}. An averaged 20 scan measurements was used and all experiments were done at room temperature.

3.2.9 Density gradient centrifugation

A linear sucrose gradient (10% - 50% w/w) was prepared in HBSS. 500µl of the liposomal Amphotericin B was layered onto the continuous sucrose gradient. The gradient was centrifuged at 285,000 x g for 17 hours at 4^oC. After centrifugation the gradient was fractionated into 150µl aliquots (using BIOCOMP gradient station) and the absorbance of the fractions determined at 405nm using microplate reader (FLUOstar®). 20µl of the fractions was diluted to 1ml with HBSS and the particle size measured by dynamic light scattering. The fractions containing drug were pooled together (upper and lower density fractions) and drug content determined with the spectrophotometer after dilution with methanol at a wavelength of 407nm.

3.2.10 Culture of Caco-2 cells

After initial culturing with 2% antibiotic-antimycotic solution (Mycokill), the Caco-2 cells (passage75) were cultured in 75cm flask in an incubator at 37°C with 5% CO_2. The culture medium was D-MEM supplemented with 10% FBS, 1% NEAA and 1% antibiotics solution (Penicillin-Streptomycin). The passaging was done weekly with one intermediate feeding. The passaging was done by washing with PBS (twice) to remove all traces of trypsin inactivating agents such as Ca^{2+}, Mg^{2+} and other serum components. 1ml of trypsin was added to the cells and incubated for 5 minutes. The trypsin was inactivated by adding 5ml of complete growth medium. The cell suspension was centrifuged at 1000rpm at 25^oC for 10 minutes. The supernatant was aspirated off and the cells re-suspended with 5ml of growth medium. The cells are counted with the help of hemocytometer and seeded into flasks or microplates.

3.2.10.1 Cytotoxicity assay

- Liposomes: At near confluence, the cells were transferred to 96-well plates and seeded at a density of 3000 cells per well and incubated for 48h for cell adhesion. Afterwards, the medium was exchanged with 180 µl of different concentrations (1, 5, 10, 25, 50, 100 µg/ml) of liposomes with and without Amphotericin B (sample C). Amphotericin B suspension in cell culture medium was used as a positive control. The cells were incubated for 1, 4 and 24 hours. After the incubation periods the medium was replaced with fresh medium and incubated for one hour. For the cell viability estimation using the MTT-test, the medium was removed and 180µl of Thiazolyl blue in colorless medium (MTT-reagent, 0.5 g/l) was added and incubated at 5% CO_2, 37°C for 1h (cellular MTT formation). After removal of the MTT-Reagent medium, the Formazan crystals were solubilized by addition of 190 µl DMSO, incubating for 30 minutes in a CO_2-incubator at 37°C and subsequent agitation with a multichannel pipette (threefold). The DMSO extracts were transferred to a non-sterile 96-well plate. The optical density was determined by the micro plate reader at 560nm and a reference of 690nm. The cell viability was then evaluated. Four replicates were done.

- Nanoemulsion: Sample G (for propylene glycol) and T_{14} (for Transcutol®) were selected for the toxicity test based upon the optimization results. The same concentrations and procedures were used.

3.2.10.2 Uptake study of liposomes

The method by Sanyog et al. (2012) was used with slight modification. After seeding and incubation for 48 hours as shown above for the cytotoxicity assay, the medium was replaced with 180 µl of 50µg/ml of liposomal Amphotericin B and incubated at 1, 4 and 24 hours. After incubation the medium was removed and cells washed three times with HBSS. 300 µl of ice-cold methanol was added and incubated for 2 hours in ice (0-4^{o}C). The cell extract was collected, vortexed and centrifuged at 14,000g for 10 minutes at 4^{o}C. The supernatant was taken and diluted with 100 µl of methanol. The absorbance of the resulting solution was determined at 407nm with the spectrophotometer. The amount of drug estimated was expressed as a percentage of the initial.

3.3 Hemolysis study

About 10 ml of fresh human blood collected into EDTA-tube was centrifuged at 2500 rpm for 10 minutes. The plasma was separated from the red blood cells and washed three times with phosphate buffered saline (pH 7.4) (Van de Ven et al., 2012). The red blood cells were then suspended at 5% v/v in the phosphate buffered saline (PBS). 300 µl of different concentrations (1, 2, 5, 10, 25 and 50 µg/ml) of the liposomal formulation and Fungizone® (as standard) prepared in PBS was added to 300 µl of cell suspension in eppendorf tubes. The samples were incubated in a shaking water bath at 37^{o}C for 1 hour. The negative control consisted of 300µl of red blood cell suspension with 300 µl of PBS, while the positive control was the same volume of red blood cell suspension diluted in distilled water. After incubation, the tubes were immersed in ice-cold water to stop hemolysis and subsequently centrifuged at

2500 rpm for 10 minutes. The absorbance of the supernatants diluted appropriately (1:1 with PBS) was measured with the spectrophotometer at a wavelength of 578 nm for the presence of released hemoglobin with PBS as the blank. The percent hemolysis was calculated according to the following equation (Fukui et al., 2003a, Van de Ven et al., 2012, Jung et al., 2009)

$$\text{Hemolysis (\%)} = (Abs - Abs_o) / (Abs_{100} - Abs_o) \times 100 \qquad \text{(eqn. 9)}$$

Where Abs is absorbance of the sample treated with amphotericin B liposomes/ Fungizone, Abs_o is absorbance of unlysed sample treated with PBS, pH 7.4 and Abs_{100} is absorbance of sample lysed with distilled water.

The same procedure was used for the nanoemulsions.

3.4 In vitro release of Amphotericin B from liposomes

4% bovine serum albumin (fatty acid free) solution was prepared with HBSS buffered to pH of 7.4. The solution was stirred overnight. It was centrifuged at 3000rpm for 10 minutes at room temperature and used as the dissolution medium. This medium is used to mimic the blood side of the gut.

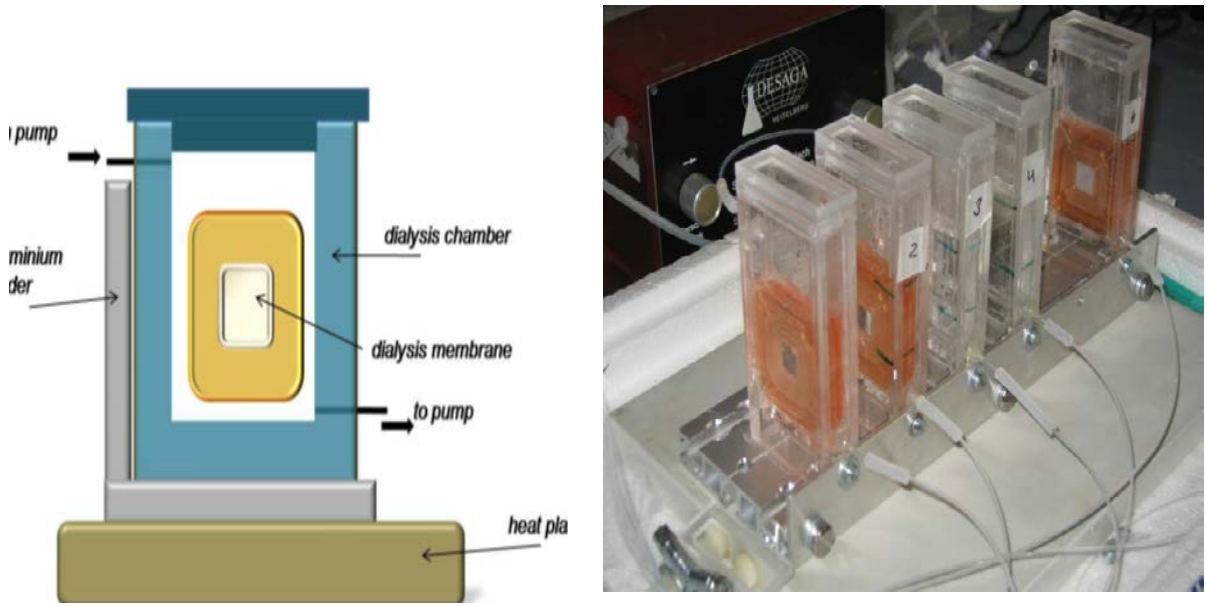

Figure 3.1: Setup for the in vitro dissolution of amphotericin B from liposomes (custom-made by Nanovel Ltd. & Co. KG, Langenlonsheim, Germany) (adapted from Diploma thesis of Eva-Christina Wurster, 2010).

An amount of liposomal formulation (or Fungizone®) containing 0.5 mg of Amphotericin B was weighed and dissolved in 0.5 ml of the release medium (1 mg/ml). The suspension was carefully filled into the dialysis cassette after hydration with the aid of syringe and needle. The cassette was inserted into the chamber containing 8 ml of the 4% BSA solution (pH 7.4) maintained at a temperature of 37°C (figure 3.1). At predetermined time intervals 1 ml of the

medium was withdrawn and spectrum measured with the spectrophotometer with the medium as blank at 300-500 nm. The sample was put back after measurement. The experiment was conducted in triplicate and for 8 hours. The amount of Amphotericin B released was evaluated at absorption maxima of 416 nm with the help of standard calibration curve of the drug in the release medium. The data was expressed as percentage released with time.

3.4.1 In vitro release study of Amphotericin B from AmB-HST

The in vitro release of Amphotericin B from AmB-HST was conducted using distilled water containing 0.25 %w/v sodium dodecyl sulphate as the release medium. An amount of sample containing 1 mg of Amphotericin B (AmB-HST or plain drug) was dispersed in 20 ml of medium and incubated in a shaking water bath at 37^{o}C (35% speed). At predetermined time intervals (5 minutes to 8 hours); 1ml of sample was withdrawn and filtered through 0.2 µm cellulose acetate membrane filter. 0.35 ml was pipetted into a 5 ml volumetric flask, 0.25 ml DMSO was added and made up to volume with methanol-water (9:1). The absorbance of the resulting mixture was measure with the spectrophotometer at 407nm. The amount of drug released was determined using standard calibration curve. The experiment was conducted in triplicate.

A graph of percentage drug released with time was established. The two dissolution curves were compared by the similarity factor according to equation 10.

$$f2 = 50 * log\left\{\left[1 + \frac{1}{n}\sum_{t=1}^{n}(R_t - T_t)^2\right]^{-0.5} * 100\right\} \quad \text{(eqn.10)}$$

where R_t and T_t are the percent drug dissolved at each time point for the reference and the test formulation respectively, and n is the number of time points. According to the guidelines profiles are denoted similar for f_2 values between 50 and 100.

3.5 Rheological properties of nanoemulsion pre-concentrates

The rheological properties of the optimized pre-concentrates were determined using the HAAKE Rheostress 1 viscometer operating at room temperature at shear rates in the range from 0 to 600 s^{-1}. The data was evaluated using attached RheoWin 4 data manager software. Graphs were plotted with Origin 7 software.

3.6 Stability study of nanoemulsion pre-concentrates

The pre-concentrates were prepared (section 3.2.4.3) and the drug content and droplet size were determined (day zero). The samples were kept in glass vials wrapped in aluminium foil and stored at room temperature (RT) and in the refrigerator (2-8^{o}C). At predetermined time intervals (every 15 days) the drug content and droplet size were measured as per methods described above. This was performed over a period of 70 days. Experiments were done in duplicate for drug content and triplicate for droplet size.

3.7 Small angle neutron scattering (SANS) experiments

The small angle neutron scattering experiments were conducted at the KWS-2 instrument of the Jülich center of neutron scattering JCNS at the FRM II high flux reactor of the Maier-Leibnitz research center MLZ at Garching. The instrument conditions used were as follows:

Table 11: Parameters of KWS-2 instrument

Neutron flux (N/cm^2 Sec)	1.3 x 10^7
Beam cross section (mm)	6 x10
Wavelength (nm)	0.4533
Detector distance (m)	1.81 and 7.76
Q range (Å)	7x10^{-4} – 0.5
Detector (60x60 cm^2)	^{6}Li

3.7.1 Contrast variation method for estimation of core-shell structure of AmB-HST

The deuterium solvent contrast method enabled a resolution of the particle and gelatin-lipid coating by nearly matching of the drug core particles with 71% D_2O buffer. 20 mg sample of AmB-HST powder was dissolved in 2 ml of the 71% D_2O buffer. The samples (350 µl) were administered to SANS in 10mm wide Teflon stoppered Quartz cuvettes of 2 mm path-length (110 QS, Hellma, Müllheim). The raw data treatment was done with the instrument software at Garching. The final evaluation was done with Origin 7 software using the procedures shown by Nawroth et al., 2011.

3.7.2 Contrast variation for evaluation of equivalent scattering length density

The deuterium contrast variation method of neutron small angle scattering SANS was applied for the structure estimation, homogeneity of the vesicles and the equivalent scattering length density of the formulations. Samples were prepared as described in section 3.2.2.2. However, the solvent was different deuterium solvent concentrations (100, 71, 56, 33 % D_2O buffer and H_2O buffer). They were administered to SANS as above (section 3.7.1). The Guinier and Kratky-Porod plots were used to estimate the radius of gyration and the thickness of the membrane span respectively (Nawroth et al, 2012). The following equations are utilized for the evaluation:

Logarithmic Guinier: $$In(I(q)) = In(I_o) - \frac{Rg^2}{3} q^2 \qquad \text{(eqn.10)}$$

Logarithmic Kratky-Porod: $$In(I_d(q)) = In(I_{do}) - R_d^2 q^2 \qquad \text{(eqn.11)}$$

Thickness scattering profile: $$I_d(q) = I(q)*q^2 \qquad \text{(eqn.12)}$$

Membrane thickness: $d = R_d * \sqrt{12}$ (eqn.13)

Liposome size S from SANS: $S = 2*r_m + d \approx 2*R_g + d$ (eqn.14)

Size of a solid sphere (e.g. micelles) $S = 2*R_g\sqrt{\frac{5}{3}}$ (eqn.15)

For spherical unilamellar liposomes the radius of gyration Rg is equivalent to the membrane radius r_m. The Guinier plot is used for the determination of the radius of gyration Rg by taking the slope $m = \frac{Rg^2}{3}$ of the linear portion of the leftmost part of the curve.

The Kratky-Porod plot enables the determination of the thickness radius R_d and it is evaluated by taking the slope $m = R_d^2$. This is related to the membrane thickness of liposomes by equation 13 above.

In addition, the particle size of the samples were measured by dynamic light scattering and data evaluated with the ALV correlator software V3.0. The liposomes were evaluated by dividing the scattering intensity, S(r), by the second power of the radius as;

$C_{m2} = \frac{S(r)}{r^2}$ C_{m2} is particle mass distribution for liposomes. (eqn.16)

The solid spheres (AmB-HST) were evaluated by dividing the intensity by the third power of the radius as;

$C_{m3} = \frac{S(r)}{r^3}$ C_{m3} is particle mass distribution for solid particles. (eqn.17)

3.7.3 Determination of internal structure of freeze-dried (final product) liposomes

The freeze-dried multilamellar (MLV) samples containing different concentrations of cholesterol (10, 20 and 30 mol%) with (5 or 10 mol%) and without drug were hydrated for about 20 minutes in 71% D_2O. Part of the multilamellar samples was sonicated for 20 minutes to produce small unilamellar vesicles (SUV). The samples were subsequently prepared in different D_2O contents at a concentration of 10 mg/ml (12% D_2O representing the equivalent scattering of the lipid, 29% D_2O for the equivalent scattering of the drug, 46% D_2O and 71% D_2O). Blank MLVs were also prepared. They were administered to small angle scattering as above but with slight variation of the instrument parameters as shown in the table 12 below.

Table 12: Parameters of KWS-2 instrument for final product

Neutron flux (N/cm^2 Sec)	1.3 x 10^7
Beam cross section (mm)	6 x 8
Wavelength (nm)	0.5151
Detector distance (m)	2.2 and 19.4
Q range (Å)	7x10^{-4} – 0.5
Detector (60x60 cm^2)	^{6}Li

3.7.4 Estimation of the structure of the nanoemulsions by SANS

350 µl of 10 mg/ml samples of drug containing nanoemulsions and their blanks were administered to SANS in 10mm wide Teflon stoppered Quartz cuvettes of 2 mm path-length (110 QS, Hellma, Müllheim). To improve contrast the samples were prepared in 71% D_2O. The experiment was conducted at the following instrument configuration as indicated in the table below:

Table 13: Parameters of KWS-2 instrument for Nanoemulsions

Neutron flux (N/cm^2 Sec)	1.3 x 10^7
Beam cross section (mm)	6 x10
Wavelength (nm)	0.527
Detector distance (m)	1.8, 7.8 and 19.8
Q range (Å)	7x10^{-4} – 0.5
Detector (60x60 cm^2)	^{6}Li

3.7.5 Statistical analysis

Student t-test was used for the evaluation of the difference between means of two samples. One-way analysis of variance (ANOVA) was used to assess the difference between means of more than two samples with post-hoc t-tests. Differences were considered statistically significant when p value was less 0.05.

4. RESULTS

4.1 AmB-HST formulation

4.1.1 Formulation of AmB-HST

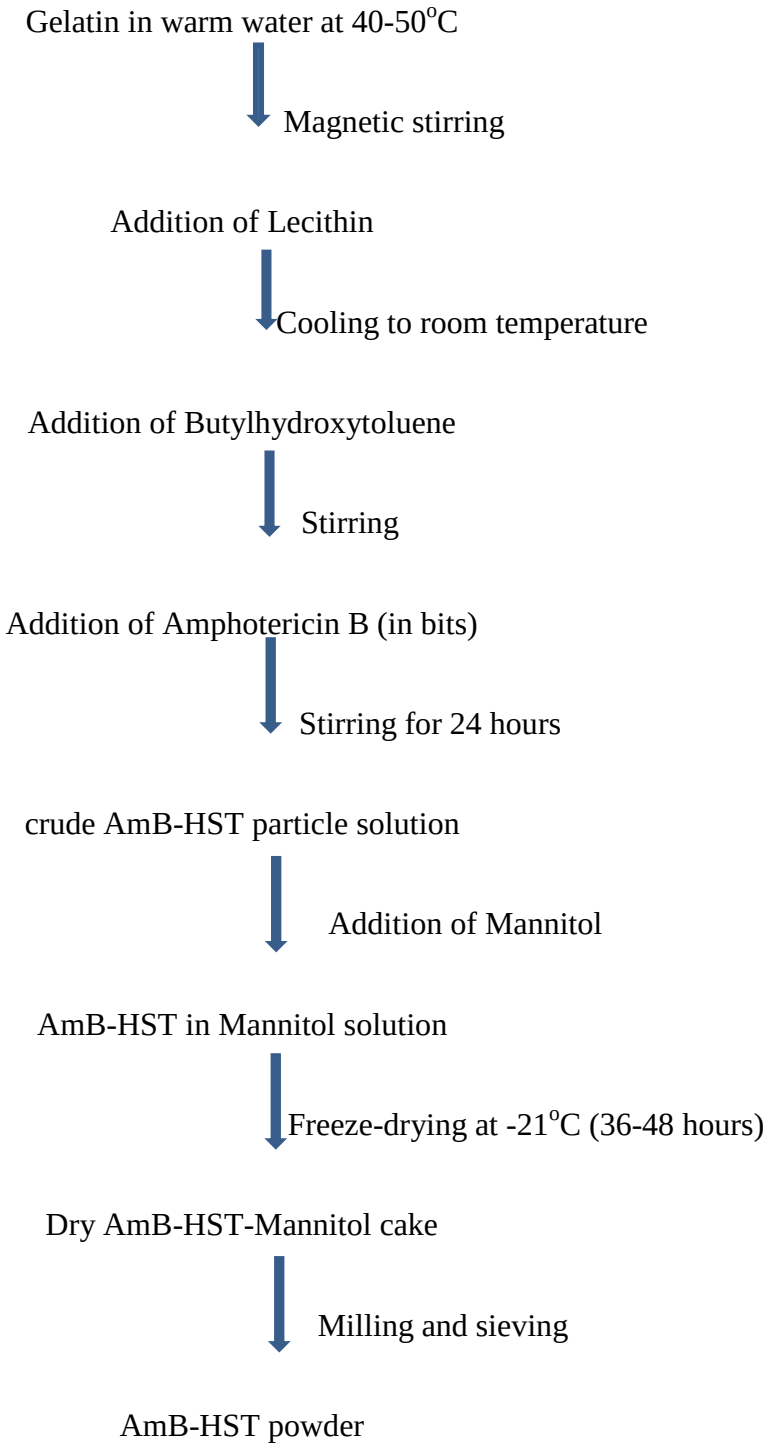

Figure 4.1**:** The stepwise embedding of Amphotericin B in lecithin-gelatin microparticles (AmB-HST). The final product was a fluffy yellow powder.

4.1.2 UV-Visible spectra of Amphotericin B

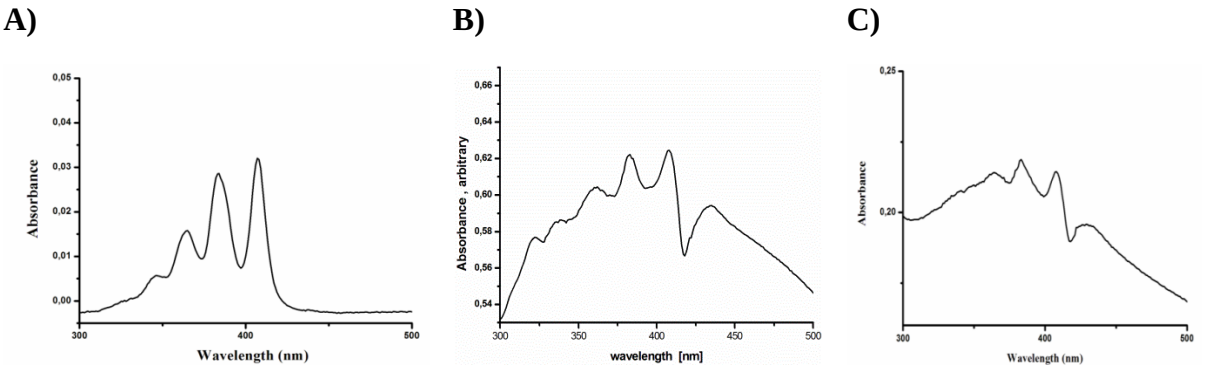

Figure 4.2: Absorption spectra of (**A)** 0.2 µM molecular resolved Amphotericin B (in methanol) depicts a dominant peak at 407 nm, while (**B)** that of the solid drug, suspended in water (arbitrary units) is combined with a broad aggregate peak (310 – 470 nm) and an additional peak at 430 nm; (**C**) The spectrum of AmB-HST microparticles (in water, 1 µM) resembles that of the pure drug suspension.

Amphotericin B shows four vibronic peaks, the wavelength of which depends on the type of solvent in which it is dissolved. In methanol the peaks occur at 407, 384, 364 and 346 nm with decreasing intensity as shown in figure 4.2A. Figure 4.2B depicts the absorption spectrum of solid pure drug suspended in water. It shows the same peaks as figure.4.2A, but positioned on a wide peak of aggregates. A dominant oligomer peak at 328-340 nm is missing. The spectrum of AmB-HST in water resembles that of the pure drug suspension; it reveals absorption peaks at 430, 408, 383 and 364 nm with increasing intensity (Figure 4.2C), i.e. absorption at the same wavelength as in free form (A), but on a broad aggregate signal and with an additional peak at 430 nm.

4.1.3 Fluorescence spectrum of Amphotericin B

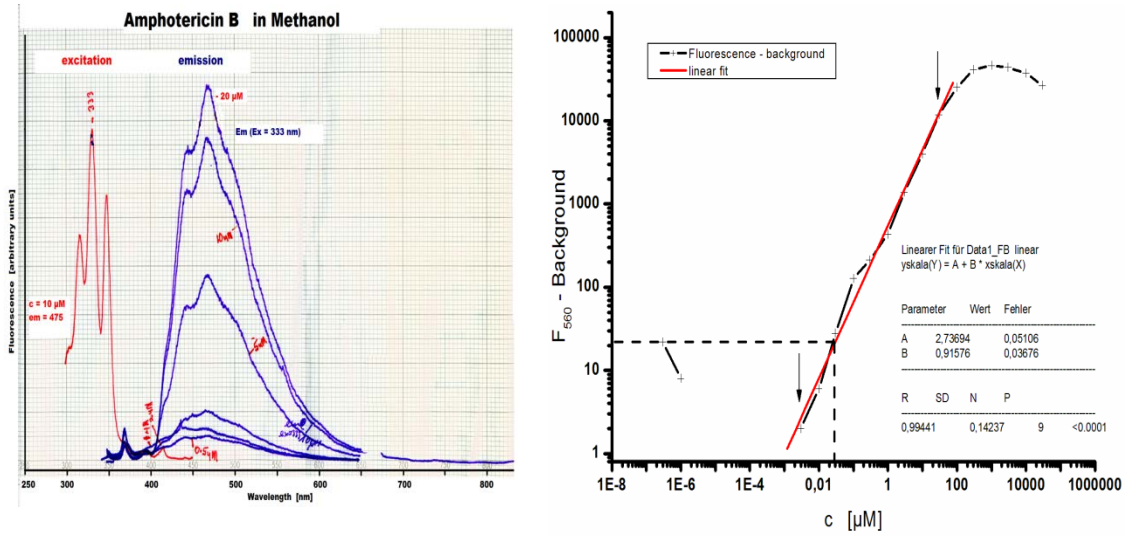

Figure 4.3: Fluorescence spectrum of Amphotericin B measured with Perkim Elmer fluorescence spectrophotometer at excitation of 333 nm and emission of 475nm (left) and a calibration curve obtained by measurement of different concentrations of the drug with the Tecan microplate reader at excitation of 340 nm and background of 560nm (right).

Results

The fluorescence spectrum of Amphotericin B at different concentrations is as shown in figure 4.3. The peak area does not increase linearly with the concentration of the drug at the excitation of 333 nm and emission of 475 nm. The calibration curve showed linearity with concentration at high concentrations as measured with the Tecan microplate reader at a wavength of 340 nm and a background of 560 nm. However, fluorescence decreases at very high concentrations due to quenching. The fluorescence emission band recorded with excitation at 333 nm has maxima located at 445,469 and 502 nm (broadening) respectively (10μM spectrum). The emission at 475 nm also shows excitation peaks at 305, 315, 333 and 348 nm respectively. This area of excitation peaks is characteristic of aggregates of Amphotericin B.

4.1.4 Microscopy of AmB-HST

A) **B)**

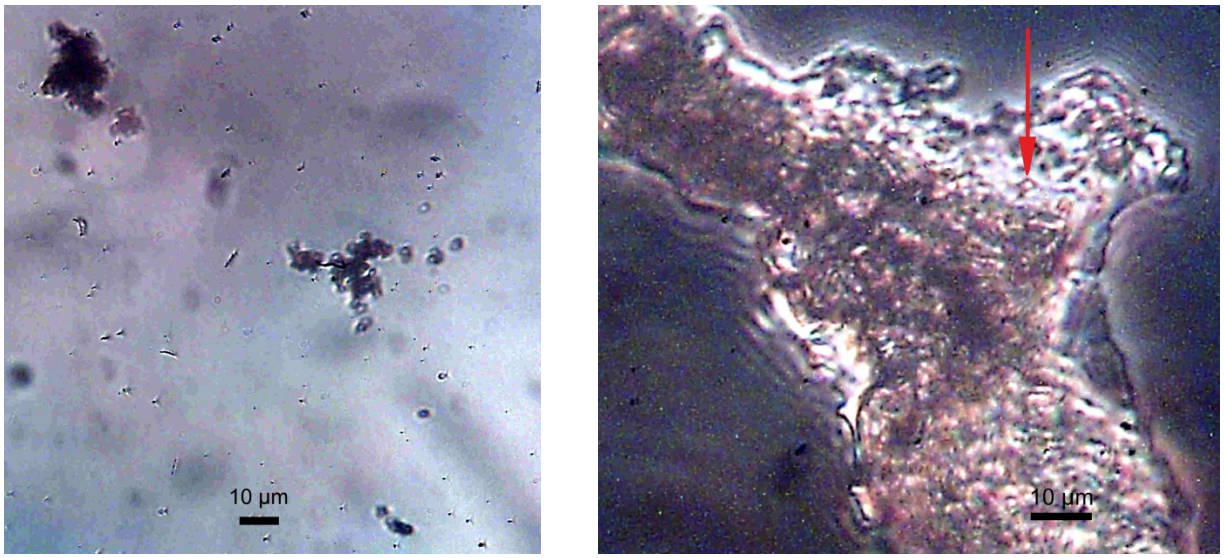

Figure 4.4: Microscopic images of (**A)** pure AmB particles (spheres) and particle aggregates (dark), and (**B)** AmB-HST microparticles in a freeze dried mannitol matrix: both contain spherical drug particles of similar size (~ 1 µm).

Amphotericin B powder appeared as spheres and aggregates under the phase contrast microscope (Figure 4.4A). Investigation was conducted to determine whether the lecithin-gelatin coating made changes to the nature of the drug. Figure 4.4B thus reveals the spherical nature of AmB-HST matrix. The particles seen under this circumstance depicts size of about a micron.

4.1.5 Particle size of formulation

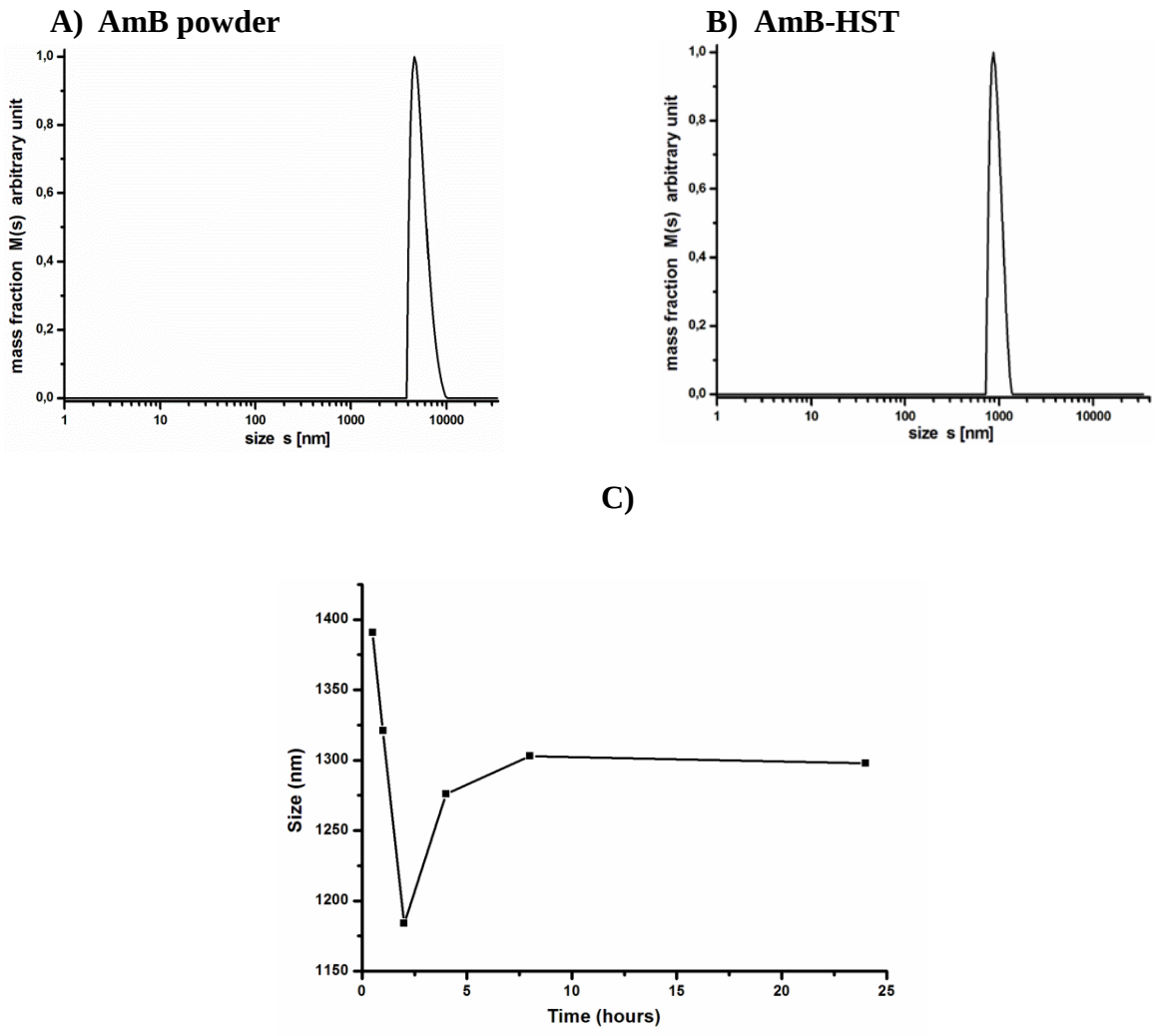

Figure 4.5: Size analysis of (**A)** Amphotericin B particles, **(B)** AmB-HST microparticles (in HBSS buffer) and **(C)** apparent size change of AmB-HST particles during preparation estimated by dynamic light scattering DLS.

The Amphotericin B powder was suspended in sucrose syrup to prevent rapid sedimentation of the particles. The suspended particles as seen in figure 4.5A have an average size of about 6 µm whilst the particles of the drug in the final product AmB-HST (figure 4.5B) recorded an average size of about 1 µm (by mass fraction [Nawroth et al., 2011]). The AmB-HST was dispersed in HBSS (cell compatible buffer).

The development of the particle size during the encapsulation of the drug by gelatin and lecithin determined after the addition of the drug during formulation (figure 4.5C) shows a decrease in the first 2 hours but increased then with subsequent time. After eight hours the size was nearly constant.

4.1.6 Small angle scattering of AmB-HST

A) **B)**

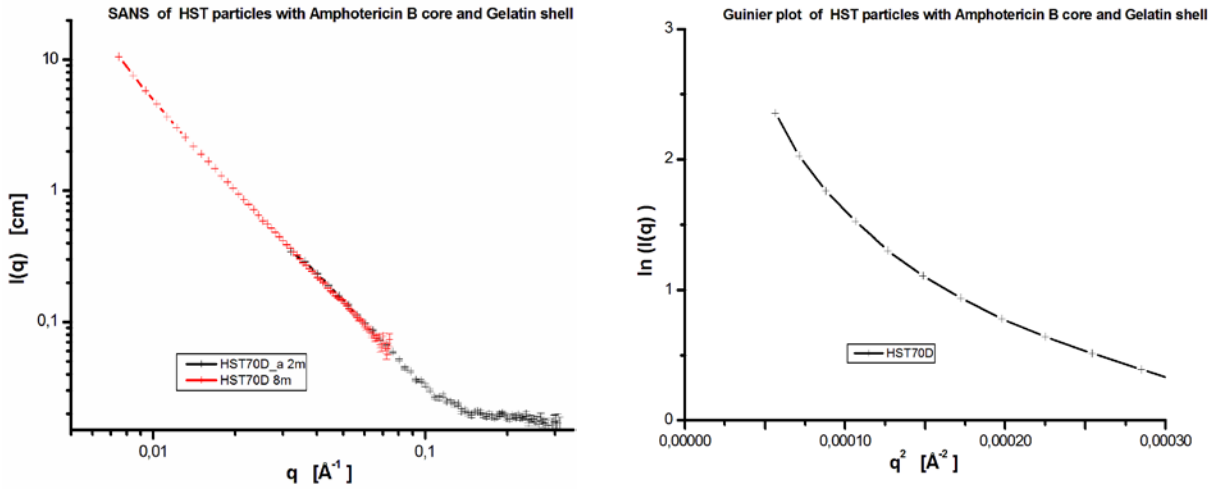

Figure 4.6: Structure analysis of AmB-HST core-shell particles by neutron small angle scattering SANS (in TM buffer, 71 % D_2O, nearly drug core matching). The scattering profile **(A)** indicates large particles (mixture), mainly above the instrument resolution (>100 nm); (**B)** the size analysis by the curved Guinier plot indicates no significant nanoparticle contribution in size range 1-100 nm (no straight line).

The details of the structure of AmB-HST particles were studied by neutron small angle scattering SANS. As buffer a partial deuterated solution was chosen, which nearly matches the drug core by deuterium contrast. The scattering profile of AmB-HST in 71% TM buffer is shown in figure 4.6A. The scattering profile was cut at the left side because of the limited length of the KWS-2 camera at FRM2 (lower q-limit). The trial evaluation of the particle size by a Guinier plot (figure 4.6B) yielded no straight line corresponding to the size range of 1-100 nm, which indicated no significant particle fraction present in this range.

The estimation of the theoretically expected small angle scattering of spherical drug particles of the size obtained by DLS (s = 1µm; Figure 4.5) yielded a radius of gyration of $R_g = (s/2 * \sqrt{(5/3)} = 645$ nm and a zero angle scattering of $I_o = 25{,}815$ (SANS origin in figure 4.5A), corresponding to $In(I_o) = 10.16$ (origin in figure 4.6B). The estimation of the SANS profile obtained at 8m distance towards a tentative shell by a Kratky-Porod plot is shown in figure 4.6. The linear range is that, which appears as weak bump between q = 0.014 and 0.025 $Å^{-1}$ in the 8m data part (red) in figure 4.6A. The evaluation of the extended linear range in figure 4.7 yielded a thickness radius of $R_d = 1.628 \pm 0.052$ nm, which is equivalent to a layer span of d = 5.64 ± 0.18 nm (statistical error only). This indicates a thin homogenous layer around the AmB-HST particles in aqueous solution.

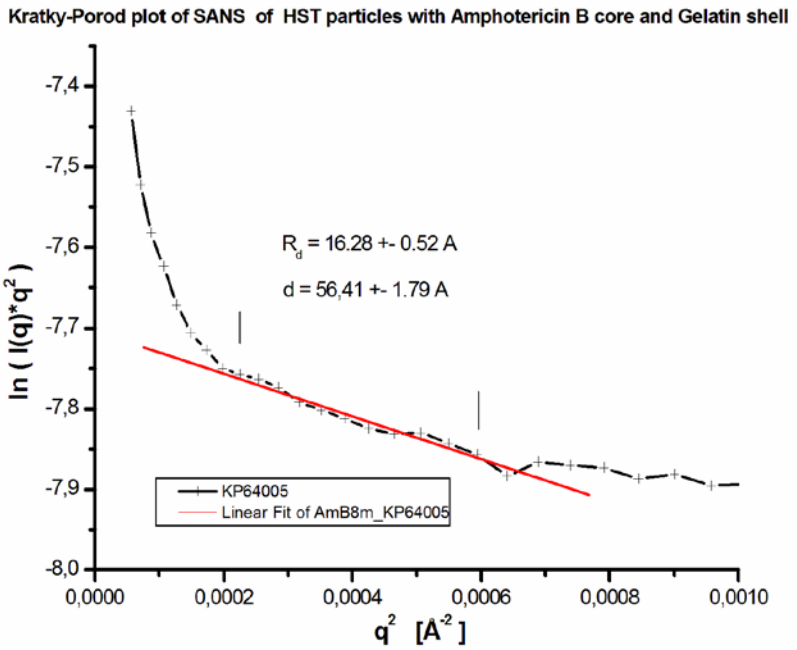

Figure 4.7: The estimation of the shell span d of AmB-HST core-shell particles in nearly core matching TM buffer (71 % D_2O) by a Kratky-Porod plot analysis yields a span radius R_d = 1.63 ± 0.052 nm, i.e. a shell span of d = 5.64 ± 0.18 nm (plus systematic error).

4.1.7 In vitro release of amphotericin B from AmB-HST

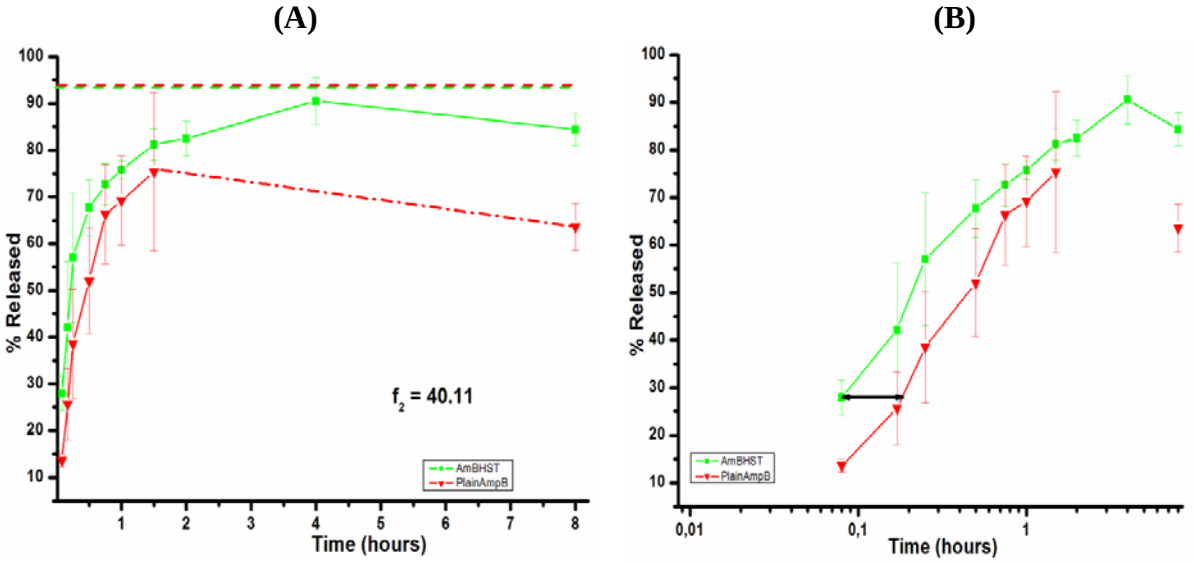

Figure 4.8: (A) The release profile of Amphotericin B from the AmB-HST microparticles in comparison with the plain drug conducted in 0.25%w/v SDS solution. (B) The graph of the percentage of drug released against the logarithm of time indicating the lag time between the release of the formulation and the plain drug.

The release profile showed a gradual release of the molecule from both the formulated and plain drug (figure 4.8A). However, the amount of drug released was higher for the formulated

drug than the plain one at all the times sampled. More than 70% of the drug was in solution after one and a half hours for both products. As expected, a comparison of the two release profiles by the similarity factor indicated a difference between the profiles (f_2 = 40.11). Evaluation of the plot of the inverse of percentage release against the inverse of time (data not shown) indicated a total amount of drug release of 94.34±4.47% and 93.72±1.83 for the plain drug and formulated AmB-HST respectively at infinity. These are indicated by the upper red and green dashed lines respectively in figure 4.8A. These values however showed no significant difference between the two products at infinity (red and green dashed lines).
Figure 4.8B indicated clearly the difference between the release profiles and shows the lag time which is calculated to be 5.62 ± 0.51 minutes.

4.2 Results of solubility of Amphotericin B in FaSSIF-C

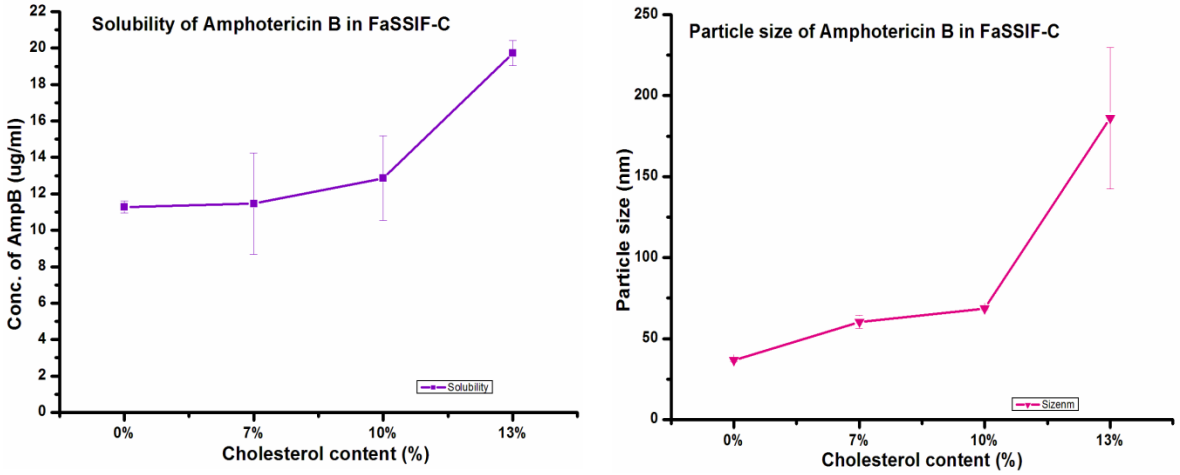

Figure 4.9: Solubility and particle size of Amphotericin B in FaSSIF-C

The solubility of Amphotericin B increased with increasing concentration of cholesterol in the medium. There was a gradual increase in solubility from 0% to 10% but at a concentration of 13% cholesterol the solubility increased significantly. Amphotericin B is known to form a complex with cholesterol and other lipids. Thus, the increase may be as a result of soluble complex of drug-lipids in the medium. Cholesterol therefore enhances the solubility of Amphotericin B.

The particle size also showed a similar trend as the solubility profile. The size of the particles increased gradually up to 10% of cholesterol and a significant increase at 13% cholesterol. This particle size increase maybe due to the formation of cholesteric particles.

4.3 Results of multilamellar liposomes formulation

4.3.1 Drug content, entrapment and particle size of liposomes

The variation of the ratio of lipids, cholesterol and drug concentration was to indirectly improve the drug load in the formulation. The different lipids with different chain length and saturation but same head group showed differences in drug loading, entrapment efficiency and particle size. Decreasing the phospholipid content and increasing the contents of cholesterol and Amphotericin B, generally increased the drug content for the lipids used. However, there was a general decrease in entrapment efficiency and particle size. The particle size and size distribution showed the formulations of the DOPC to have smaller particle size and narrower size distribution compared to the other lipids (Table 13). The other lipids (DSPC, DPPC and DMPC) had particles within the micrometer range with particle size increasing in the order DPPC < DSPC < DMPC which reflects the decreasing chain length of the fatty acid component of the lipids. It is worth noting that the larger the particle size the greater the polydispersity index of the particles. The particle size and polydispersity index of the DOPC and DSPC samples after freeze drying were larger than before freeze drying (Table 13). The reverse was the case for DPPC and DMPC.

With regards to the blank formulations, DOPC and DPPC had particle sizes within the nanometer range whilst that of DSPC and DMPC was within the micrometer range (Table 14). The blanks of DOPC had larger sizes and polydispersity index before and after freeze drying than the drug containing formulations. The same can be said for DSPC before freeze drying but in terms of the polydispersity index there was no significant difference. The opposite was the case for the blanks of DPPC compared to its drug containing formulations. DMPC also had blanks with lower particle sizes and polydispersity index before and after freeze drying than the drug loaded formulations. Based on the above analysis DOPC formulations were chosen for further characterization.

Results

Table 14: Drug content, entrapment efficiency, particle size and size distribution of liposomal formulation of the different lipids with cholesterol and Amphotericin B

Sample	**Drug content (mg)**	**Entrapment (%)**	**Particle size and distribution**			
			Drug loaded			
DOPC			**Before freeze dry**	**PDI**	**After freeze dry**	**PDI**
A	1.887 ± 0.025	77.00 ± 1.00	239.0 ± 17.1	0.438 ± 0.170	399.5 ± 23.0	0.489 ± 0.062
B	1.883 ± 0.021	77.72 ± 0.82	233.2 ± 56.5	0.413 ± 0.064	381.0 ± 19.0	0.469 ± 0.043
C	3.917 ± 0.005	76.35 ± 0.11	324.2 ± 198.0	0.543 ± 0.068	519.7 ± 79.2	0.635 ± 0.034
DSPC						
A	1.075 ± 0.012	50.59 ± 4.01	2053.3 ± 63.7	1.000 ± 0.000	1542.7 ± 320.2	0.460 ± 0.312
B	1.247 ± 0.007	52.12 ± 3.26	1592 ± 111.6	0.330 ± 0.061	2129.7 ± 255.9	1.000 ± 0.000
C	1.572 ± 0.081	28.33 ± 1.73	1378.0 ± 171.3	0.801 ± 0.344	1875.3 ± 262.7	1.000 ± 0.000
DPPC						
A	1.055 ± 0.021	53.59 ± 0.28	953.1 ± 146.6	0.866 ± 0.103	701.5 ± 134.0	0.633 ± 0.121
B	1.309 ± 0.043	56.65 ± 0.85	1715.3 ± 114.4	1.000 ± 0.000	1076.0 ± 123.0	0.741 ± 0.002
C	2.119 ± 0.000	48.86 ± 1.50	1497.7 ± 276.8	0.564 ± 0.379	1557.7 ± 168.6	0.975 ± 0.043
DMPC						
A	0.861 ± 0.005	47.18 ± 1.14	4018.3 ± 629.0	1.000 ± 0.000	1462.7 ± 173.5	0.856 ± 0.250
B	1.070 ± 0.038	42.02 ± 3.38	1194.4 ± 359.7	0.873 ± 0.111	1140.3 ± 86.6	0.939 ± 0.073
C	2.608 ± 0.020	51.10 ± 1.96	2214.7 ± 291.2	1.000 ± 0.000	1235.0 ± 19.8	0.684 ± 0.424

Results

Table 15: Particle size and size distribution of the blank formulation of the different lipids with cholesterol

Sample	**Particle size and distribution**			
	Blanks			
DOPC	**Before freeze dry**	**PDI**	**After freeze dry**	**PDI**
A	445.3 ± 40.1	0.517 ± 0.196	571.3 ± 22.8	0.504 ± 0.092
B	306.1 ± 71.4	0.489 ± 0.056	662.1 ± 50.4	0.629 ± 0.035
C	473.6 ± 15.4	0.539 ± 0.127	1190.0 ± 181.8	0.966 ± 0.058
DSPC				
A	1618.0 ± 270.5	0.157 ± 0.061	2298.7 ± 271.7	1.000 ± 0.000
B	1768.7 ± 151.2	0.255 ± 0.139	1599.7 ± 67.4	1.000 ± 0.000
C	3134.3 ± 390.0	0.404 ± 0.100	1314.7 ± 79.0	0.990 ± 0.017
DPPC				
A	244.1 ± 41.5	0.352 ± 0.054	273.4 ± 20.0	0.410 ± 0.057
B	509.2 ± 20.2	0.525 ± 0.028	280.3 ± 60.6	0.487 ± 0.052
DMPC				
A	1165.0 ± 36.2	0.327 ± 0.020	1490.7 ± 93.2	0.849 ± 0.072
B	400.6 ± 57.4	0.423 ± 0.037	952.8 ± 28.6	0.657 ± 0.011
C	1346 ± 402.2	0.959 ± 0.072	589.6 ± 10.9	0.442 ± 0.010

4.3.2 Microscopy of liposomes

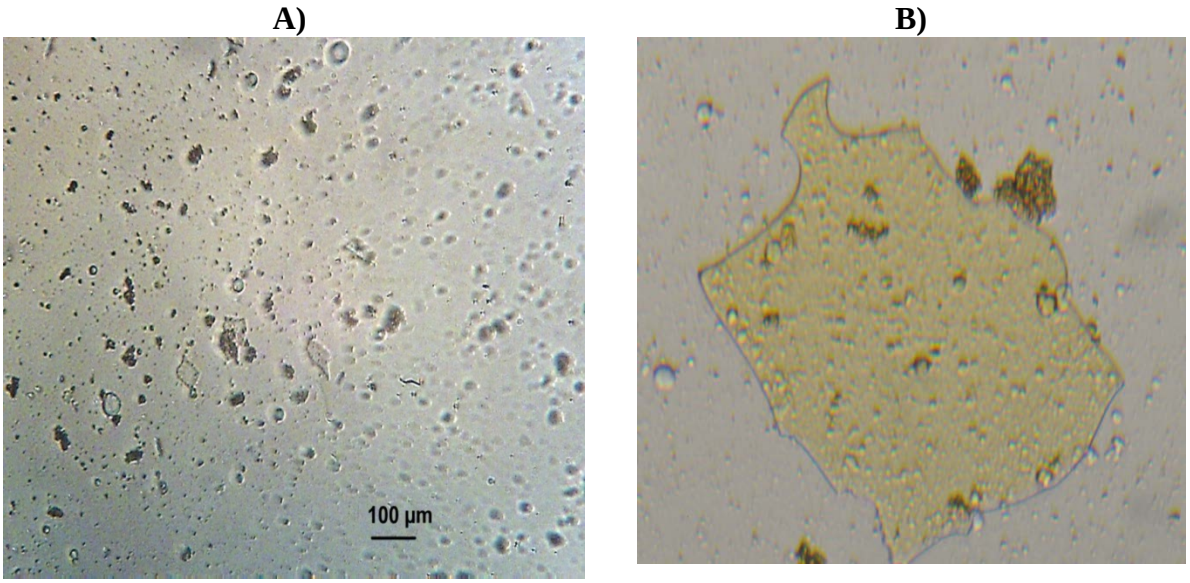

Figure 4.10: Microscopic images of A) dispersion of sample C and B) a focused sheet-like structure that was identified and increases with increasing drug content.

Using the light microscope various structures were observed. Figure 4.10A shows liposomes, drug crystals and sheet-like structures which are enlarged in Figure 4.10B. These structures were observed in all formulations. Increasing the drug content increased the number of the sheet-like structures. However the colour of the sheet was uniform (yellowish) in all formulations.

4.3.3 Spectrum of Amphotericin B in Liposomes

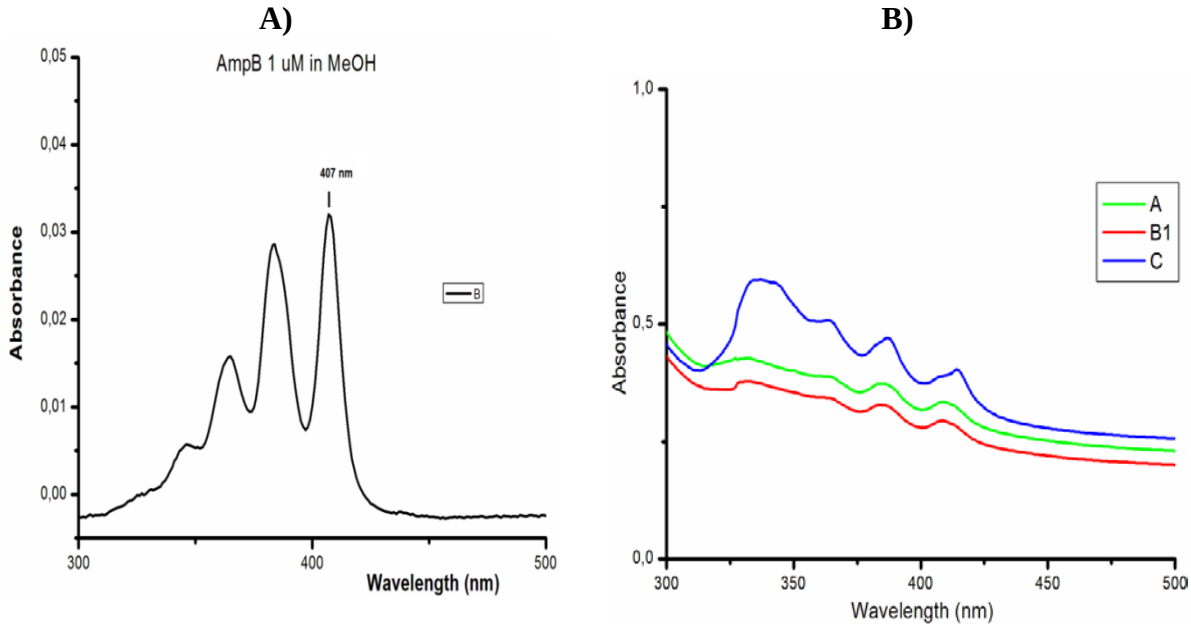

Figure 4.11: Absorption spectra of A) pure Amphotericin (in methanol) and B) Liposomal formulations (in HBSS). The drug in the liposomes appears as molecular aggregates and its concentration dependent, while it is monomeric in methanol.

Results

Amphotericin B shows four vibronic peaks, the wavelength of which depends on the type of organic solvent in which it is dissolved. In methanol the peaks occur at 407, 384, 364 and 346 nm with decreasing intensity as shown in figure 4.11. In HBSS, the Amphotericin B liposomes reveals a slight bathochromic shift of the peaks at 409, 385, 364 and a broad peak at 330 nm with increasing intensity showing molecular aggregation of the amphotericin B for samples A and B (Figure B). The peaks for sample C are located at 414, 387, 364 and a broad peak between 334 and 344. Sample C shows a higher molecular aggregation.

4.3.4 DSC of Amphotericin B, liposomes and blanks

(A) (B)

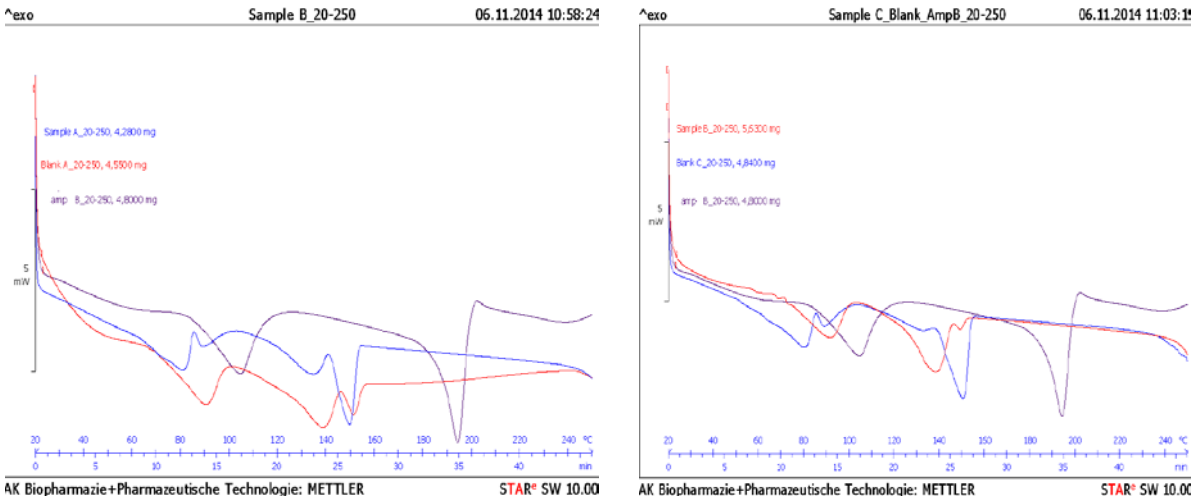

Figure 4.12: Thermograms of (a) sample A, blank and Amphotericin B and (b) Sample C, blank and Amphotericin B.

The thermograms of samples A and C with their blanks as well as Amphotericin B are shown in figure 4.12. The thermogram of Amphotericin B shows two endotherms with peak temperatures at 104.49^{o}C and 194.07^{o}C with enthalpies of transition of 63.20 J/g and 79.50 J/g respectively (see Appendix B). Samples A, C and their blanks however showed two major peaks with other minor peaks. The peak temperatures and the enthalpies of transition of the drug loaded liposomes were different from those of the blank samples. However, the thermograms are similar in pattern. In both cases the melting peak of the drug at 194.07^{o}C was completely missing. The peak temperatures and enthalpies of transition are summarized in table 16.

Results

Table 16: Peak temperatures and enthalpies of transition of drug loaded liposomes and their blanks

Sample	Major Peaks		Minor peaks	
	Peak temperature / ^{o}C	Enthalpy of transition /J/g	Peak temperature /^{o}C	Enthalpy of transition/ J/g
A	80.60	34.65	88.78	3.51
	149.39	39.26	135.04	11.47
Blank A	89.97	39.77	151.06	8.96
	138.56	25.61		
C	91.19	29.49	149.15	1.20
	138.10	38.04		
Blank C	79.94	27.94	88.70	2.90
	150.22	51.99		

4.3.5 FTIR of liposomes and their physical mixtures

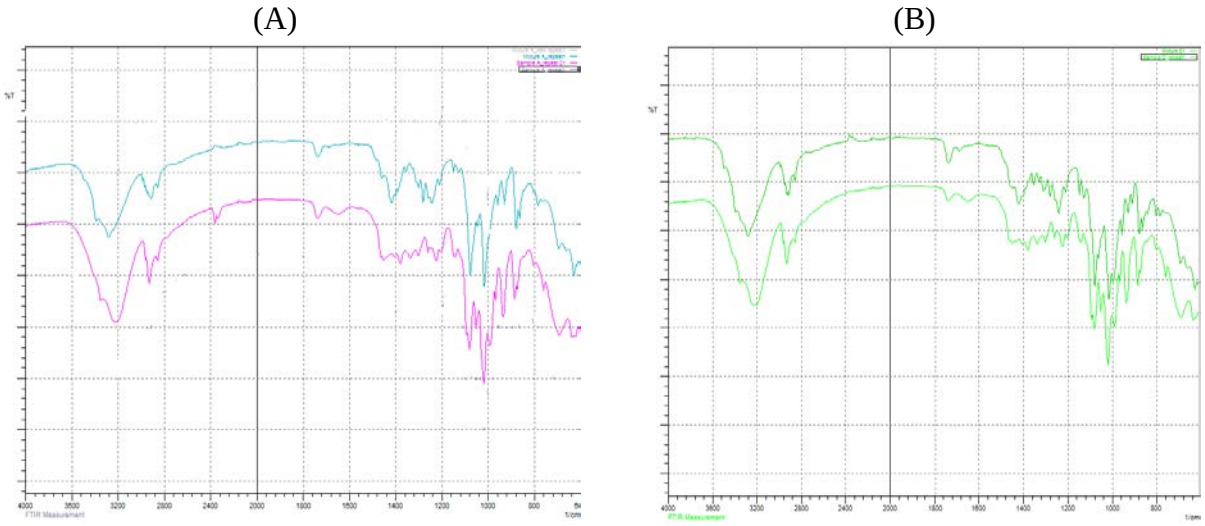

Figure 4.13: FTIR spectra of (A) Sample A (below) and its physical mixture (above) and (B) Sample C (below) and its physical mixture (above).

FTIR spectroscopy is used to investigate either drug-excipient or excipient-excipient interactions. Figure 4.13A and B shows the main absorption bands for both the formulated and physical mixtures of samples A and C. The absorption band between 3200 and 3600 cm^{-1} is attributed to stretching mode of either O-H or N-H. The peaks between 2800 and 3000 cm^{-1} are symmetric and asymmetric vibrations of CH_2 bonds. In both formulated and physical mixtures are two short peaks at 1735 cm^{-1} and 1631 cm^{-1} indicative of stretching vibrations of C=O and C=C respectively. The strong peak at 1016 cm^{-1} can be assigned to C-C-H bending in plane and a C-O asymmetric stretching vibrations at 1078 cm-1. Of prominence in both spectra are –CH and OH bending at 1417 cm^{-1} and 1280 cm^{-1} respectively. These peaks are strong in the physical mixtures (upper spectrum) but diminished in the formulated samples. These are the most observable difference between the formulated samples and their physical mixtures.

4.3.6 Density gradient centrifugation of liposomes

A

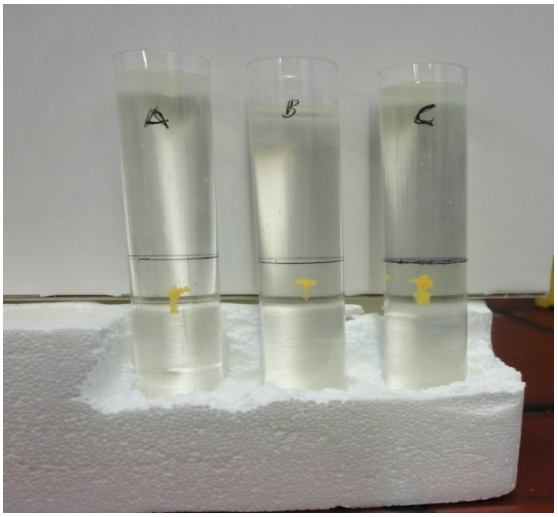

B

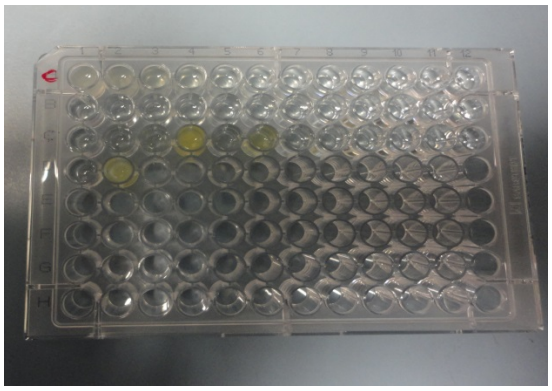

C

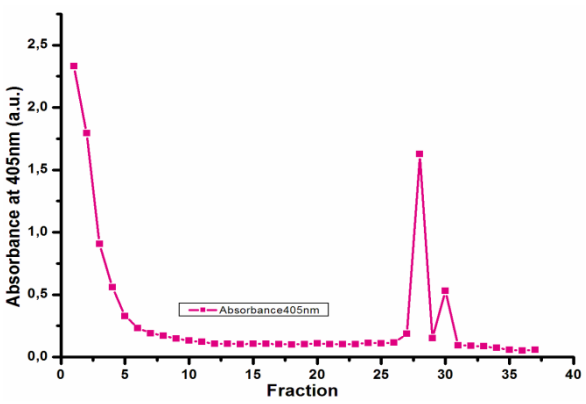

D

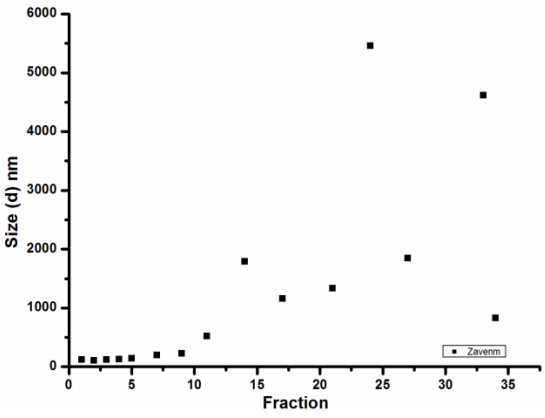

E

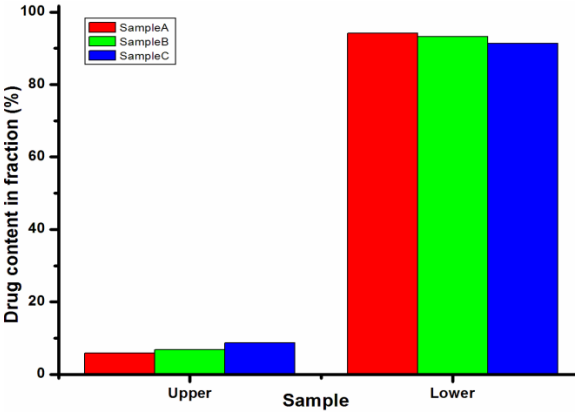

F

Figure 4.14: Density gradient centrifugation of the amphotericin B liposomes: (A) sample in fractionation column after centrifugation showing two bands. (B) Sample in tubes indicating the two regions. (C) Sample fractionated into 96- well plate. (D) Absorbance measurement of the fractions. (E) Particle size of some selected fractions and (F) determined drug content.

Results

After centrifugation the sample separated into two regions of different densities as shown in figures 4.14 A and B. The upper layer may represent liposomes associated with drug and the middle band could be drug associated lipid complexes. The absorbance and drug content analysis graphs (Figure 4.14D and F) confirm the two regions of drug association as the absorbance was higher in the upper and middle region of the fractionated samples. The particle size analysis of the fractions indicated the upper fractions of less than 200 nm diameter particles. The middle region which showed the aggregates of drug-lipid complexes recorded particles with diameter of about 6 µm (Figure 4.14E).

4.3.7 Cytotoxicity test of liposomes

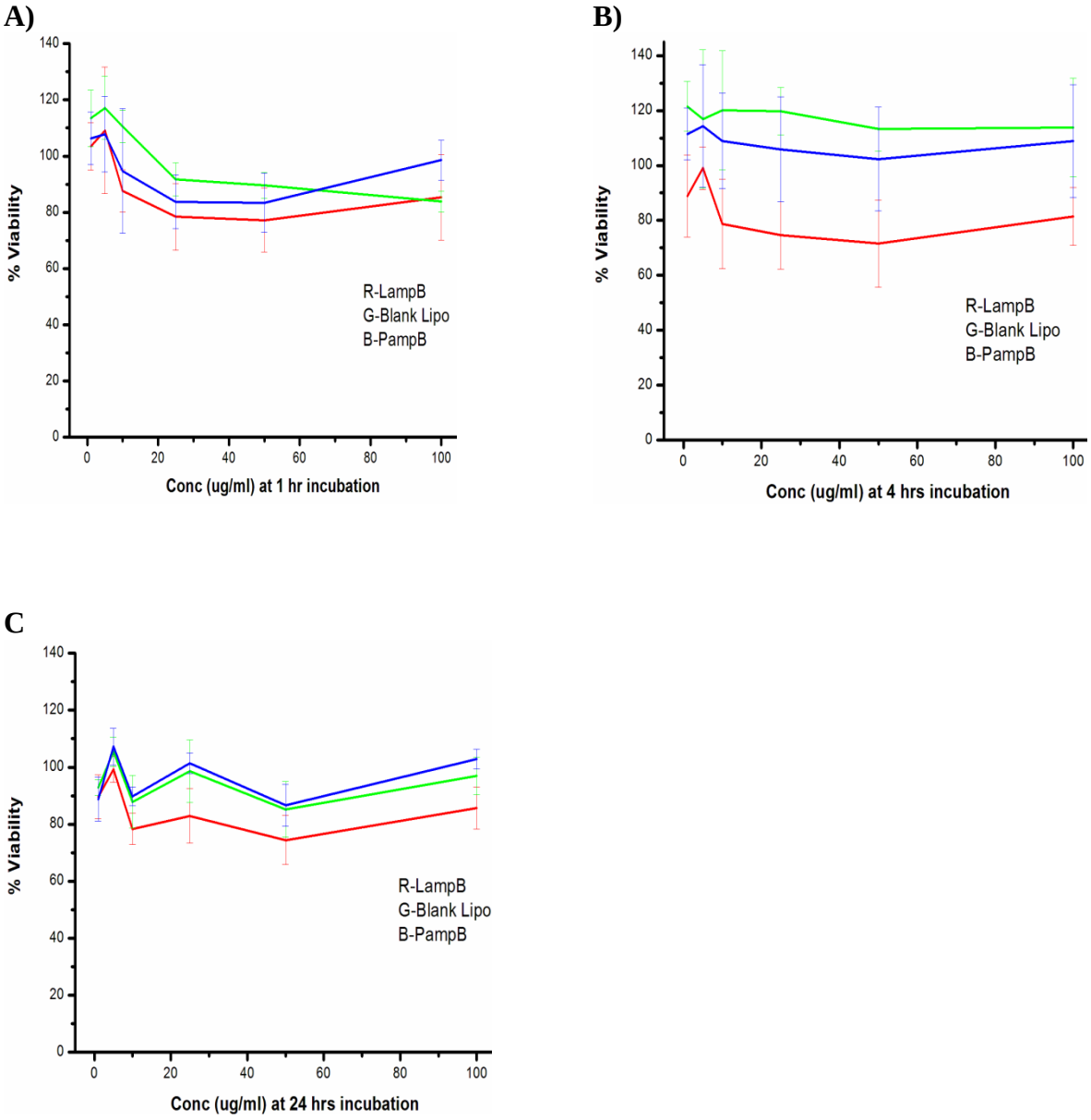

Figure 4.15: Caco-2 cell viability at A) 1 hour incubation B) 4 hours incubation and C) 24 hours incubation with different concentration of formulated Amphotericin B, Blank liposomes and Amphotericin B suspension.

Results

After one hour incubation the cell viability was above 75 % for the drug loaded liposomes, blank liposomes and the drug suspension. It was observed that the viability of the blank and plain drug was higher than that of the drug loaded liposomes at all the concentrations tested (Figure 4.15A). Incubation at 4 and 24 hours also resulted in the same trend as that of the one hour incubation (Figure 4.14B and C). The viability of the blank liposomes was comparatively higher than the drug loaded and the plain drug at 1 and 4 hours incubation. However, the viability at 24 hours incubation was the same for both the blank and the plain drug suspension at all concentrations tested. Thus, at 100µg/ml the liposomal formulation of Amphotericin B was not toxic to Caco-2 cells. The cell viability at all concentration levels for the drug loaded liposomes was lower at 4 hour incubation than at one and 24 hours.

4.3.8 Liposomal Amphotericin B uptake study

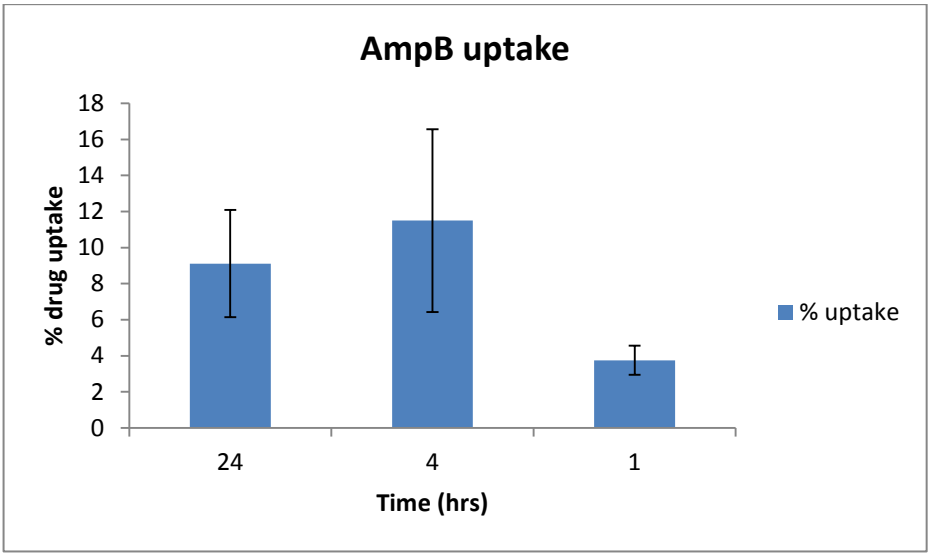

Figure 4.16: Percentage uptake of Amphotericin B by Caco-2 cells after incubation for 1, 4 and 24 hours.

The first step in drug permeation into the blood stream is the internalization by the enterocytes by either endocytosis or other mechanisms. Thus, the uptake of the formulated liposomes was assessed using Caco-2 cells. The formulation was incubated at 1, 4 and 24 hours. The percentage uptake was highest at 4 hours incubation, followed by 24 hours and was lowest at 1 hour incubation (figure 4.16).

4.3.9 In vitro release study of Amphotericin B from liposomes

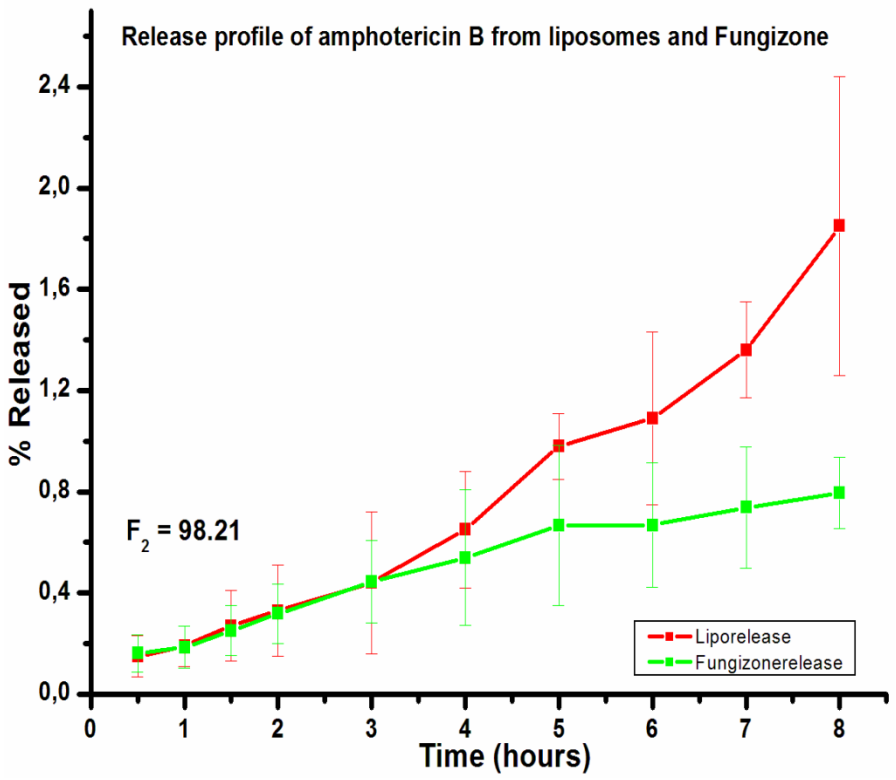

Figure 4.17: In vitro release of Amphotericin B from liposomes by dialysis method in comparison to Fungizone® which is a micellar suspension of Amphotericin B and sodium deoxycholate).

Membrane dialysis method has been used for the in vitro release of Amphotericin B from formulations in the literature (Hsiue et al, 2009; Kumar et al, 2010; Zhiwen et al, 2012; Abeer et al, 2013). These studies used phosphate buffer (pH 7.4) with either surfactants or dimethylsulfoxide as the release medium. In this study 4% bovine serum albumin in HBSS buffer (pH 7.4) was used as the medium to mimic the physiological body condition or as the blood side of the intestine and also to provide sink condition for the drug. The dialysis cassette with a molecular weight cut off of 10,000 was employed. The release of the drug from the liposomes and reference (Fungizone®) which is a micellar preparation was almost the same from 30 minutes to 3 hours. Thereafter, the release of the drug from the liposomes was higher than the reference due to observed precipitation of the drug. After 8 hours the amount of Amphotericin B released was 1.85% as against 0.80% for Fungizone®. Comparison of the release profiles of the liposomes and the Fungizone® by the similarity factor, f_2, revealed no difference (f_2 = 98.21).

4.3.10 Hemolysis test of liposomes

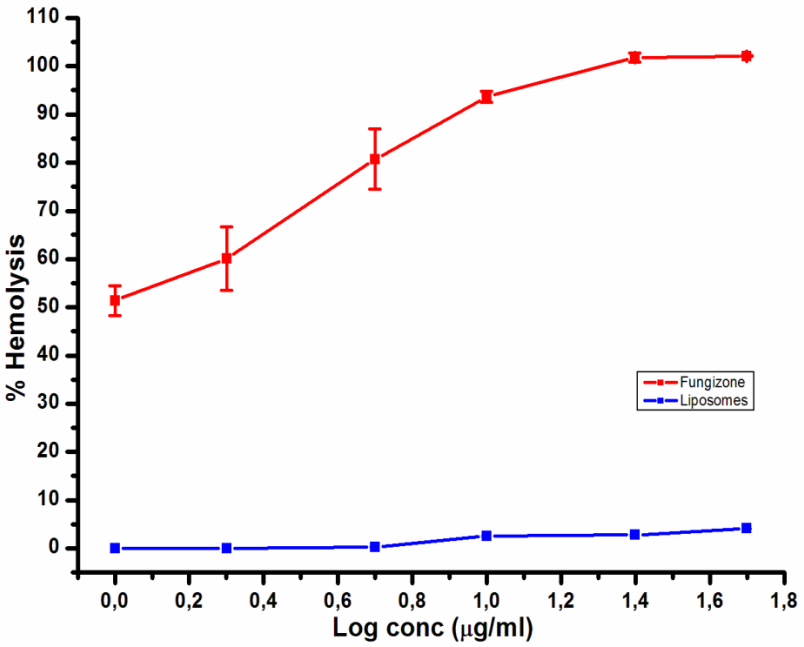

Figure 4.18: Effect of liposomal Amphotericin B formulation on human red blood cells in comparison to Fungizone®.

The graph showed an increase in hemolysis with increasing concentration of both formulated liposomes and Fungizone®. However, the multilamellar liposome formulation containing amphotericin B showed no significant ($p<0.05$) hemolytic property up to 50µg/ml (4.1%) while the micellar formulation of Fungizone® showed about a 100% hemolysis at the same concentration of amphotericin B (Figure 4.18).

4.4 Small angle neutron scattering SANS

The scattering profiles for both buffer and solution of samples with buffer were obtained. The scattering of the sample alone was obtained by subtracting the buffer scattering from the solution scattering. Standard linear plots such as the Guinier and Kratky-Porod were used for the evaluation of structural parameter according to equations 10 to 15 in section 3.7.2. The slope of the Guinier curve gives the Radius of Gyration (Rg) and that of the Kratky-Porod results in the thickness radius (R_d), and from that the membrane span d.

4.4.1 Scattering profiles of DOPC-Amphotericin B small unilamellar liposomes in 100% D_2O buffer

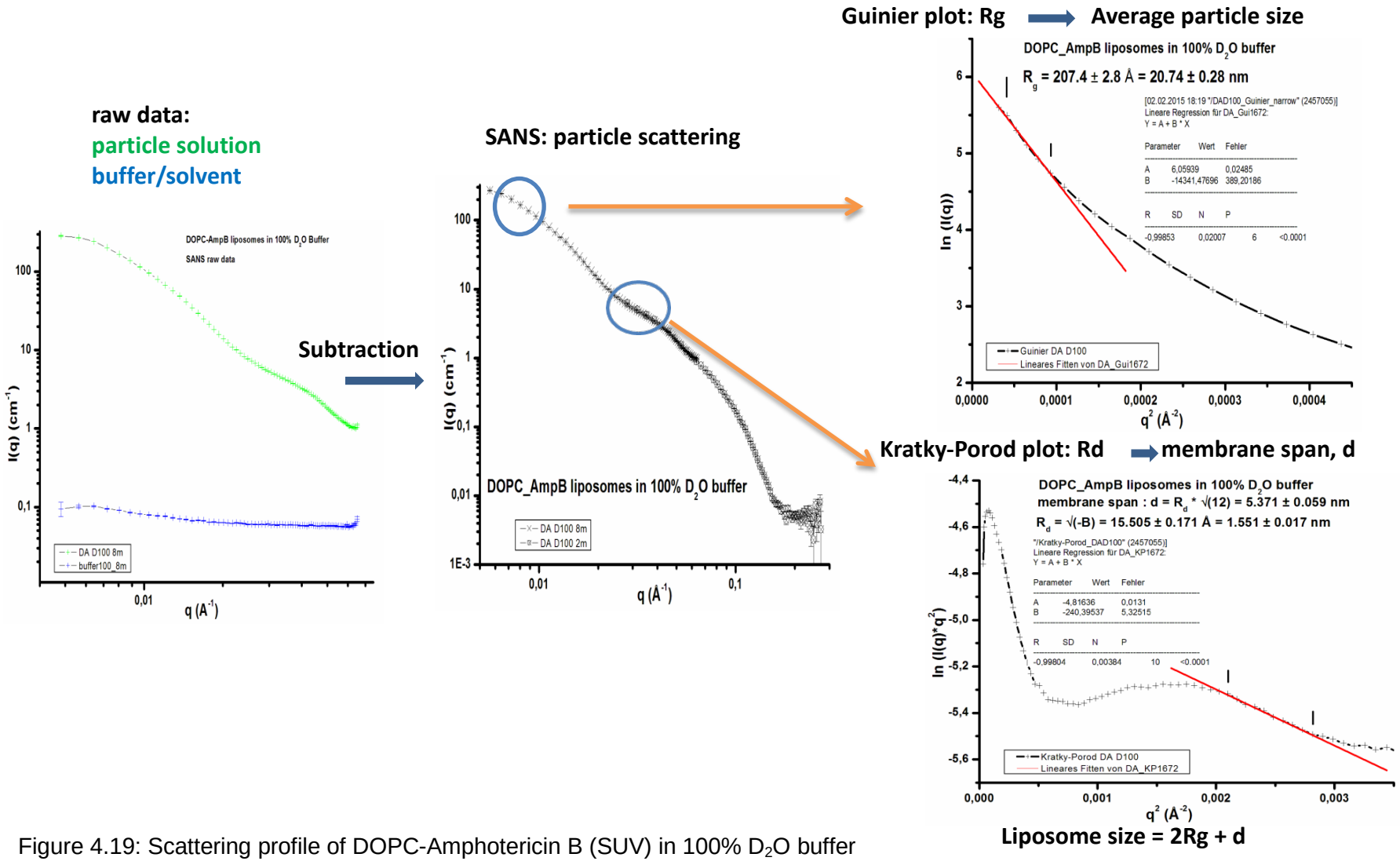

Figure 4.19: Scattering profile of DOPC-Amphotericin B (SUV) in 100% D_2O buffer

4.4.2 Analysis of the scattering profiles

The leftmost part of the scattering profile of the particle below q = 0.01Å gives the Guinier portion. The slope of the linear regression analysis gives the radius of gyration, Rg. Thus, from the above;

$$Rg = \sqrt{-3B} \qquad \text{(eqn.18)}$$

B is taken from the Guinier plot.

The Kratky-Porod graph is obtained by plotting In ($I(q)*q^2$) against q^2 according to equations 11 and 12. The slope of the linear regression analysis gives the thickness radius, Rd. Hence from the Kratky-Porod plot above;

$$Rd = \sqrt{-B} \qquad \text{(eqn.19)}$$

The membrane thickness is then evaluated using equation 13.

The size of the liposome (small unilamellar vesicle) is therefore calculated using equation 14.

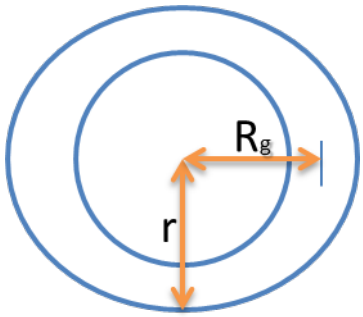

Figure 4.20: Representation of SUV liposome showing radius of gyration (Rg) and radius of vesicle (r).

For solid spheres such as micelles and in this thesis, AmB-HST, the size is calculated using equation 15.

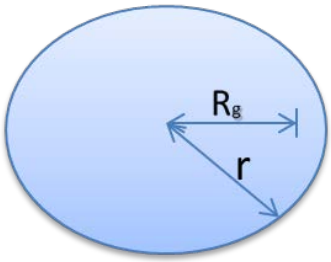

Figure 4.21: Representation of solid sphere showing the radius of gyration, R_g and radius of sphere (r).

4.4.3 Scattering profile of DOPC-Cholesterol-Amphotericin B liposomes (SUV)

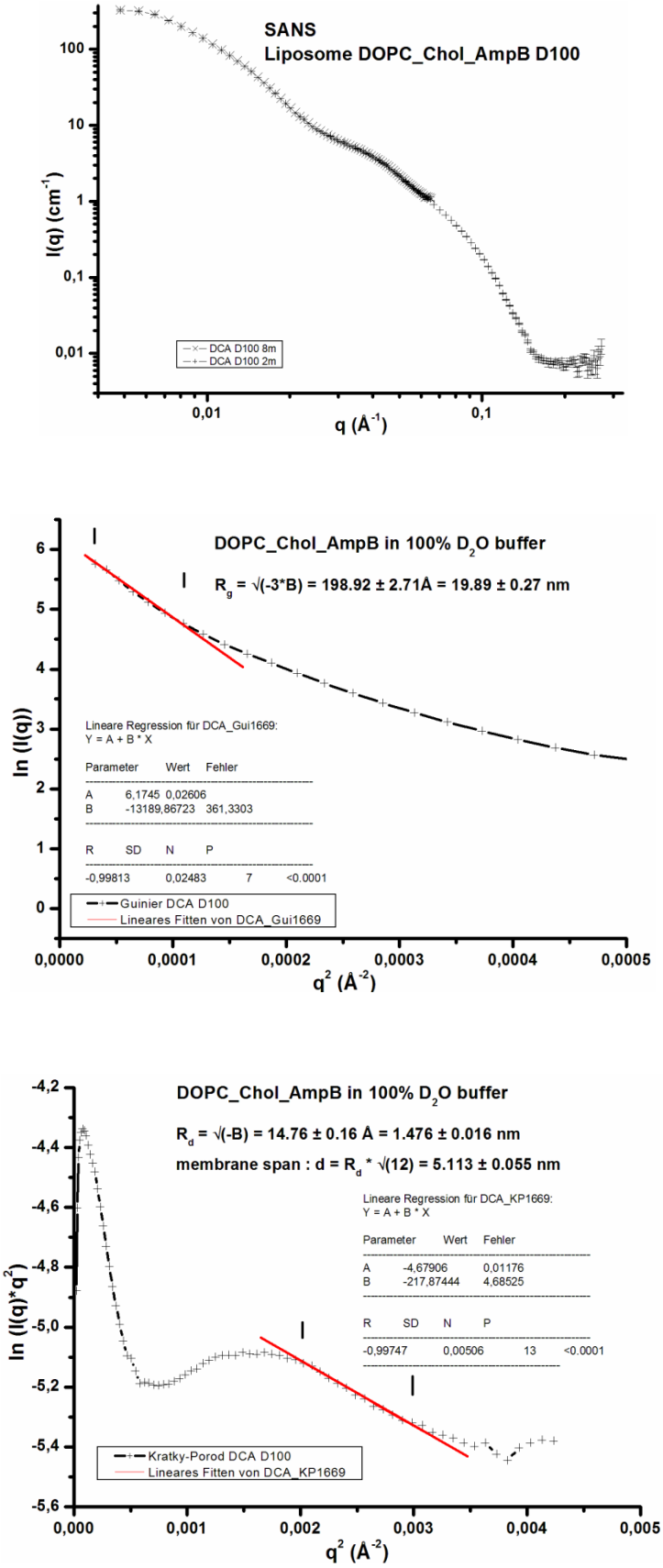

Figure 4.22: Scattering curve (top), Guinier (middle) and Kratky-Porod (bottom) plots for DOPC-Cholesterol-Amphotericin B (10g/L) in 100% D_2O buffer

4.4.4 Scattering profile of DOPC liposomes (SUV) in H_2O buffer

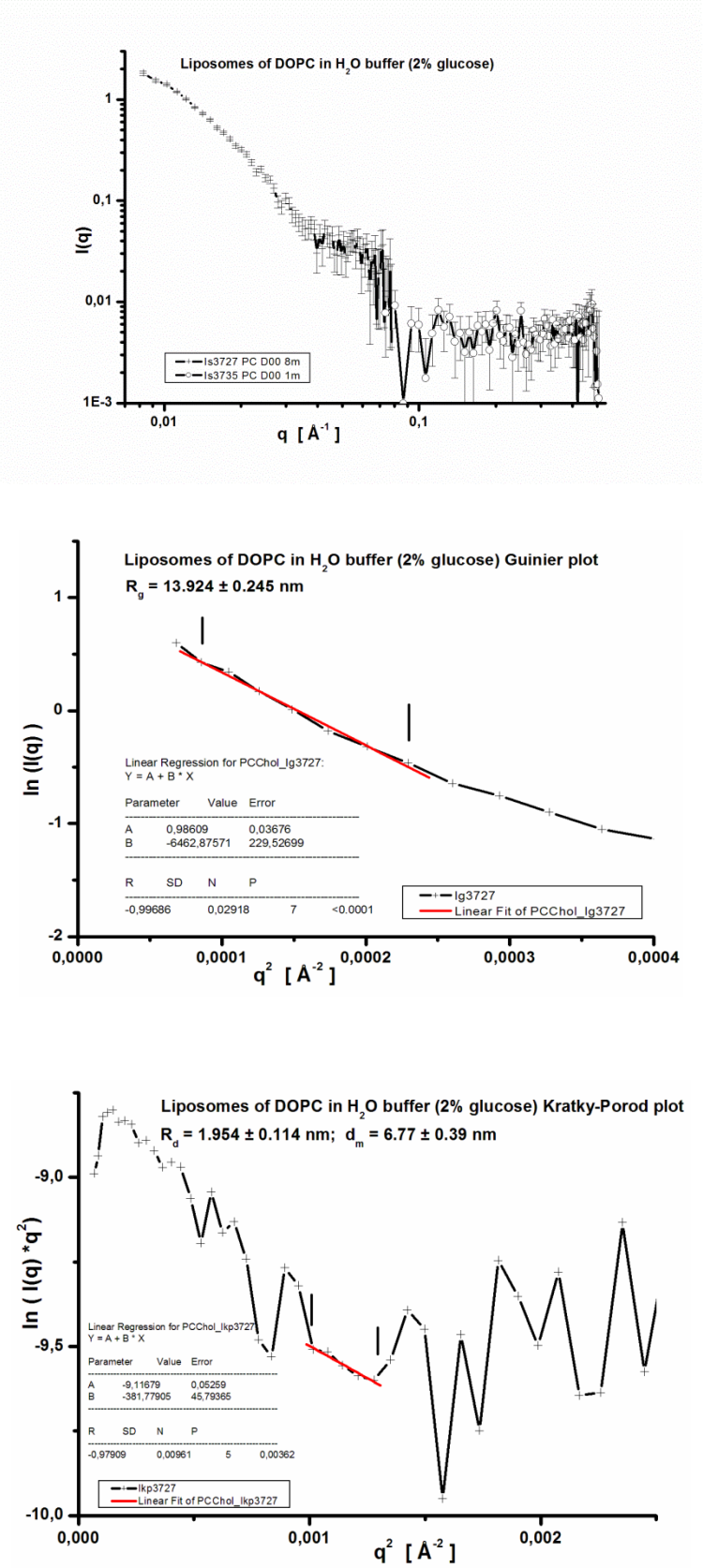

Figure 4.23: Scattering curve (top), Guinier (middle) and Kratky-Porod (bottom) plots for DOPC liposomes (10g/L) in H_2O buffer.

4.4.5 Scattering profile of DOPC-Cholesterol (SUV) in H_2O buffer

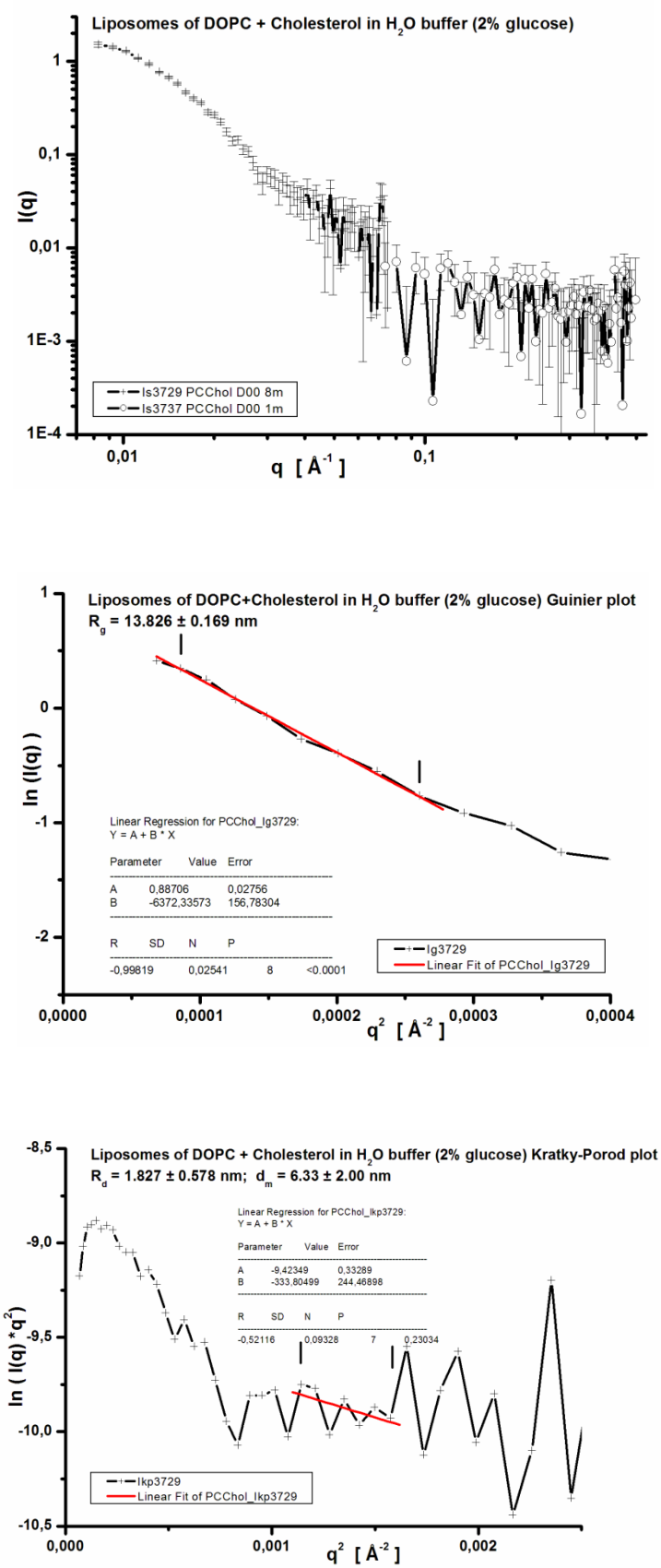

Figure 4.24: Scattering curve (top), Guinier (middle) and Kratky-Porod (bottom) plots for DOPC-Cholesterol liposomes (10g/L) in H_2O buffer.

4.4.6 Scattering profiles of AmB-HST

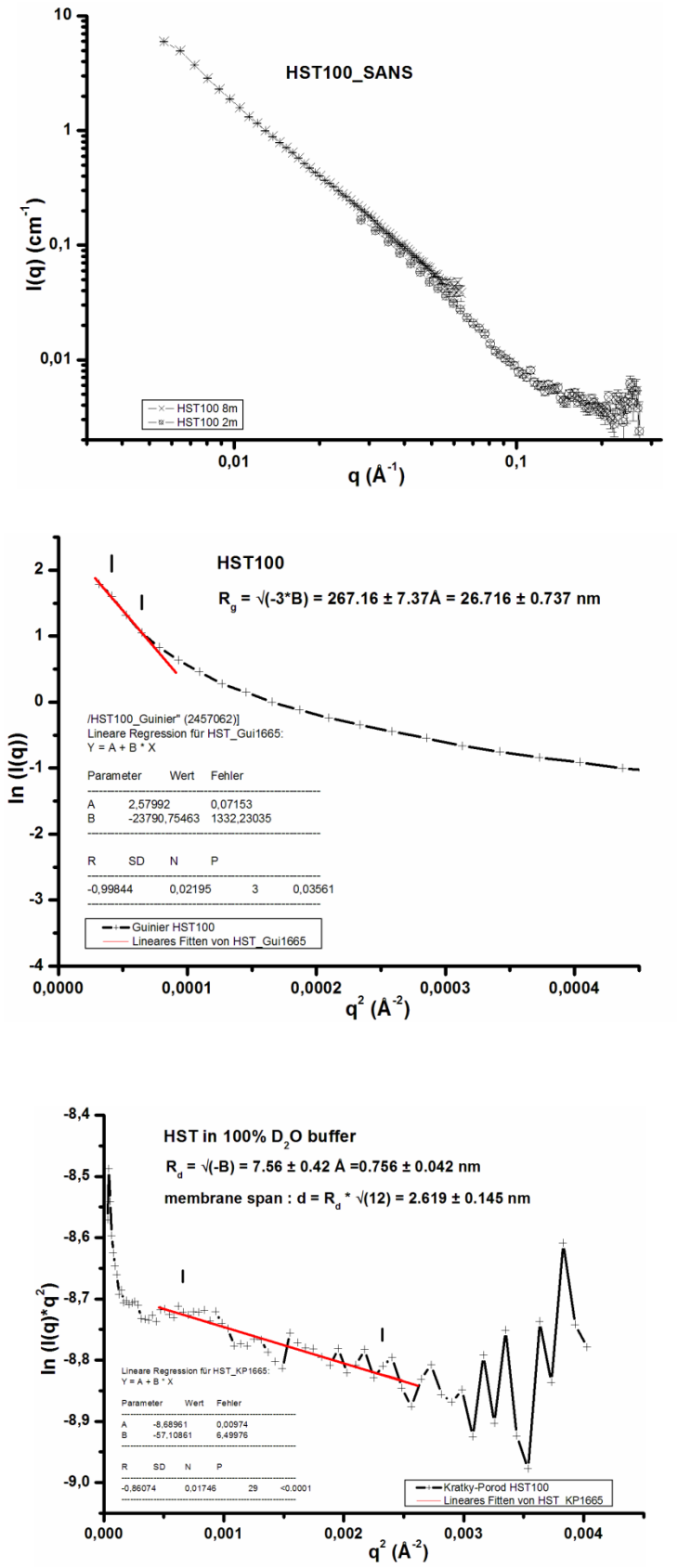

Figure 4.25: Scattering curve (top), Guinier plot (middle) and Kratky-Porod plot of AmB-HST in 100% D_2O buffer.

Results

The scattering profiles for 71, 56, 33% D_2O and H_2O buffers for the liposomes with drug and the blank as well as AmB-HST can be found at the appendices D1 to D5. The nominal buffer concentrations and the actual deuterium content as well as their scattering length densities are given in table 17. These buffers were used for the neutron scattering experiments.

Table 17: Buffer concentration and actual deuterium content

sample	**D_2OBuffer**	**dD_2OBuffer**	**D_2O**	**dD_2O**	**H_2O**	**Ndensity**	**dNdensity**
	% D_2O buf	**error**					
B0	0	0	0,06183	0	99,93817	-5,5574E9	0
TM12	12	0,06	11,74385	0,05872	88,25615	2,50893E9	4,03316E7
TM29	29	0,16	28,29338	0,1561	71,70662	1,39362E10	1,07551E8
B33	33	0,17	32,18739	0,16581	67,81261	1,6625E10	1,14273E8
TM46	46	0,19	44,84291	0,18522	55,15709	2,53635E10	1,27717E8
B56	56	0,19	54,57793	0,18518	45,42207	3,20855E10	1,27717E8
B71	71	0,15	69,18045	0,14616	30,81955	4,21684E10	1,00829E8
B100	100	0,1	97,412	0,09741	2,588	6,1662E10	6,72194E7
H_2O	-0,0076	0	0	0	100	-5,6E9	0
D_2O	102,588	0	100	0	0	6,33E10	0

Ndensity = Scattering length density of the buffers

4.4.7 Evaluation of particle size of samples measured after SANS contrast variation

The intensity data were evaluated using equations 16 and 17 for the liposomes and AmB-HST respectively.

4.4.7.1 Particle size for DOPC-Amphotericin B (SUV)

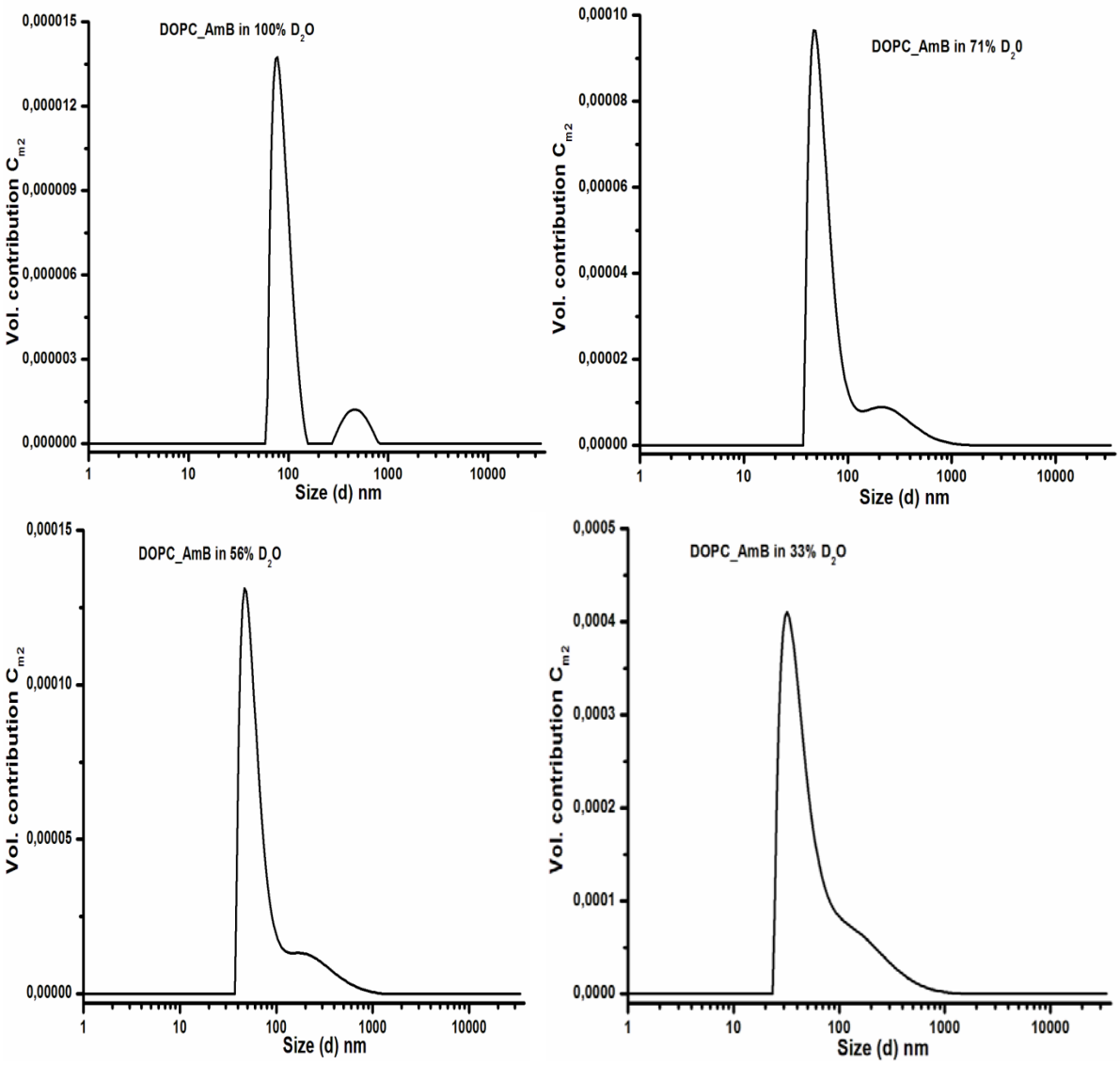

Figure 4.26: Particle size of DOPC-Amphotericin in different concentrations of D_2O buffer as determined after SANS.

The graphs showed a bimodal distribution of particles in all the different deuterated buffer concentrations. With the exception of the sample in 100% D_2O buffer that showed distinct vesicles, the others indicated a fusion of membranes.

4.4.7.2 Particle for DOPC-Cholesterol-Amphotericin B (SUV)

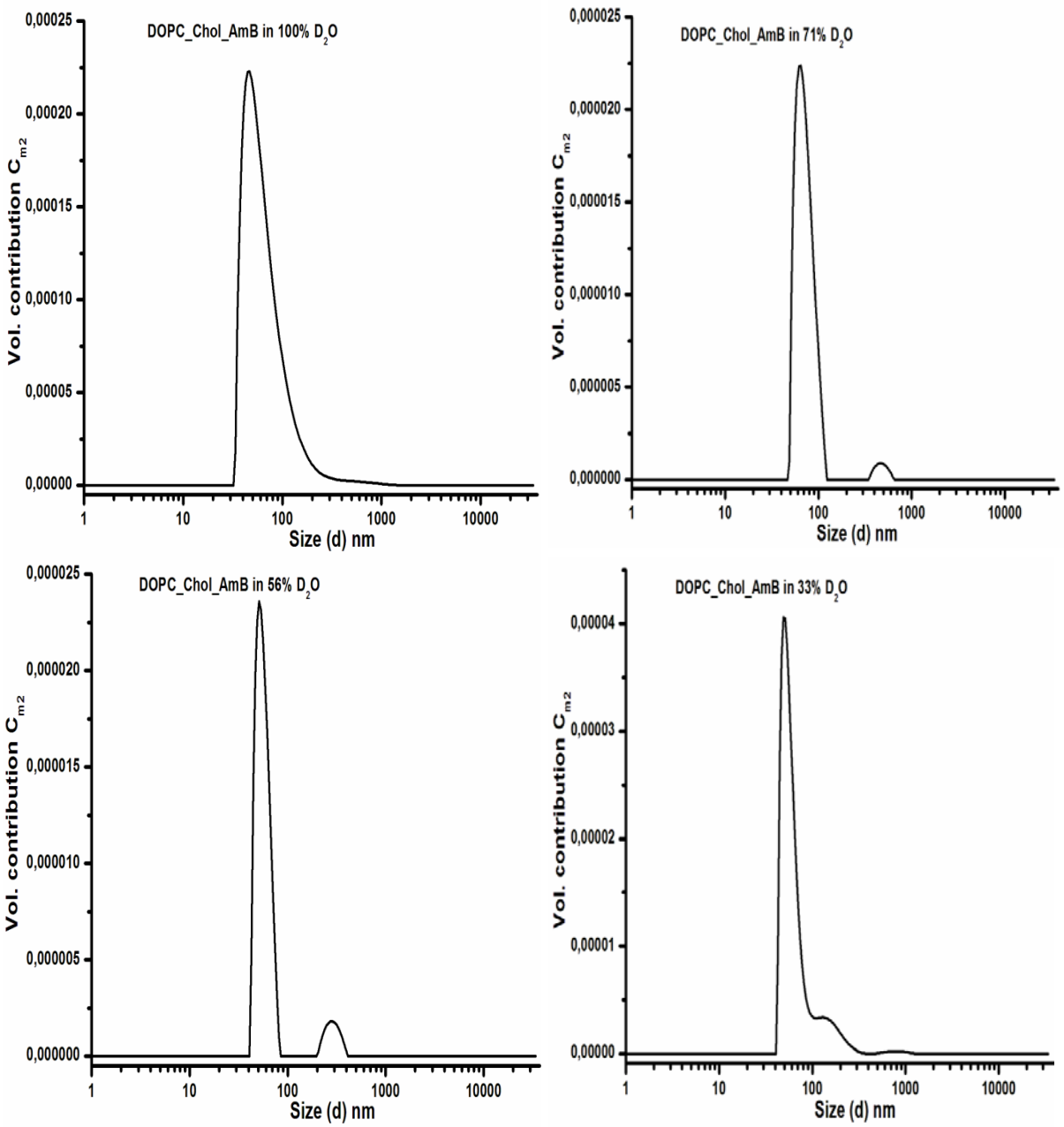

Figure 4.27: Particle size of DOPC-Cholesterol-Amphotericin B (SUV) in buffer of different D_2O concentrations determined after SANS.

The graphs indicated a bimodal particle size for the 71% and 56% D_2O buffers. The sample in 100% buffer was unimodal whilst that in 33% D_2O buffer contained three vesicles with indication of fusion of vesicles.

4.4.7.3 Particle size for AmB-HST in D_2O buffers

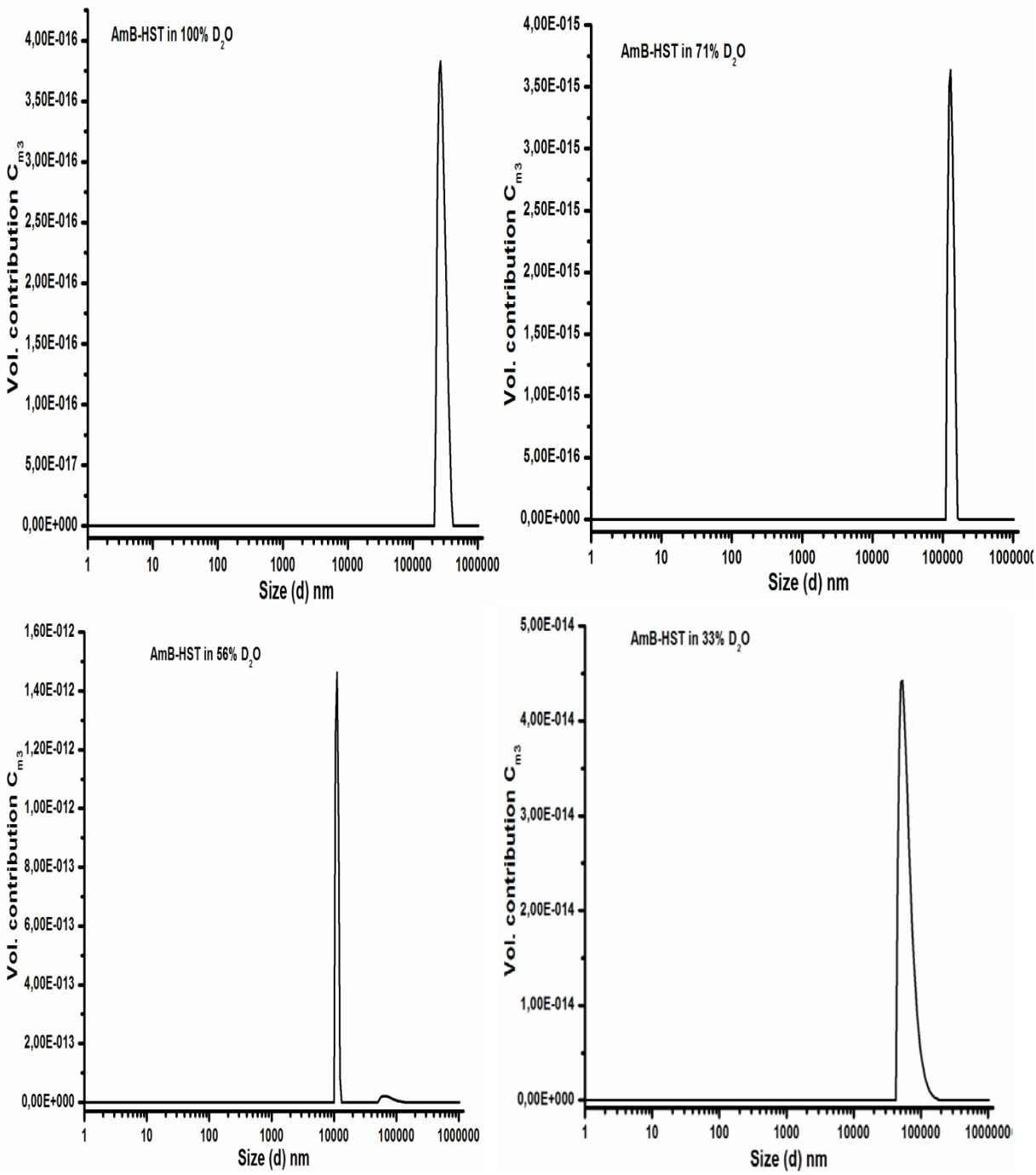

Figure 4.28: Particle size of AmB-HST in buffer of different D_2O content after SANS

The particle size of this core-shell formulation showed micron particles of large nature in deuterated water. The large particles could either be due to aggregation or sedimentation. All the particles were above 100 µm with the exception of the 33% D_2O sample (51.67µm).

4.4.7.4 Structural parameters of SANS in comparison with DLS

4.4.7.4.1 Structural parameters for DOPC-Amphotericin B (SUV)

Table 18: SANS parameters of DOPC-Amphotericin B (SUV) in comparison to DLS

D_2O buffer	Rg ≈ Rm	D (nm)	Size (SANS) (nm)	Size DLS (nm)
33	19.47 ± 0.36	5.86 ± 0.42	44.80 ± 0.73	32.03 / 202.67
56	19.68 ± 0.35	6.27 ± 0.09	45.63 ± 0.69	46.75 / 215.53
71	19.71 ± 0.39	5.51 ± 0.13	44.94 ± 0.77	48.26 / 240.98
100	20.74 ± 0.28	5.37 ± 0.06	46.85 ± 0.06	76.28 / 475.07

*Rg ≈Rm = radius of gyration; D = membrane thickness

4.4.7.4.2 Structural parameters for DOPC-Cholesterol-Amphotericin B (SUV)

Table 19: SANS parameters of DOPC-Cholesterol-Amphotericin B in comparison to DLS

D_2O buffer	Rg ≈ Rm	D (nm)	SANS size (nm)	DLS size (nm)
33	20.01 ± 0.39	1.69 ± 0.65	41.71 ± 0.77	50 / 150.05/ 773.47
56	19.51 ± 0.34	5.72 ± 0.10	44.74 ± 0.69	51.32 / 286.52
71	19.00 ± 0.33	5.21 ± 0.06	43.22 ± 0.66	64.01 / 482.71
100	19.89 ± 0.27	5.11 ± 0.06	44.89 ± 0.54	46

4.4.7.4.3 Structural parameters for AmB-HST

Table 20: SANS parameters of AmB-HST in comparison to DLS

D_2O buffer	Rg	SANS size (nm)	DLS size (µm)
33	24.94 ± 3.74	64.39 ± 9.66	51.67
56	31.32 ± 1.07	80.87 ± 2.76	11.2 / 65.03
71	25.30 ± 0.08	65.32 ± 0.20	130.07
100	26.72 ± 0.74	68.98 ± 1.90	270.61

As expected, the size measured by dynamic light scattering (DLS) was higher than that from the small angle neutron scattering (SANS) (Tables 18, 19 and 20). In light scattering particles

are measured in addition to the hydration shell that surrounds the particles in solution. The light scattering data of the liposomes with and without cholesterol contained both small unilamellar and multilamellar vesicles (Tables 18 and 19) which is characteristic of liposomes prepared by the sonication method. The cholesterol containing vesicles had marginally smaller sizes compared to the drug and lipid vesicles alone as measured by the SANS. The neutron scattering only indicated one kind of vesicles due to the limit of the KWS-2 instrument (<100nm). By neutron scattering, smaller particles were identified for the AmB-HST which was not detected by the light scattering (Table 20). The big particles (> 50µm) which are the majority overshadowed the small particle light scattering.

4.4.8 Determination of equivalent scattering length density by SANS contrast variation

The Guinier plot of the scattering profile enables the evaluation of the zero angle scattering (I_o) according to equation 10. A graph of the square root of the zero angle scattering intensity $\sqrt{Io}$ against the deuterated water concentration yields the equivalent scattering length density of the particle after extending the line to zero scattering.

Table 21: Zero angle scattering intensity data for the different formulations

AmB-HST			
D_2O buffer	**In(I_o)**	**I_o**	**$\sqrt{Io}$**
33	0.80423 ± 0.359	2.235 ± 0.996	1.495 ± 0.294
56	1.5161 ± 0.122	4.554 ± 0.589	2.134 ± 0.134
71	1.54421 ± 0.007	4.684 ± 0.032	2.164 ± 0.008
100	2.57992 ± 0.072	13.196 ± 0.979	3.633 ± 0.132
DOPC-Cholesterol-Amphotericin B (SUV)			
33	3.191985 ± 0.040	24.334 ± 0.99	4.933 ± 0.039
56	4.7221 ± 0.037	112.40 ± 4.22	10.602 ± 0.197
71	5.26947 ± 0.039	194.31 ± 7.59	13.940 ± 0.269
100	6.1745 ± 0.026	480.34 ± 12.69	21.917 ± 0.287
DOPC-Amphotericin B (SUV)			
33	2.92702 ± 0.039	18.67 ± 0.74	4.321 ± 0.085
56	4.51126 ± 0.038	91.04 ± 3.51	9.541 ± 0.183
71	5.16959 ± 0.042	175.84 ± 7.59	13.261 ± 0.283
100	6.05939 ± 0.025	428.11 ± 10.78	20.691 ± 0.259

Results

The corresponding contrast variation curves showing the equivalent scattering length densities of the liposomes with and without cholesterol, and the AmB-HST are given in figure 4.29.

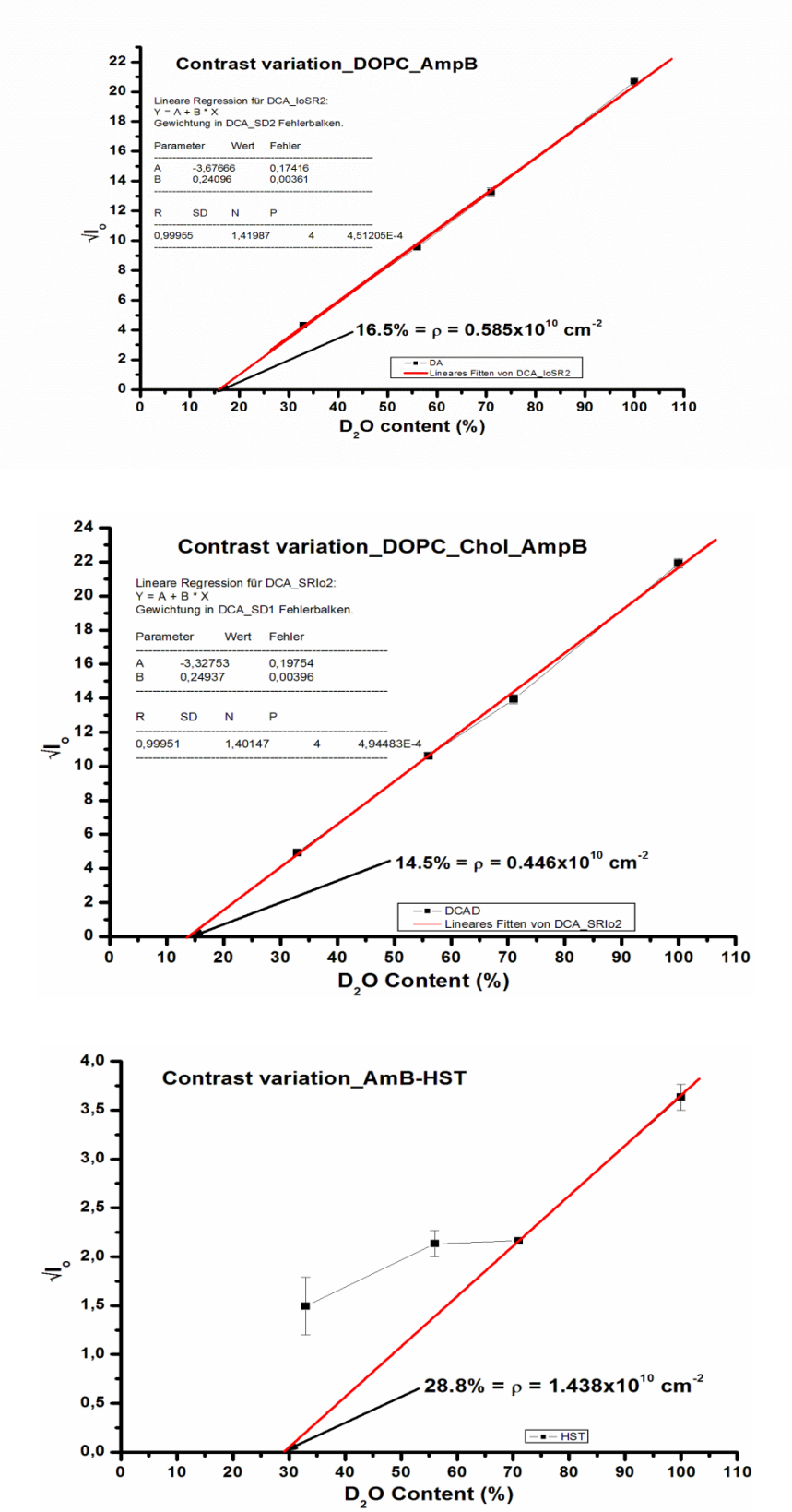

Figure 4.29: Graphs of $\sqrt{I_0}$ against the D_2O content showing the equivalent scattering length density of DOPC-Amphotericin liposomes (top), DOPC-Cholesterol-Amphotericin B liposomes (middle) and AmB-HST (bottom).

Results

The equivalent scattering length density for the DOPC and Amphotericin B was 16.5% D_2O which on an absolute scale corresponds to $0.585x10^{10}cm^{-2}$. The presence of cholesterol (~20 mole %) changed the equivalent scattering density to 14.5% D_2O ($0.446x10^{10}$ cm^{-2}). This change in density presumes a possible in situ complex formation between the other components of the liposomes and cholesterol. Thus, the cholesterol causes a change of 2% D_2O equivalent in the scattering density of the formulation.

The AmB-HST had an equivalent scattering density of 28.8% D_2O ($1.438x10^{10}$ cm^{-2}) indicating the denser among the formulations as well as confirming the large particulate nature of the core-shell formulation (Figure 4.29).

The equivalent scattering density of the blank liposomes with and without cholesterol is needed for the thorough evaluation of the scattering density of the drug (Amphotericin B). The contrast variation graphs are as shown in figure 4.30 below.

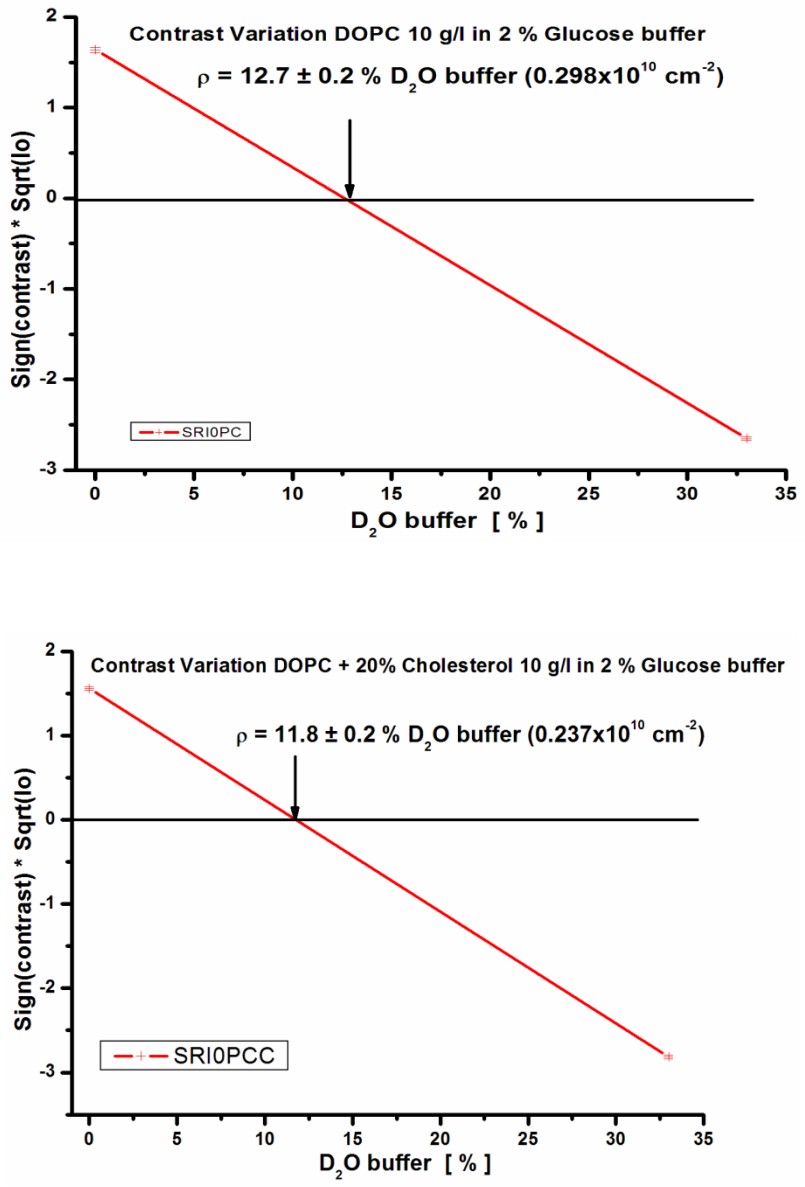

Figure 4.30: Contrast variation curves showing the equivalent scattering length density for blank DOPC liposome without cholesterol (top) and with cholesterol (bottom).

Results

In the literature the equivalent scattering length density for lipids is quoted as 5-20% D_2O which strongly depends on the nature of the head-group and the number of exchangeable protons (Svergun et al, 2013). The average scattering length density for the DOPC liposomes was equivalent to 12.7% D_2O ($0.298x10^{10}$ cm^{-2}) which is consistent with the literature whiles that containing cholesterol had an average equivalent of 11.8% D_2O as its scattering density ($0.237x10^{10}$ cm^{-2}).

The radius of gyration (R_g) obtained from the Guinier curves is analogous to the mechanical radius of gyration where mass is replaced by scattering length density. The mechanical R_g is given by

$$R_g^2 = \sum_i miri^2 / \sum_i mi \qquad \text{(eqn.20)}$$

where m_i is a mass located at distance r_i from the centre of mass. $\sum_i miri^2$ is the moment of inertia, and $\sum_i mi$ is the total mass of the particle. Replacing m_i by the excess scattering density (contrast) the expression for the Rg of the scattering particle becomes

$$R_g^2 = \int_{Vp}(p(r) - ps)r^2\, dr / \int_{Vp}(p(r) - ps)dr \qquad \text{(eqn.21)}$$

where $p(r)$ is the scattering length density at position r (measured from the centre of gravity in terms of scattering) of the particle, and Vp, is the particle volume including atoms of the hydration layer which may have a density different from the bulk solvent. ps is the scattering length density of the solvent. R_g^2 can be negative or positive since the contrast can be positive or negative (Svergun et al. 2013). For neutrons, the contrast between solvent and macromolecules can vary enormously and therefore R_g of a macromolecular complex comprising two or more components such as nucleic acids, proteins and lipids depends strongly on the relative contrast of the components. Stuhrmann and Kirste (1965) showed the dependence of the R_g on the contrast according to the equation

$$R_g^2 = Rc^2 + \frac{\alpha}{\rho} + \frac{\beta}{\rho^2} \qquad \text{(eqn.22)}$$

By rearrangement

$$\rho R_g^2 = \rho Rc^2 + \alpha + \frac{\beta}{\rho} \qquad \text{(eqn.23)}$$

where Rc is the radius of gyration at infinite contrast, β is the displacement of the centre of scattering within the particle and α, relates to the internal density fluctuations within the scattering object.

Equation 22 denotes that R_g is a quadratic function of the inverse of the contrast. For a complex having two components with strongly different scattering densities the constant β is an indication of the distance (d) between the centres of mass of the two components. If β is zero the two components have the same centre of mass and a plot of ρR_g^2 against $\frac{1}{\rho}$ will be

linear with α as the slope. If the value of α is positive then the component of higher scattering density is farther from the centre of mass, and the component of lower scattering density is closer to the centre of mass. The opposite is the case when α is negative. Table 22 is a compilation of the radius of gyration and the contrast on absolute scale. Stuhrmann plots were then deduced for the formulations.

Table 22: Scattering length density (SLD), contrast and radius of gyration (R_g) for the liposomes and core-shell AmB-HST.

DOPC-Amphotericin B (SUV)						
% D_2O buffer	**% H_2O buffer**	**SLD (soln) Absolute x10^{10} (cm^{-2})**	**Contrast ($\rho_p - \rho_s$) x10^{10} (cm^{-2})**	**1/($\rho_p - \rho_s$) x10^{-10} (cm^2)**	**R_g (nm)**	**R_g^2 (nm^2)**
16.5	83.5	0.585				
33	67	1.730	-1.145	-0.87	19.47 ± 0.36	379.08 ± 14.15
56	44	3.327	-2.742	-0.36	19.68 ± 0.35	387.30 ± 13.90
71	29	4.368	-3.783	-0.26	19.71 ± 0.39	388.48 ± 15.53
100	0	6.38	-5.795	-0.17	20.74 ± 0.28	430.15 ± 11.69
DOPC-Cholesterol-Amphotericin B (SUV)						
14.5	85.5	0.446				
33	67	1.730	-1.284	-0.78	20.01 ± 0.39	400.40 ± 15.76
56	44	3.327	-2.881	-0.35	19.51 ± 0.34	380.64 ± 13.38
71	29	4.368	-3.922	-0.25	19.00 ± 0.33	361.00 ± 12.65
100	0	6.38	-5.934	-0.17	19.89 ± 0.33	395.61 ± 10.82
AmB-HST						
28.8	71.2	1.438				
33	67	1.730	-0.292	-3.42	24.94 ± 3.74	622 ± 200.54
56	44	3.327	-1.889	-0.53	31.32 ± 1.07	980.94 ± 68.17
71	29	4.368	-2.930	-0.34	35.30 ± 0.08	640.09 ± 4.05
100	0	6.38	-4.942	-0.20	26.72 ± 0.74	713.96 ± 40.09

*ρ_p = Scattering length density of particle ρ_s = Scattering length density of solvent

Results

The stuhrmann graphs are given below:

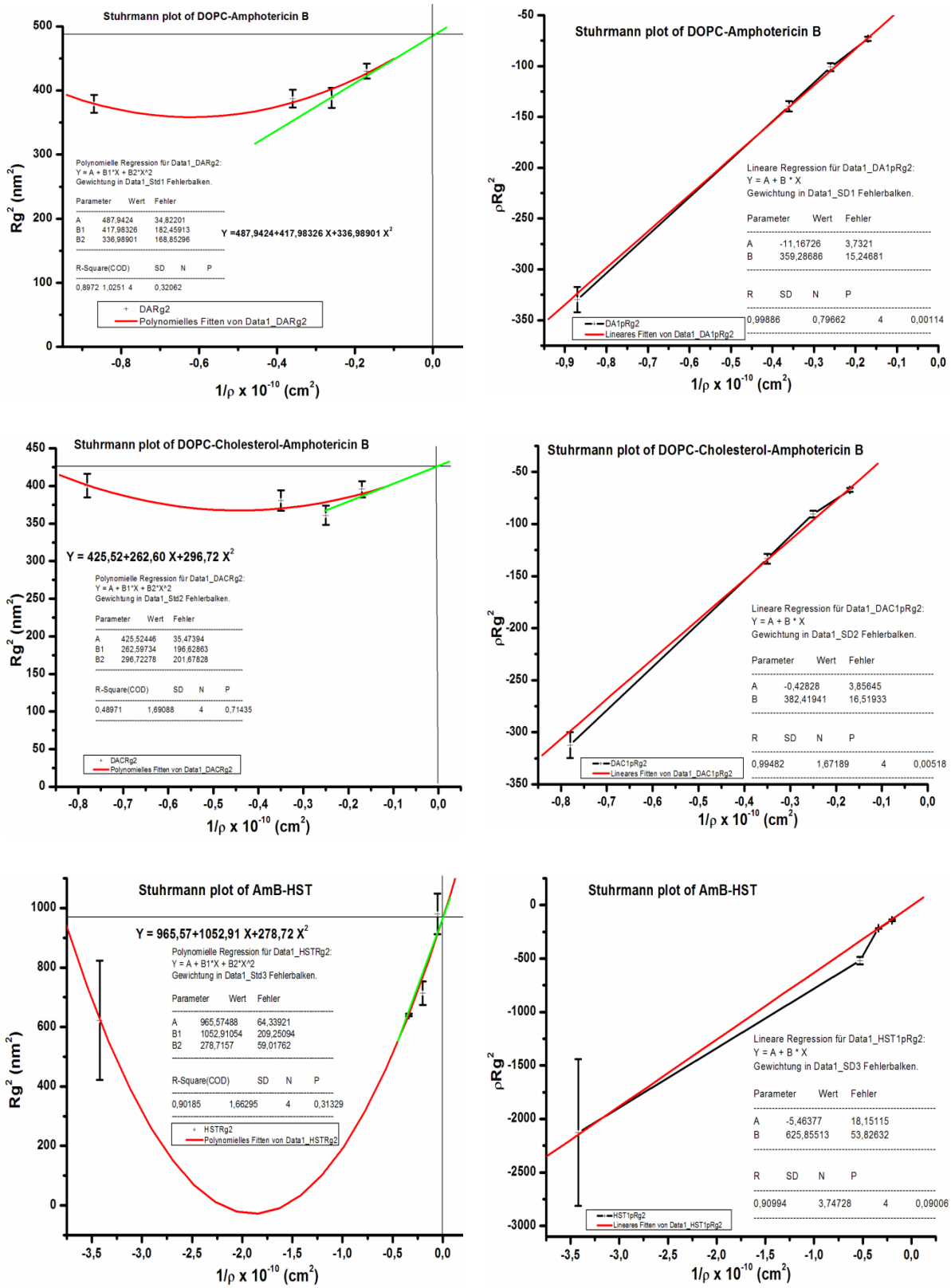

Figure 4.31: Stuhrmann plot for DOPC-AmB (top), DOPC-cholesterol-AmB (middle) and AmB-HST (bottom). The left plots utilize equation 22 and the right ones, equation 23 above.

Results

The contrast variation curves of $\sqrt{I_o}$ against the volume fraction of D_2O for the small unilamellar liposomes of the amphotericin B prepared with DOPC, with and without cholesterol showed a linear function (figure 4.29). Linearity was also observed for the blank preparations (figure 4.30). This implies that the solutes of these preparations are significantly homogenous or monodisperse. The graph for the AmB-HST was linear at high contrast but showed some deviation towards the matching point. There is a slight heterogeneity in the scattering density among the AmB-HST particles which could be due to either lecithin-gelatin shell without drug, sedimentation or demixing.
The Stuhrmann plot is used to determine the distribution of neutron scattering density of the solute and hence the shape dimensions (Schoenborn et al. 1987). The experimental points plotted in figure 4.31 clearly show that ρR_g^2 is linearly dependent on the inverse of the contrast ($1/\rho$) for the DOPC-Amphotericin B and DOPC-Cholesterol-Amphotericin B small unilamellar liposomes. This linearity implies that $\beta = 0$ for these two vesicle particles. This means that the components of the particle (vesicle) have the same centre of mass. This is true for liposomes which are hollow spheres and are symmetrical. The same cannot be said of the AmB-HST particle as the graph is not absolutely linear (figure 4.31 bottom) towards the match point. AmB-HST has been investigated with SANS to be a core-shell particle. It is therefore likely that the spherical core can be asymmetric with respect to the shell. The positive values of α for all the samples means that the higher scattering components are far away from the centre of mass of the particles. In this case the hydrophilic portions are more towards the outside and the hydrophobic portions are more towards the inside of the particles.

4.4.9 Internal structure evaluation of the freeze-dried liposomes

In an initial experiment multilamellar (MLV) and small unilamellar vesicles (SUV) were prepared as in section 3.2.3.2 but were not freeze-dried. These were administered to small angle scattering. The scattering profiles of the multilamellar liposomes without and with 20% cholesterol are as shown in figure 4.32 below:

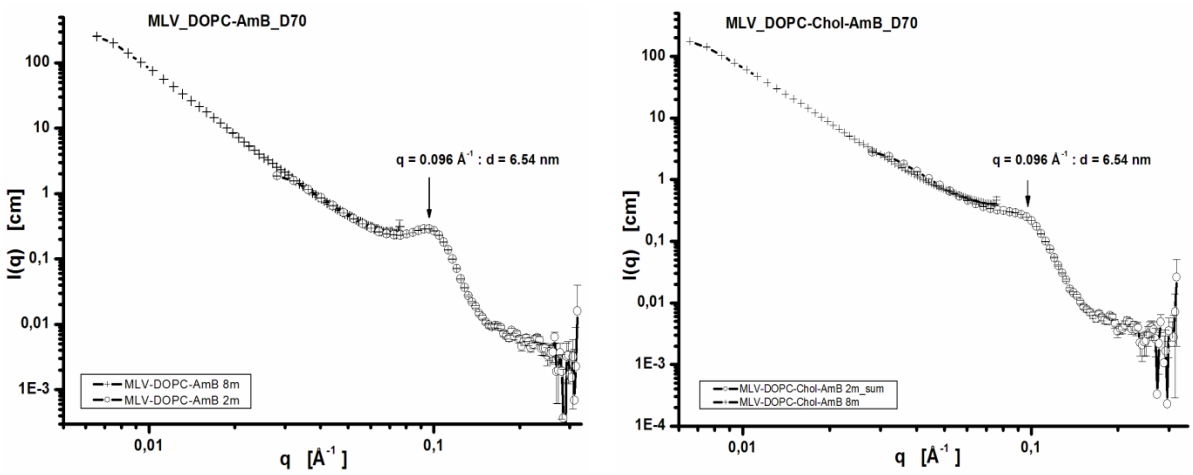

Figure 4.32: Scattering profile of multilamellar vesicles with and without cholesterol (non-freeze-dried)

Results

Both profiles show a peak at q value of 0.096 $Å^{-1}$. This represents the inter-lamellar distance within the vesicles and has a value of 6.54 nm in both cholesterol and non-cholesterol containing liposomes. However, it can be observed that the cholesterol causes a slight broadening (smearing) of the peak (side maxima). There are aggregates as indicated at the lowest q range. The smearing effect by cholesterol was a matter for investigation.

The profiles for the small unilamellar vesicles are as indicated in figure 4.33 below:

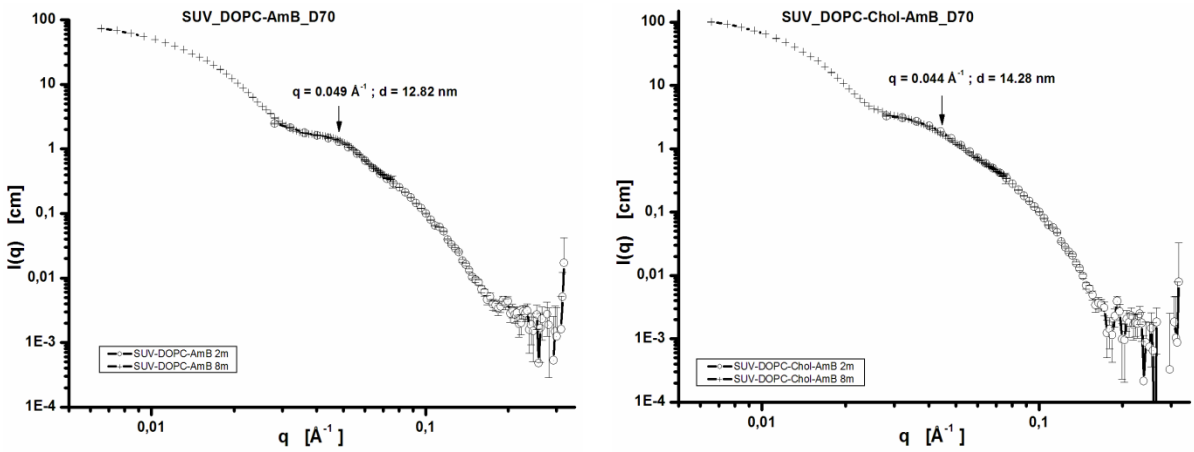

Figure 4.33: Scattering profile of small unilamellar vesicles without and with 20% cholesterol (non-freeze-dried)

Lateral phase separation is seen in both profiles at different q values (0.049 $Å^{-1}$ and 0.044 $Å^{-1}$for without cholesterol and with cholesterol respectively). The distance between these phases are 14.28 nm for cholesterol containing vesicles and 12.82 nm for vesicles without cholesterol. Here too, cholesterol influences the nature of the lateral phase separation.
Domains are observed in the scattering profiles of amphotericin B with the lipids (DOPC and cholesterol). These are seen as bumps in the scattering profiles and occur in DOPC-Amphotericin B liposomes as well as in the DOPC-cholesterol-Amphotericin B liposomes. By observation that cholesterol improves the solubility of Amphotericin B by forming complexes, further experiment was set out to investigate the organization of the drug-lipid complexes in the membrane vesicles. The final freeze-dried products containing different Amphotericin B and lipids were investigated with neutrons and light scattering. Small unilamellar vesicles of the products were used to resolve the domains by deuterium contrast variation. The deuterium content was set out to eliminate the scattering by the lipids at 12% D_2O buffer and that of the drug at 29% D_2O buffer from the results of the above contrast variation experiments of the liposomes and the AmB-HST core shell particles.
The scattering profiles of the freeze-dried multilamellar vesicles containing different concentrations of drug and lipids are shown in the figure 4.34 below:

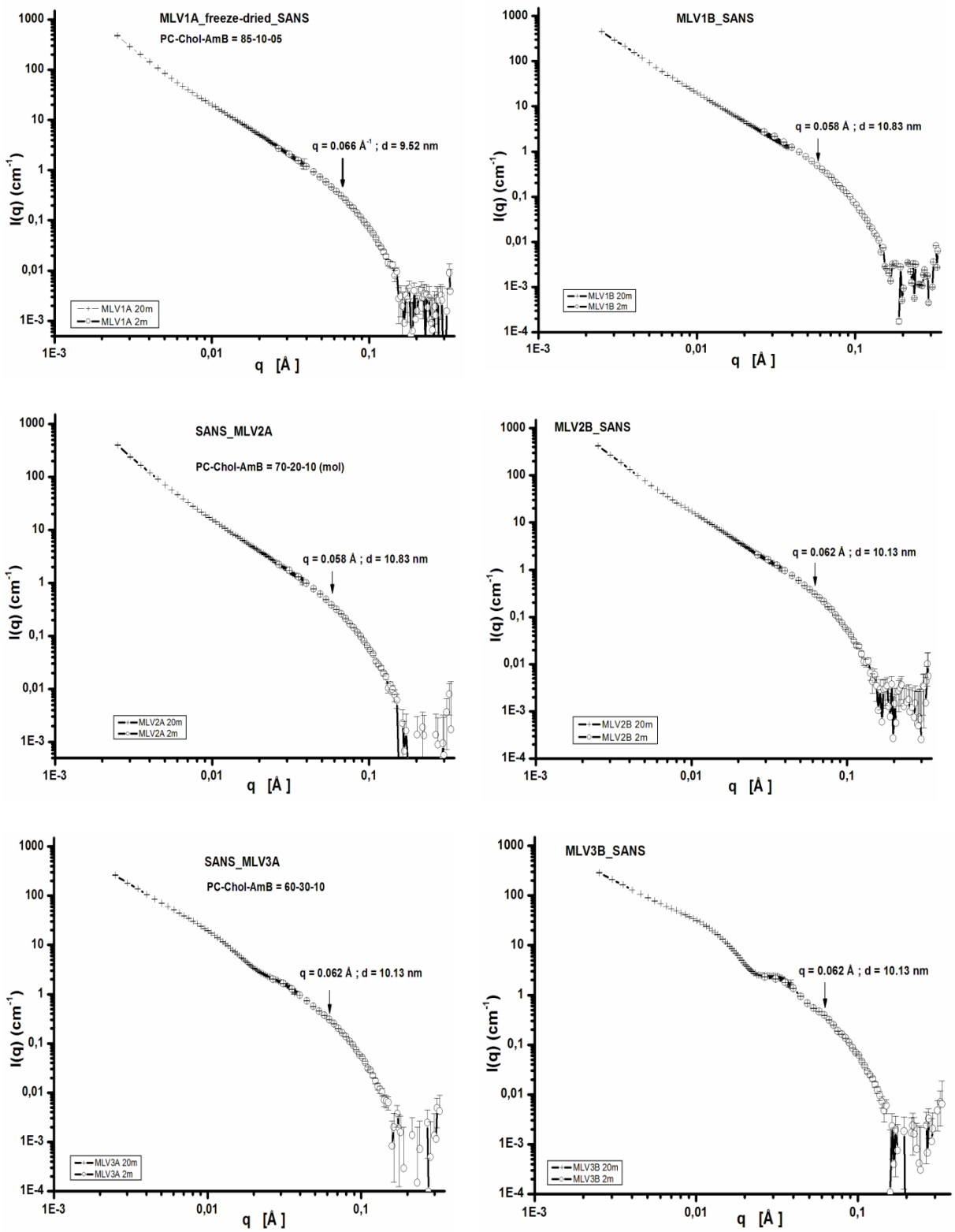

Figure 4.34: Scattering profiles of MLV containing drug and their blanks: top – 85:10:5 mol% DOPC-Cholesterol-Amphotericin B (MLV1A & MLV1B). Middle – 70:20:10 mol% DOPC-Cholesterol and Amphotericin B (MLV2A & MLV2B). Bottom – 60:30:10 mol% DOPC-Cholesterol-Amphotericin B (MLV3A & MLV3B)

Results

The curvature of the scattering curves at the 2m distance of the drug containing vesicles is different from that of the blanks. The scattering curves were cut at the left side (low q) due to the limit of the instrument with all samples showing some level of aggregation. The smearing of the lamellar peak was however more pronounce in comparison to the non-freeze-dried multilamellar vesicles. The inter-lamellar distance was different but not significant. The determined parameters from the scattering curves are thus summarized in table 23.

Table 23: Structural parameters of the freeze-dried MLVs with Amphotericin B and drug-free reference (blanks)

Sample	Radius of gyration (R_g) nm	Membrane span (d) nm	Inter-lamellar distance (nm)	Size (nm) $S = 2^* \sqrt{\frac{5}{3}} R_g$	DLS size (Peak values) nm
MLV1A	19.48 ± 0.21 14.42 ± 0.26	2.45 ± 0.31	9.52	50.29 ± 0.55 37.23 ± 0.67	4.12 25.57
MLV2A	19.91 ± 0.46 14.85 ± 0.15	3.78 ± 0.02	10.83	51.41 ± 1.17 38.34 ± 0.37	19.55
MLV3A	20.96 ± 0.31 16.21 ± 0.32	4.43 ± 0.03	10.13	54.12 ± 0.80 41.87 ± 0.82	31.48
Blanks					
MLV1B	17.36 ± 0.30	2.61 ± 0.39	10.83	44.82 ± 0.54	11.08
MLV2B	24.98 ± 0.24	6.58 ± 0.31	10.13	64.49 ± 0.62	22.00
MLV3B	17.18 ± 0.20 15.50 ± 0.17	4.42 ± 0.01	10.13	44.36 ± 0.50 40.37 ± 0.50	29.65

The same samples measured by dynamic light scattering showed different particles as evidenced in the raw intensity plot below (figure 4.35). However, the data was scaled assuming massive particles (spheres) by dividing the intensity by the third power of the radius (r^3). The scaled graphs of the MLVs and their blanks are given in figure 4.36 below.

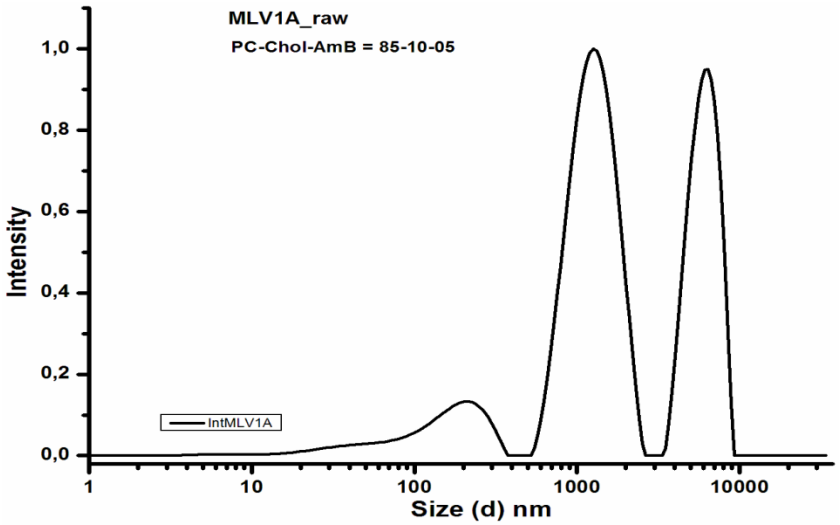

Figure 4.34: A sample graph of intensity (raw) against diameter for the freeze-dried MLVs.

Results

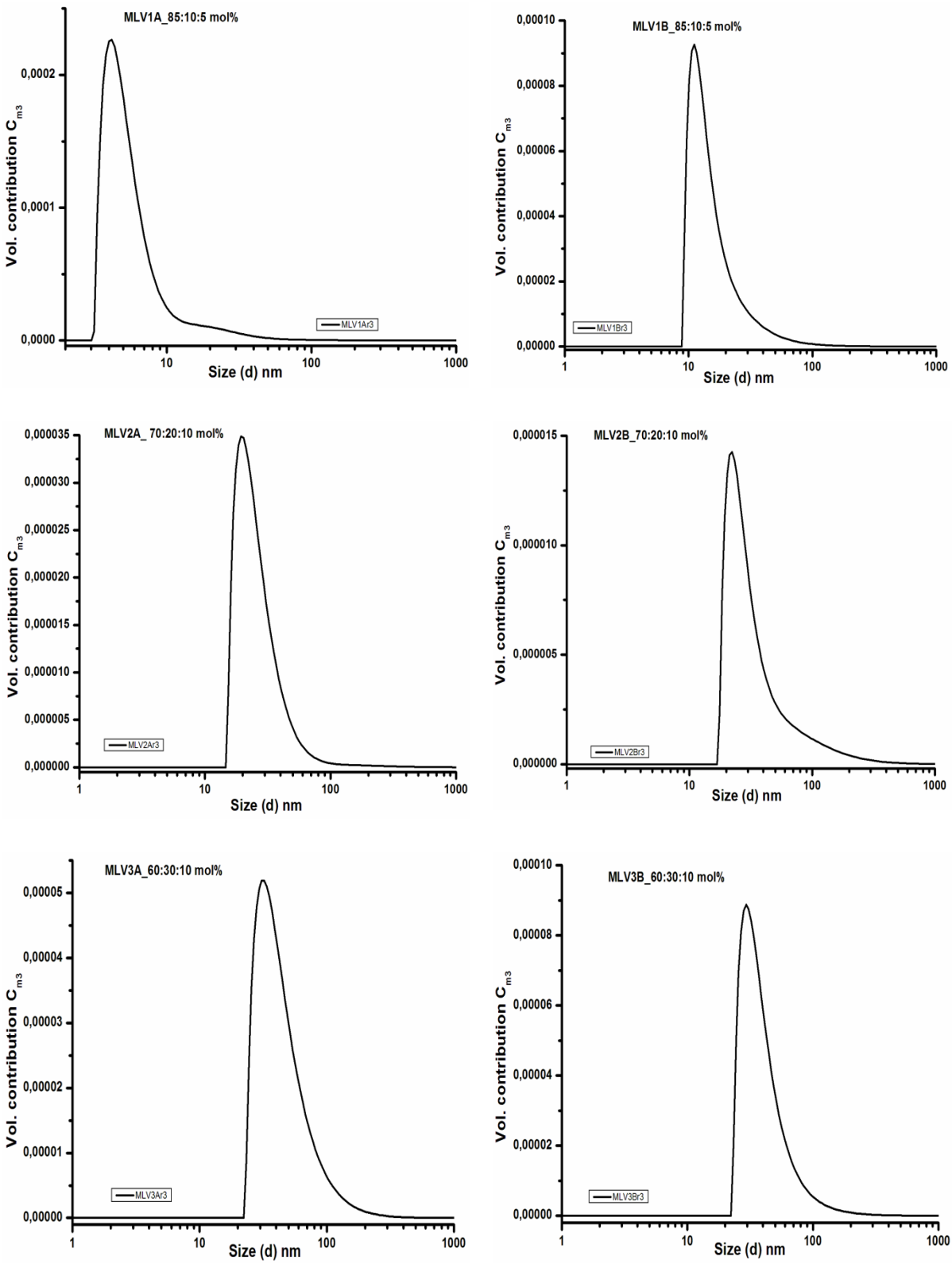

Figure 4.36: Graphs showing particle size of the multilamellar vesicles measured by dynamic light scattering (DLS) after being administered to small angle neutron scattering (SANS). MLV1A & 1B are samples containing 85:10:5 mol% DOPC-Cholesterol-AmB and blank respectively. MLV2A & 2B for 70:20:10 mol% DOPC-Cholesterol-AmB and blank, whiles MLV3A & 3B represents 60:30:10 DOPC-Cholesterol-AmB and its blank.

Results

It is clear from the intensity graph (raw) that the samples are polydispersed and only particles that are below 100 nm would be resolved by the neutron instrument. Thus all the sizes determined for the drug containing samples and blanks are below 100 nm as indicated in table 23. The particles show a slight increase in size with increase in cholesterol and drug contents as expected. The DLS scaled graphs also show a tailing towards larger particle size and a broad area of the peak for all samples measured, confirming the polydispersity. It is thus clear that the organization of the drug-lipid complexes cannot be resolved using MLVs.
To enable the tentative evaluation of the structure of the formulation and internal organization of the drug-lipid complexes in the membrane-like vesicles, small unilamellar vesicles of the formulations were prepared. This was also to meet the size limit of the instrument. In this regard, the drug containing vesicles were administered to the neutrons and the particle size measured as well by dynamic light scattering. The graphs by dynamic light scattering are given below in figure 4.37

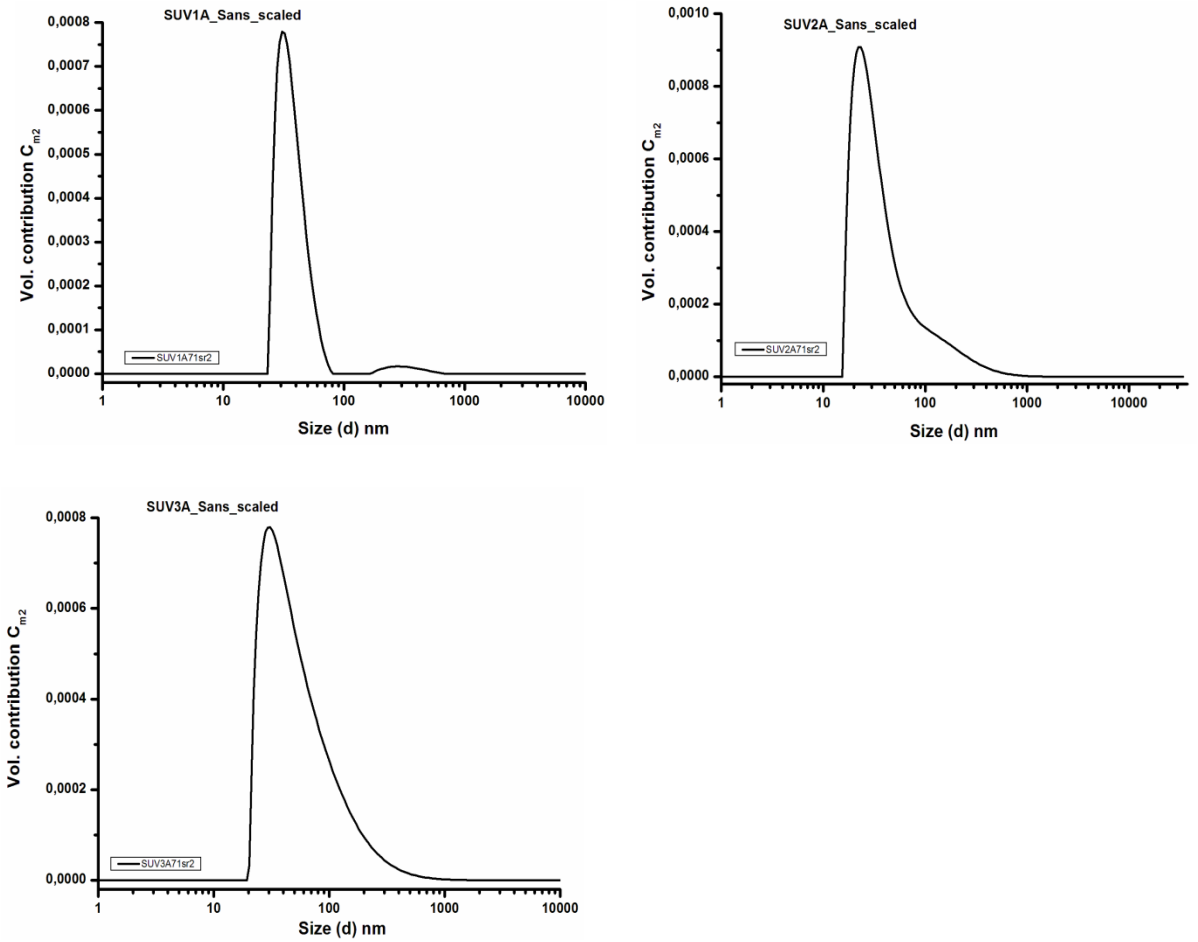

Figure 4.37: Particle size of the small unilamellar vesicles measured by dynamic light scattering after being measured by small angle neutron scattering. The intensity data was scaled by dividing by the second power of the radius (r^2) for liposomes. SUV1A for 85:10:5 mol% vesicles; SUV2A for 70:20:10 mol% vesicles and SUV3A for 60:30:10 mol% vesicles.

The neutron scattering curves, the Guinier plots for the determination of radius of gyration (R_g) and the Kratky-Porod plots for estimation of the membrane span for the vesicles containing different lipids and drug contents are given in figures 4.38 and 4.39.

Results

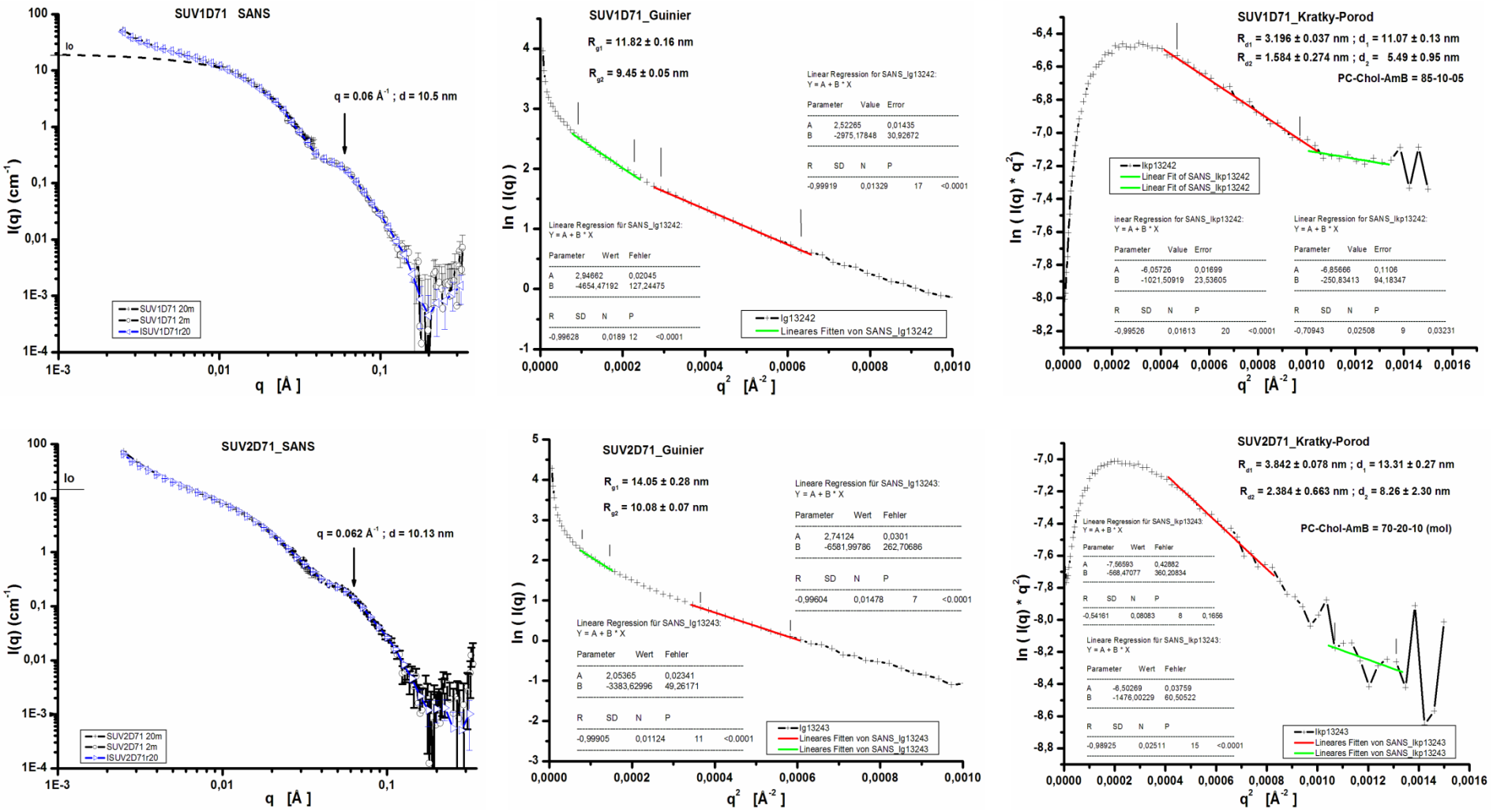

Figure 4.38: Scattering curves, Guinier and Kratky-Porod plots for 85:10:5 mol% DOPC-Cholesterol-AmB small unilamellar vesicles (SUV1) (top) and 70:20:10 DOPC-Cholesterol-AmB small unilamellar vesicles (SUV2) (bottom). The scattering curves reveal the lateral phase separation at q = 0.06 $Å^{-1}$ and 0.062 $Å^{-1}$ for SUV1 and SUV2 respectively.

Results

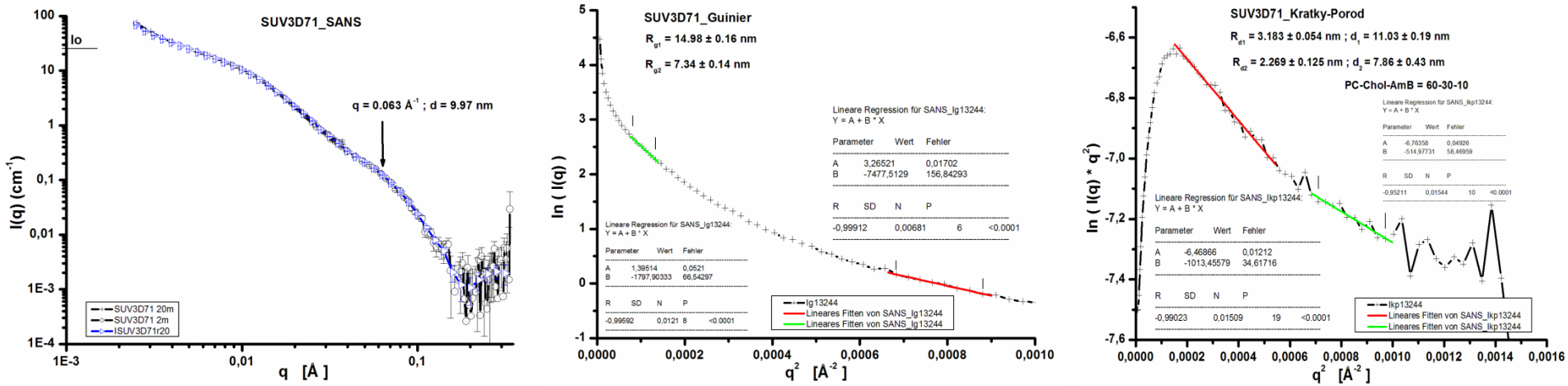

Figure 4.39: The scattering curve, Guinier and Kratky-Porod plots for 60:30:10 DOPC-Cholesterol-AmB (SUV3). The lateral phase separation occurs as a bump with peak at q = 0.063 $Å^{-1}$.

A summary of estimated parameters are indicated in table 24.

Table 24: Parameters evaluated from the scattering curves of the small unilamellar vesicles containing different concentrations of drug and lipids

Sample	Radius of gyration (R_g) nm	Membrane span (d) nm	Distance between domains (d_{dd})	Zero angle scattering (Io)	Size (DLS) nm
SUV1	11.82 ± 0.16 9.45 ± 0.05	11.07 ± 0.13 5.49 ± 0.95	10.5	19.04 ± 0.39 12.46 ± 0.18	31.37 306.92
SUV2	14.05 ± 0.28 10.08 ± 0.07	13.31 ± 0.27 8.26 ± 2.30	10.13	15.51 ± 0.47 7.80 ± 0.18	23.02 148.69
SUV 3	14.98 ± 0.16 7.34 ± 0.14	11.03 ± 0.19 7.86 ± 0.43	9.97	26.19 ± 0.45 4.04 ± 0.22	30.15

Results

The DLS results indicate fractions of large particles in addition to the small vesicles which are expected for liposomes prepared by sonication. However, vesicles larger than 100 nm will escape resolution by the instrument. Particles of about 30 nm were obtained as measured by both the DLS and SANS (figure 4.37 and Table 24). The scattering profiles show minimal aggregation with increase in cholesterol content even with increased amount of drug (figures 4.38 and 4.39). Thus, it can be assumed that the lipids could form a solvent for the drug.
With the model of a spherical membrane for small unilamellar vesicles, one expects a single radius of gyration (R_g) and a single membrane span (d).

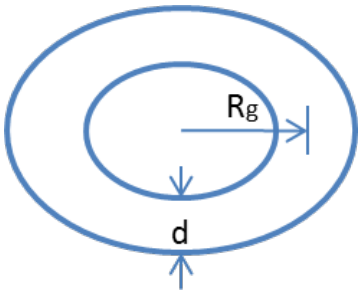

Figure 4.40: A model of a small unilamellar vesicle showing radius of gyration (R_g) and the membrane span (d).

The scattering profiles show that there are domains in the vesicles with distances which vary with the composition of the components. The inter-domain distance was evaluated to be 10.5 nm, 10.13 nm and 9.97 for SUV1, SUV2 and SUV3 respectively. The distance decreases with increase in the cholesterol and drug contents. The analysis of the scattering data by Guinier and Kratky-Porod plots reveal two radii of gyrations and two membrane spans for all the samples as indicated in table 24. The smaller values of the calculated membrane spans are slightly higher than normal membrane span due to the fact that amphotericin B is known to cause membrane thickening. Thus, a novel model could be assumed for the DOPC-Cholesterol-Amphotericin B vesicles to depict the organization of the Amphotericin B-lipid complexes in model membranes.

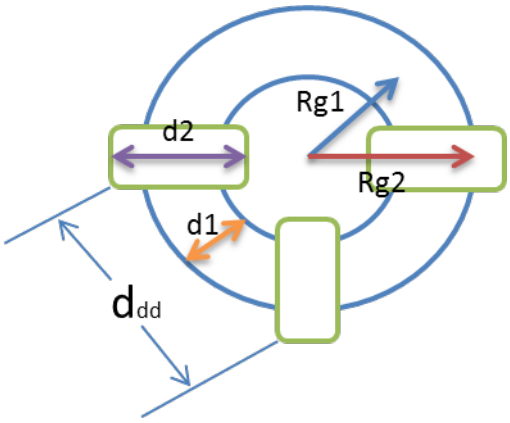

Figure 4.41: Assumed model of the organization of domains of Amphotericin B-lipid complexes in membranes

The two radii of gyration suggest that the domains are not symmetrical. If they were to be symmetrical, only one radius of gyration would have been observed. This presupposes that

the domains are more towards the outside of the membrane than the inside. In taking the geometry of a sphere and the evaluated parameters the number of domains could be roughly estimated. For example, using the parameters of the SUV1:

R_{g1}= 9.45 nm R_g2 = 11.82 nm d_1 = 5.49 nm d_2 = 11.07 nm d_{dd} = 10.5 nm
The circumference of a sphere L = 2πR where R is the radius of the sphere.
Hence from the above model,

$$L = 2\pi (Rg_1 + d_1/2) = 3.14159*2 (9.45 + 5.49/2) = 76.62 \text{ nm}$$

The distance between domains (d_{dd}) is calculated as 10.5 nm. Therefore the number of domains will be given by 76.62/10.5 = 7.30 ≈ 7.
By following the same procedure, SUV2 and SUV3 have almost 9 and 7 domains respectively. Thus as the ratio of lipid to Amphotericin B increases the number of domains increases and decreases again as more cholesterol is added.
The equivalent scattering length densities of the domains were probed by contrast variation method of the small angle neutron scattering. The scattering curves of the different D_2O contents of the different samples can be found at appendix D6, D7 and D8. The contrast variation curves are as shown below:

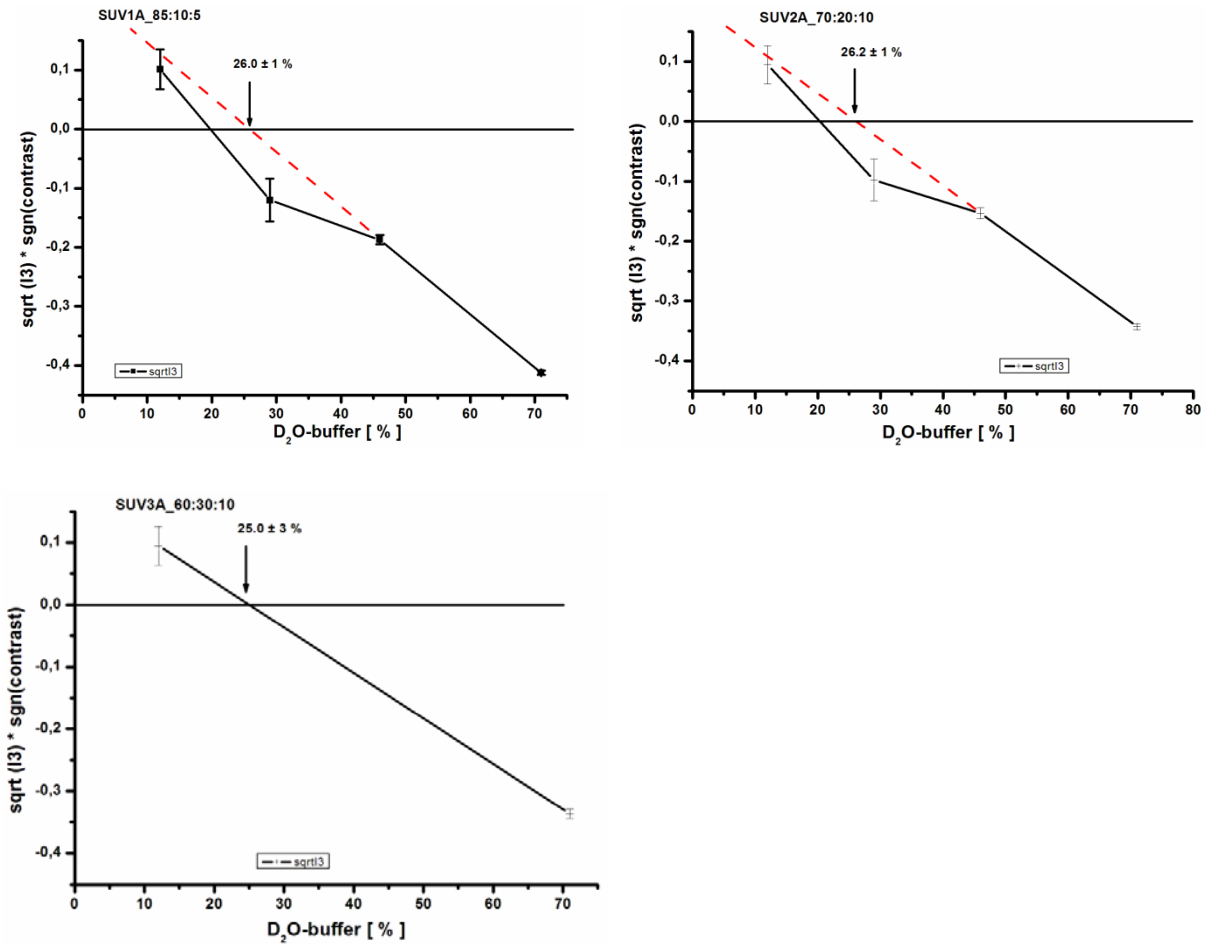

Figure 4.42: Contrast variation curves of SUV1, SUV2 and SUV3 showing the equivalent scattering length densities of the domains of the Cholesterol-Amphotericin B complexes in the model DOPC membranes.

Results

The domain of the 85:10:5 DOPC-Cholesterol-Amphotericin B (SUV1) indicated an equivalent scattering density of 26.0±1 % D_2O (absolute = $1.243x10^{10}$ cm^{-2}) while that of the 70:20:10 DOPC-Cholesterol-Amphotericin B (SUV2) recorded 26.2±1 % D_2O ($1.258x10^{10}$ cm^{-2}). SUV3 with composition of 60:30:10 DOPC-Cholesterol-Amphotericin B had a scattering length density equivalent of 25.0±3 % D_2O ($1.175x10^{10}$ cm^{-2}). The scattering length density is proportional to the density of the material. Thus, the density of the domains in the various formulations is almost the same irrespective of the concentration of drug and lipids.

4.5 Results of self-nanoemulsifying system

4.5.1 Solubility of Amphotericin B in excipients

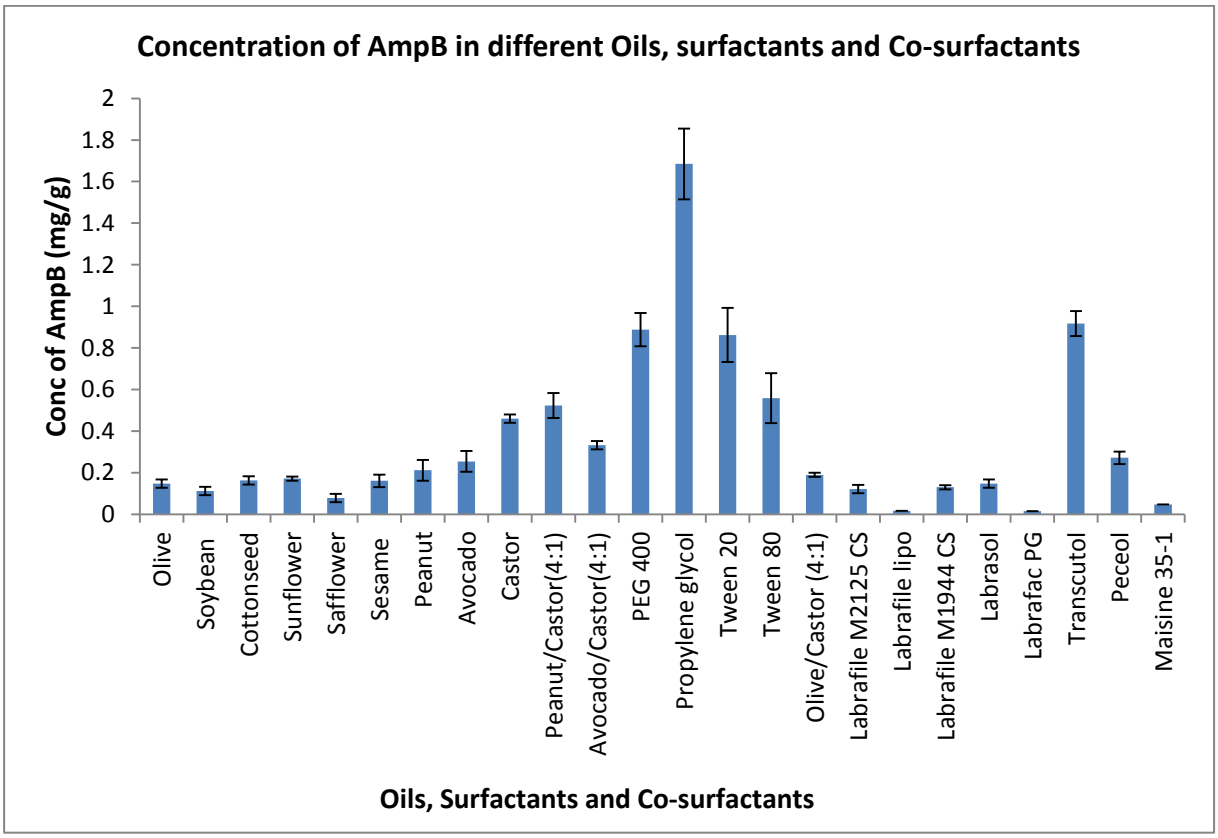

Figure 4.43: solubility of Amphotericin B in different excipients

The solubility of Amphotericin B in various oils, surfactants and co-surfactants are as indicated in figure 4.43. Among the oils, castor oil showed the highest solubility of the drug recording a value of 0.46 ± 0.02 mg/ml followed by Peceol® (0.272±0.03 mg/ml). Combinations of peanut and avocado oils with castor oil also showed improve solubility. Out of the surfactants, Tween 20 solubilized the highest among of the drug and propylene glycol dissolved the highest amount of drug amongst the co-surfactants.

4.5.2 Ternary phase diagrams

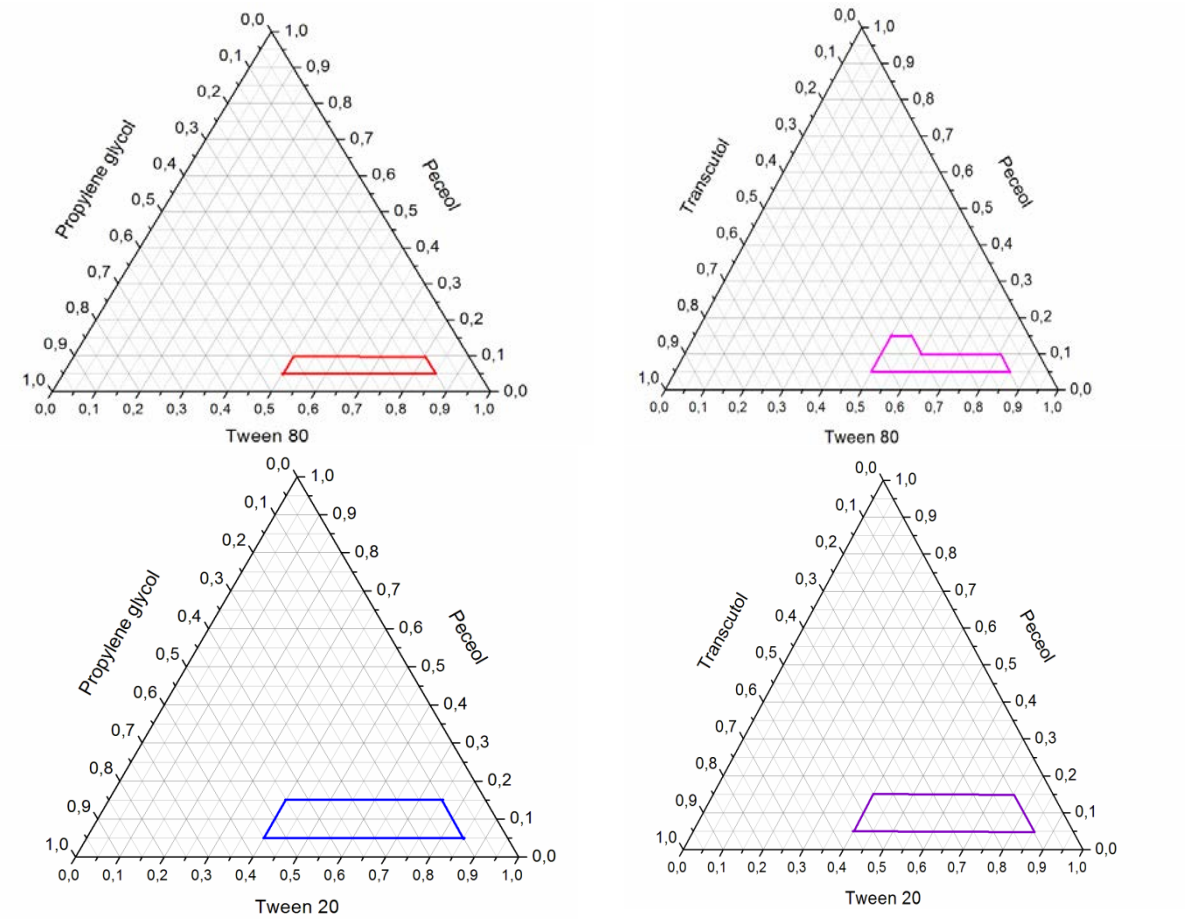

Figure 4.44: Ternary phase diagram with the following components: Peceol, Tween 80, Tween 20, propylene glycol and Transcutol® P.

It is observed from the ternary phase diagrams (Figure 4.44) that the region of emulsification for Tween 20 was larger than Tween 80 with the two co-surfactants and could have some emulsification with oil content up to 15 %. Its minimum surfactant ratio for self-emulsification was 40% as compared to 50 % for Tween 80. The Transcutol® with Tween 80 had a small region of emulsification with 15% of oil.

4.5.3 Emulsification properties of blanks

Sample	Peceol	Tween 80	PG	t_1	t_2	t_3	t-ave (secs)	Result/Grading	Comment	Size (d) nm	PDI
A	5	50	45	18	27	22	22.33 ± 4.51	formed / I	Clear	14.9 ± 0.3	0.334 ± 0.013
B	5	60	35	27	27	30	28.00 ± 1.73	formed / I	Clear	40.0 ± 0.5	0.418 ± 0.019
C	5	70	25	32	30	36	33.07 ± 3.06	formed / I	Clear	14.8 ± 0.3	0.332 ± 0.009
D	5	75	20	48	44	45	46.07 ± 2.08	formed / I	Clear	27.7 ± 0.2	0.530 ± 0.006
E	5	80	15	38	40	42	40.00 ± 2.00	formed / I	Clear	53.0 ± 0.4	0.310 ± 0.006
F	5	85	10	68	88	76	77.33 ± 10.07	formed / I	Clear	15.4 ± 1.4	0.393 ± 0.047
G	10	50	40	34	34	32	33.33 ± 1.15	formed / I	Bluish	63.8 ± 0.5	0.233 ± 0.005
H	10	60	30	34	44	39	39.00 ± 5.00	formed / I	Bluish	72.6 ± 0.8	0.202 ± 0.005
I	10	70	20	95	95	83	91.00 ± 6.93	formed / II	bluish white	156.2 ± 42.1	0.283 ± 0.075
J	10	80	10	> 5	> 5	> 5	> 5 mins	formed / IV	greyish white	184.6 ± 0.6	0.430 ± 0.004
K	8	50	42	90	110	89	96.33 ± 12.25	formed / II	Bluish	42.7 ± 0.6	0.306 ± 0.002
L	8	55	37	77	104	136	105.67 ± 29.54	formed /II	Bluish	77.5 ± 1.0	0.182 ± 0.004
M	8	60	32	132	214	114	153.33 ± 53.30	formed / II	Bluish	65.5 ± 1.4	0.207 ± 0.009
N	8	65	27	200	220	133	184.33 ± 45.57	formed / II	Bluish	74.6 ± 1.3	0.185 ± 0.005
O	8	70	22	107	131	154	131.07 ± 23.50	formed / II	Bluish	76.0 ± 0.5	0.200 ± 0.002
P	8	76	16	150	80	88	106.00 ± 38.31	formed / II	Bluish	73.6 ± 0.7	0.211 ± 0.006

Table 25: Particle size and emulsification time for blank samples of Peceol, Tween 80 and Propylene glycol

Results

Sample	Peceol	Tween 80	Transcutol	t_1	t_2	t_3	t-ave (secs)	Result/Grade	Comment	Size (d) nm	PDI
T_1	15	50	35	47	43	57	49.00 ± 7.21	formed/ II	Bluish white	130.6 ± 2,6	0.177 ± 0.023
T_2	15	55	30	161	179	202	180.07 ± 20.55	formed / IV	Oily surface	196.0 ± 3.1	0.345 ± 0.054
T_3	15	60	25	> 5	> 5	> 5	> 5 mins	Poor / V	Large droplets	221.8 ± 4.2	0.414 ± 0.017
T_4	5	50	45	30	28	22	27.07 ± 4.16	formed / I	Clear	19.8 ± 0.1	0.269 ± 0.035
T_5	5	60	35	21	20	23	21.33 ± 1.53	formed / I	Clear	15.2 ± 1.0	0.340 ± 0.054
T_6	5	66	29	41	36	39	39.07 ± 2.52	formed / I	Clear	11.6 ± 0.2	0.175 ± 0.012
T_7	5	70	25	26	28	25	26.33 ± 1.53	formed / I	Clear	13.4 ± 0.8	0.263 ± 0.037
T_8	5	80	15	37	34	36	33.07 ± 1.53	formed / I	Clear	17.7 ± 0.7	0.416 ± 0.055
T_9	5	85	10	41	38	47	42.00 ± 4.58	formed / I	Clear	13.8 ± 1.5	0.294 ± 0.064
T_{10}	10	50	40	21	29	24	25.07 ± 4.04	formed / I	Bluish	71.7 ± 0.6	0.210 ± 0.007
T_{11}	10	60	30	44	33	36	38.07 ± 5.69	formed / I	Bluish	101.1 ± 0.2	0.139 ± 0.008
T_{12}	10	65	25	51	70	106	76.07 ± 28.33	formed / II	Bluish	76.3 ± 1.1	0.161 ± 0.017
T_{13}	10	70	20	38	40	40	39.33 ± 1.15	formed / I	bluish	76.0 ± 2.6	0.183 ± 0.010
T_{14}	10	76	14	107	102	78	96.07 ± 15.50	formed /II	Bluish	90.3 ± 1.2	0.187 ± 1.2
T_{15}	10	80	10	50	93	83	75.33 ± 22.50	formed / II	Bluish-white	153.7 ± 0.6	0.437 ± 0.020

Table 26: Particle size and emulsification time for blank samples of Peceol, Tween 80 and Transcutol P

Results

Tables 25 and 26 indicate the various parameters determined for blank samples prepared with propylene glycol and Transcutol® respectively using Peceol and Tween 80. It was generally observed that oil content above 15 % resulted in mixtures with large droplet size which had poor self-emulsification properties with some not forming the emulsion at all. It is also observed that mixtures that formed large droplets in aqueous medium resulted in increased emulsification time and that correlated with its appearance (Tables 25 and 26).

4.5.4 Emulsification properties of pre-concentrates

Table 27: Drug content, particle size and emulsification time of Peceol, Tween 80 and propylene glycol pre-concentrate

Sample	**Peceol**	**T80**	**PG**	**t_1**	**t_2**	**t_3**	**t-ave (secs)**	**Amount of AmpB (mg/g)**	**Fate of drug in emulsion after 24 hrs**	**Size (d) nm**	**PDI**	**Stability:one week**
A	5	50	45	46	48	35	43.00 ± 7.00	1.114 ± 0.079	No visible ppt	615 ± 130.7	0.706 ± 0.051	SDMT
B	5	60	35	57	44	60	54.07 ± 8.50	1.070 ± 0.058	No visible ppt	1158.1 ± 337.5	0.934 ± 0.025	SDMT
C	5	70	25	66	67	84	72.33 ± 10.12	0.890 ± 0.056	No visible ppt	1410.8 ± 619.8	0.915 ± 0.137	SDMT
D	5	75	20	84	74	90	83.07 ± 8.08	1.065 ± 0.163	No visible ppt	1341 ± 448.6	0.877 ± 0.107	SDMT
E	5	80	15	152	139	200	164.07 ± 32.13	0.705 ± 0.019	No visible ppt	977 ± 598.6	0.789 ± 0.193	SDMT
F	5	85	10	225	237	230	231.07 ± 6.03	1.083 ± 0.153	No visible ppt	1169.3 ± 181.7	0.884 ± 0.110	SDMT
G	10	50	40	74	62	70	69.07 ± 6.11	1.063 ± 0.016	No visible ppt	118.3 ± 4.9	0.278 ± 0.045	SDMT
H	10	60	30	140	98	121	120.07 ± 21.03	1.058 ± 0.181	No visible ppt	96.5 ± 1.7	0.302 ± 0.035	SDMT

Results

I	10	70	20	135	110	225	157.07 ± 60.48	0.898 ± 0.065	No visible ppt	112.7 ± 22.7	0.309 ± 0.045	SDMT
K	8	50	42	48	43	41	44.00 ± 3.61	1.288 ± 0.220	No visible ppt	115 ± 21.8	0.353 ± 0.080	SDMT
L	8	55	37	32	33	35	33.33 ± 1.53	0.933 ± 0.081	No visible ppt	283.5 ± 108.9	0.373 ± 0.071	SDMT
M	8	60	32	38	42	43	41.00 ± 2.65	1.407 ± 0.175	No visible ppt	146.2 ± 6.2	0.459 ± 0.244	SDMT
N	8	65	27	35	38	30	34.33 ± 4.04	0.777 ± 0.086	No visible ppt	153.3 ± 65.1	0.306 ± 0.040	SDMT
O	8	70	22	35	32	37	35.07 ± 2.52	0.749 ± 0.132	No visible ppt	135.9 ± 57.5	0.331 ± 0.034	SDMT
P	8	76	16	52	56	55	54.33 ± 2.08	0.781 ± 0.150	No visible ppt	106.5 ± 27.8	0.387 ± 0.007	SDMT

- ppt = precipitate
- SDMT = Sedimentation

Results

Table 28: Drug content, particle size and emulsification time of Peceol, Tween 80 and Transcutol P pre-concentrate

Sample	Peceol	T80	Trans	t_1	t_2	t_3	t-ave (secs)	Amount of AmpB (mg/g)	Fate of drug in emulsion after 24 hrs	Size (d) nm	PDI	Stability:one week
T_4	5	50	45	39	32	29	33.33 ± 5.13	0.295 ± 0.009	No visible ppt	673.5 ± 70.4	0.745 ± 0.127	SDMT
T_6	5	66	29	30	33	40	34.33 ± 5.13	0.749 ± 0.066	No visible ppt	1072.2 ± 176.1	0.849 ± 0.055	SDMT
T_7	5	70	25	36	38	37	37.00 ± 1.00	0.787 ± 0.065	No visible ppt	936.2 ± 248.0	0.794 ± 0.062	SDMT
T_8	5	80	15	60	81	80	74.07 ± 11.85	1.071 ± 0.155	No visible ppt	1524.2 ± 563.9	0.930 ± 0.122	SDMT
T_9	5	85	10	110	80	78	89.33 ± 17.93	0.964 ± 0.060	No visible ppt	1760.0 ± 622.3	0.992 ± 0.014	SDMT
T_{10}	10	50	40	40	50	54	48 ± 7.21	0.323 ± 0.098	No visible ppt	91.3 ± 0.3	0.305 ± 0.002	SDMT
T_{11}	10	60	30	49	57	48	51.33 ± 4.93	0.827 ± 0.073	No visible ppt	99.3 ± 9.8	0.291 ± 0.049	SDMT
T_{12}	10	65	25	93	73	82	83.07 ± 10.02	1.086 ± 0.054	No visible ppt	97.7 ± 12.4	0.316 ± 0.071	SDMT
T_{13}	10	70	20	71	92	88	80.07 ± 11.15	1.082 ± 0.024	No visible ppt	98.6 ± 6.0	0.359 ± 0.014	SDMT
T_{14}	10	76	14	115	119	112	115.33 ± 3.51	1.270 ± 0.021	No visible ppt	123.3 ± 4.3	0.304 ± 0.022	SDMT
T_1	15	50	35	140	161	266	189.00 ± 67.51	0.627 ± 0.050	No visible ppt	226.5 ± 5.3	0.379 ± 0.026	SDMT
T_2	15	55	30	207	184	180	190.33 ± 14.57	0.792 ± 0.124	No visible ppt	232.9 ± 5.7	0.435 ± 0.018	SDMT

- ppt = precipitate
- SDMT = Sedimentation

The above tables (tables 27 and 28) show the parameters evaluated for the drug containing pre-concentrates for the propylene glycol and Transcutol®. In general terms, the amount of drug solubilised by the propylene glycol emulsion decreased with increased surfactant concentration at a fixed oil and co-surfactant (table 27). This also resulted in increase in emulsification time. Increasing the co-surfactant concentration also resulted in increased drug load and faster emulsification. These trends are depicted graphically in figures 4.45A and 4.46A.

The Transcutol® emulsion on the other hand showed increased drug load with increasing surfactant at a fixed oil and co-surfactant concentrations (Table 28 and figure 4.45B). This led to faster emulsification. Contrary to the effect of co-surfactant on the propylene glycol emulsion, the Transcutol® emulsion showed a decrease drug solubilisation with increasing co-surfactant concentration (Table 28 and figure 4.46B)

4.5.5 Effect of surfactant and co-surfactant on drug content

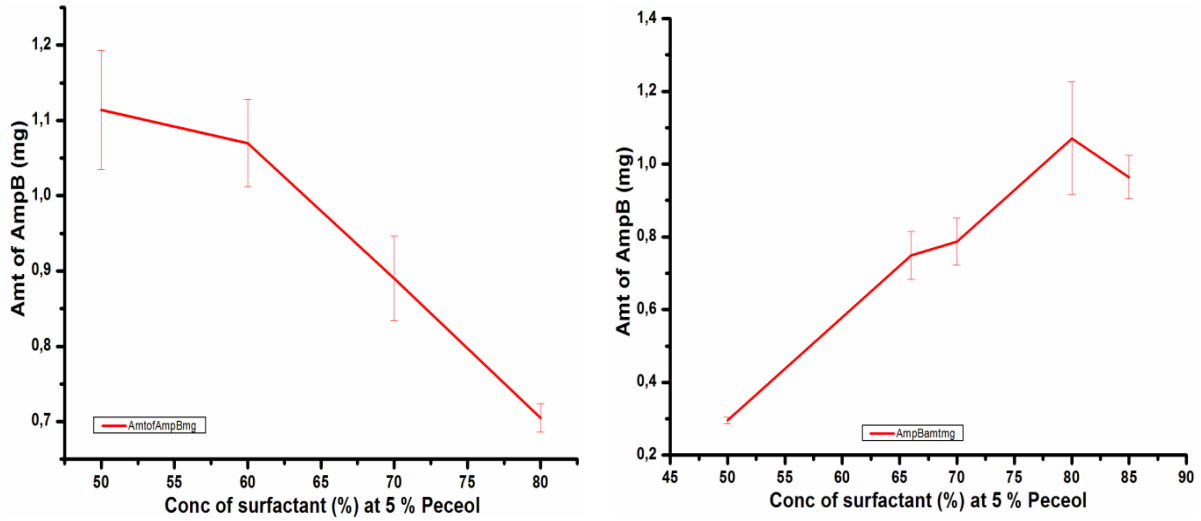

(A) Surfactant with drug (PG) (B) Surfactant with drug (Transcutol)

Figure 4.45: Effect of surfactant concentration on drug content

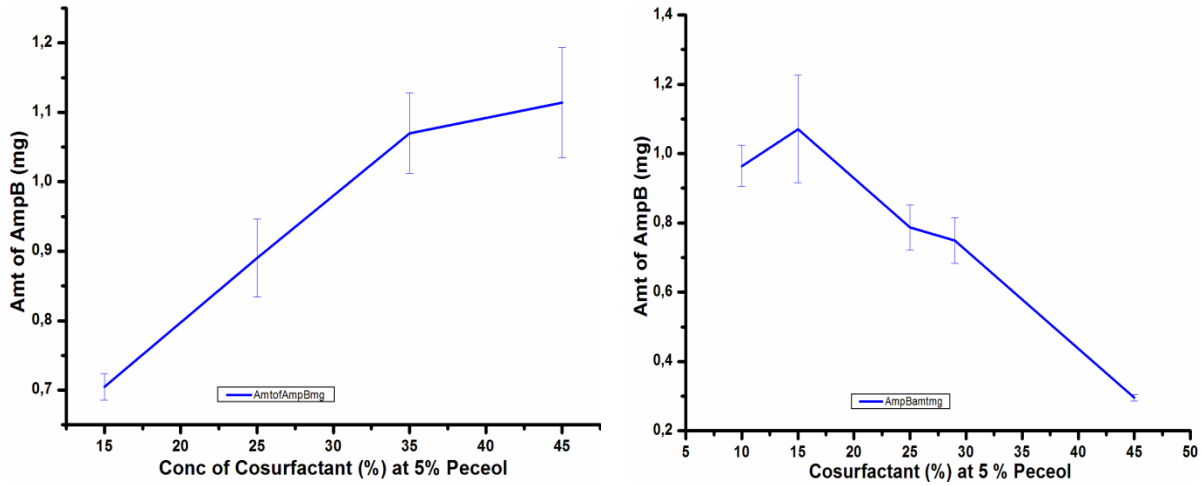

(A) Propylene glycol (B) Transcutol P

Figure 4.46: Effect of co-surfactants concentration on drug content

4.5.6 Effect of surfactant and co-surfactants on droplet size

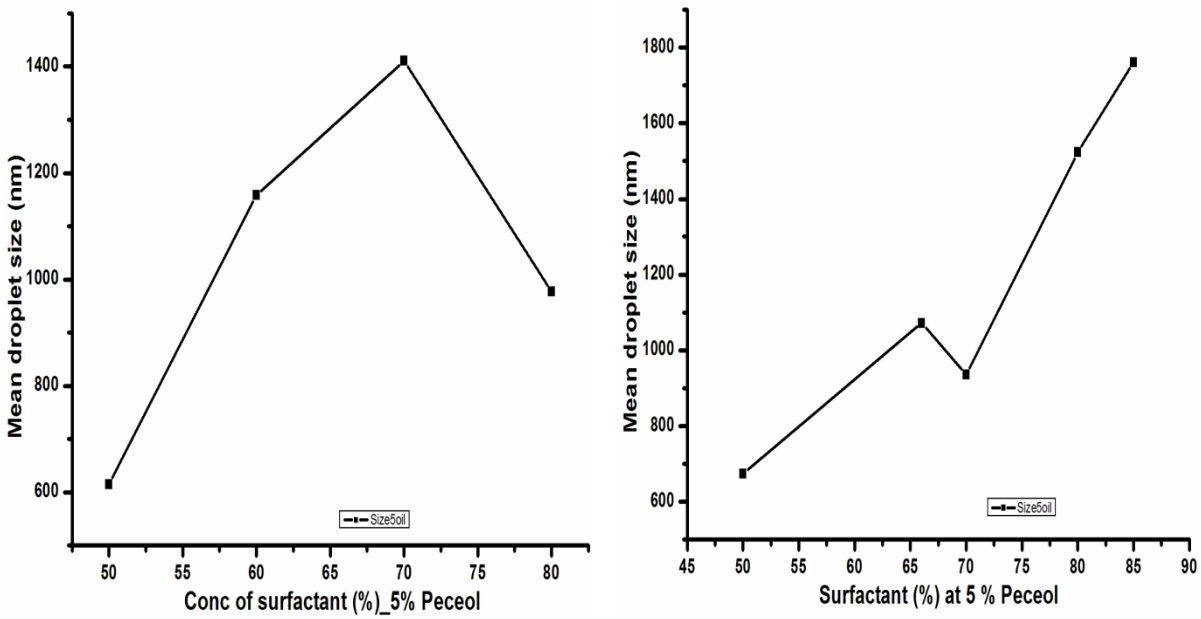

(A) Propylene glycol (B) Transcutol

Figure 4.47: Effect of surfactant on droplet size

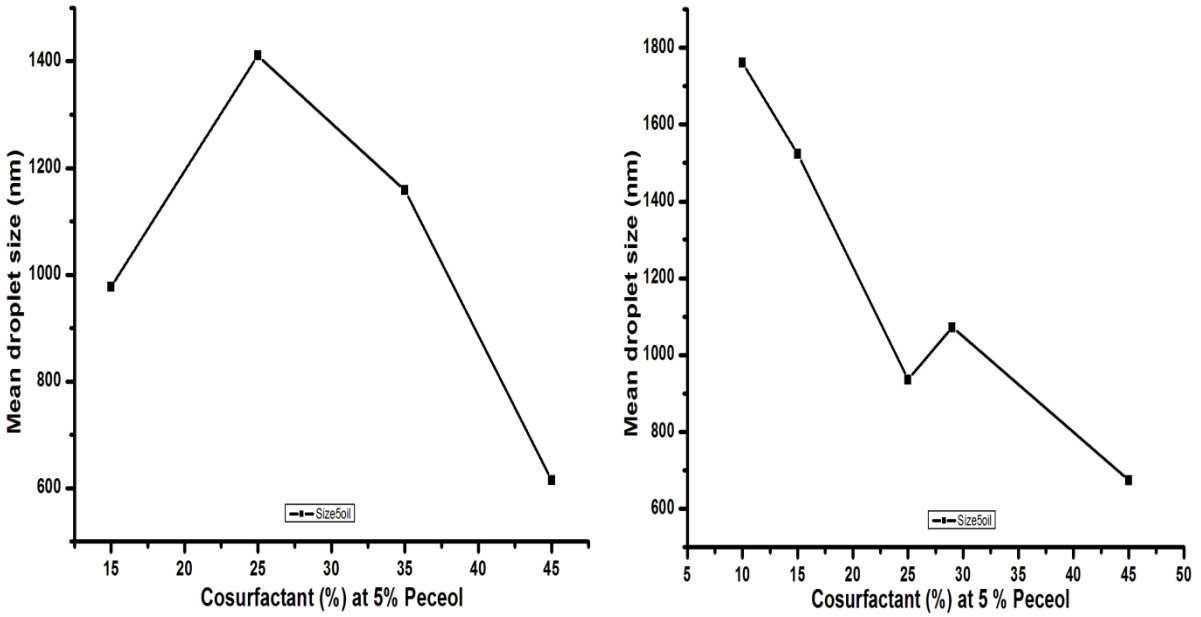

(A) Propylene glycol (B) Transcutol

Figure 4.48: Effect of co-surfactants on droplet size

The increase in surfactant concentration generally increased the droplet size of both formulations as depicted in figure 4.47A and B. After 70% of Tween 80 the droplet size decreased for the propylene glycol emulsion whilst there was a continuous increase for that containing Transcutol®.

Figures 4.48A and 4.48B show graphical representation of the effect of the co-surfactants on the droplet size of the emulsions. As shown above, there was a general decrease in droplet size for the Transcutol® as co-surfactant. However, for the propylene glycol the size increased from 15% to 25% before decreasing afterwards with increasing content of propylene glycol.

4.5.7 Precipitation study of nanoemulsions

The nanoemulsion produced after dilution in water was kept at ambient temperature for 24 hours and some for 72 hours. No precipitate was observed after 24 hours for all samples. However, after 72 hours sedimentation of the drug was visually observed for samples with higher drug load.

4.5.8 UV-Visible spectrum of Amphotericin B in nanoemulsion

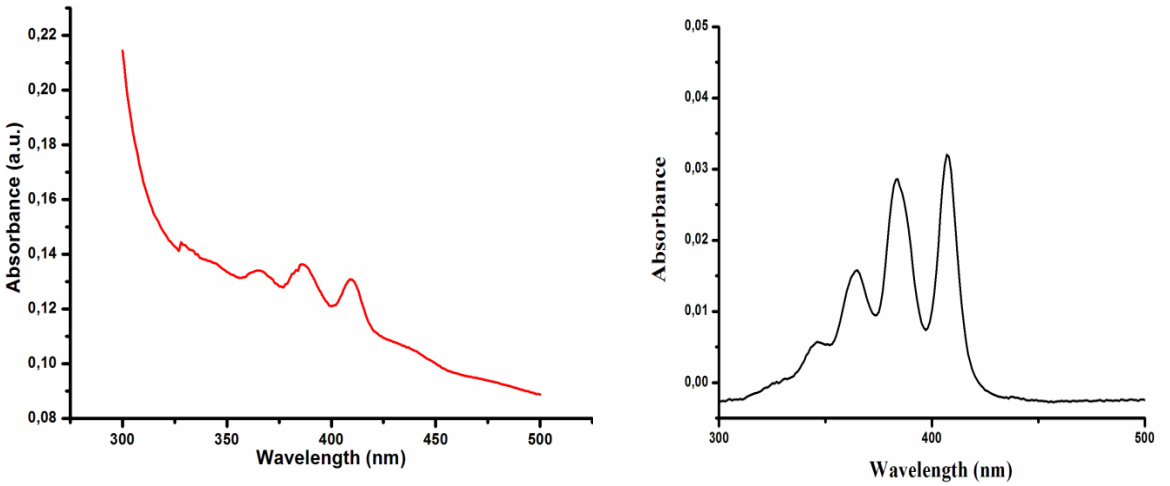

Figure 4.49: Spectrum of Amphotericin B in nanoemulsion diluted in water (left) and in methanol (right)

The spectrum of Amphotericin B in methanol shows four peaks with decreasing intensity. The drug in the aqueous nanoemulsion has three peaks with diminished intensity occurring at wavelengths of 409, 386 and 366 nm which depict the drug as also in monomeric form. The spectrum is identical for all tried formulations irrespective of the excipient concentration.

4.5.9 Optimisation of formulations

The drug content for the formulations of both the propylene glycol and the Transcutol® were less than 2 mg per gram of total excipients. This amount is highly inadequate for oral application considering even the dose that is used parenterally. The formulations were optimised based on process conditions. The maximum saturated solubility for the propylene glycol emulsion was 2.197 ± 0.049 mg/g at 20 minutes sonication and 2500 rpm centrifugation and that for the Transcutol® was 1.814 ± 0.063 mg/g at 40 minutes sonication and same speed of centrifugation as the propylene glycol emulsion.

Results

Table 29: Optimisation of Peceol®, Tween 80 and propylene glycol nanoemulsion pre-concentrate

Parameter	Variable	Sample	Drug content (mg/g)	Emulsification Time (secs)	Particle size (d) nm	PDI
Centrifugation Speed at 20 mins sonication	4000 rpm	G	1.320 ± 0.094	70.33 ± 2.52	115.5 ± 3.9	0.332 ± 0.043
		K	1.482 ± 0.068	48.00 ± 3.61	105.5 ± 10.1	0.348 ± 0.057
		M	1.609 ± 0.056	55.33 ± 3.51	132.1 ± 34.2	0.307 ± 0.071
	2500 rpm	G	2.197 ± 0.049	87.00 ± 10.44	116.8 ± 1.0	0.300 ± 0.022
		K	1.712 ± 0.107	68.07 ± 4.73	117.5 ± 26.6	0.317 ± 0.018
		M	1.760 ± 0.141	68.00 ± 7.07	119.2 ± 17.0	0.365 ± 0.046
Time of sonication at 2500 rpm centrifugation	30 mins	G	2.062 ± 0.125	102.00 ± 26.06	119.3 ± 1.7	0.346 ± 0.034
		K	1.687 ± 0.088	142.00 ± 7.21	429.6 ± 25.6	0.481 ± 0.026
		M	1.888 ± 0.110	125.00 ± 5.57	311.0 ± 140	0.488 ± 0.136
	40 mins	G	2.007 ± 0.093	98.07 ± 22.01	122.5 ± 5.3	0.374 ± 0.055
		K	2.041 ± 0.054	91.00 ± 8.14	157.1 ± 40.4	0.356 ± 0.046
		M	2.033 ± 0.089	105.33 ± 20.55	270.3 ± 69.4	0.408 ± 0.017

Results

Table 30: Optimisation of Peceol®, Tween 80 and Transcutol® P emulsion pre-concentrate

Parameter	Variable	Sample	Drug content (mg/g)	Emulsification Time (secs)	Particle size (d) nm	PDI
Centrifugation Speed at 20 mins sonication	4000 rpm	T_{12}	1.378 ± 0.038	111.00 ± 24.30	116.9 ± 29.4	0.311 ± 0.073
		T_{13}	1.452 ± 0.050	95.33 ± 28.54	123.8 ± 13.2	0.278 ± 0.026
		T_{14}	1.622 ± 0.050	98.00 ± 12.12	154.1 ± 4.4	0.344 ± 0.030
	2500 rpm	T_{12}	1.557 ± 0.108	137.00 ± 13.17	117.3 ± 29.8	0.314 ± 0.075
		T_{13}	1.657 ± 0.113	142.07 ± 26.17	119.7 ± 19.9	0.365 ± 0.080
		T_{14}	1.643 ± 0.063	93.07 ± 10.21	131.0 ± 22.2	0.285 ± 0.076
Time of sonication at 2500 rpm centrifugation	30 mins	T_{12}	1.534 ± 0.177	140.07 ± 17.04	163.9 ± 21.0	0.269 ± 0.024
		T_{13}	1.852 ± 0.098	122.33 ± 13.05	130.2 ± 13.8	0.399 ± 0.160
		T_{14}	1.690 ± 0.068	109.07 ± 21.01	123.3 ± 2.7	0.371 ± 0.031
	40 mins	T_{12}	1.562 ± 0.024	131.00 ± 21.06	99.8 ± 1.3	0.280 ± 0.023
		T_{13}	1.813 ± 0.109	128.07 ± 21.22	112.0 ± 23.7	0.336 ± 0.065
		T_{14}	1.814 ± 0.063	136.00 ± 17.35	110.8 ± 7.9	0.353 ± 0.048

Results

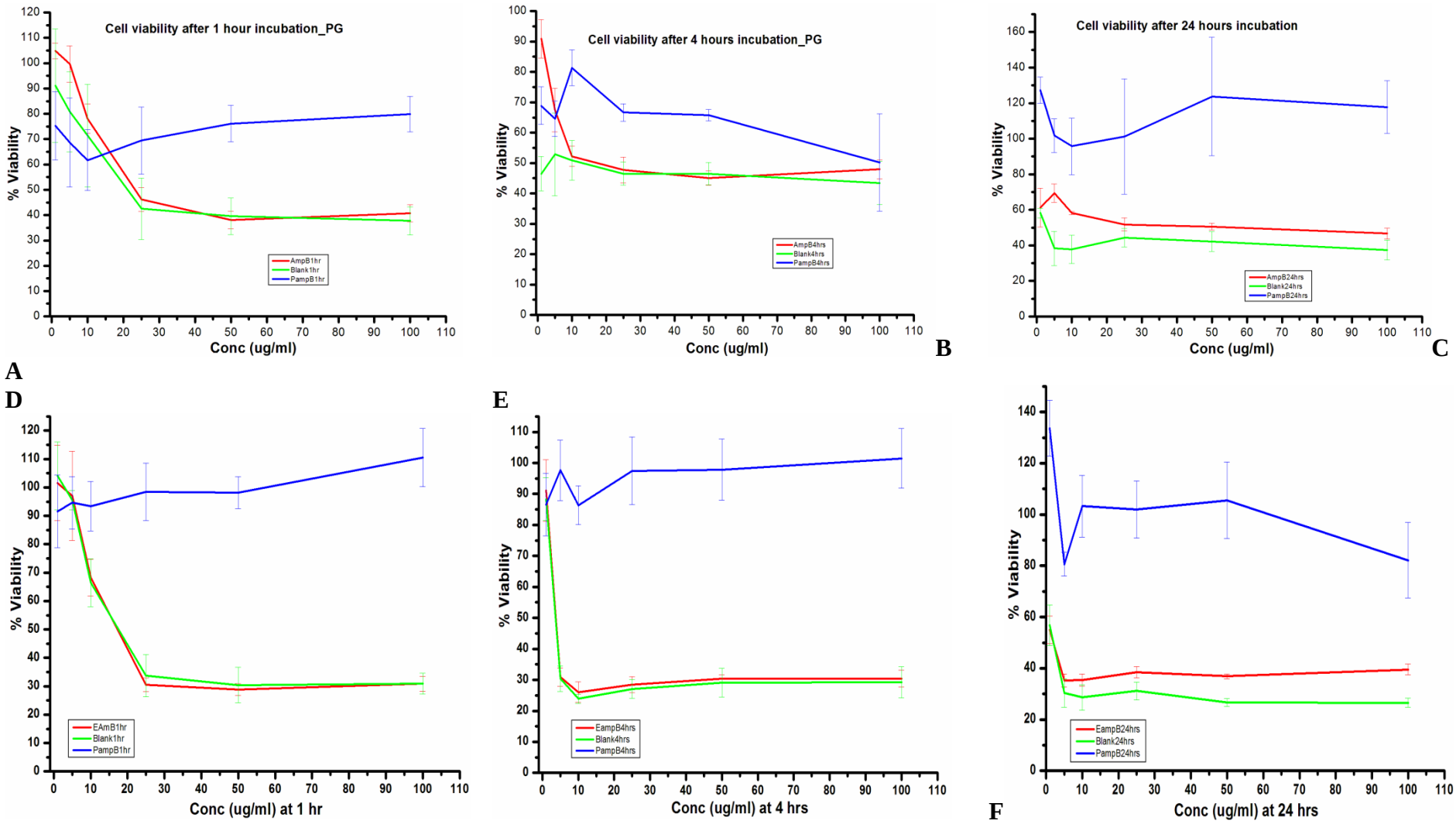

Figure 4.50: Cell viability test for propylene glycol (A, B and C) and Transcutol® P (D, E and F) emulsions at 1, 4 and 24 hours incubation.

Results

After incubation for 1, 4 and 24 hours, the cell viability test for emulsion containing Peceol®, Tween 80 and propylene glycol indicated viability above 50% at concentrations less than or equal to 10 µg/ml (figure 4.50A, B and C). There was no significant difference ($p>0.05$) between the viability of the drug containing emulsion, blank and the plain drug suspension for the one hour incubation by a one-way analysis of variance (ANOVA). For the four hours incubation, cell viability were 47.93±3.08, 43.46±7.12% and 50.16±16.02% respectively at 100µg/ml. Analysis of the viability for the four hours incubation period also showed no significant difference ($p>0.05$). The blank and the drug containing emulsions were more toxic ($p<0.05$) than the plain drug suspension to the Caco-2 cells for the 24 hours incubation. Cell viability was about 40% for the blank and 50% for the drug containing emulsion at concentrations of above 25µg/ml. In all cases the blank showed more toxicity than the drug containing emulsion.

In comparison to the propylene glycol emulsion, the Transcutol® P containing emulsion was more toxic to the growing cells. The concentration of drug with above 50% viability was 1 µg/ml for 4 and 24 hours incubation. For 1 hour, the viability above 50% was 10 µg/ml (figure 4.50 C, D and E). Above 25 µg/ml the viability had reduced to about 30%. The 100 µg/ml concentration recorded about 25% viability at all incubation times. Here too, there was no significant difference between the drug containing emulsion and the blank ($p>0.05$) but both were significantly different from the plain drug suspension ($p<0.05$) for the one hour incubation. The same trend was observed for incubation times of 4 and 24 hours. In all cases the suspension of the plain drug recorded cell viability above 70%.

4.5.10 Hemolysis test of nanoemulsions

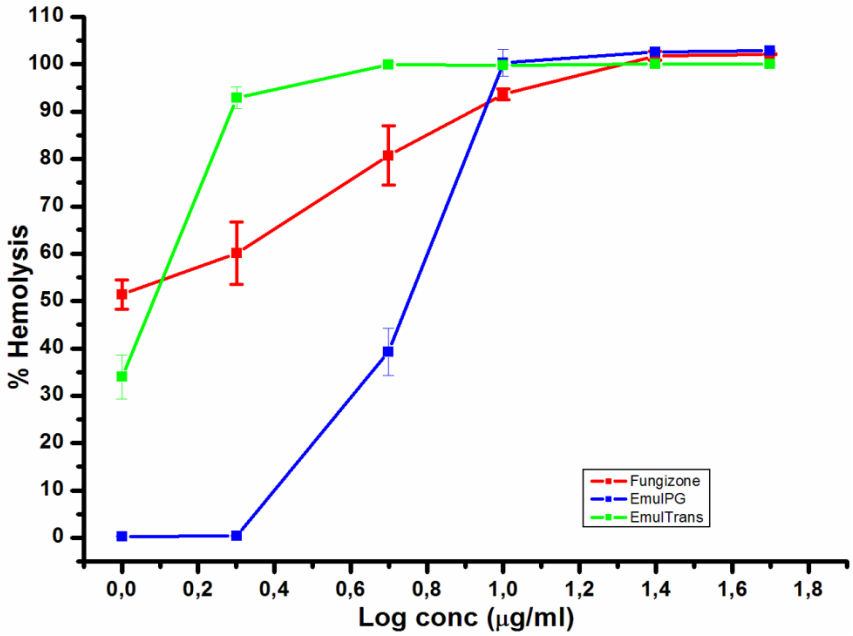

Figure 4.51: Hemolysis effect of Amphotericin B nanoemulsions on human red blood cells in comparison to Fungizone®.

Results

Figure 4.51 shows the hemolytic effect of the various formulations on human red blood cells. There was a general increase in hemolysis with increasing concentration. The effect of the emulsion with propylene glycol was less as compared to the emulsion with the Transcutol® and the Fungizone® at lower concentrations. The concentration causing 50% hemolysis of red blood cells (HC_{50}) was 0.85µg/ml, 5.89µg/ml and 1.33µg/ml respectively for Fungizone®, propylene glycol and Transcutol emulsions. However, there was no significant difference ($p>0.05$) between the hemolytic effect of the three formulations.

4.5.11 Rheology of pre-concentrates

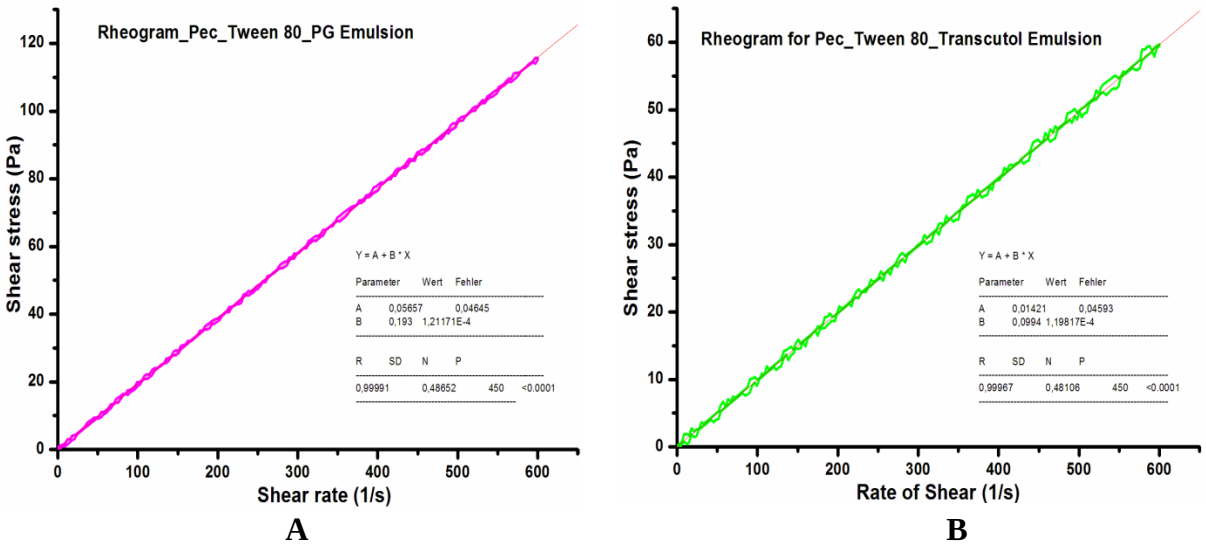

A **B**

Figure 4.52: Flow curves of shear stress against shear rate for the optimized formulations: A) rheogram for Peceol®, tween 80 and propylene glycol and B) rheogram for Peceol®, tween 80 and Transcutol®.

The two formulations exhibited Newtonian properties as indicated in figure 4.52. The slope of the curve gives the viscosity of the emulsions. Thus, the Transcutol® emulsion is slightly less viscous (0.0994±0.0001 Pas) than the propylene glycol emulsion with a viscosity of 0.193±0.0001 Pas at room temperature (Reference: Water is 0.000890 Pas at 25^{o}C or 0.890 cP).

4.5.12 Structure determination of nanoemulsion by small angle neutron scattering

Micoemulsions are considered as droplets of internal phase dispersed in a continuous phase. Droplets are assumed to be spherical in shape. This is the envisaged model in the investigation of the structure of the prepared nanoemulsions with drug and blank. The contrast between droplets and continuous phase was improved with 71% D_2O buffer. The scattering curves, Guinier and Kratky-Porod plots of the drug containing nanoemulsions and their blanks are given below.

Results

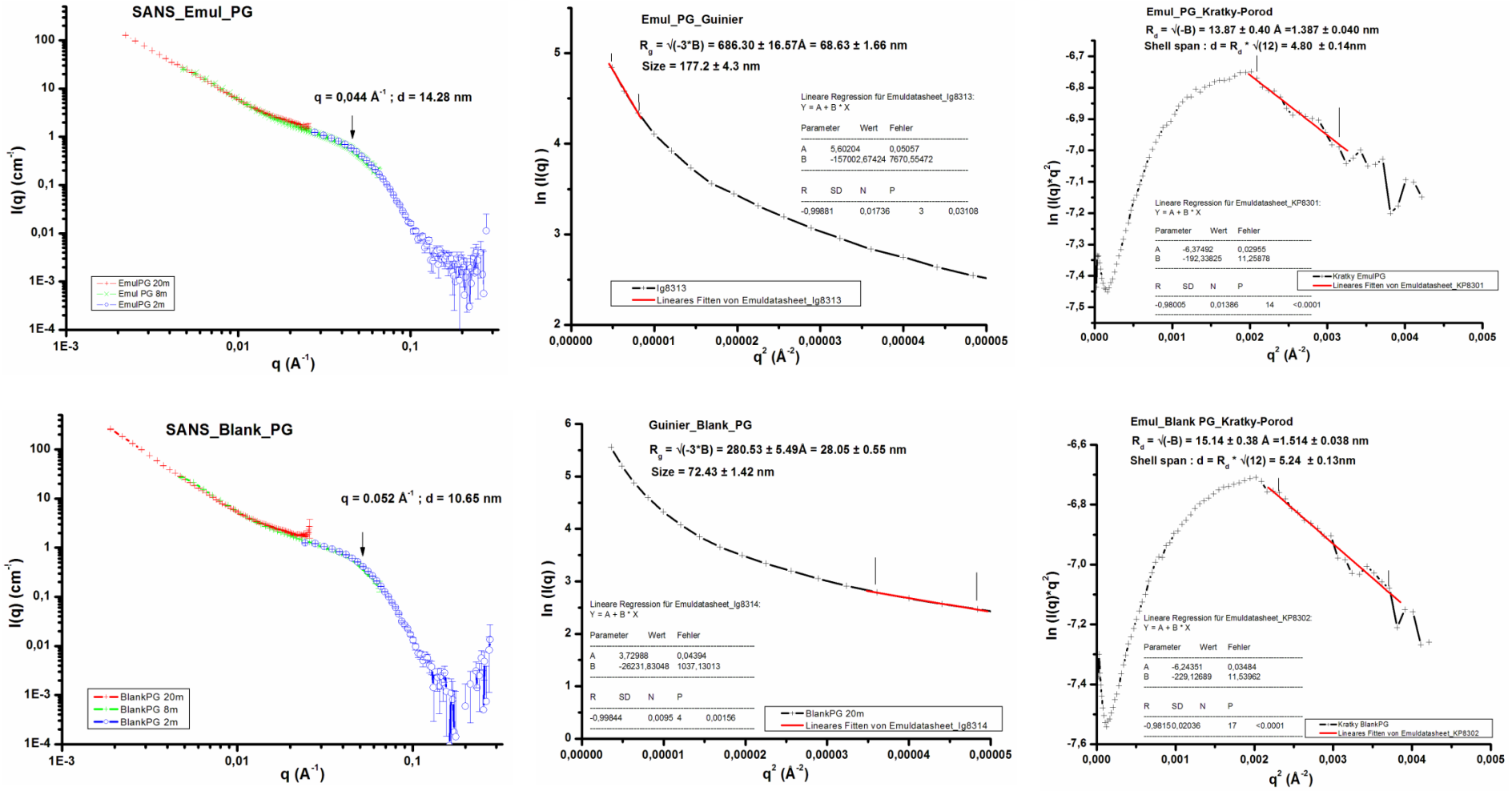

Figure 4.53: The scattering profile, Guinier plot for the estimation of radius of gyration (R_g) and Kratky-Porod plot for the estimation of interfacial film layer (d) of the propylene glycol nanoemulsion containing Amphotericin B (top) and its drug-free reference (bottom).

Results

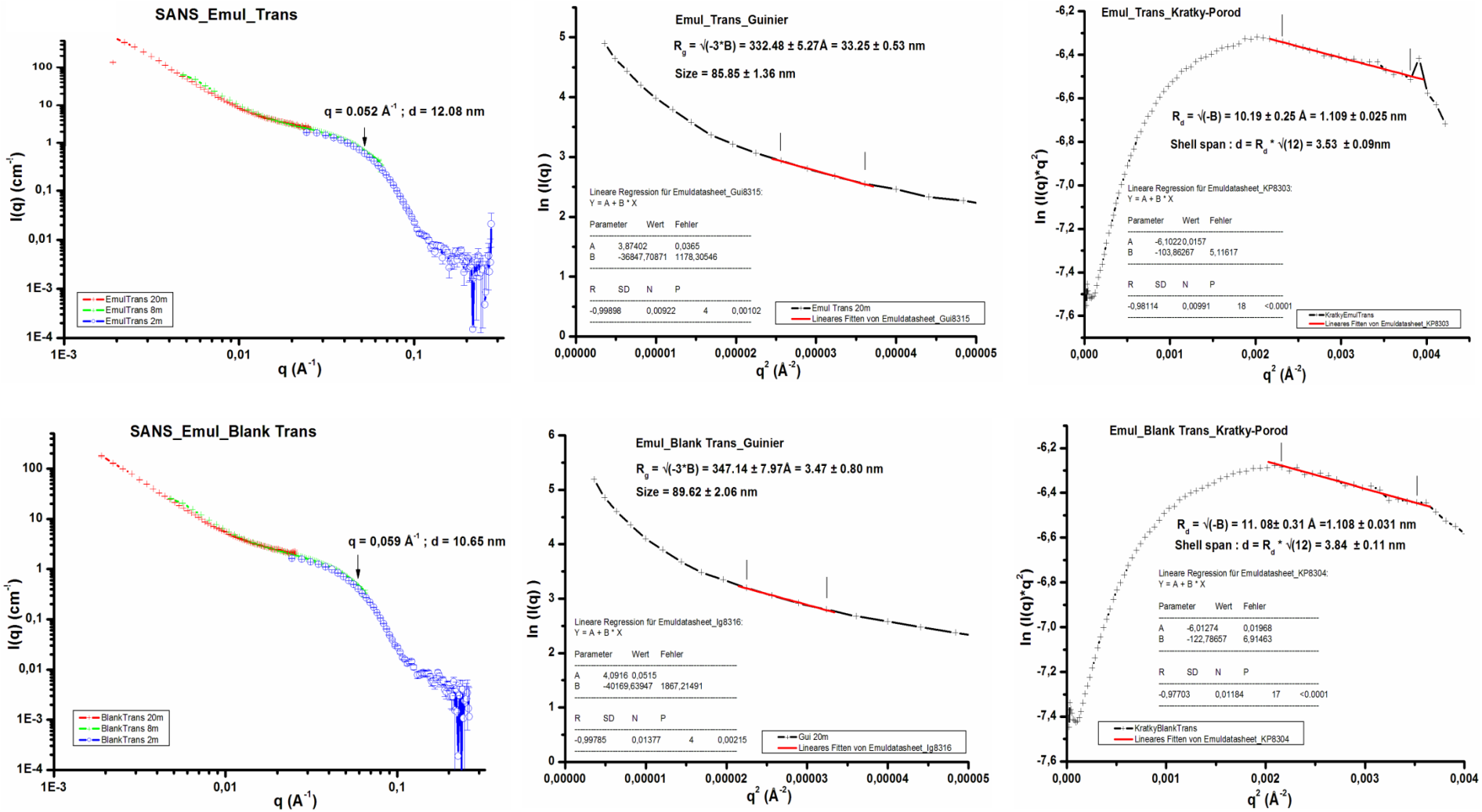

Figure 4.54: The scattering profile, Guinier plot for the estimation of radius of gyration (R_g) and Kratky-Porod plot for the estimation of interfacial film layer (d) of the Transcutol® nanoemulsion containing Amphotericin B (top) and its drug-free reference (bottom).

The evaluated parameters are summarized in table 31.

Table 31: SANS parameters evaluated for the nanoemulsions

Sample	Droplet size (SANS) nm	Inter-droplet distance (nm)	Interfacial film span (nm)
Emulsion with Propylene glycol (PG)	177.20 ± 4.30	14.28	4.80 ± 0.14
Blank with Propylene glycol	72.43 ± 1.42	10.65	5.24 ± 0.13
Emulsion with Transcutol®	85.85 ± 1.36	12.08	3.53 ± 0.09
Blank with Transcutol®	89.62 ± 2.06	10.65	3.84 ± 0.11

The scattering curves showed Bragg peaks in both drug containing and blank emulsions and seemed to have the same curvature. These peaks are representative of inter-droplet distance. This distance was higher in the drug containing emulsions as compared to the blanks. The blank emulsion containing propylene glycol and that containing Transcutol® had the same inter-droplet distance. The extension of the curves at lower q shows some level of droplet aggregation in all the samples. The droplet size calculated out of the Guinier plots for the propylene glycol nanoemulsion confirmed that measured by dynamic light scattering where the drug containing emulsion had larger size than the blank. The droplet size for the Transcutol® emulsion and its blank was however comparable. The interfacial film span calculated from the Kratky-Porod plots indicated the blanks having higher span than the drug containing emulsions. The Transcutol® emulsions have span slightly lower than normal biological membrane span (4–5 nm). However, the drug containing propylene glycol emulsion had interfacial film span similar to that of a biological membrane with that of its blank slightly higher.

4.5.13 Stability study of nanoemulsions

The two pre-concentrates were both kept at room temperature and in the refrigerator to evaluate their stability. The drug content and the droplet size were determined periodically. The study was to assess if they could be kept at room temperature without any adverse effect on drug content and droplet size as this would be cost effective. The results are indicated in figures 4.55 and 4.56 respectively for drug content and droplet size.

Results

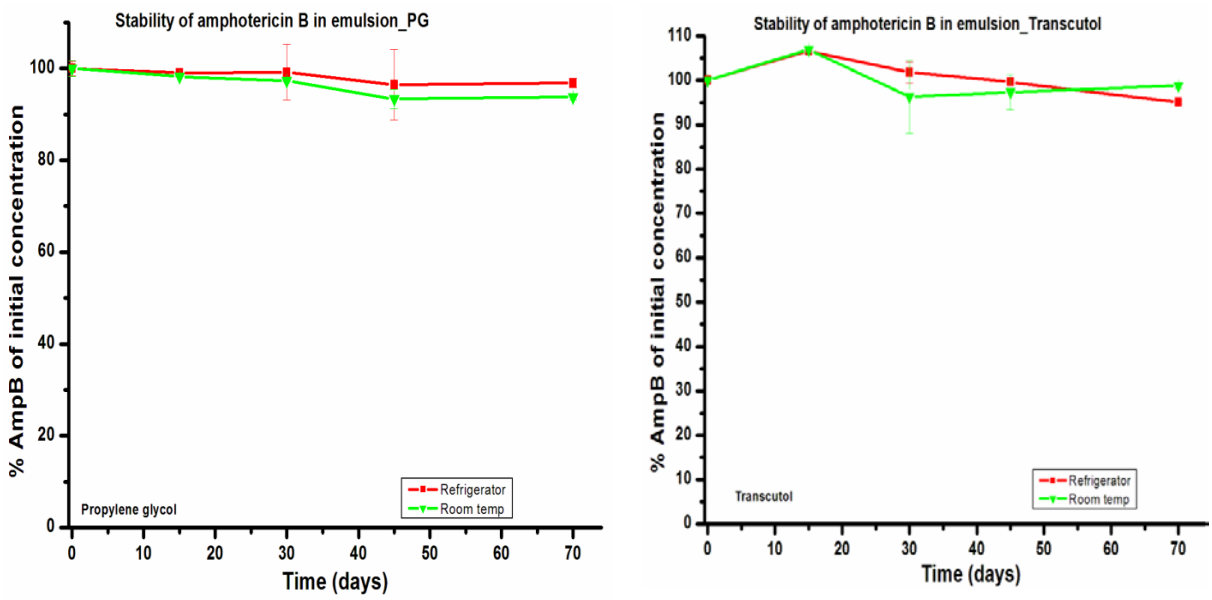

Figure 4.55: Drug content of the pre-concentrates of the propylene glycol and Transcutol® kept at room temperature (RT) and in the refrigerator (2-8^{o}C) for a period of 70 days.

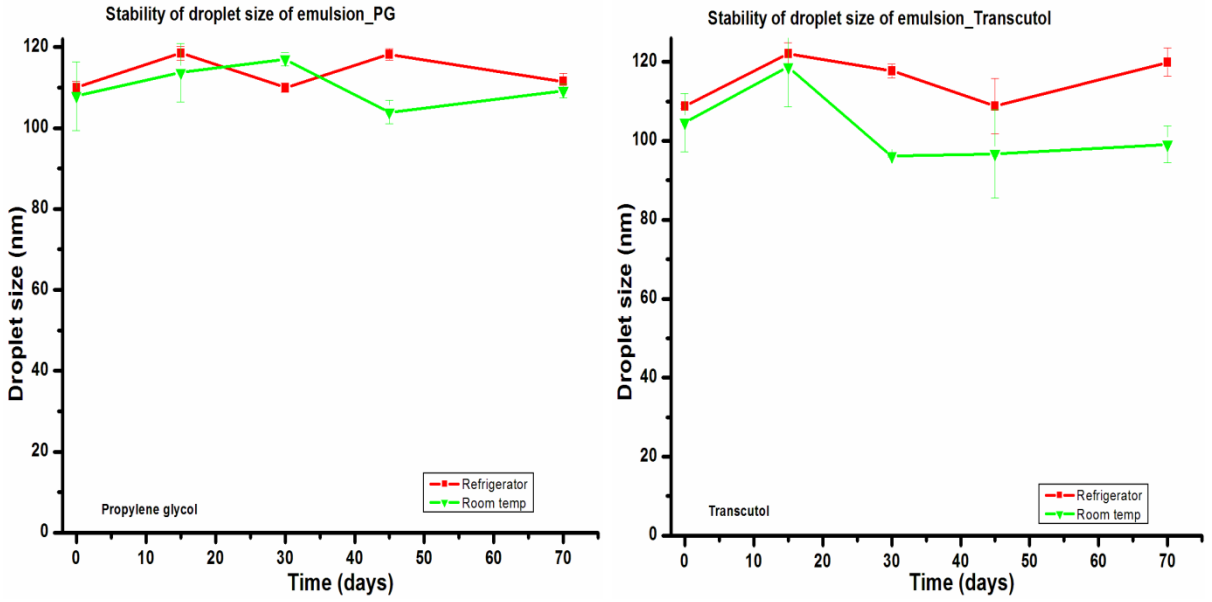

Figure 4.56: Droplet size of the pre-concentrates of propylene glycol and Transcutol® kept at room temperature (RT) and in the refrigerator for 70 days.

The drug contents were determined as a percentage of the initial. There was no significant difference ($p>0.05$) between the propylene glycol pre-concentrate stored at room temperature and in the refrigerator for the 70 days period. The same effect was also observed for the pre-concentrate prepared with the Transcutol®, Peceol® and Tween 80.

There was no considerable difference ($p>0.05$) in droplet size of the propylene glycol, Peceol® and Tween 80 pre-concentrate stored at room temperature and in the refrigerator over the period of the study. However, the was a decrease in droplet size of the Transcutol® pre-concentrate kept at room temperature in comparison to the one kept in the refrigerator ($p<0.05$).

5. DISCUSSION

Disseminated fungal infections such as candidiasis, histoplasmosis and aspergillosis are on the increase, mostly affecting patients with immunocompromised diseases such as cancer and HIV/AIDS. In these patients, invasive fungal infections account for about 30% of deaths (Wasan et al.2009). Despite advances in development of antifungal agents, Amphotericin B remains one of the most effective drugs for the treatment of systemic fungal infections and also effective against the protozoan infection, leishmaniasis. The delivery systems developed so far for the use of this important and effective drug is for parenteral administration due to the poor aqueous solubility and permeability properties of the drug. This route of administration of the drug has its intended safety issues such as indwelling catheter, rigors due to red blood cell hemolysis and dose dependent renal toxicity. This requires that the drug has to be administered under surveillance, hence by hospitalization. This adds to the cost of treatment in addition to the cost of the products and storage conditions.

The search for an effective and safe oral formulation of Amphotericin B has been on the increase over the decades. This work thus attempts to improve the solubility of the drug by employing solubility enhancing excipients such as lipids, surfactants, co-solvents and low molecular weight polymers. These agents are also known to enhance the permeation and hence the bioavailability of poorly soluble drugs. The amount of drug solubilized by the application of these agents partly determines the suitability of the delivery system for oral administration. Due to hepatic first pass effect and intestinal metabolism, drugs administered orally must have a higher dose than that used parenterally. Most surfactants and co-solvents have toxicity limits. Thus, the amount of such excipients administered per day or per treatment is very critical especially for long term treatments. With these considerations, this work incorporated Amphotericin B into three different nanoformulations to assess its suitability for oral use.

The first was using soybean lecithin (lipid) and gelatin (polymer) to solubilize the drug by the Hydrophilic Solubilisation Technology developed by Hilfinger et al. 2005. The structure of this formulation was investigated and elucidated for the first time.

Liposomal formulations using synthetic phospholipids with same head-group but different acyl chain lengths and saturation were developed and characterized for oral delivery. Lipids are known to enhance solubility and improve bioavailability through lymphatic uptake.

The last of the nanoformulations was a self-nanoemulsifying drug delivery system developed using synthetic long chain triglycerides (Peceol®), non-ionic surfactants (Tween 80 and Tween 20) and co-solvents (Propylene glycol and Transcutol P®). The amount of drug solubilized in relation to the amount of excipients used as well as toxicity was paramount.

5.1 Development and structural evaluation of Amphotericin B core-shell microparticles

The majority of orally administered drugs gain access to the systemic circulation by direct absorption into the portal blood [Porter et al., 2001; Wasan et al., 2002]. However, for some water-insoluble compounds and those with low permeability, a transport by way of the intestinal lymphatic system may provide a pathway to the systemic circulation. Such compounds are transported in association with the lipid core of intestinal lipoproteins (triglyceride-rich chylomicrons) thereby requiring co-administration with lipids to stimulate lipoprotein formation. This route has contributed to the successful absorption of a number of highly lipophilic compounds such as Halofantrine, Probucol and Cyclosporine [Hauss et al., 1994; Holm et al., 2002; Palin et al., 1984; Ueda et al., 1983]. Amphotericin B with its unfavourable properties therefore requires lipids to enhance its solubility and improve its intestinal permeability. Lecithin was chosen as a lipid in this formulation due to proven efficiency in deliverability, inexpensiveness and established compatibility with biological systems. Gelatin is biocompatible, biodegradable, inexpensive, and easily available from several origins and has low immunogenicity. An encapsulation procedure of drug powders or granules by hydrophilic polymer and insoluble amphiphile, e.g. gelatin and lecithin, was introduced for some drugs such as Simvastatin by Hilfinger et al. In the current study the procedure has been modified for the strongly hydrophobic drug, Amphotericin B. The procedure, shown in figure 4.1, yields the drug formulation as a fluffy powder after milling and sieving. The material was characterized structurally with respect to the entrapped drug and shell entities.

UV-visible spectroscopy has proven to be a useful technique for the study of the interaction of Amphotericin B with its molecular environment since it is sensitive to the aggregation state of the drug [Fournier et al., 1998]. The technique was therefore applied to study the interaction of the Amphotericin B with the lecithin-gelatin mixture. Amphotericin B is characterized by molecular aggregation in aqueous medium at certain concentrations which is related to its activity [Sanchez-Brunette et al., 2004; Carter et al., 1997; Espada et al., 2008] and toxicity [Espada et al., 2008; Lamy-Freund et al., 1993; Legrand et al., 1992; Barwicz et al., 1992]. According to pharmaceutical literature, three forms of the drug are identified in aqueous solution: monomers at 0.2 µg/ml, water-soluble aggregates (e.g. of oligomers) at above 1 µM and water insoluble aggregates at a concentration above 10 µM [Brajtburg et al., 1996; Kajtar et al., 1989; Abeer et al., 2013]. Oligomers display an absorption maximum between 328 and 340 nm whilst aggregates show wide absorption [Torrado et al., 2008]. The solution of Amphotericin B in methanol (figure 4.2A) depicted the four peaks, which are reported as typical for a molecular solution of the monomers. The suspension of the original solid drug in water (figure 4.2B) showed similar peaks, but as an overlay on a wide peak (310-470 nm), which could be interpreted as a scattering peak of the aggregates of spherical particles, visualized in figure 4.4A by microscopy. A dominant peak at 328-340 nm [Torrado et al., 2008] is missing. Thus it can be concluded that the material is not in the oligomeric state. Figure 4.2C depicts the absorption spectrum of the AmB-HST formulation in water, which had an opaque yellow appearance. A wide peak from 310 to 470 nm, as is typical for aggregates, is overlaid by a series of individual peaks. The three peaks at lower wavelength of

364, 383, 408 nm appear within the limit of the instrument at the same wavelength as that for the molecular form in methanol (figure 4.2A). Thus it can be inferred that the core of the AmB-HST form is aggregated, but not in the oligomeric state, and hence in an uptake competent form.

The fluorescence properties of pure Amphotericin B in organic solvent and its formulation in the form of Fungizone® (micellar dispersion of Amphotericin B and sodium deoxycholate) has been studied (Gruszecki et al., 2003; Stoodley et al., 2007). The conjugated system composed of seven double bonds is responsible for the fluorescence behavior. As a possible tool for the analysis of the drug in formulations, the fluorescence spectrum of the drug was obtained in methanol and a calibration curve evaluated to ascertain its linearity. Figure 4.3 showed the spectrum of different concentrations of Amphotericin B in methanol. The excitation spectrum at emission of 475 nm revealed four strong bands at 305, 315, 333 and 348 nm. An excitation wavelength of 333 nm resulted in emission peaks at 420, 445, 469 and 502 nm (seen clearly with the 5µM sample, figure 4.3). This result conforms to that obtained by Gruszecki et al. and Stoodley et al. at excitation wavelength of 350 nm and emission at 471 nm. However, the positions of the peaks varied due to the use of different solvents. The occurrence of the excitation peaks between 305 and 350 nm is indicative of the drug in the dimer state (aggregates). Thus, the fluorescence behavior of Amphotericin B is dependent on its concentration and molecular environment. The calibration curve showed an increase in fluorescence with increased drug concentration (also in spectrum) but linearity was at high concentrations. The fluorescence reduced at a much higher concentration and this could be due to quenching. The higher concentration of drug required for measurable fluorescence is indicative of a lower sensitivity as compared to its absorption spectrum. Thus, its analysis by fluorescence was not encouraging and hence not used.

In its commercial forms, Amphotericin B may be present in both amorphous and crystalline form [Duddu et al., 2008]. The phase contrast microscopy of our starting material revealed single and clustered drug spheres in its raw form (Figure 4.4A). Our final product, amphotericin B in the formulated powdered sample of AmB-HST (Figure 4.4B), appeared in a sugar matrix with embedded orange drug spheres depicting a similar size of ~1 µm as the sub-particles in the original drug (Figure 4.4A). Obviously the initial clusters were resolved during the lipid-gelatin embedding procedure.

The structure of the initial and HST drug particles in aqueous solutions was studied with dynamic light scattering (DLS) and neuron scattering (SANS). The DLS investigation of the raw material (Figure 4.5A) depicted large particles of 6 µm apparent size, which corresponds to the clusters in the microscopic picture (Figure 4.4A). After the formulation to AmB-HST (Figure 4.5B) the clusters disappeared and smaller particles of a narrow size distribution (s = 1 µm) were detected. This corresponds to the microscopic image of the solid AmB-HST form (Figure 4.4B). The development of the particle size during the AmB-HST formation process as estimated by time resolved DLS is shown in figure 4.5C. After a short phase (2h) with a fast size reduction, the particle diameter increased during 8 h to a stable level. The result is interpreted as a disruption of the Amphotericin B sphere clusters (Figures 4.4A and 4.5A) by

the lecithin-gelatin solution without mannitol, and a slower encapsulation accompanied by a slight size increase.

The internal structure of all HST-like drug formulations was unknown until now. The particle domain structure is here resolved by neutron small angle scattering using the deuterium solvent contrast method. By the drug composition, a partially deuterated biocompatible buffer was prepared (71% D_2O gastrointestinal transport medium TM [Kataoka et al., 2006]), which partly matches the Amphotericin B drug core. In the scattering profile (Figure 4.5A) the top of the tentatively bell shaped scattering profile is cut because of the low q-limit of the available instrument KWS-2 (0.008$Å^{-1}$, corresponding to <100 nm particle size). In the current case this is no problem, as the size was estimated by DLS (~1 µm, Figure 4.5C). The trial evaluation of SANS by a Guinier plot (Figure 4.6B) indicated that smaller particles of 1-100 nm size were not present at a significant level (%). The straight part of the drug particle scattering, expected by theory assuming the 1µm size from DLS (R_g = 645 nm; $In(I_o)$ = 10.16) was not visible by the q limits of the KWS2 instrument. The most important result was the estimation of the span of the AmB-HST particle shell, depicted in figure 4.7 by a Kratky-Porod plot. The shell span d = 5.64 ± 0.18 nm (statistical error only) indicates a thin layer of material with low scattering density, as expected for lecithin and gelatin. The value is similar, but slightly higher as that reported for the biological lipid membrane core (tail region) in comparable studies of liposomes (d = 4-4.5 nm).

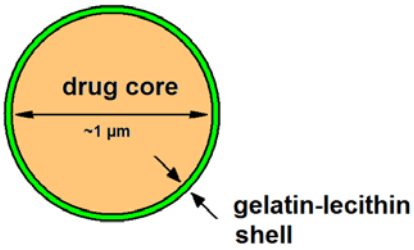

Figure 5.1: The structure sketch (core: not true scale) of AmB-HST core-shell microparticles combines the results of microscopy, DLS and SANS with deuterium contrast matching: the particles consist of a massive drug core (AmB), embedded in a lecithin-gelatin shell of 5.64 nm width, similar to biological lipid membranes (4-5 nm).

Thus the shell around AmB-HST particles is assumed to be a lipid-bilayer with some attached gelatin, resembling biological membranes. The results of core investigation by DLS, microscopy, spectroscopy, and the shell structure obtained by SANS are summed up in the structure sketch of AmB-HST presented in figure 5.1. In the case of Amphotericin B, the HST formulation appears as drug sphere of 1 µm diameter, embedded in a thin lecithin-gelatin layer of 5.64 ± 0.18 nm span. This structure explains the potential of the HST formulations for the solubilisation of hydrophobic drugs of the BCS classes II and IV.

The in vitro release of the established core-shell microparticles was conducted with the plain drug as a reference using a solution of 0.25% w/v sodium dodecyl sulphate (SDS) as the dissolution medium to create a sink condition for the drug. The cumulative drug release against time is indicated by figure 4.8A. The release from the AmB-HST was higher than the plain drug at all the sampled times confirming the increased solubility of the formulation in aqueous medium. This confirms the improved solubility of hydrophobic drugs by the

Hydrophilic Solubilisation Technology (HST). More than 70% of the drug had been released for both the formulated product and the reference before 2 hours. The increased release by the two products could also be attributed to the micellar solubilisation of the sodium lauryl sulphate solution. Two release profiles are judged similar by the calculation of the similarity factor, f_2 (f_2>50). The f_2 value estimated indicated a difference in the cumulative release of the AmB-HST and the plain drug. However, an assumed infinity release of the drug (calculated from linear regression of inverse of percentage release against inverse of time) as indicated by the red and green lines in figure 4.8A showed no difference. The logarithm plot (figure 4.8B) is shown to indicate the lag time between the dissolution of the formulated product and the plain drug since the dissolution of the formulation was higher at all times. The lipid- gelatin shell enhances solubilisation of the molecular drug faster as compared to the plain molecule. Thus, a lag time of 5.62 ± 0.51 minutes was estimated.

It is anticipated from the structure of the formulation and the release profiles that there is a likelihood of drug precipitation in the intestinal milieu after removal or digestion of the lipid-gelatin shell. The particle size of the core drug (~1µm) was not modified in the formulation.

5.2 Development of self-microemulsifying drug delivery system

The choice of excipients for the formulation of microemulsions depends on the solubility of the active pharmaceutical ingredient in the excipient as well as the miscibility of the various components. Amphotericin B solubility was determined in 13 oils, 5 surfactants and 3 co-solvents. The data for the oil solubility screening indicated castor oil as the highest solubilizer of Amphotericin B in this work. Castor oil is known to have purgative action and irritates the gastrointestinal tract. Therefore combinations of castor oil with peanut and avocado oils (1:4) with the intention of reducing the amount of castor oil were also tried. There was an increase in the solubility of the drug (figure 4.43). However, there was phase separation of the oils in combination with the surfactant and co-surfactants. Based on these, Peceol® (glyceryl monooleate) was chosen as the oil, Tween 80 and Tween 20 were chosen as surfactants and Propylene glycol and Transcutol® P (Highly purified diethylene glycol monoethyl ether) as co-surfactants. Also, with the exception of propylene glycol, none of the excipients could solubilize about 1 mg/ml of the drug making the drug not readily lipophilic. Therefore, a closer look at the solubility data puts Amphotericin B as a non-lipophilic hydrophobic drug, popularly referred to as ‘brick dust’ (Müllertz et al.2010).

Microemulsion preparations are depicted with the help of phase diagrams. Construction of phase diagram is a useful approach to study the complex series of interactions that can occur when different components are mixed and the ratios thereof. A ternary phase diagram of oil, surfactant and co-surfactant without drug (blank) was thus prepared by considering the speed of emulsification, appearance and dispersibility of the formed nanoemulsion in water at 37^{o}C (Table 10). It was observed from the ternary phase diagrams (Figure 4.44) that the region of emulsification for Tween 20 was larger than Tween 80 with the two co-surfactants and could have some emulsification with oil content up to 15 %. Its minimum surfactant ratio for self-emulsification was 40% as compared to 50 % for Tween 80. However, all formulations

prepared with Tween 20 and Amphotericin B showed sedimentation of the drug in less than two hours due to low viscosity of the surfactant. Although they both have hydrophilic and hydrophobic portions like the drug, Tween 80 has a longer chain length and unsaturated than Tween 20. Tween 20 has lauric acid whiles Tween 80 has oleic acid in their hydrophobe. Tween 80 by appearance is more viscous than Tween 20 and could account for the less viscous nature of the Tween 20 formulations. Thus, formulations with Tween 80 were developed and further evaluated. Tables 25 and 26 indicate the various parameters determined for blank samples prepared with propylene glycol and Transcutol® respectively using Peceol® and Tween 80. Large droplet size of emulsion was observed with mixtures having more than 15% content of oil. Such mixtures also had poor self-emulsification properties and cloudy appearance according to the criteria specified in table 10.

It has been reported in literature that the drug incorporated in self-emulsifying delivery systems may have some effect on the emulsifying performance (Pouton et al, 1985). The effect of the drug is therefore indicated in tables 27 and 28 for the propylene glycol and Transcutol® respectively. The maximum equilibrium solubility of a drug in a formulation is of utmost importance since it dictates the maximum dose that can be incorporated in a unit dose capsule (Pouton et al, 2009). The most important parameter was the amount of the Amphotericin B that could be incorporated into the pre-concentrate. The role of surfactants in self-emulsifying systems is to reduce the interfacial tension and adjust the spontaneous curvature of the interface so as to enable the dispersion process and provide a flexible film that can easily cover the lipid core (Müllertz et al, 2010). The presence of co-surfactants (co-solvents) facilitates the dispersion process and results in faster dispersion rate. In addition, they are known to improve the solubility of the drug in the self-emulsifying pre-concentrate. Figures 4.45 and 4.46 show the effect of the surfactant and the different co-solvents on the amount of drug incorporated into the pre-concentrate. Increasing the surfactant concentration indirectly reduces the co-solvent concentration at fixed oil content. The amount of drug reduced with increasing Tween 80 from 50 % to 80 %. This indirectly showed the amount of drug to increase with increasing content of propylene glycol from 15 % to 45 % (Figures 4.45A and 4.46A). However, the reverse was the case for Transcutol® P as the co-solvent (Figures 4.45B and 4.46B). This observation maybe due to the more hydrophilic nature of the propylene glycol which therefore has a higher solvent capacity for the Amphotericin B since the drug is amphiphilic. This is also evident in the solubility profile of the drug in propylene glycol and the Transcutol® in figure 4.43. This trend was also observed for higher oil contents (8 % and 10 %) as shown in tables 27 and 28.

The addition of Amphotericin B did not visually modified the viscosity of the pre-concentrate but did modify the particle size and size distribution of the nanoemulsion which is consistent with reported findings (Butani et al, 2014) as compared to the droplet size of the blanks (Tables 25 and 26). At a fixed concentration of oil (e.g. 5 %), the droplet size of the nanoemulsion increased with increase in surfactant concentration with corresponding increase in polydispersity index for both formulations (Figures 4.47A and 4.47B, Tables 27 and 28). Thus, as expected the droplet size decreased with increase in co-solvent content. The amphiphilic nature of the drug enables it to intermingle with the amphiphilic nature and hydrophobic chains of the surfactant as well as hydroxyl groups of co-surfactants at the interface resulting in changes in their packing arrangement which in turn can affect the

curvature of the interface and interfacial energy (Eccleston et al, 1992). Generally, the droplet sizes of the Transcutol® formulations were smaller than that of the propylene glycol ones. This is also consistent with findings by Jeoung et al on Transcutol® whose self-emulsifying nanoemulsion of Lutein with Transcutol HP resulted in smaller droplets compared to that of Lutrol E-400 as co-surfactants (Jeoung et al.2010). The spontaneity of emulsification was linearly related to the amounts of surfactant and co-solvent. The higher the co-solvent the faster the dispersion rate (Tables 27 and 28).

Many poorly-water soluble drugs are much more soluble in co-solvents than oils as is the case of Amphotericin B. Formulation of such compounds has the tendency of precipitation after dilution in excess water due to loss of solvent capacity. Therefore one has to balance the advantage of including co-solvents with the risk of inducing drug precipitation on dispersion. The precipitation tendency was assessed after dilution in water at 37^{o}C. The resulting emulsion was left to stand for a day and sometimes three days. There were no visible precipitation of the drug after 24 hours in all formulations, both propylene glycol and Transcutol®. Precipitation was however observed when the nanoemulsions were kept for three days and this was drug load dependent. Even though there was sedimentation of the drug with the pre-concentrate, no visible grains of the drug were seen and the components were miscible upon slight agitation (shaking by hand). Sedimentation was observed after a week of preparation.

The spectrum of Amphotericin B in methanol shows four peaks with decreasing intensity at wavelengths of 407, 384, 364 and 346 nm signifying the drug in monomeric state (Abeer et al. 2013; Bolard et al. 1995, and Milhaud et al. 2002). The drug in the aqueous nanoemulsion has three peaks with diminished intensity occurring at wavelengths of 409, 386 and 366 nm which depict the drug also in monomeric form. The slight bathochromic shift could be drug interaction with excipients and water. The spectrum is identical for all tried formulations irrespective of the excipient concentration (see Appendix E). Thus, the extent of sonication had no effect on the molecular state of the drug. It is probable that the presence of the co-solvent kept the drug in the monomeric state which is preferable for uptake and activity with reduced side effects.

Due to the peculiar solubility and permeability properties of Amphotericin B which warrants its parenteral administration, an oral formulation should contain a higher amount of drug to overcome the intestinal barriers and present sufficient blood levels for efficacy. The drug load in the formulation is the prime factor. The drug content for the formulations of both the propylene glycol and the Transcutol were less than 2 mg per gram of total excipient. This amount is highly inadequate for oral application considering even the dose that is used parenterally. Thus, there was the need for optimisation of process parameters to assess the effect on the drug load. The two major process conditions were the time of sonication and the speed of centrifugation to separate non-solubilized drug. In view of this, three (3) samples from each was selected based on the pre-concentrate that solubilised high amount of drug and which dispersed in water within 2 minutes generating droplet sizes below 200 nm as measured by dynamic light scattering (DLS). The results are as indicated in Tables 27 and 28 for samples with propylene glycol and Transcutol® as co-surfactants respectively. The maximum saturated drug load for the nanoemulsion of Peceol®, Tween 80 and propylene glycol was 2.197 ± 0.049 mg per gram of total excipient at a time of sonication of 20 minutes

and centrifugation speed of 2500 rpm. The nanoemulsion of Peceol®, Tween 80 and Transcutol® P also had a saturated solubility of 1.814 ± 0.063 mg per gram of total excipient at 40 minutes sonication and 2500 rpm centrifugation. At a centrifugation speed of 1000 rpm drug grains were observed in the pre-concentrate. The optimisation had a slight improvement on the amount of drug incorporated into the formulation.

Excipients used for the delivery of drugs as well as formulated products should not be toxic systemically and to tissues of the body. In vitro assessment of the permeability of the formulation thus requires its evaluation of toxicity to both red blood cells and intestinal enterocytes. Caco-2 cells have been one of the cells used for intestinal permeability studies since the differentiated cells have the same morphological features as the human intestines. It should be emphasized that the mass transport of drug across a membrane is dependent not only on drug concentration but also on the excipient effect on the permeability of the biological membrane (Saha and Kou, 2000). Thus, the nanoemulsions and their blanks together with a suspension of the drug in culture medium were tested against Caco-2 cells in the same manner as the liposomes. The nanoemulsions comparatively reduced the Caco-2 cell viability. The excipients used are generally regarded as safe (GRAS) by the U.S. FDA (www.fda.gov) and have been included in a great number of formulations for various routes of administration. The inclusion of the Tween 80 and the co-solvents probably had the major effect on the cells in addition to the drug which is known to cause toxic effects to certain cells in the human body. The effect may either be direct cell death or modification of membrane integrity. Saha and Kou in their work reported that 1% propylene glycol and Tween 80 (3:2) reduced the transepithelial electrical resistance (TEER) of Caco-2 cell monolayers by 14% and 16% in the study of the donor solubility and permeability of an imidazole derivative, Sch-Y and a himbacine analog, Sch-X respectively which is an effect on membrane integrity.

Another study by Takahashi et al stated that a 10% propylene glycol had a significant effect on a 3-day culture Caco-2 cells whilst about 20% did not have any effect on a 21-day culture of the same type of cells. Tween 80 at 1% significantly affected the TEER of the 3-day cultured cells but for the 21-days culture, a concentration of 10% showed the significant effect. Transcutol® P on the other hand was only investigated on the 21-days culture and the results showed that a significant reduction only occurred at a 20% concentration. The authors therefore concluded that propylene glycol and Tween 80 are appropriate for permeability studies but Transcutol® P heightens permeation and therefore not appropriate (Takahashi et al. 2002). Even though most of the excipients used for the nanoemulsions and their blends have been investigated on Caco-2, their effects on the monolayer have been found to be concentration dependent (Saha and Kou, 2000; Takahashi et al. 2002; Xianyi et al. 2005; Alvi and Chatterjee, 2014; Liang et al. 2014). The concentration dependent effect as indicated in figure 4.49 is therefore in agreement with what is stated in the literature at all the times of incubation for both the drug containing and blanks even though the viability of the cell was determined by the MTT test. The cells were used 48 hours after seeding. At the highest concentration tested (100 µg/ml), cell viability was only reduced by about 50% for the propylene glycol emulsion at all the incubation times. The effect was more pronounced for the blank than the drug containing emulsion. This highlights the fact that it is not the effect of the drug but rather the excipient. Statistically, there was no significant difference between the viability of the cells at the 1hr and 4hrs incubation periods for the drug containing emulsion,

blank and the suspension of the drug ($p>0,05$). However, the drug containing emulsion and the blank were more toxic than the drug suspension at 24 hrs incubation ($p<0.05$).
Transcutol nanoemulsions (both drug containing and blank) were more toxic to the Caco-2 cells at all concentrations and incubation times. The concentration used in the formulation was only 14% (lower than stated by Takahashi et al) but significantly reduced the cell viability in comparison to the drug suspension ($p<0.05$).
The toxicity of the nanoemulsions was evaluated further using fresh human red blood cells. They were compared with Fungizone®, a micellar preparation of Amphotericin B, which has a known hemolytic effect. The results indicated a linear increase in haemolysis with increase in concentration of the drug for all the three formulations studied. The haemolytic effect of the propylene glycol emulsion was observed at a concentration of 5µg/ml whereas that of Transcutol® and Fungizone® occurred at 1µg/ml. However, at the highest dose tested (50µg/ml) the haemolytic effect was almost 100% (figure 4.51) for all the formulations and the concentration that caused 50% haemolysis were 0.85µg/ml, 1.33µg/ml and 5.89mg/ml for Fungizone®, Transcutol® nanoemulsion and propylene glycol nanoemulsion respectively. There was no significant difference in haemolysis between the three formulations ($p>0.05$).
There exists a close association between the states of aggregation of amphotericin B and its toxicity. Monomeric Amphotericin B associates more with ergosterol in the fungal membranes, whereas self-associated Amphotericin B form pores in cholesterol-containing membranes leading to toxicity towards host cells (Bolard et al. 1991). The spectrum in figure 4.49 (and Appendix E) indicated the drug to be in monomeric form in the nanoemulsions due to the presence of the co-solvents. The haemolytic effect may not be due to the drug alone but also the surfactant and the co-solvents present in the formulations. Italia et al. explained that the haemolytic activity of Fungizone® is not caused by Amphotericin B alone but also by the sodium deoxycholate which is a surfactant (Italia et al. 2009). Surfactants have been used extensively as drug solubilizers by either a direct co-solvent effect or by uptake into micelles (Strickley, 2004). Strickley concluded that the commonly used surfactants such as cremorphors, polysorbates, Labrafils, TPGS, and Span 20 are proven useful but they have limitations. Thackaberry et al. conducted a comprehensive toxicological study of hydroxypropylmethyl cellulose (HPMC), propylene glycol, Tween 80 and Hydroxypropyl-beta-cyclodextrin (HPβCD) in mice, rats, dogs and monkeys by oral gavage. The authors stated that the excipients are suitable for use in preclinical formulations containing up to 20mg/kg for HPMC, 10mg/kg for Tween 80 and 1000mg/kg for propylene glycol. The United States Food and Drugs Administration (USFDA) have listed propylene glycol, Transcutol®P and Tween 80 in their Inactive Ingredients Database as oral excipients and are generally considered safe (21 CFR 184.1666). Although propylene glycol is rated safe and commonly used in parenteral formulations, it is considered as one of the more haemolytic co-solvents (Fort et al. 1984; Reed and Yalkowsky, 1985). The concentration of propylene glycol in the nanoemulsion formulation was 40% w/w and that of the Transcutol®P was 14% w/w. Tween 80 has a concentration of 50% w/w in propylene glycol nanoemulsion and 76% w/w in the Transcutol® nanoemulsion. Thus, the haemolytic effect of the nanoemulsions could be as a result of the surfactant and the co-solvents. This is substantiated by the MTT tests with the Caco-2 cells as the blanks were more toxic than the drug containing emulsions (figure 4.49).

Discussion

The exact amounts of organic co-solvents in formulations are usually not reported, but in those formulations where the amount is stated, the maximum amount of solvent used is up to 55% for propylene glycol (Strickley et al.2004). The nanoemulsion contains only 40%. A 1000mg/kg/day Transcutol®P was considered acceptable for use as a vehicle for poorly soluble drugs following oral administration to Wistar rats in a toxicity study (Delongeas et al.2010; Sulllivan Jr. et al.2014). The amounts of Amphotericin B solubilised in the nanoemulsions are 2.197±0.049 mg and 1.184±0.063 mg per gram of total excipients for the propylene glycol and Transcutol® respectively. These amounts are inadequate for oral administration. The intravenous preparations like Fungizone® and Ambisome® are reconstituted to a concentration of 4 mg/ml of Amphotericin B with a recommended maximum dose of 1 mg/kg/day and 5 mg/kg/day respectively. An adult person of 70kg weight would therefore have to consume higher amounts of the excipients if intestinal metabolism and first pass effect are taken into consideration. The Food and Agriculture Organisation/World Health Organization Expert Committee on Food Additives has set the acceptable human intake of these excipients at 25mg/kg/day (Lowest oral LD50 for propylene glycol is 18-23.9g)(www.fao.org; www.inchem.org). Therefore oral application of Amphotericin B in this regard seemed impossible but other factors need to be considered.

Density and viscosity of dosage forms affect their transit in the gastrointestinal tract (Amidon et al.1991; Clark et al.1993; Tuleu et al.1991). The flow properties of the pre-concentrates were therefore evaluated at room temperature. They were found to be Newtonian as the up-curve and the down-curve coincided at almost the same points (figure 4.52). The viscosity was then evaluated from the slope of the curve. The pre-concentrates were as expected, more viscous than water due to the excipients but would be even less viscous when the emulsion is formed in situ upon dilution with intestinal fluids.

A preliminary structure of the emulsions was investigated by small angle neutron scattering. Various structures have been proposed for emulsions depending on the emulsion type and composition. Spherical, lamellar, bicontinuous (sponge), rod-like micelles, onions and vesicles are some suggested structures in the literature. The general structure mostly obtained for oil-in-water microemulsions is a spherical droplet (Hellweg, 2002; Shukla et al, 2002). The oil (Peceol®) is assumed to be the core with the surfactant and co-surfactant forming the interfacial film, and water as the continuous phase. This shape was assumed in the analysis of the data. Thus, the droplet size and the interfacial film layer were evaluated. A critical look at the oil, surfactant and drug structures show they all have both hydrophobic and hydrophilic domains. Thus the core of the droplet is likely to be the hydrophobic portion of these components. The interfacial film would compose of the hydrophilic portions as well as the co-surfactants and water bound molecules. The inter-droplet distance for the drug containing emulsions was higher than their blanks. This could be due to some repulsive forces induced by the presence of the drug as it interacts with both the hydrophilic and hydrophobic domains of the excipients. The high interdroplet distance of the propylene glycol microemulsion as compared to the Transcutol® is due to the decreased chain length of the propylene glycol since the surfactant and oil are the same in both formulations (Moulik et al, 1998). Generally, the interfacial film layer of the blank emulsions was higher than the drug containing emulsions. The presence of the drug influenced the curvature of the droplets. The propylene glycol emulsions however had higher interfacial film layer compared to that of the

Transcutol® (diethylene glycol monoethyl ether). Co-surfactants are proposed to introduce disorder in the interfacial film more especially when their chain lengths differ from the surfactant (Moulik et al, 1998). Propylene glycol has a shorter chain length and differ more from the surfactant in terms of structure, thus has the tendency to induce more disorder in the interfacial film. This effect could account for the large interfacial film span in comparison to the Transcutol® which has a longer chain. Interfacial film decreases with increase in chain length of the alcohol. A more critical structural evaluation can be done by contrast variation method of small angle neutron scattering and other techniques such as cryo-transmission electron microscopy.

The stability of the pre-concentrates was evaluated in terms of drug content and droplet size. The pre-concentrates were kept in glass vial wrapped with aluminium foil. They were stored in the refrigerator (5 $\pm 3^{o}$C) and at room temperature (25$\pm 2^{o}$C) without any humidity control over 70-days period. This was to assess if the product could be stored at room temperature to save cost. The pre-concentrates were very stable in terms of drug content and there was no significant difference ($p>0.05$) between the two storage conditions for both the propylene glycol and Transcutol® (figure 4.55). In all cases the drug content was 93% of the initial amount. The droplet size analysis for the propylene glycol pre-concentrate revealed no significant difference ($p>0.05$) between storage in the refrigerator and at room temperature. The complex interaction of the hydrophilic and hydrophobic components of the excipients and drug molecules was very stable culminating in a stable droplet size. The assessment of the Transcutol® pre-concentrate was however different in terms of droplet size. There was a significant difference ($p<0.05$) in droplet size between storage at room temperature and in the refrigerator. The droplet size of the refrigerated sample was more stable than at room temperature. The droplet size reduced with time at room temperature (figure 4.56). This may be due to rearrangement of the hydrophilic and hydrophobic domains of components resulting in changes in curvature of the droplets due to temperature. There was however, no change in appearance of the two products.

5.3 Solubility of Amphotericin B in FaSSIF-C

The solubility of Amphotericin B increased with increasing concentration of cholesterol in the medium. Amphotericin B is known to form complexes with cholesterol and other lipids that constitute major components of cell membranes (Herve et al, 1989; Baginski et al, 2002; Matsumori et al, 2005 and Crub et al, 2006). Thus, the increase may be as a result of soluble complex of drug-lipids in the medium. Cholesterol therefore enhances the solubility of Amphotericin B in fasted state simulated intestinal fluid (figure 4.9).

The size of the particles formed in the medium also showed a similar trend as the solubility profile. There was a gradual increase in size up to 10% of cholesterol and a significant increase at 13% cholesterol. This result conforms to the observation made by Khoshakhlagh et al in their solubility and particle size determination of BCS class II drugs in the same model media (Khoshakhlagh et al. 2015). In that study the solubility of Fenofibrate was increased with increasing concentration of cholesterol in the medium. Large particles believed to be cholesteric particles were observed at 13% cholesterol. Therefore the high cholesterol content increased the drug-sterol complex with a corresponding increase in solubility. This therefore

suggested that lipids and sterols could act as solubilisation agents for the formulation of Amphotericin B. Thus, the drug was incorporated into the probable lipid delivery system which is liposomes.

5.4 Development of Amphotericin B liposomes

Liposomes are well recognised for their ability to improve the delivery of drugs which can be entrapped in the lumen (hydrophilic) or embedded in the membrane (hydrophobic). However, due to their structural attributes they have been employed as solubilising agents for low solubility drugs. The liposomal formulations of Amphotericin B investigated so far are made with either positively or negatively charged lipids (Manosroi et al, 2004; Santangelo et al, 2000; Delmas et al, 2002 and Zarif, 2005). With the exception of the study by Santangelo et al. and Zarif, the rest were evaluated for parenteral administration. Santangelo et al and Zarif prepared Amphotericin B cochleates for oral delivery using phophatidylserine (negatively charged) and demonstrated complete survival of mice infected with *Candida albicans*. In the present study DOPC (18:1) (unsaturated), DSPC (18:0), DPPC (16:0), and DMPC (14:0) were chosen as the lipids with cholesterol as sterol for the preparation of multilamellar vesicles intended for oral administration. The chosen lipids have different acyl chain lengths with DOPC as the unsaturated one. It is the hypothesis of this work that there could be a possible π-π interaction between DOPC and the polyene group of the drug. Neutral lipids have been added to charge ones in drug targeting to form stable liposomes. This property is also explored in this formulation.

An important parameter of consideration for the use of Amphotericin B by the oral route is the drug load due to its low solubility. Ali et al. reported that incorporation of low soluble drugs into liposomes does not only depend on the physicochemical properties of the drug but also on the composition of the liposomes. The choice of the phosphatidylcholine and the cholesterol concentration within the bilayer has an impact on drug loading (Ali et al., 2013). Although cholesterol is known to improve bilayer stability, the amount can also reduce drug incorporation efficiency (drug dependent). Therefore, the amount of lipid and cholesterol was varied. The film hydration method was employed for this formulation since it is simple and widely used for the preparation of multilamellar liposomes. The films were hydrated with the buffer before vortexing to generate the liposomes. Preliminary investigations were conducted by decreasing the lipid content from 85 to 50 mole % with resulting increase in cholesterol and drug from 10 to 40 mole % and 5 to 10 mole % respectively. It was observed that increasing the cholesterol content led to the formation of hard films that required longer hydration times and the suspension of film was very difficult. This could be attributed to the strong binding of the drug to either cholesterol or to the phospholipid. Thus, some films were left on the tubes at above 30 mole % of cholesterol. Grains of Amphotericin B were visibly observed at higher cholesterol and drug concentrations. This finding supports what Ali et al. reported that high cholesterol content reduces encapsulation efficiency. This resulted in the use of the combination of the excipients as indicated in table 9 (see section 3.2.3.1). However, such observation was not made with the blanks.

Discussion

The type and nature of the lipid had a profound effect on the particle size and size distribution, drug content and entrapment efficiency. All these stated parameters were better with DOPC as compared to the other lipids in all concentrations. This gave an indication that there could be a possible interaction between the drug and the lipid in addition to the binding affinity for cholesterol. This interaction could also explain the smaller particle size of the drug loaded formulations in comparison to the blank formulations. The particle size result is similar to a reported one by Lawrence et al. who also used the same lipids to prepare small unilamellar liposomes but without drug (Lawrence et al, 2004(1)). The knowledge that the drug embeds in membranes by association with cholesterol results in lower entrapped volume and hence relatively lower size (Table 14 and 15). The saturated lipids (DSPC, DPPC and DMPC) had particle sizes in the micrometer range with particle size of DPPC liposomes much smaller than DSPC and DMPC after freeze drying. Amphotericin B is reported to change its conformation upon binding to liposomes and this conformational change is dependent on the type of lipid, drug-lipid ratio, curvature of the vesicles and the transition temperature of the lipid. These factors could account for the particle size difference between the lipids. Particle size after freeze drying was much smaller compared to prior lyophilisation for all lipids with the exception of DOPC. This could be an indication of fusion of the liposomes. Freeze-drying has been used to improve encapsulation efficiency of some hydrophilic drugs. However, this did not improve the encapsulation efficiency of the Amphotericin B which is hydrophobic. The only possible explanation is a reduction in lamellarity of the liposomes. The DMPC liposomes were very much affected compared to the others. It is known that longer acyl chain lipids produce more stable liposomes due to stronger chain-chain interaction (Gaines, 1966). All the formulations recorded high polydispersity index (> 0.4) with that of DOPC being relatively low. Less than 5% of the particles were above 2µm as measured by dynamic light scattering for some of the drug loaded samples showing sometimes two or more populations. The heterogeneity is one of the drawbacks of multilamellar liposomes (Sriwongsitanont et al, 2011). DOPC was selected as the best lipid based on the above analysis for the formulation and characterisation of the drug. Lawrence et al. in their work with the above lipids and the Tweens also concluded that DOPC allows incorporation of large amounts of Tween surfactants into its vesicles and could be potentially useful vehicles for drug delivery purposes. Amphotericin B has both hydrophilic and hydrophobic domains just like the Tween surfactants. This could also explain the favourable characteristics of the formulation of the drug with DOPC and cholesterol (Lawrence et al. 2004 (2)).

It is known in the literature that Amphotericin B exists in three different states in aqueous medium depending on its concentration. The different states can be assessed spectrophotometrically by the intensity and wavelength of the four vibronic peaks of the drug. The state determines the extent of activity and toxicity of the drug in vivo (Espada et al, 2008; Legrand et al, 1992; Barwicz et al, 1992). It is therefore important to determine the aggregation state of formulations in aqueous medium to predict the extent of toxicity before administration. Figure 4.11B revealed an increase in intensity of peaks towards shorter wavelength as compared to that in methanol (figure 4.11A). The drug therefore occurs in aggregated form in all formulations but the extent of aggregation is highest when the

concentration of lipid is low with a higher drug load. The highest drug load showed a broad peak between 328 to 340 nm depicting oligomeric state of the drug's aggregation.

Structural analysis of formulation is very crucial since it affects stability, absorption and performance. The morphology of the formulation was observed microscopically aside using dynamic light scattering. Two different structures were identified in addition to the liposomes; drug crystals and yellow sheet-like structures which are uniform in colour. The number of sheets increased with drug content vis-à-vis the lipid and cholesterol (figure 4.10B). The density of the crystals and sheets are the same and inseparable by sucrose density gradient centrifugation (see figure 4.14). Vyas and Gupta (2007) observed comma shaped ribbons and other unspecified structures in their bid to develop emulsomes (lipid particles) of Amphotericin B. These structures were observed at a drug concentration of above 6 % w/w ratio of drug to lipid. Abelcet, a lipid complex of Amphotericin B (DMPC and DMPG) is also ribbon-like in structure (Torrado et al, 2008; Janoff et al, 1993 and 1998). It is very difficult to offer an explanation to the occurrence of these structures but Brajtburg and Bolard, as well as Janoff et al. attributed them to collapsed and aggregated membranes existing as interdigitated bilayers (Brajtburg and Bolard, 1996). However, their appearance could be as a result of a high energetic mixture held by strong forces with the tendency towards crystallization.

Sucrose density gradient centrifugation was employed to investigate if the different structural components (liposomes, sheets and drug crystals) of the formulation could be separated as observed under the microscope (figure 4.10A). The results as shown in figure 4.14A and B revealed a bimodal density distribution. Visual observation showed the drug to be more associated with the high density band. The absorbance measured at 405 nm confirmed the distribution of the drug (figure 4.14D). Particle size analysis of the different fractions indicated the lower density population as having about 200 nm size which is predictive of liposomes. The higher density population recorded a size of about 6 µm which depicts a mixture of drug-lipid complexes and aggregates of drug. Microscopic pictures were not different from that observed in figure 4.10A as both layers had the sheets and crystalline drug. This result resembles that reported by Janoff et al. Ribbon-like structures were observed when 5 to 10 mole % of Amphotericin B was incorporated into liposomal formulation of DMPC/DMPG (7:3 mol/mol). Sucrose density gradient centrifugation data also revealed a bimodal population with the 5 mole % Amphotericin B in which the bulk of the drug did not migrate with the bulk of the lipid. However, above 10 mole % (25 and 50 mole %), greater than 95% of the drug migrated with the lipid in a single band (Janoff et al, 1993; 1988). Analysis of the drug content in the two bands showed 5.83%, 6.80% and 8.73% of Amphotericin B in samples A, B and C respectively in the low density portion (upper). The high density fractions recorded concentrations of 94.17, 93.20 and 91.28% respectively (figure 4.14F). Ribbons of size 6-11 µm are also reported for Abelcet® which is an Amphotericin B-lipid complex preparation. The particle size of the unidentified structures and ribbons prepared by Gupta et al. was not determined and could probably be of large size. The formulation was prepared with soy phosphatidylcholine, cholesterol and trilaurin. It can be deduced that the type of lipid and concentration of lipid to drug results in creation of different kinds of structures. Amphotericin B complexed with cholesteryl sulfate produced disc-like structures at a lipid-drug ratio of 1:1 (Hamill, 2013).

Discussion

Differential scanning calorimetry (DSC) is a tool for measuring how the physical properties of a sample change, along with temperature and time. Thus, the technique was used to verify if the melting peak of the crystalline Amphotericin B is still prominent in the formulation as seen under the light microscope. In view of this, drug loaded samples and their blanks as well as pure drug were investigated. The thermogram of Amphotericin B showed two endotherms which is consistent with the literature (Sanyog et al, 2012 and Manosroi et al, 2004). The first peak is as a result of the evaporation of water and the second is the melting peak of the drug which occurred at 194.09^{o}C (>170^{o}C). The drug loaded liposomes and their blanks also showed two or more peaks (Figure 4.12A and B). The first peak in the formulations is attributed to water evaporation. The second peak expressed physical interaction either between lipid components or melting peak of the sugar component in the formulation (trehalose and mannitol). The melting point of the used mannitol was determined as 166.56^{o}C (164-169^{o}C) and when it was freeze-dried, the peak occurred at 152.27^{o}C. Trehalose dihydrate had a melting point of 97.76^{o}C (97-99^{o}C) and cholesterol's melting point was determined as 149.08^{o}C (148-150^{o}C) (see Appendix B). The second major peaks in the thermograms for both drug-loaded and blanks occurred between 138 and 151^{o}C (see Table 16) which represents either the cholesterol or mannitol in the samples. Even though crystal-like structures were observed under the microscope, the melting peak of Amphotericin B was completely absent which could be explained as either complexation to the lipid excipients (embedding in the membrane) or that the amount is completely masked out of the formulation. It was also generally observed that the higher the melting point (major peaks), the greater the value of the enthalpy of transition (Table 16). The thermograms of the blanks and samples were similar.

To investigate drug-excipient or excipient-excipient interactions, Fourier Transform Infra-red Spectroscopy (FTIR) is one of the techniques mostly applied. Formulated samples and their physical mixtures were investigated. There are no striking differences between the spectrum of the formulations and their physical mixtures as indicated in the FTIR spectra (Figure 4.13A and B). However, both spectra are different from the spectrum of Amphotericin B (see Appendix C). An intense peak at 1562 cm^{-1} attributable to NH_3^+ is missing in the formulation. This functional group could be used in the interaction with the cholesterol or phospholipid head group.

The cell viability test revealed a value of above 75 % for the drug loaded liposomes, blank liposomes and the suspension of the plain drug at all concentrations and times of incubation. The drug loaded liposomes however, showed lower cell viability compared to the blank and the suspension at all concentrations and time of incubation. The blank liposomes could serve as food to the cells whiles the suspension may not be internalised by the cells as it is not readily permeable. Therefore at one and four hours the cell viability of the blank was higher than the suspension and the drug loaded liposomes. The cell viability recorded at 24 hours incubation was virtually similar for the suspension and the blank liposomes. The data gives evidence that the drug loaded liposomes were internalised by the cells and hence produced reduced viability but not toxic to the cells even at 24 hours incubation at a concentration of 100 µg/ml. The highest internalisation occurred at 4 hour incubation (Figure 4.15A, B and C).

Discussion

The internalisation or uptake of the drug loaded liposomes was confirmed by a cell uptake study. Figure 4.16 shows the percentage uptake of the amphotericin B by Caco-2 cells after 1, 4 and 24 hours. The highest drug uptake occurred at 4 hours incubation. There is therefore correlation between the cell viability and the uptake tests. This readily suggests that the liposomal formulation could be a potential oral delivery system for Amphotericin B.

The in vitro release of Amphotericin B from the liposome formulation was conducted by the membrane dialysis method over an 8 hour period due to stability consideration for the lipid components at 37^{o}C (see section 3.4). Most of the release studies conducted was done over 24 hours to several days (Italia et al. 2009; Abeer et al. 2013; Kumar and Jain, 2010; Yang et al. 2012; Chae-Eun et al. 2008). After 8 hours the cumulative release of Amphotericin B was 1.85% and 0.8% for the liposomal formulation and Fungizone® (reference) respectively. The retarded release from the liposomes may be due to the strong binding of the drug to the lipids (DOPC and cholesterol) and hence a stable complex or hindrance by the dialysis membrane. Yang et al. in their study recorded a release of only 12.3% of Amphotericin B after 96 hours from cubosomes made from Phytantriol and poloxamer 407. Kumar et al. also stated 10% release in the first 24 hours from their PLGA nanoparticle preparation. An in vitro release study of the drug into serum from a complex of Amphotericin B with poly (α-glutamic acid) (PGA) also indicated an amount of 9.74% released after 24 hours. The same complex dialysed in phosphate buffered saline (PBS) containing 5% DMSO (pH 7.4); only 1.46% of the total drug was released after 24hr incubation (Abeer et al. 2013). These results clearly indicate that the release of Amphotericin B from formulation matrices is generally slow due to its hydrophobic nature which could be advantageous in vivo by reducing the toxicity effect of the drug. Thus the 1.85% after 8 hours, though very low, is seemingly comparable to the other results in the literature. The release of the drug from the Fungizone® preparation was extremely low due to precipitation and sedimentation of the drug in the medium in the dialysis cassette. The release of Fungizone® was comparable to the liposomes during the first 3 hours. The release profiles were however similar by the calculation of the f_2 value (f_2 = 98.21). Reproducibility of the experiment was a major problem as it is evident in the error bars of the graph (figure 4.17). Kumar and Jain in their study of the release of Amphotericin B from polymerosomes tried different media such as phosphate buffer (0.1M, pH 7.4) and buffer with varying strengths of Tween 80 (1,2 and 2.5% w/v) and sodium dodecyl sulphate (0.1, 0.25, 0.5, 1, and 2% w/v). They concluded that in all cases the results were not reproducible with their formulation (Kumar and Jain, 2010). This notwithstanding, the complex formed between the drug and the components of the vesicle can be said to be stable to enhance lymphatic uptake of the liposomes.

Amphotericin B is well known for its severe and potentially lethal side effects. Its use in the form of Fungizone® causes several forms of anaemia and other blood dyscrasias. This is one of the major factors that limit the use of Fungizone®. The toxicity of the liposomal formulation was again evaluated using freshly obtained human red blood cells (RBCs) to determine haemolysis in comparison to Fungizone®. Figure 4.17 revealed a haemolysis of 4.1% by the formulation as compared to almost 100% by Fungizone® at a concentration of 50µg/ml. Thus, the liposomes are significantly non-haemolytic ($p<0.05$). The literature reports low haemolytic activity of lipid based formulations of Amphotericin B. The damaging

effect of the drug depends on its ability to dissociate from complexes. The affinity between the drug and deoxycholate in Fungizone® is very weak compared to that between the drug and lipids (Brajtburg and Bolard, 1996). Thus, the drug dissociates easily from the deoxycholate and hence exerts its damaging effect. The drug's dissociation from lipids is concentration dependent. Therefore, at the concentrations tested there was no haemolysis as compared to the reference.

5.4.1 Equivalent scattering length density determination by SANS

Small angle neutron scattering has been an important tool for the elucidation of structures and domains of many macromolecules, complexes and biochemical reactions. The technique has been applied to study the assembly, dispersion, alignment and mixing of nanoscale condensed matter. It is also used to characterise the internal structure of organic films and porous structures (Hollamy, 2013). Recently, the technique has been used pharmaceutically to study structure interaction between drugs and colloids of biorelevant media in drug development of poorly soluble drugs (Khoshakhlagh et al. 2014, 2015; Nawroth et al. 2011). Neutrons are non destructive and the high scattering length difference between hydrogen and its isotope, deuterium, makes neutron scattering a favorite tool for membrane research (table 8). The deuterium contrast variation method enabled the AmB-HST structure to be resolved (see section 5.1). This method was extended to the liposome formulation as well as the AmB-HST to determine the equivalent scattering length density of the liposomes with and without cholesterol, and the lecithin-gelatin matrix with Amphotericin B. The Guinier and Kratky-Porod plots are the standard plots that were used to determine the radius of gyration and layer span thickness respectively. The sizes of the particles were calculated from these parameters and compared to measurements from dynamic light scattering (DLS). It is worth stating that small unilamellar liposomes (SUV) were prepared for the neutron scattering experiments due to the size limit of the KWS-2 instrument (<100nm).

The scattering profiles, Guinier and Kratky-Porod plots of selected samples for the liposomes of Amphotericin B with and without cholesterol as well as their blanks are shown in sections 4.4.1 to 4.4.5 (see also Appendix D1, D2, D4 and D5). Table 18 indicated that the DLS size for the DOPC-Amphotericin B was higher than measured by SANS. This is expected as light scattering measures the solvated particles in solution (hydrodynamic size) whereas SANS measures the particles only. In comparison to the cholesterol containing vesicles, the size as measured by SANS for the DOPC-Amphotericin B vesicles were marginally larger, though not significant. The membrane thickness was however comparable. Both membrane thicknesses were larger than a normal biological membrane (4 – 4.5 nm). The DLS measurements on the other hand had the sizes of the cholesterol containing vesicles being larger than without cholesterol vesicles in almost all the D_2O concentrations. The sizes of the blanks as measured by SANS were smaller than the drug containing vesicles (32.47±0.22 nm for DOPC liposomes and 33.95±0.19 nm for DOPC-cholesterol, all measured in 33% D_2O buffer) but the thickness of the membrane were higher (6.06±0.77 nm for DOPC vesicles only and 6.44±0.63 nm for DOPC-cholesterol vesicles). The drug certainly has a profound effect on the size of the vesicles but minimal on the membrane thickness. Herec et al reported no significant change in bilayer thickness when Amphotericin B at 1 mole% was added to vesicles made from egg yolk phosphatidylcholine investigated with SANS and SAXS.

However, at 5 mole% drug incorporation, there was a significant change in the lipid acyl chain ordering which is consistent with the incorporation of the drug into the hydrophobic layer of the membrane (Herec et al. 2007; Foglia et al. 2011). Thus the slight thinning of the drug containing vesicles in relation to the blanks may be due to binding of the drug within the lipid head groups which leads to a disturbance of the lipid packing. This has been concluded by Gruszecki et al. on the basis of UV-Vis-linear dichroism (Gruszecki et al. 2003a, b). The increase in size as measured by SANS for the drug containing vesicles may be due to molecular aggregation of the drug-cholesterol complexes in the vesicles as was evident in the UV-Visible spectrum (Figure 4.11B). It is stated in the literature that Amphotericin B binds to lipid membranes and to cholesterol containing lipid membranes preferentially in the dimeric form (Gruszecki et al. 2009).

The DLS results revealed a bimodal distribution of particles as expected from liposomes prepared by sonication which comprises of both small unilamellar and multilamellar vesicles depending on the time of the sonication (Figure 4.26 and 4.27). The multilamellar liposomes escaped detection by the SANS due to the size limit of the instrument (Tables 18 and 19).

With regards to the AmB-HST, the neutron scattering revealed particles in the size range of 60 to 90 nm which could not be detected by the DLS measurements in parallel with larger particles (Table 20). The DLS measurements however revealed microparticles which increased in size with increasing deuterium content (see Table 20 and Figure 4.28). The large particles fell into the beamstop of the SANS instrument hence not detectable. The large particles could be aggregates of the core-shell particles or drug aggregates (see Figure 4.4A) as a result of sedimentation.

Small-angle neutron scattering experiments require preparations that are homogenous, monodisperse and non-interacting (Schoenborn et al. 1987). An inhomogeneous sample with particle interaction would result in Guinier plots which are non-linear near the origin. All the Guinier plots for the small unilamellar liposomes with and without cholesterol as well as blanks were initially linear. This was confirmed by the deuterium contrast variation plots of the square root of the intensity at zero scattering against the deuterium content (Figure 4.29 and 4.30). The DOPC had an equivalent scattering length density absolute of 0.298×10^{10} cm^{-2} which is consistent with the literature for phospholipids. The presence of the cholesterol in the blank vesicles resulted in an equivalent scattering length density absolute of 0.237×10^{10} cm^{-2} (0.9% D_2O equivalent difference). This indicates an alteration of the internal structure of the DOPC-cholesterol bilayer. The same effect was realised for the vesicles containing drug. The equivalent scattering length density absolute for the DOPC-Amphotericin B liposomes was 0.585×10^{10} cm^{-2} and that for DOPC-Cholesterol-Amphotericin B was 0.446×10^{10} cm^{-2} (2% D_2O equivalent difference). However, the densities were higher due to the high density nature of Amphotericin B in the complex with the lipid and cholesterol. The density distribution in the internal structure of the vesicles was investigated with the Stuhrmann plots. The linear nature of the graphs explains that the components of the drug containing liposomes with and without cholesterol have the same centre of mass. The β factor in the Stuhrmann equation (eqn. 23) is thus zero. The α-factor which is the slope of the line indicates the distribution of the scattering densities. Since the values for both formulations are positive, it means that the components with the higher scattering length density are located farther away from the centre

of mass (outside). This implies that the hydrophilic portions of the complex are located farther away from the centre of mass whiles the hydrophobic regions are towards the centre of mass. The parameters of the AmB-HST were completely different from the liposomes. The contrast variation graph was not linear (see figure 4.29 bottom) as well as the Stuhrmann plot (see figure 4.31 bottom). The contrast variation graph was not linear at the lower deuterium content indicating that it could be closer to the equivalent scattering length density of the complex which was estimated to be $1.438x10^{10}$ cm^{-2} (28.8% D_2O as against the measurement of 33% D_2O buffer). This is far higher than that for the liposomes and establishes the denser nature of the core-shell structure. The non-linearity of the graphs proves the mixture is not homogenous and that there could be sedimentation of particles or demixing. It is also possible to have a shell of lecithin-gelatin without drug, by deducing from the core-shell nature of the formulation. The components of the core-shell particle do not have the same centre of mass as depicted by the Stuhrmann plot. However, like the liposomes, the α-value is positive signifying the higher scattering components are farther from the centre of mass of the core-shell particle. The above analysis highlights the anticipation that the AmB-HST formulation is likely to precipitate in the intestinal environment even though solubility and dissolution of the drug are improved. The high density nature of the formulation causes rapid sedimentation and likely aggregation (see DLS results-Table 20).

5.4.2 Internal structure of Amphotericin B-lipid complexes in a model membrane

A number of research by way of experimental and molecular dynamics simulations have been conducted to elucidate the molecular organisation of the complexes formed between Amphotericin B and sterols as well as lipids in model biological membranes. Most of these researches confirm the importance of sterols in the activity of Amphotericin B (and other polyene macrolides) in pore formation in fungal membranes (Matsumori et al, 2005; Baginski et al, 2002; Milhaud et al, 1999; Herve et al, 1989; Czub et al, 2006; Bolard et al, 1991). It is confirmed that the antibiotic inserted into cholesterol containing membranes induces ordering of the hydrocarbon chain (acyl) of the lipids (Czub et al, 2007). The molecular simulations as well as experimental findings confirm the increase in membrane thickness by Amphotericin B in the presence of sterols (Czub et al, 2006 and Lopes et al, 2002). Recently Foglia et al have investigated the effect of Amphotericin B on phospholipid and phospholipid-sterol membrane structure by small angle neutron scattering (SANS). They used POPC as the phospholipid and cholesterol and ergosterol as the sterols. The samples were mixtures of MLVs and SUVs with 30% of either sterol. The study was able to calculate the lamellar to lamellar distance even though there were no visible Bragg peaks in the scattering profiles. They however confirmed an increase in membrane thickness caused by the drug in sterol containing membranes (Foglia et al, 2011). The increase in membrane thickness is attributed to two possible modes of insertion of the drug in the membrane: (1) the drug inserts itself in the lipid head groups and lies more or less flat on the membrane surface or (2) the drug embeds itself vertically into the outer leaflet of the bilayer with its amino-sugar protruding above the level of the phospholipid head groups. Foglia et al SANS modelling could not distinguish between the two situations but speculated that the most likely increase in

membrane thickness could be due to vertical insertion of the drug in the membrane. This posture has also been supported by Lopes et al. using UV-Vis linear dichroism (Lopes et al, 2002).

In an initial experiment, the inter-lamellar Bragg peaks which were not identified by Foglia et al were seen in the scattering profiles of Amphotericin B in DOPC with and without cholesterol. This was observed in both MLVs and SUVs (Figures 4.32 and 4.33). The samples were not finished products for final application (not lyophilised). Therefore the final freeze-dried products were used after re-hydration to investigate the internal orientation of the drug-lipid complexes in the model DOPC membrane. The products contained different cholesterol to drug concentrations. The Bragg peaks were identified as a broad curvature for all the multilamellar liposomes, both drug containing nanoparticles and blanks (Figure 4.34). The inter-lamellar distances ranged between 9.52 and 10.83 nm for both blanks and drug containing vesicles. The membrane thickness results indicated some membrane thickening and some thinning which was also identified by Foglia et al. (Table 23).

Of interest to this work is the domains observed by Bragg peaks in the small unilamellar liposomes obtained by sonication of the re-hydrated final product (MLV). The drug containing liposomes of the finished products containing different cholesterol to drug ratios were used. The deuterium contrast variation was employed by choosing the deuterium content based on the experiment conducted to determine the scattering length densities of the formulations as discussed in section 5.4.1. The scattering of the lipids and drug were eliminated by 12% and 29% D_2O buffer respectively. The Bragg peaks were clearly seen (Figures 4.38 and 4.39). The peak however was smeared at the higher cholesterol concentration. These peaks are however not inter-lamellar distances as is the case in multilamellar vesicles but rather are lateral domains in the membranes. Results by Guinier and Kratky-porod approximations revealed two radii of gyrations and two membrane spans (Table 24, Figures 4.38 and 4.39). The lower values calculated for the membrane spans are higher than normal membranes confirming membrane thickening by Amphotericin B. The distance between seperated domains decreased with the increase in cholesterol from 10 mol% to 30 mol%. In view of the results and using the geometry of small unilamellar liposomes as spherical in shape, the model in figure 4.41 was assumed for the organisation of the drug in the sterol containing membrane model of DOPC and cholesterol. The sizes were confirmed by dynamic light scattering (figure 4.37). If the domains were axially symmetrical to the membrane centre, one radius of gyration would have been observed. The existence of two radii of gyrations and membrane spans suggests that the domain is not axially symmetrical to the membrane centre but occur more towards the outer leaflet of the membrane. These findings confirmed the Stuhrmann results above where the higher scattering density domains occur more towards the outside. The number of drug-rich domains was calculated from the geometry of a model small unilamellar vesicle as spherical and the domains increased from 7 to 9 with increase in cholesterol and drug contents. This supports the decrease in inter-domain distance observed. A further increase in cholesterol however reduced the domains. This effect may be due to the probable solubilisation of the drug in the presence of excess lipids (as a solvent for the drug). A proposed novel model for the internal organisation of Amphotericin B in membranes is shown in figure 5.2 below.

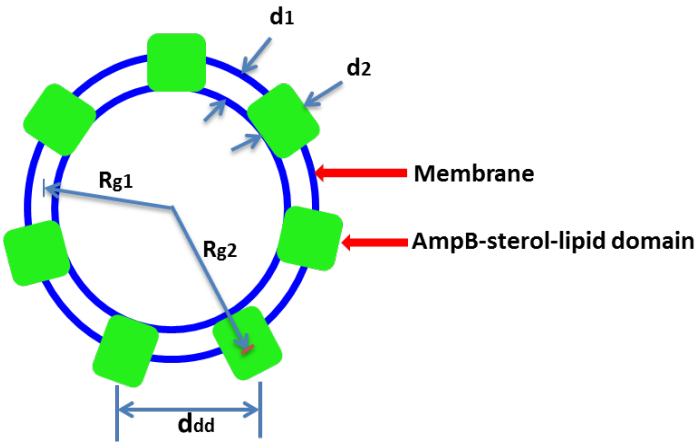

d_{dd} = Distance between two drug domains

Figure 5.2: Block model showing internal organisation of Amphotericin B-cholesterol-lipid complex in DOPC-cholesterol membranes

The equivalent scattering length densities of the lateral domains were investigated by deuterium contrast variation. The equivalent scattering length density of the domains in the different formulations was almost the same (figure 4.42). Thus, the density of the domains is independent of the concentration of lipid (DOPC), drug (Amphotericin B) and sterol (cholesterol).

The conclusion is drawn that the contrast variation method of the small angle scattering of freeze-dried small unilamellar liposomes showed domains. The membrane thickening by Amphotericin B was confirmed and that the drug inserts vertically in cholesterol containing membranes as proposed in the literature. The number of domains increased as the drug and cholesterol increased but to a certain limit. The tentative structure of the drug containing multilamellar vesicles is thus proposed in figure 5.3.

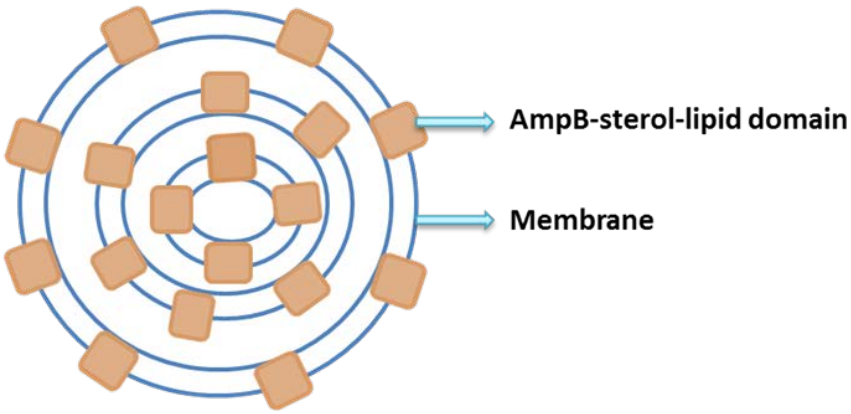

Figure 5.3: Block model showing internal organisation of Amphotericin B-sterol-lipid complex in DOPC-cholesterol multilamellar vesicles.

Discussion

The dosage regimen for Amphotericin B is disease and product specific. Treatment ranges from 3 days to several months depending on the type of infection. A dose ranges from 0.25 mg/kg body to 1 mg/kg body weight per day for Fungizone® (micellar dispersion of Amphotericin B with sodium deoxycholate). For Ambisome® (liposomal formulation), dosage is 3 to 5 mg/kg body weight per day and can be higher depending on the type of infection and its severity. A total treatment dose of 2 to 4 g of Amphotericin B is recommended. In using Fungizone® as a guide which is the conventional formulation, one would require between 17.5 mg to 70 mg of Amphotericin B per day. Assuming a bioavailability of 50% by the oral route, one would require between 35 mg to 140 mg of Amphotericin B per day.

The formulated freeze-dried liposomes could be used as a core for an enteric coated tablet. 245 mg of the matrix contains about 4 mg of Amphotericin B. Thus, about 3 g matrix could be compressed into 6 standard tablets for oral administration per day (in divided doses). It is recommended that an alternative cheaper lipid like purified soy bean lecithin could be used for the reduction of cost and drug load improvement. The compressed core matrix should be sealed with some sugar solution since it is porous and then enteric coated for intestinal dissolution. The developed multilamellar vesicles in this work open a new perspective for the oral delivery of Amphotericin B.

6. CONCLUSION

Three drug formulations for oral administration of Amphotericin B were developed, characterized and compared namely core-shell particles (AmB-HST), nanoemulsion and multilamellar vesicles (MLV). The novel homogenous core-shell formulation of the hydrophobic antifungal polyene drug Amphotericin B was prepared from the pure drug, lecithin and gelatin with the HST process, analogous to that established earlier for Simvastatin and some other drugs. The photometric investigation revealed the final product as an aggregate of drug monomers. The microscopic investigation depicted a resolution of aggregates in the starting material to individual drug spheres preceding the encapsulation in lecithin and gelatin. The structure investigation indicated a narrow distribution of encapsulated drug particles of ~ 1 µm size. The shell structure of HST particles was the first time resolved by neutron scattering using the deuterium solvent contrast method. The neutron scattering of the particles upon partly contrast matching of the drug core depicted the lecithin-gelatin shell as a thin layer of 5.64 ± 0.18 nm span, which is similar, but slightly larger as compared to the biological lipid membrane. The finding offers opportunities for further improvements of the formulation, e.g. by surface modification. A further small angle neutron scattering investigation by contrast variation method indicated that the components of the core-shell particles do not have the same centre of mass and have the higher scattering domains more towards the outside and are asymmetric. The particles are denser as compared to liposomes. In vitro release study proved the solubilizing power of the HST system as the drug release was higher for the formulation than the pure drug at all sampled time points.

The nanoemulsion formulation of Amphotericin B with the same oil and surfactant but different co-solvents was successfully formulated. The drug was shown to be non-lipophilic and non-hydrophilic by the solubility determination in the various excipients. Determination of the concentration of excipients necessary for emulsification by ternary phase diagrams showed that high oil and surfactant contents led to no emulsion formation. Thus the highest oil content was 10%. Droplet size was found to increase with increasing surfactant concentration which indirectly decreased co-solvent amount for the propylene glycol nanoemulsion. However, the reverse was the case for the Transcutol®P nanoemulsion where increasing the surfactant concentration rather decreased the droplet size. The inclusion of the drug did not change the viscosity of the formulation but influenced the droplet size. The drug incorporation increased the droplet size of the formulations. Drug content increased with increasing propylene glycol content and decreased when Transcutol®P content was increased. UV-Visible spectral analysis indicated the Amphotericin B to be in the monomeric state in both formulations. The formulations were however toxic to Caco-2 cells and to human red blood cells. The toxicity was not only due to the Amphotericin B but also to the excipients as the blanks were even more toxic than the drug containing formulations. The amount of drug solubilized in both preparations was inadequate in comparison to the amount of excipients to be consumed as set by the WHO. The formulations by this analysis do not look suitable for oral administration but there is the need for animal studies to ascertain the effect on the animals and how much drug reaches the systemic circulation. This will enable justified conclusions to be made and the possible prospects of the formulations. This notwithstanding, the pre-concentrates are very stable and can be stored at room temperature.

Conclusion

Multilamellar vesicular formulations of Amphotericin B with unsaturated and saturated neutral phospholipids and cholesterol were successfully formulated and revealed not only vesicles but other additional structures at increasing cholesterol concentration. The particle size analysis showed microparticles with the saturated lipids and was acyl chain length dependent. Nanoparticles were however formed with the unsaturated lipid (DOPC) with favourable encapsulation and particle size distribution. Thermal analysis and FTIR spectroscopy showed the absence of the influence of the drug confirming the probability of drug insertion in lipid and/or cholesterol rich membranes as reported in the literature. The formulation fractionated by a linear sucrose density gradient indicated a bimodal distribution of vesicles and drug-lipid complexes with the drug associated more with the complexes than the vesicles. Experiments by the contrast variation method of the small angle neutron scattering was successfully conducted and revealed that cholesterol formed a complex with Amphotericin B in situ. This was indicated partly by the difference in the equivalent scattering length density of the drug-lipid and drug-lipid-cholesterol small unilamellar vesicles. The scattering profiles showed Bragg peaks indicating domains and critical investigation revealed that the number of domains increased with increasing cholesterol content but to a certain limit as further increase caused a decrease in the number of domains. The domains occur more towards the outside of the model membrane and confirms the vertical insertion of the drug in cholesterol rich membranes. The formulation was not toxic to Caco-2 cells as well as human red blood cells and showed promise for oral administration as it was taken up by Caco-2 cells. This formulation has prospect and could be compressed into tablets. A film coating will enable the drug to withstand the acidic environment of the stomach. Animal studies are required to assess the systemic availability of the formulation. The developed multilamellar formulation including drug-cholesterol complexes opens a perspective for medical application.

6.1 Zusammenfassung

In der Form von Nanokapseln (AmB-HST), Nanoemulsion beziehungsweise multilamellaren Vesikeln (MLV) wurden drei Amphotericin-B-Formulierungen für die orale Applikation entwickelt, charakterisiert und verglichen. Die neuartige homogene Nanokapsel-Formulierung des hydrophoben Polyen-Antimykotikums Amphotericin B wurde in Analogie zu einem für Simvastatin und andere Arzneistoffe etablierten Prozess aus der Reinsubstanz, Lezithin und Gelatine mit Hilfe des HST-Verfahrens hergestellt. Photometrische Untersuchungen zeigten, dass das Endprodukt aus Monomeren aufgebaut ist. Mittels Mikroskopie ließen sich die Aggregate vor der Umhüllung mit Lezithin und Gelatine im Ausgangsmaterial als individuelle kugelförmige Arzneistoffpartikel darstellen. Strukturuntersuchungen mit dynamischer licht streuung (DLS) zeigten eine enge Größenverteilung der verkapselten Partikel von ca. 1 µm. Die Struktur der Hülle der HST-Partikel wurde erstmalig mit Neutronenstreuung unter Verwendung der Deuterium-basierten Lösungsmittel kontrastmethode aufgeklärt. Durch die teilweise Kontrastmaskierung des Partikelkerns bei der Neutronenstreuung konnte die Lezithin-Gelatine-Hülle als eine dünne, 5,64 ± 0.18 nm dicke Schicht aufgelöst werden, welche der biologischen Lipidmembran ähnlich, im Vergleich aber geringfügig größer ist. Dieses Resultat eröffnet Wege für die Optimierung der Formulierung von pharmazeutischen Nanopartikeln, z.B. durch Oberflächenmodifizierungen. Weitere Untersuchungen mittels Kleinwinkelneutronenstreuung unter Verwendung der D-Kontrastvariation deuten darauf hin, dass die Komponenten der Nanokapseln nicht den gleichen Masseschwerpunkt haben, sondern asymmetrisch aufgebaut sind und dass die stärker streuenden Domänen weiter außen liegen. Die Partikel sind im Vergleich zu Liposomen dichter. In-Vitro Freisetzungsstudien belegen das Solubilisierungsvermögen des HST-Systems, wonach die Freisetzung des Arzneistoffes aus der Formulierung zu allen gemessenen Zeitpunkten höher als diejenige der Reinsubstanz war.

Die Nanoemulsion-Formulierung von Amphotericin B wurde mit einem Öl und Tensid system, jedoch mit unterschiedlichen Co-Solvenzien, erfolgreich entwickelt. Gemäß der Bestimmung der Löslichkeit in verschiedenen Hilfsstoffen erwies sich der Arzneistoff Amphotericin B als nicht-lipophil, gleichzeitig aber auch als nicht-hydrophil. Die zur Ermittlung der für die Emulsionsbildung notwendigen Hilfstoffkonzentrationen erstellten ternären Diagramme veranschaulichten, dass hohe Öl- und Tensidgehalte zu keiner Emulsionsbildung führten. Dementsprechend betrug der höchste Ölgehalt 10%. Die Tröpfchengröße wuchs mit zunehmender Tensidkonzentration, wobei die Co-Solventmenge der Propylenglykol-haltigen Nanoemulsion indirekt verringert wurde. Für die Transcutol®P-haltige Nanoemulsion hingegen wurde das Gegenteil beobachtet, nämlich eine Abnahme der Tröpfchengröße bei steigenden Tensidkonzentrationen. Durch den Einschluss des Arzneistoffes wurde nicht die Viskosität der Formulierung, sondern die Tröpfchengröße beeinflusst. Der Wirkstoffeinschluss führte zu höheren Tröpfchengrößen. Mit zunehmender Propylenglykolkonzentration wurde der Wirkstoffgehalt erhöht, mit zunehmender Transcutol®P-Konzentration dagegen vermindert. UV/VIS-spektroskopische Analysen deuten darauf hin, dass in beiden Formulierungen Amphotericin B als Monomer vorliegt. Allerdings erwiesen sich die Formulierungen Caco-2-Zellen und humanen roten Blutkörperchen gegenüber als toxisch. Da die Kontrollproben eine höhere Toxizität als die wirkstoffhaltigen Formulierungen zeigten, ist die Toxizität nicht nur auf Amphotericin, sondern auch auf die Hilfsstoffe zurückzuführen. Die solubilisierte Wirkstoffmenge ist in beiden Formulierungen nicht ausreichend im Hinblick auf die eingesetzte Menge an Hilfsstoff

nach WHO-Kriterien. Gemäß diesen Untersuchungen erscheinen die Emulsions-Formulierungen für die orale Gabe nicht geeignet. Dennoch sind Tierstudien notwendig, um den Effekt bei Tieren sowie die systemisch verfügbare Wirkstoffmenge zu ermitteln. Dies wird bestandskräftige Schlussfolgerungen bezüglich der Formulierung und Aussagen über mögliche Perspektiven erlauben. Nichtsdestotrotz sind die Präkonzentrate sehr stabil und können bei Raumtemperatur gelagert werden.

Die multilamellar-vesikulären Formulierungen von Amphotericin B mit ungesättigten und gesättigten neutralen Phospholipiden und Cholesterin wurden erfolgreich entwickelt und enthielten nicht nur Vesikel, sondern auch zusätzliche Strukturen bei zunehmender Cholesterinkonzentration. Mittels Partikelgrößenanalyse wurden bei den Formulierungen mit gesättigten Lipiden Mikropartikel detektiert, was abhängig von der Alkylkettenlänge war. Mit dem ungesättigten Lipid (DOPC) konnten hingegen Nanopartikel mit hinreichender Verkapselung und Partikelgrößenverteilung gebildet werden. Die Ergebnisse der thermischen und FTIR-spektroskopischen Analyse, welche den Einfluss des Arzneistoffes ausschließen ließen, liefern den Nachweis für die mögliche, bereits in der Literatur beschriebene Einlagerung des Wirkstoffs in lipid- und/oder cholesterinreiche Membranen. Mit Hilfe eines linearen Saccharosedichtegradienten konnte die Formulierung in Vesikel und Wirkstoff-Lipid-Komplexe nach bimodaler Verteilung aufgetrennt werden, wobei der Arzneistoff stärker mit den Komplexen als mit den Vesikeln assoziiert ist. Bei den Kleinwinkelneutronenstreu-Experimenten wurde die Methode der Kontrastvariation mit Erfolg angewendet. Dabei konnte gezeigt werden, dass Cholesterol in situ einen Komplex mit Amphotericin B bildet. Diesen Sachverhalt legt unter anderem die beobachtete Differenz in der äquivalenten Streulängendichte der Wirkstoff-Lipid- und Wirkstoff-Lipid-Cholesterin-haltigen kleinen unilamellaren Vesikeln nahe. Das Vorkommen von Bragg-Peaks im Streuprofil weist auf Domänen hin und systematische Untersuchungen zeigten, dass die Anzahl der Domänen mit steigendem Cholesteringehalt zunimmt, ab einem bestimmten Grenzwert jedoch wieder abnimmt. Die Domänen treten vor allem nahe der Außenfläche der Modellmembran auf und bestätigen, dass der Wirkstoff in den Cholesterinreichen Membranen vertikal eingelagert ist. Die Formulierung war sowohl Caco-2-Zellen als auch humanen roten Blutkörperchen gegenüber nicht toxisch und erwies sich unter Berücksichtigung der Aufnahme in Caco-2-Zellen als vielversprechend für die orale Applikation. Die Formulierung zeigt sich somit aussichtsreich und könnte in Tabletten weiterverarbeitet werden. Ein Filmüberzug würde den Wirkstoff gegen die saure Umgebung im Magen schützen. Für die Bestimmung der systemischen Verfügbarkeit der Formulierung sind Tierstudien notwendig. Die entwickelten multilamellaren Formulierungen einschließlich der Wirkstoff-Cholesterin-Komplexe bieten somit gute Aussichten auf die mögliche medizinische Anwendung.

7. REFERENCES

Abeer H.A.M.A., Karolina, A.L., Karin, S., Croft, S.L., Brocchini, S., 2013. Noncovalent complexation of amphotericin B with poly (α-glutamic acid). Mol. Pharmaceutics., 10(3), 940-950.

Abrahamsson, H. Lennernas, 2005. Application of the biopharmaceutic classification system now and in the future. Drug Bioavailability, Estimation of Solubility, Permeability, Absorption, and Bioavailability. Waterbeemd, H. v. d., Lennernas, H. & Artursson, P., WILEY-VCH. 18 495 531.

Adams, M.L., Andes, D.R., Kwon, G.S., 2003. Amphotericin B encapsulated in micelles based on poly(ethylene oxide)-block-poly(L-amino acid) derivatives exerts reduced in vitro hemolysis but maintains potent in vivo antifungal activity. Biomolecules, 4(3): 750-757.

Ahmad, I., Longenecker, M., Samuel, J., Allen, T.M., 1993. Antibody-targeted delivery of doxorubicin entrapped in sterically stabilized liposomes can eradicate lung cancer in mice. Cancer Res. 53, 1484-1488.

Akbarzadeh, A., Sadabay, R.R., Davaran, S., Sang, W.O., Zarghami, N., Hanifehpour, Y., Samie, M., Kouhi, M., Kazem, N.K., 2013. Liposome: classification, preparation, and applications. Nanoscale Research Letters. 8(102): 1-9.

Ali, M.H., Behfar, M., Kirby, D.J., Afzal, R.M., Perrie, Y. 2013. The role of lipid geometry in designing liposomes for the solubilisation of poorly water soluble drugs. Int. J. Pharm. 453 (1):225-232.

Alvi, M.M. and Chatterjee, P. 2014. A prospective analysis of co-processed non-ionic surfactants in enhancing permeability of a model hydrophilic drug. AAPS PharmSiTech. 15(2): 339-353.

Amidon, G.L., DeBrincat, G.A., Najib, N., 1991. Effects of gravity on gastric emptying, intestinal transit and drug absorption. J. Clin. Pharmacol., 31: 968-973.

Amidon, G.L., Lennernas, H., Shah, V.P., Crison J.R., 1995. A theoretical basis for the biopharmaceutic drug classification: The correlation of in vitro drug product dissolution and in vivo bioavailability, Pharm. Res., 12, 413-420.

Anderson, B.D., 1999. Chemical and related factors controlling lipid solubility. Bull. Tech. Gattefosse 92: 11-18.

Aramwit P, Yu BG, Lavasanifar A, Samuel J, Kwon GS. 2000. The effect of serum albumin on the aggregation state and toxicity of amphotericin B. J Pharm Sci 89:1589–1593.

Baginski, M., Resat, H., Borowski, E. 2002. Comparative molecular dynamics simulations of amphotericin B-cholesterol/ergosterol membrane channels. Biochim. Biophys. Acta 1567: 63-78.

References

Bangham, A.D., Horne, R.W., 1964. Negative staining of phospholipids and their structural modification by surface-active agents as observed in the electron microscope. J. Mol. Biol. 8, 660-668.

Barlett K, Yau E, Hartsel SC, Hamer A, Tsai G, Bizzotto D, Wasan KM. 2004. Effect of heat-treated amphotericin B on renal and fungal cytotoxicity. Antimicrob Agents Chemother 48:333-336.

Barwicz, J., Christian, S., Gruda, I., 1992. Effects of the aggregation state of amphotericin B and its toxicity to mice. Antimicrob. Agents Chemother., 36, 2310-2315.

Barwicz, J., Christian, S., Gruda, I., 1992. Effects of the aggregation state of amphotericin B and its toxicity to mice. Antimicrob. Agents Chemother., 36, 2310-2315.

Bekersky I, Fielding RM, Dressler DE, Lee JW, Buell DN, Walsh TJ. 2002. Pharmacokinetics, excretion, and mass balance of liposomal amphotericin B (AmBisome) and amphotericin B deoxycholate in humans. Antimicrob Agents Chemother 46:828–833.

Bennett J. 1995. Antimicrobial agents: antifungal agents. In: Hardman J., Limbird L (eds) Goodman & Gillman's pharmacological basis of therapeutics. McGraw-Hill, New York, pp 1175-1790.

Betlach, C.J., Gonzalez, M.A., McKiernan, B.C., Neff-Davis, C., Bodor, N.J., 1993. Oral pharmacokinetics of carbamazepine in dogs from commercial tablets and a cyclodextrin complex. Pharmaceutical Sciences 82 (10), 1058–1060.

Bolard, J., Legrand, P., Heitz, F., Cybulska, B., 1991. One-sided action of amphotericin B on cholesterol-containing membranes is determined by its self-association in the medium. Biochemistry, 30: 5707-5715.

Bolard J, Marzeski J., Borowski E., 1995. Effect of the modifications of ionizable groups of amphotericin B on its ability to form complexes with sterols in hydroalcoholic media, Biochimica et Biophysica Acta 1236: 170-176.

Bolard J, Seigneuret M, Boudet G. 1980. Interaction between phospholipid bilayer membranes and the polyene antibiotic amphotericin B: Lipid state and cholesterol content dependence. Biochim Biophys Acta 599:280–293.

Brajtburg, J., Bolard, J. 1996. Carrier effects on biological activity of amphotericin B. Clin. Microbiol. Rev., 9, 512-531.

Butani,D., Yewale, C., Misra, A. 2014. Amphotericin B topical microemulsion: Formulation, characterisation and evaluation. Colloids and Surfaces B: Biointerfaces 166: 351-358.

Byrn, S.R., Pfeiffer, R.R., Stowell, J.G., 1999. Solid State Chemistry of Drugs, 2nd edn . SSCI, West Lafayette, IA.

Carriera EM, Szpilman AM, Volmer AA, 2010. Synthesis and biological evaluation of Amphotericin B derivatives. Nat. Prod. Rep. 27: 1329-1349.

References

Carter, K.C., Baille, A.J., Mullen, A.B., 1997. Comparison of the efficacies of various formulations of amphotericin B against murine visceral leishmaniasis. Antimicrob. Agents Chemother., 41, 2089-2092.

Chae-Eun, S., Choi, K.C., Bang, J.Y., Kim, P., Kim, C. 2008. Amphotericin B-incorporated polymeric micelles composed of poly (D,L-lactide-co-glycolide)/dextran graft copolymer. Int. J. Pharm. 355:224-230.

Charvalos E, Tzatzarakis MN, Van Bambeke F, Tulkens PM, Tsatsakis AM, Tzanakakis GN, Mingeot-Leclercq MP. 2006. Water-soluble amphotericin B-polyvinylpyrrolidone complexes with maintained antifungal activity against Candida spp. and Aspergillus spp. and reduced haemolytic and cytotoxic effects. J Antimicrob Chemother 57: 236–244.

Chatterjee, I., Kumar, A., Gill, R., Alrefai, W.A., Dudeja, P.K., 2014. M01765 3D Cell culture of Caco-2: A better model to study the functionality and regulation of intestinal ion transporters. Gastroenterology. 146 (5): S654.

Clarke, G.M., Newton, J.M., Short, M.D., 1993. Gastrointestinal transit of pellets of differing size and density. Int. J. Pharm., 100: 81-92.

Coa, Y., Marra, M., Anderson, B.D., 2004. Predictive relationship for the effects of triglyceride ester concentration and water uptake on solubility and partitioning of small molecules into lipid vesicles. J. Pharm. Sci. 93: 2768-2779.

Czub, J., Baginski, M., 2006. Modulation of Amphotericin B membrane interaction by cholesterol and ergosterol-a molecular dynamics study. J. Phys. Chem. B. 110: 16743-16753.

Daneshmend TK, Warnock DW. 1983. Clinical pharmacokinetics of systemic antifungal drugs. Clin Pharmacokinet 8:17–42.

Delmas, G., Park, S., Chen, Z.W. 2002. Efficacy of orally delivered cochleates containing amphotericin B in a murine model of aspergillosis. Antimicro. Agents Chemother.. 46: 2704-2707.

Delongeas, J.L., de Conchard, G.V., Beamonte, A., Bertheux, H., Spire, C., Maisonneuve, C., Becourt-Lhote, N., Goldfain-Blanc, F., Claude, N., 2010. Assessment of Labrasol/Labrafil/Transcutol (4/4/2, v/v/v) as a non-clinical vehicle for poorly water-soluble componds after 4-week oral toxicity study in Wistar rats. Regul. Toxicol. Pharmacol., 57: 284-290.

DeSesso, J.M., and Jacobson, C.F., 2001. Anatomical and physiological parameters affecting gastrointestinal absorption in humans and rats. Food Chem. Toxicol., Vol. 39, No.3, 209-228.

Duddu, S., Srinvivas, P., Ballesteros, D.L., Miller, D., Kugler, R., Frantz, C., Tan, T., Malcolmson, R., Washcok, K., Sweeny, T., Tarara, T.E., Dwivedi, S., Eldon, M.E., 2008. Compositions comprising Amphotericin B, methods and systems. United States patent US7326691 B2.

References

Eccleston, G.M. 1992. Microemulsions. In: Swarbrick, S., Boylan, J.C. (Eds), Encyclopedia of Pharmaceutical Technology. Marcel Dekker, New York, pp. 375-421.

El-Kattan, A., Varma, M., 2012. Oral absorption, Intestinal metabolism and Human oral bioavailability. INTECH open science. DOI. 10.5772/31087. www.intechopen.com.

Ellen K. Wasan, Karen Bartlett, Pavel Gershkovic, Olena Sivak, Brian Banno, Zhao Wong, Jeffrey Gagnon, Byron Gates, Carlos G. Leon, Kishor M. Wasan 2009. Development and characterisation of oral lipid-based amphotericin B formulations with enhanced drug solubility, stability and antifungal activity in rats infected with Aspergillus fumigatus or Candida albicans. Int. J Pharmaceutics 372:76-84.

Espada, R., Valdespina, S., Alfonso, C., Rivas, G., Baallesteros, M.P., Torrado, J.J., 2008. Effect of aggregation state on the toxicity of different amphotericin B preparations. Int. J. Pharm., 361, 64-69.

Espada, R., Valdespina, S., Dea, M.A., Molero, G., Ballesteros, M.P., Bolas, F., Torrado, J.J., 2008. In vivo distribution and therapeutic efficacy of a novel amphotericin B poly-aggregated formulation. J. Antimicrob. Chemother., 61, 1125-1131.

Foglia, F., Drake, A.F., Terry, A.E., Rogers, S.E., Lawrence, M.J., Barlow, D.J. 2011. Small-angle neutron scattering studies of the effect of amphotericin B on phospholipid and phospholipid-sterol membrane structure. Biochimi et Biophysica Acta 1808:1574-1580.

Fort, F.L., Heyman, I.A., Kesterson, J.W., 1984. Hemolysis study of aqueous polyethylene glycol 400, propylene glycol and ethanol combinations in vivo and in vitro. J. Parent. Sci. Technol. 38, 82.

Fournier, I., Barwicz, J., Tancrede, P., 1998. The structuring effects of amphotericin B on pure and ergosterol- or cholesterol-containing dipalmitoylphosphatidylcholine bilayers: a differential scanning calorimetry study. Biochemica et Biophysica Acta, 1373, 76-86.

Fricker, G., Kromp, T., Wendel, A., Blume, A., Zirkel, J., Rebmann, H., Setzer, C., Quinkert, R.O., Martin, F., Goymann-Müller, C., 2010. Phospholipids and Lipid-Based Formulations in oral drug delivery. Pharm. Res. 27:1469-1486.

Fukui, H., Koike, T., Saheki, A., Sonoke, S., Tomii, Y., Seki, J., 2003a. Evaluation of the efficacy and toxicity of amphotericin B incorporated in nano-sphere (LNS®). Int.J.Pharm. 236: 51-60.

Gaboriau F, Cheron M, Leroy L, Bolard J. 1997. Physicochemical properties of the heat-induced superaggregates of amphotericin B. Biophys Chem 66:1–12.

Gaines, G.L., 1966. Insoluble Monolayers at Liquid-Gas Interfaces. John Wiley & Sons Inc. New York (1966).

References

Garcia April, Jill Adler-Moore and Richard T. Proffitt, 2000. Single-Dose AmBisome (Liposomal Amphotericin B) as prophylaxis for murine systemic candidiasis and Histoplasmosis. Journal of Antimicobial chemotherapy. 44(9): 2327 – 2332.

Granger, D.N., Barrowman, J.A., Kvietys, P.R., 1985. Clinical gastrointestinal physiology. W.B. Saunders, Philadelphia.

Gruda I, Milette D, Brother M, Kobayashi GS, Medoff G, Brajtburg J. 1991. Structure-activity study of inhibition of amphotericin B (Fungizone) binding to sterols, toxicity to cells, and lethality to mice by esters of sucrose. Antimicrob Agents Chemother 35:24–28.

Gruszecki, W.I., Gagos, M. Herec, M. 2003a. Dimers of polyene antibiotic amphotericin B detected by means of fluorescence spectroscopy: molecular organization in solution and in lipid membranes. J. Photochem. Photobiol. B: Biol. 69:49-57.

Gruszecki, W.I., Gagos, M., Herec, M., Kernen, P. 2003b. Organisation of antibiotic amphotericin B in model lipid membranes. A mini review. Cell. Mol. Biol. Lett. 8:161-170.

Gruszecki, W.I., Luchowski, R., Gagos, M., Arczewska, M., Sarkar, P., Herec, M., Mysliwa-Kurdziel, B., Strzalka, K., Gryczynski, I., Gryczynski, Z. 2009. Molecular organisation of antifungal antibiotic amphotericin B in lipid monolayers studied by means of Fluorescence Lifetime Imaging Microscopy. Biophys. Chem. 143 (1-2): 95-101.

Hamill, R.J., 2013. Amphotericin B Formulations: A comparative review of efficacy and toxicity. Drugs, 73: 919-934.

Hassan P., Suman R., Verma G., 2015. Making sense of Brownian motion: Colloid characterization by Dynamic Light Scattering. Langmuir 31: 3-12.

Hauss, D., Fogal, S.E., Ficorilla, J.V., 1998. Lipid-based delivery systems for improving the bioavailability and lymphatic transport of a poorly water-soluble LTB4 inhibitor. J. Pharm. Sci. 87: 164-169.

Hauss, D.J., Mehta, S. and Radebaugh, G.W., 1994. Targeted lymphatic transport and modified systemic distribution of CI-976, a lipophilic lipid-regulator drug, via a formulation approach. Int. J. Pharmaceutics, 108, 85-93.

Hellweg, T., 2002. Phase structures of microemulsions. Current opinion in Colloids & Interface Science, 7, 50-56.

Herec, M., Islamov, A., Kuklin, A., Gagos, M. Gruszecki, W.I. 2007. Effect of antibiotic amphotericin B on structural and dynamic properties of lipid membranes formed with egg yolk phosphatidylcholine. Chem. Phys. Lipids 147:78-86.

Herve, M., Debouzy, J.C., Borowski, E., Cybulska, B., Gary-Bobo, C.M., 1989. The role of the carboxyl and amino groups of polyene macrolides in their interactions with sterols and their selective toxicity. A P-NMR study. Biochim. Biophys. Acta. 980: 261-272.

References

Heshmati, N., Cheng, X., Eisenbrand, G., Fricker G. 2013. Enhancement of oral bioavailability of E804 by self-emulsifying drug delivery system (SNEDDS) in Rats. J. Pharm. Sci. 102: 3792-3799.

Hilfinger, J., Kim J.S., Kijek, P. 2005. Methods and composition of extended delivery of water insoluble drugs. United States Patent 0220879A1.

Hollamy, M.J., 2013. Practical applications of small angle neutron scattering. Phys. Chem. Chem. Phys. 15: 10566-10579.

Holm, R., Jensen, I.H.M., Sonnergaard, J., 2006a. Optimization of self-microemulsifying drug delivery systems (SMEDDS) using a D-optimal design and the desirability function, Drug Dev. Ind. Pharm, 32: 1025-1032.

Holm, R., Porter, C.J., Mullertz, A., Kristensen, H.G., Charman, W.N., 2002. Structured triglycerides vehicles for oral delivery of halofantrine: Examination of intestinal lymphatic transport and bioavailability in conscious rats. Pharm. Res., 19, 1354-1361.

Horter, D and Dressman, J.B., 2001. Influence of physicochemical properties on dissolution of drugs in the gastrointestinal tract. Advanced Drug Delivery Reviews, Vol 46, No. 1-3, 75-87.

Hostetler, J.S., Hanson, L.H., Stevens, D.A., 1993. Effect of hydroxypropyl- β -cyclodextrin on efficacy of oral itraconazole in disseminated murine cryptococcosis. The Journal of Antimicrobial Chemotherapy 32(3), 459 – 463.

Hsiue, G., Wang, W.T., Wang C.H., 2009. Development of polyion complex micelles for encapsulating and delivering amphotericin B. Biomaterials, 30: 3352-3358.

Italia, J.L., Yahya, M.M., Singh, D., 2009. Biodegradable nanoparticles improve oral bioavailability of amphotericin B and show reduced nephrotoxicity compared to intravenous Fungizone. Pharm. Res., 26(6): 1324-1331.

Janoff AS, Boni LT, Popescu MC, Minchet SR, Cullis PR, Mallen TD, Taraschi T, Gruner SM, Shyamsunder E, Tate MW, Mendelshon R, Bonner D. 1988. Unusual lipid structures selectivity reduces the toxicity of amphotericin B. Proc Natl Acad Sci USA 85:6122–6126.

Janoff, A.S., Perkins, S.L., Saletan, S.L., Swenson, C.E. 1993. Amphotericin B lipid complex (ABLC®): A molecular rational for the attenuation of Amphotericin B related toxicities. J. Lip. Res, 3(3), 451-471.

Järvinen, T., Järvinen, K., Schwarting, N., Stella, V.J., 1995. Beta-cyclodextrin derivatives, SBE4-beta-CD and HP-beta-CD, increase the oral bioavailability of cinnarizine in beagle dogs. Journal of Pharmaceutical Sciences, 84 (3), 295–299.

References

Jeoung HY., Shanmugam, S., Thapa, P., Lee, E.S., Balakrishnan, P., Baskaran, R., Yoon, SK., Choi, HG., Yong CS., Yoo, BK.,Han, K. 2010. Novel self-emulsifying drug delivery system for enhanced solubility and dissolution of Lutein. Arch Pharm Res. Vol 33, (3): 417-426.

Jung, H.S., Deok, H.L., Soon H.J., Jung, E.L., Jeong, K.S., Seong, H., Byung, C.S., 2009. Amphotericin B-entrapping lipid nanoparticles and their in vitro and in vivo characteristics, Eur. J. Pharm. Sci, 37: 313-320.

Kajtar, M., Vikmon, M., Morlin, E., Szejtli, J., 1989. Aggregation of amphotericin B in the presence of γ-cyclodextrin. Biopolymers, 28, 1585-1586.

Kanchan K., Ahmad, J. Showkat R. M., Saima A., 2012. Self-Emulsifying Nano Carriers for Improved Oral Bioavailability of Lipophilic Drugs. Rev. Adv. Sci. Eng., 1(2): 1-14.

Kataoka, M., Masaoka, Y., Sakuma, S., Yamashita, S., 2006. Effect of food intake on the oral absorption of poorly water-soluble drugs: In vitro assessment of drug dissolution and permeation assay system. Journal of Pharmaceutical Sciences, 95, 2051-2061.

Khoo, SM., Humberstone, A.J., Porter, C.J.H., Edwards, G.A., Charman, W.N. 1998. Formulation design and bioavailability assessment of lipidic self-emulsifying formulations of Halofantrine. Int. J. Pharm. 167 (1-2): 155-164.

Khoshakhlagh P., Johnson R., Nawroth T., Langguth P., Schmueser L., Decker H., Hellmann N., Szekely N. 2015. Fasted-State Simulated Intestinal Fluid 'FaSSIF-C', a cholesterol containing Intestinal Model Medium for In vitro Drug Delivery Development. J. Pharm Sci., Vol 166, pp 1155 – 1166.

Khoshakhlagh P., Johnson R., Nawroth T., Langguth P., Schmueser L., Decker H., Hellmann N., Szekely N. 2014. Nanoparticle structure development in the gastrointestinal model fluid FaSSIFmod6.5 from several phospholipids at various water content relevant for oral administration. Eur. J. Lipid Sci. Technol., Vol 166, pp 1155 – 1166.

Kimura, M., Shizuki, M., Miyoshi, K., Sakai, T., Hidaka, H., Takamura, H., Matoba, T., 1994. Relationship between the molecular structures and emulsification properties of edible oils. Biosci. Biotechnol. Biochem. 58: 1258-1261.

Kommuru, T.R., Gurley, B., Khan, M.A., Reddy, I.K. 2001. Self-emulsifying drug delivery systems (SEEDS) of coenzyme Q10: formulation development and bioavailability assessment. Int. J. Pharm. 212: 233-246.

Kumar, N., Jain, J.P., 2010. Development of amphotericin B loaded polymersomes based on $(PEG)_3$-PLA co-polymers: Factors affecting size and in vitro evaluation. Eur. J. Pharm. Sci. 40: 456-465.

Kwon GS, Monica LS, 2003. Relative aggregation state and hemolytic activity of amphotericin B encapsulated by poly (ethylene oxide)-block–poly(N-hexyl-L-aspartamide)-acyl conjugate micelles: effects of acyl chain length. J controlled release 87:23-32.

References

Lamy-Freund, M.T., Ferreira, V.F., Faljoni-Alario, A., Schreier, S., 1993. Effect of aggregation on the kinetics of autoxidation of the polyene antibiotic amphotericin B. J.Pharm. Sci., 82, 162-166.

Langowski, J. Kremer, W., Kapp, U. 1992. Dynamic light scattering for study solution conformation and dynamics of superhelical DNA. Methods in enzymology, 211: 430-448.

Lavasanifar A, Samuel J, Satari S, Kwon GS. 2002. Block copolymer micelles for the encapsulation and delivery of amphotericin B. Pharm Res 91:125–133.

Lawrence, M.J., Lim, W.H. 2004. Aggregation behaviour of mixtures of phosphatidylcholine and polyoxyethylene sorbitan monoesters in aqueous solution. Phys. Chem. Chem. Phys. 6:1380-1387.

Lawrence, M.J., Lim, W.H. 2004. Influence of surfactant and lipid chain length on the solubilisation of phosphatidylcholine vesicles by micelles comprised of polyoxyethylene sorbitan monoesters. Colloids and Surfaces A: Physicochem. Eng. Aspects 250, 449-457.

Legrand P, Cheron M, Leroy L, Bolard J. 1997. Release of amphotericin B from delivery systems and its action against fungal and mammalian cells. J Drug Target 4:311–319.

Legrand, P., Romero, E.A., Cohers, B.E., Bolard, J., 1992. Effects of aggregation and solvent on the toxicity of amphotericin B to human erythrocytes. Antimicrob. Agents Chemother., 36,2518-2522.

Lemke A., A. F. Kiderlen, O. Kayser, 2005. Amphotericin B. Appl Microbiol Biotechnol, 68: 151 – 162.

Liang, L., Tao, Y., Lam, W.K., 2014. Inhibition of the human efflux transporter ABCC2 (MRP2) by self-emulsifying drug delivery system: Influences of concentration and combination of excipients. J.Pharm Pharm Sci. 17(4): 447-460.

Lipinski, C.A., 1995. Computational alerts for potential absorption problems: profiles of clinically tested drugs. In: Tools for Oral Absorption, Part Two. Predicting Human Absorption. AAPS Meeting. Miami, AAPS.

Lipinski, C.A., 2000. Drug-like properties and the causes of poor solubility and poor permeability. J. Pharmacol. Tox. Methods, Vol. 44, No. 1, pp 235-249.

Lipinski, C.A., 2004. Solubility in water and DMSO: Issues and potential solutions: Pharmaceutical Profiling in Drug Discovery for Lead Selection: Borchardt, R.T., Kerns, E.H., Lipinski, C.A., Thakker, D.R. & Wang, B.W. Washington DC, AAPS Press.

Lipinski, C.A., Lombardo, F., Dominy, B.W., Feeny, P.J., 2001. Experimental and computational approaches to estimate solubility and permeability in drug discovery and development settings. Adv. Drug Deliv. Rev., Vol. 46, No. 1-3, pp 3-26.

Liu YT, 1984. Biosynthetic studies of amphotericins, candicidin and nystatin by means of mutation. Proc Natl Sci Counc Repub China B 8:182-186.

References

Lopes, S., Castanho, M.A.R.B., 2002. Revealing the orientation of Nystatin and Amphotericin B in lipidic multilayers by UV-Vis linear dichroism. J. Phys. Chem. 106: 7278-7282.

Lopez-Berestein, G., Fainstein, V., Mehta, K.R., Sullivan, M., Keating, M., Luna, M., Hersh, E.M., 1985. Liposomal amphotericin B for the treatment of systemic fungal infections in patients with cancer. J. Infect. Diseases. 151: 704-710.

Matsumori, N., Sawada, Y., Murata, M., 2005. Mycosamine orientation of Amphotericin B controlling interaction with ergosterol: Sterol-dependent activity of conformation-restricted derivatives with an Amino-Carbonyl bridge. J. Am. Chem. Soc. 127: 10667-10675.

Manosroi, A., Kongkaneramit, L., Manosroi, J., 2004. Characterisation of amphotericin B liposome formulations. Drug. Dev. and Ind. Pharm. 30 (5): 535-543.

Milhaud J., Ponsinet V., Takashi M., Michels B. 2002. Interactions of the drug amphotericin B with phospholipid membranes containing or not ergosterol: new insight into the role of ergosterol, Biochim. Biophys. Acta 1558, 95-108.

Monji N, Mechlinski W, Shaffer CP, 1976. Microbial production of amphotericin B-3H and the synthesis of its sodium desoxycholate (carboxyl-14C) complex and methyl-14C-ester. J Antibiot 29:438-443.

Moore-Adler, J. and Richard T. Proffitt, 2002. Liposomal formulation, structure, mechanisms of action and pre-clinical experience. Journal of Antimicobial chemotherapy. 49: 21 – 30.

Moulik, S.P., Paul, B.K., 1998. Structure, dynamics and transport properties of microemulsions. Adv. Colloid Interface Sci. 78: 99-195.

Müllertz, A. Ogbonna, A., Ren. S., Rades, T. 2010. New perspectives on lipid and surfactant based drug delivery systems for oral delivery of poorly soluble drugs. J. Pharm. Pharmacol. 62: 1622-1636.

Nakanishi, K., Nadai, T., Masada, M., Miyajima, K., 1992. Effect of cyclodextrins on biological membrane. II. Mechanism of enhancement on the intestinal absorption of non-absorbable drug by cyclodextrins. Chemical and Pharmaceutical Bulletin 40 (5), 1252–1256.

Nawroth, T., Buch, P., Buch, K., Langguth, P., Schweins, R., 2011. Liposome formation from bile salt-lipid micelles in the digestion and drug delivery model FaSSIF(mod) estimated by combined time-resolved neutron and dynamic light scattering. Mol. Pharm. 8:2162-2172.

Ohsawa, T., Miura, H., Harada, K., 1984. A novel method for preparing liposomes with a high capacity to encapsulate proteinous drugs: freeze-drying method. Chem. Pharm. Bull. 32, 2442-2445.

Palin, K.J., Wilson, C.L., 1984. The effect of different oils on the absorption of probucol in the rat. J. Pharm. and Pharmacology, 36, 641-643.

References

Papahalopoulos, D., Watkins, J.C., 1967. Phospholipid model membranes, II. Permeability properties of hydrated liquid crystals. Biochem. Biophys. Acta 135, 639-652.

Patterson TF, Miniter P, Dijkstra J, Szoka FC Jr, Ryan JL, Andriole VT, 1989. Treatment of experimental invasive aspergillosis with novel amphotericin B/cholesterol sulfate complexes. J. Infect Dis. 159(4):717-24.

Plumb, D. 1999. Veterinary Drug Handbook. White Bear Lake, PharmaVet Publishing, USA. p. 853.

Polacheck, I., Domb, A.J., Falk, R., 1999. A novel injectable water-soluble amphotericin B-Arabinogalactan conjugates. Antimicro. Agent Chemor., 43(8): 1975-1981.

Porter, C.J.H., Charman, W.N., 2001. Intestinal lymphatic drug transport: An update. Adv. Drug Del. Rev., 50, 61-80.

Pouton CW, 2006. Formulation of poorly water-soluble drugs for oral administration: Physicochemical and physiological issues and the lipid formulation classification systems. Eur. J. Pharm. Sci 29 (3-4): 278-287.

Pouton, C.W. 1985. Self-emulsifying drug delivery systems: assessment of the efficiency of emulsification. Int. J. Pharm. 27: 335-348.

Pouton, C.W. and Porter, C.J.H., 2008. Formulation of lipid-based delivery systems for oral administration: Materials, methods and strategies. Adv. Drug dev. Rev. 60: 625-637.

Pouton, C.W., 2006. Formulation of poorly water-soluble drugs for oral administration: Physicochemical and Physiological issues and the lipid formulation classification system. Eur. J. Pharm. Sci., Vol 29, 3-4, 278-287.

Pouton, C.W. 2000. Lipid formulations for oral administration of drugs: non-emulsifying, self-emulsifying and 'self-microemulsifying' drug delivery systems. Eur. J. Pharm. Sci. 11 (sup 2): S93-S98.

Pouton, W.C., 2007. Properties and Uses of Common Formulation Lipids, Surfactants and Cosolvents, in AAPS Workshop. March 2007.

Pouton. CW., Mohsin, K., Long, M.A., 2009. Design of lipid-based formulations for oral administration of poorly water-soluble drugs: Precipitation of drugs after dispersion of formulations in aqueous solution. J. Pharm. Sci. 98 (10): 3582-3595.

Reed, K.W. and Yalkowsky, S.H., 1985. Lysis of human red blood cells in the presence of co-solvents. J. Parent. Sci. Technol. 38: 64-69.

Saha, P and Kou, J.H. 2000. Effect of solubilising excipients on permeation of poorly water-soluble compounds across Caco-2 cell monolayers. Eur. J. Pharm Biopharm. 50 (3): 403-411.

References

Sanchez-Brunette, J.A., Dea, M.A., Rama, S., Bolas, F., Alund, J.M., Torrado-Santiago, S., Torrado, J.J., 2004. Amphotericin B molecular organisation as an essential factor to improve activity/toxicity ratio in the treatment of visceral leishmaniasis. J. Drug Targeting, 12, 453-460.

Sanchez-Brunette, J.A., Dea, M.A., Rama, S., Bolas, F., Alund, J.M., Torrado-Santiago, S., Torrado, J.J., 2004. Amphotericin B molecular organisation as an essential factor to improve activity/toxicity ratio in the treatment of visceral leishmaniasis. J. Drug Targeting, 12, 453-460.

Santangelo, R., Paderu, P., Delmas, G. 2000. Efficacy of oral cochleate-amphotericin B in a mouse model of systemic candidiasis. Antimicrob Agents Chemother., 44: 2356-60.

Sanyog, J., Valvi, P.U., Swarnakar, N.K., Thanki, K., 2012. Gelatin coated hybrid lipid nanoparticles for oral delivery of amphotericin B. Mol. Pharm., 9 (9): 2542-2553.

Schoenborn, B.P., Pachence, J.M., Edelman, I.S.,1987. Low angle neutron scattering analysis of Na/K-ATPase in detergent solution. J. Biol. Chem. 262(2):702-709.

Shao, Z., Li, Y., Chermak, T., Mitra, A.K., 1994. Cyclodextrins as mucosal absorption promoters of insulin. II. Effects of β -cyclodextrin derivatives on α -chymotryptic degradation and enteral absorption of insulin in rats. Pharmaceutical Research 11(8), 1174–1179.

Sharma, A. and Sharma, U., 1997. Liposomes in drug delivery: progress and limitations. Int. J. Pharm. 154:123-140.

Sharma, A., Mayhew, E., Bolcsak, L., Cavanaugh, C., Harmon, P., Janoff, A., Bernacki, R.J., 1997. Activity of paclitaxel liposome formulations against human ovarian tumor xenografts. Int. J. Cancer. 71, 103-107.

Sharma, A., Straubinger, R.M., Ojima, I., Bernacki, R.J., 1995. Antitumor efficacy of Taxane liposomes on a human ovarian tumor xenograft in nude athymic mice. J. Pharm. Sci. 84, 1400-1404.

Shen, H.Z., Kang, M., 2006. Preparation and evaluation of self-microemulsifying drug delivery systems (SMEDDS) containing atorvastatin. J. Pharm. Pharmacol 58: 1183-1191.

Shukla, A., Janich, M., Jahn, K., Krause, A., Kiselev, M.A., Neubert, R.H.H., 2002. Investigation of pharmaceutical microemulsions by small angle scattering. Pharm. Res. 19(6): 881-886.

Sriwongsitanont, S., Masaharu, U., 2011. Effect of freeze-thawing process on the size and lamellarity of PEG-Lipid liposomes. The open colloid science journal, 4: 1-6.

Stephen M. K., 2013. Small Angle Neutron Scattering. www.isis.stfc.ac.uk.

Strickley, R. 2004. Solubilizing excipients in oral and injectable formulations. Pharm. Res. 21(2): 201-230.

References

Stoodley, R., Wasan, K.M., Bizzotto, D., 2007. Fluorescence of Amphotericin B-deoxycholate (Fungizone) monomers and aggregates and the effect of heat-treatment. Langmir, 23:8718-8725.

Stuhrmann, H.B., Kirste, R.G., 1965. Elimination der intrapartikulaeren Untergrundstreuung bei der Röntgenkleinwinkelstreuung an Kompakten Teilchen (Proteinen). Zeitschr. Physik. Chem. Neue Folge 46: 247-250.

Sullivan Jr., D.W., Gad, S.C., Julien, M., 2014. A review of the non-clinical safety of Transcutol®, a highly purified form of diethylene glycol monoethyl ether (DEGEE) used as a pharmaceutical excipient. Food and chemical Toxicology, 72: 40-50.

Svergun, D.I., Koch, M.H., Timmins, P.A., May, R.P. 2013. Small angle X-ray and Neutron scattering from solutions of biological macromolecules. Oxford university press.

Swenson, E.S., Milisen, W.B., Curatolo, W., 1994. Intestinal permeability enhancement: efficacy, acute local toxicity, and reversibility. Pharmaceutical research, 11(8): p. 1132-1142.

Takahashi, Y., Kondo, H., Yasuda, T., Watanabe, T., Kobayashi, S., Yokohama, S., 2002. Common solubilisers to estimate the Caco-2 transport of poorly water-soluble drugs. Int. J. Pharm. 246: 85-94.

Talegaonkar, S., Azeem, A., Fahran, J.A., Roop, K.K., Shadab, A.P., Zeenat, I.K., 2008. Microemulsions: A novel approach to enhanced drug delivery. Recent patents on drug delivery & formulation, 2, 238-257.

Talsma, H., Jousma, H., Nicolay, K., Commelin, D.J.A., 1987. Multilamellar or Multivesicular vesicles? Int. J. Pharm. 37: 171-173.

Tenjarla, S., 1994. Microemulsions: an overview and pharmaceutical applications. Critical reviews in therapeutic drug carrier systems, 16(5): p. 461.

Tevyashova, A.N., Olsufyeva, E.N., Solovieva, S.E., Printsevskaya, S.S., Reznikova, M.I., Trenin, A.S., Galatenko, O.A., Treshalin, I.D., Pereverzeva, E.R., Mirchink, E.P., Isakova, E.B., Zotchev, S.B., Preobrazhenskaya, M.N., 2013. Structure-Antifungal Activity Relationship of Polyene antibiotics of the Amphotericin B Group. Antimicrob. Agents Chemother, 57(8): 3815-3822.

Thackaberry, E.A., Kopytek, S., Sherratt, P., Trouba, K., McIntyre, B., 2010. Comprehensive investigation of hydroxypropyl methylcellulose, propylene glycol, polysorbate 80, and hydroxypropyl-beta-cyclodextrin for use in general toxicological studies. Toxicological Sciences, 117(2): 485-492.

Torrado JJ, Espada MP, Ballesterus, Torrado-Santiago. Reviews-Amphotericin B formulations and Drug Targeting. www.interscience.wiley.com. Accessed on 20th April, 2013.

Torrado, J.J., Espada, R., Ballesteros, M.P., Torrado-Santiago, S., 2008. Amphotericin B formulations and drug targeting. J. Pharm. Sci., 97, 2405-2425.

References

Tuleu, C., Andrieux, C., Boy, P., Chaumeil, J.C., 1999. Gastrointestinal transit of pellets in rats: effect of size and density. Int. J. Pharm. 180: 123-131.

Ueda, C.T., Lemaire, M., Gsell, G., Nussbaumer, K., 1983. Intestinal lymphatic absorption of cyclosporin A following oral administration in an olive oil solution to rats. Biopharm. & Drug Disposition, 4, 113-124.

Vakil R, Kwon GS. 2005. PEG-phospholipid micelles for the delivery of amphotericin B. J Control Release 101:386–388.

Van de Ven H, C. Paulussen, P.B. Feijens, A. Matheeussen, P. Rombaut, P. Kayaert, G. Van den Mooter, W. Weyenberg, P. Cos, L. Maes, A. Ludwig,. 2012. PLGA nanoparticles and nanosuspensions with amphotericin B: Potent in vitro and in vivo alternatives to Fungizone and AmBisome. J controlled Release, 161:795-803.

Vander, A.J., Sherman, J.H., Luciano, D.S., 1985. Human physiology: The mechanisms of body function, 4th Edition. McGraw Hill, New York

Vandermeulen G, Rouxhet L, Arien A, Brewster ME, Preat V. 2006. Encapsulation of amphotericin B in poly (ethylene glycol)-block-poly (e-caprolactone-co-trimethylenecarbonate) polymeric micelles. Int J Pharm 309:234–240.

Veerareddy PR, Vobalaboina V. 2004. Lipid-based formulations of amphotericin B. Drugs Today 40:133–145.

Vingerhoeds, M.H., Steerenberg, P.A., Hendriks, J.J.G.S., Crommelin, D.J.A., Storm, G., 1996. Targeted delivery of diphtheria toxin via immunoliposomes: efficient antitumor activity in the presence of inactivating anti-diphtheria toxin antibodies. FEBS Lett. 395, 245-250.

Vyas, S.P., Gupta, S., 2007. Development and characterisation of amphotericin B bearing emulsomes for passive and active macrophage targeting. Journal of Drug Targeting, 15(3), 206 – 217.

Walsh TJ, Goodman JL, Pappas P, Bekersky I, Buell DN, Roden M, Barret J, Anaissie EJ. 2001. Safety, tolerance, and pharmacokinetics of high-dose liposomal amphotericin B (Ambisome) in patients infected with Aspergillus species and other filamentous fungi: Maximum tolerated dose study. Antimicrob Agents Chemother 45:3487–3496.

Wasan M. Kishor, Ellen K. Wasan, Pavel Gershkovic, Xiaohua Zhu, Richard R. Tidwell, Karl A. werbovetz, John G. Clement and Sheila J. Thornton, 2009. Highly effective oral amphotericin B formulation against murine visceral Leishmaniasis. J. Inf. Diseases 200: 357 – 360.

Wasan, K. M. 2002. The role of lymphatic transport in enhancing oral protein and peptide drug delivery. Drug Development and Industrial Pharmacy, 28, 1047-1058.

Windholz M, Budavari S, Blumetti, R. Otterbein E., 1983. The Merck Index. Merck & Co Inc, Rahway (USA); p. 2194

References

Wingard JR, White MH, Anaissie E, Raffalli J, Goodman J, Arrieta A. L AmpB/ABLC Collaborative Study Group. 2000. A randomized, double blind comparative trial evaluating the safety of liposomal amphotericin B versus amphotericin B lipid complex in the empirical treatment of febrile neutropenia. Clin Infect Dis 31:1155–1163.

www.druginfosys.com. Amphotericin B. Accessed on 16th April, 2013

www.fao.org. Propylene glycol. Assessed on 27th August 2015.

www.inchem.org. Propylene glycol. Assessed on 27th August 2015.

www.pfizer.com/files/products/material-safety-data/Amphocin(R) injection. Accessed on 17th April, 2013.

www.sigmaaldrich.com Product Information: Amphotericin B. Accessed on 16th April, 2013.

Xianyi, S., Guijun, Y., Yunjuan, W., Junchan, L., Xiaoling, F. 2005. Effect of self-emulsifying drug delivery systems containing Labrasol on tight junctions in Caco-2 cells. Eur. J. Pharm. Sci. 24: 447-486.

Yu, B.G., Okano, T., Kataoka, K., Kwon, G. 1998. Polymeric micelles for drug delivery: solubilization and haemolytic activity of amphotericin B. J. Cont. Rel., 53: 131-136.

Zarif, L. 2005. Drug delivery by lipid cochleates. Meth Enzymol.. 391: 314-29.

Zhiwen, Y., Tan, Y., Chen, M., Dian, L., Shan, Z., Peng, X., Wu, C., 2012. Development of amphotericin B-loaded cubosomes through the SolEmuls technology for enhancing the oral bioavailability. AAPS PharmSciTech, 13(4): 1483-1491.

8. APPENDIX

A- UV spectra of DMPC, DPPC and DSPC liposomes

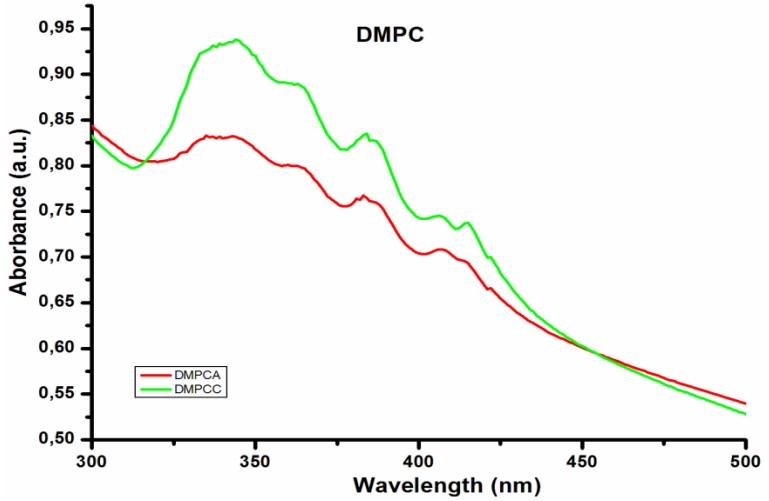

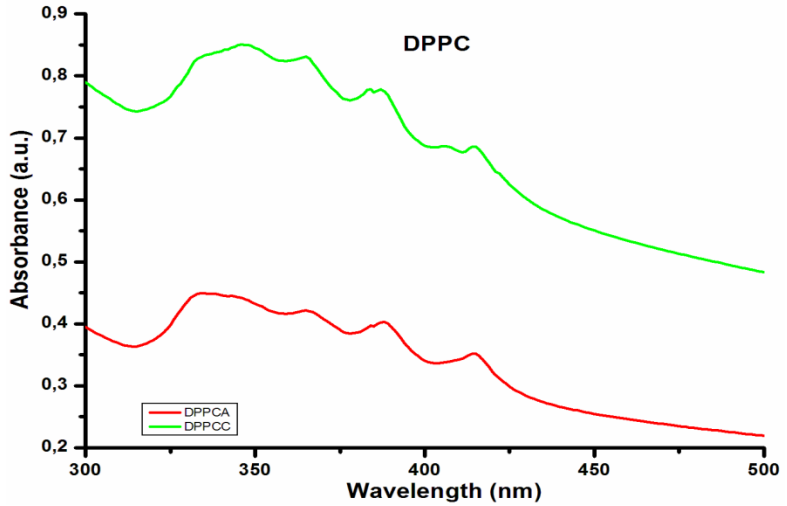

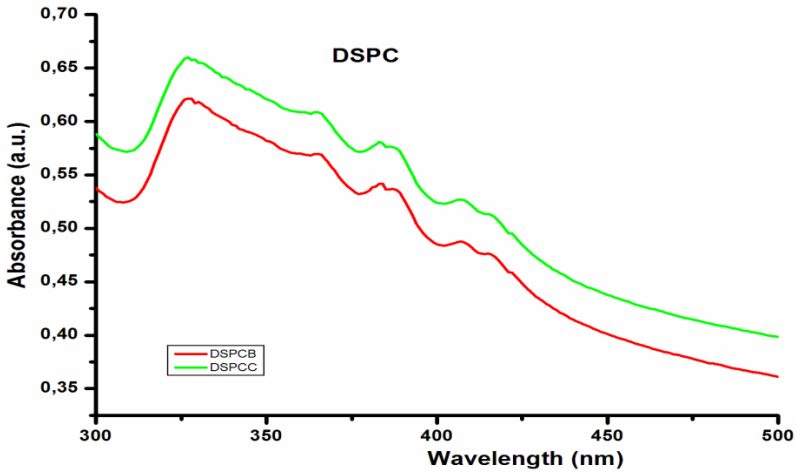

Appendix

B- DSC spectra of Amphotericin B, Cholesterol, Trehalose, Mannitol and freeze-dried mannitol.

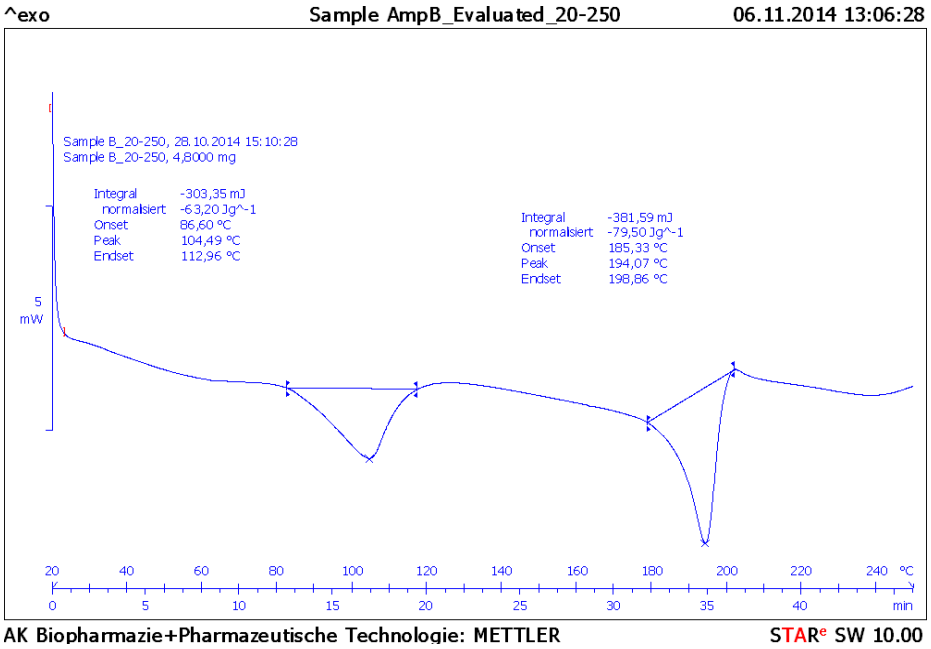

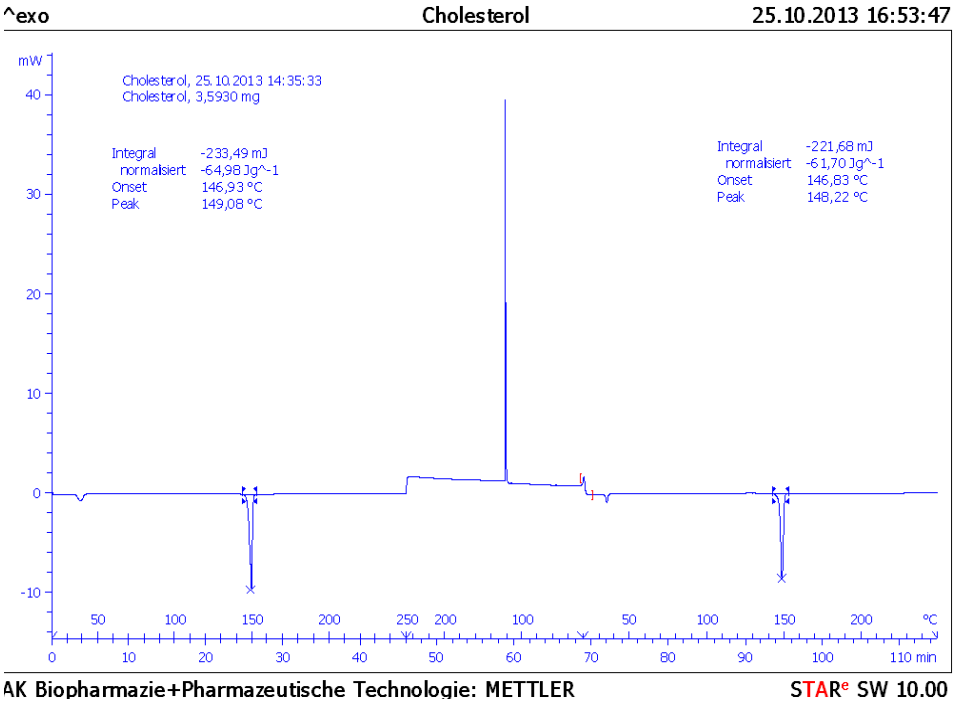

Appendix

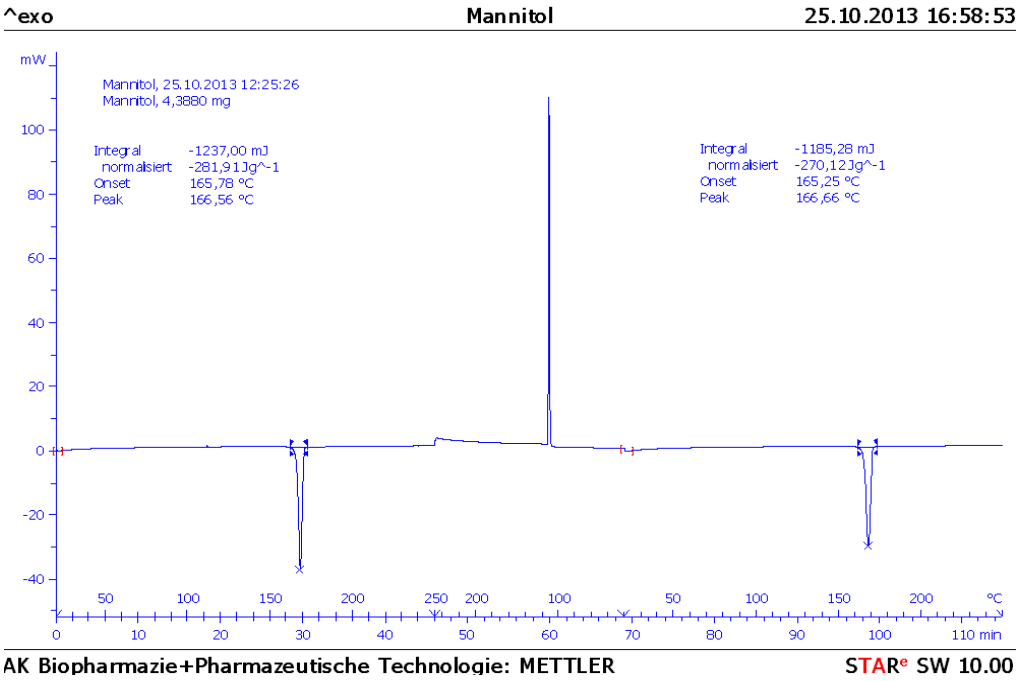
^exo
Mannitol
25.10.2013 16:58:53
mW
Mannitol, 25.10.2013 12:25:26
Mannitol, 4,3880 mg
Integral -1237,00 mJ
normalisiert -281,91 Jg^-1
Onset 165,78 °C
Peak 166,56 °C
Integral -1185,28 mJ
normalisiert -270,12 Jg^-1
Onset 165,25 °C
Peak 166,66 °C
°C
min
AK Biopharmazie+Pharmazeutische Technologie: METTLER
STARe SW 10.00

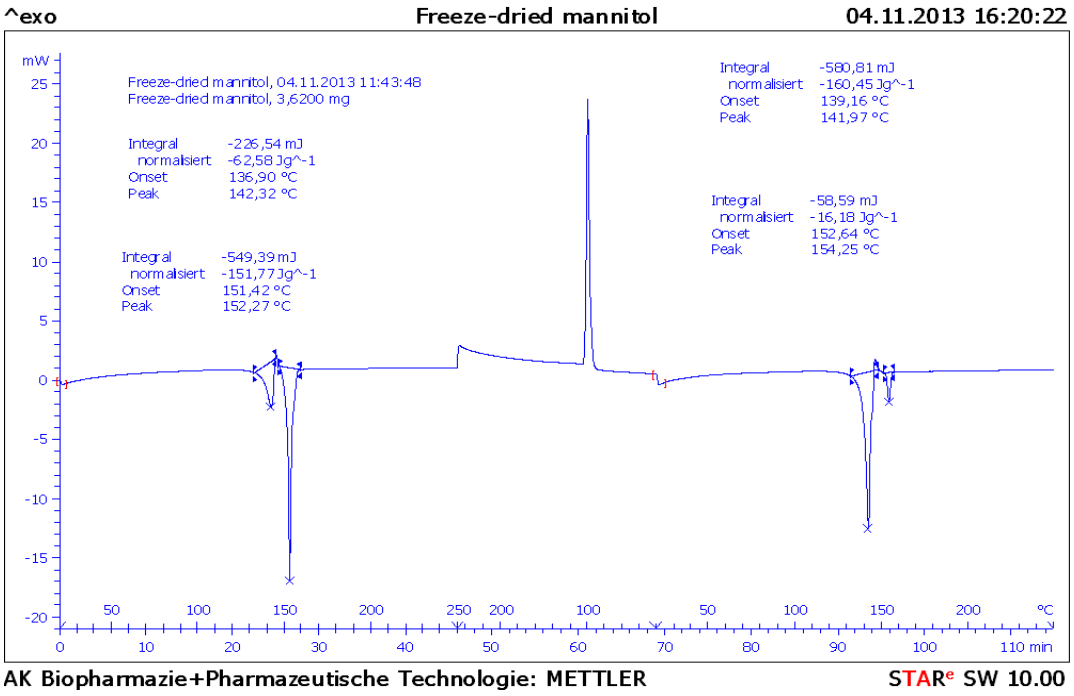
^exo
Freeze-dried mannitol
04.11.2013 16:20:22
mW
Freeze-dried mannitol, 04.11.2013 11:43:48
Freeze-dried mannitol, 3,6200 mg
Integral -226,54 mJ
normalisiert -62,58 Jg^-1
Onset 136,90 °C
Peak 142,32 °C
Integral -549,39 mJ
normalisiert -151,77 Jg^-1
Onset 151,42 °C
Peak 152,27 °C
Integral -580,81 mJ
normalisiert -160,45 Jg^-1
Onset 139,16 °C
Peak 141,97 °C
Integral -58,59 mJ
normalisiert -16,18 Jg^-1
Onset 152,64 °C
Peak 154,25 °C
°C
min
AK Biopharmazie+Pharmazeutische Technologie: METTLER
STARe SW 10.00

Appendix

C- FTIR spectra of Amphotericin B, Cholesterol, DOPC, Mannitol and Trehalose

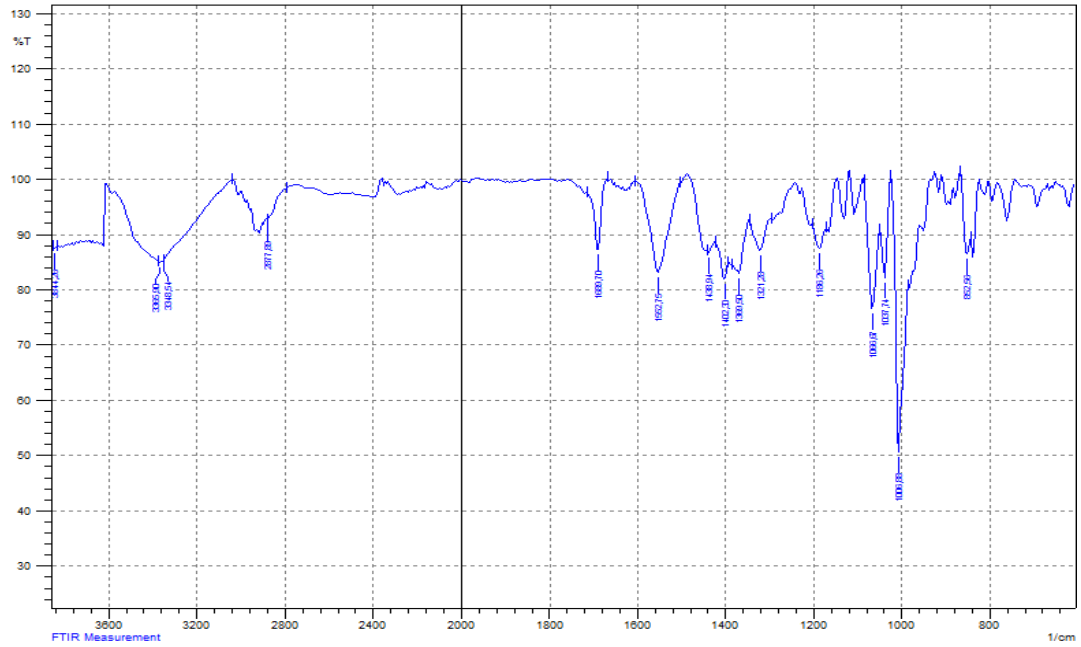

IR-Amphotericin B

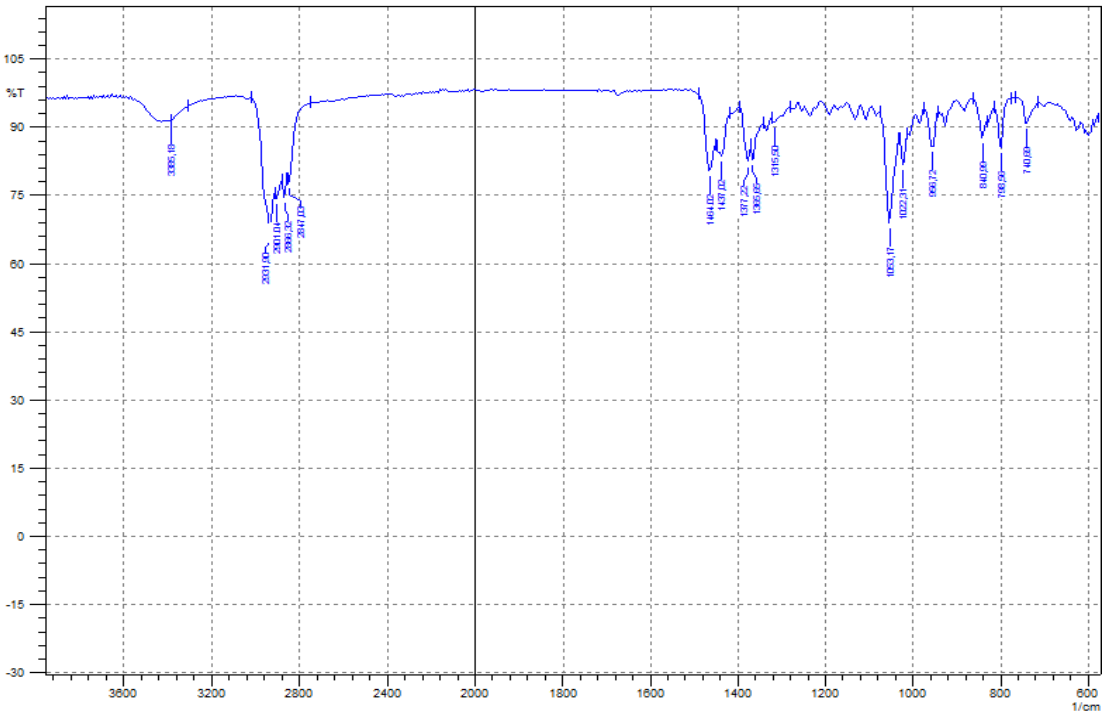

IR-Cholesterol

Appendix

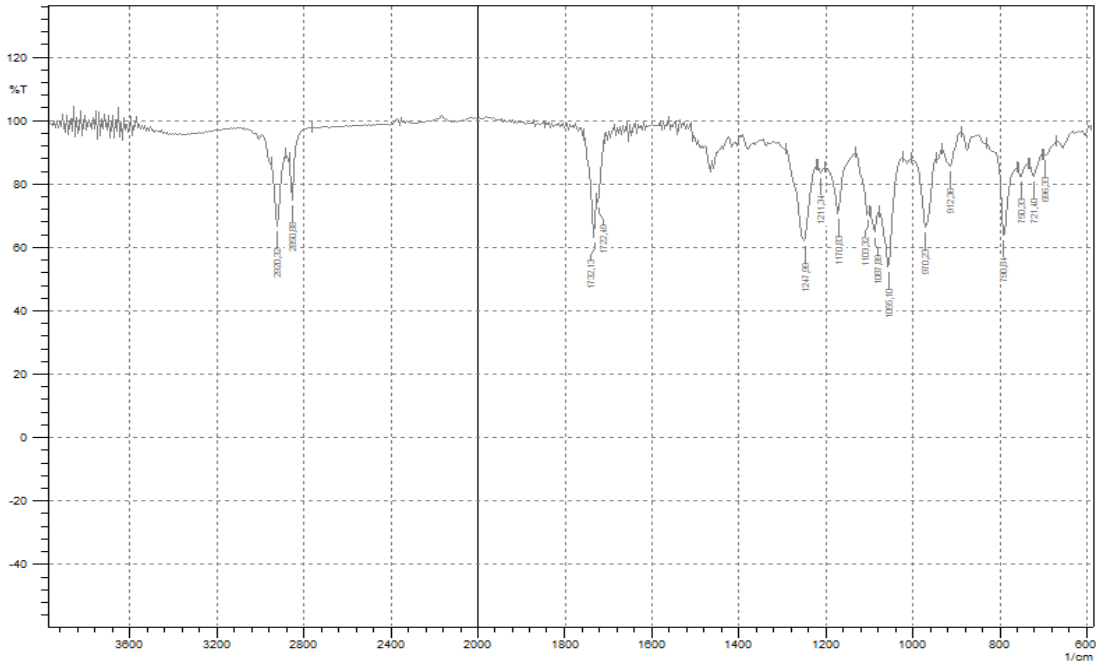

IR-DOPC

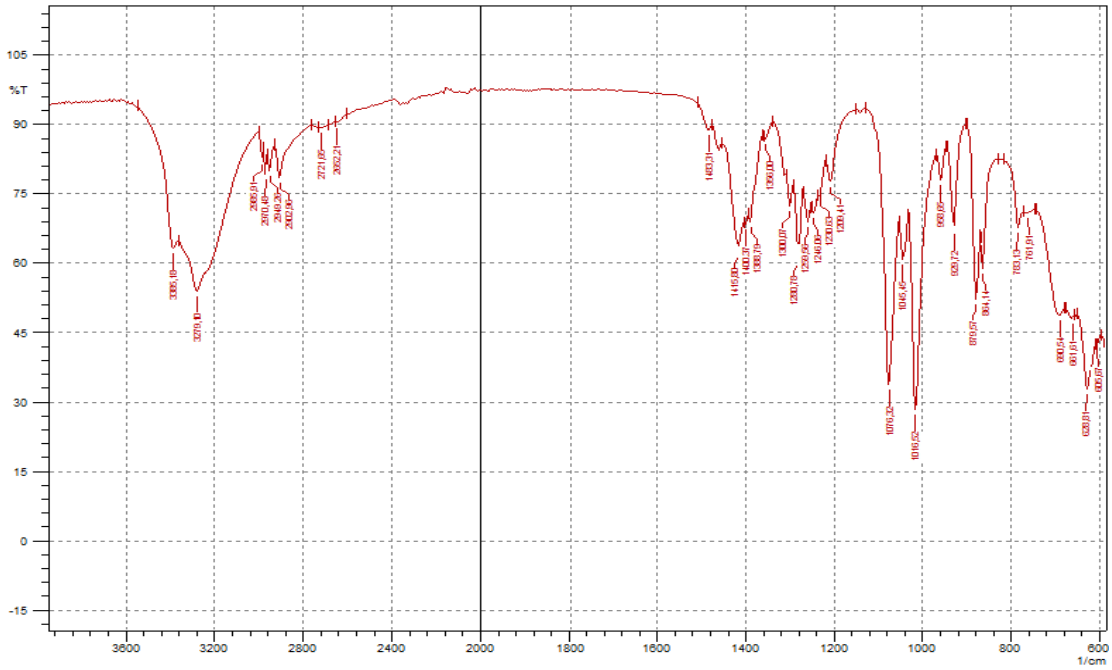

IR-Mannitol

Appendix

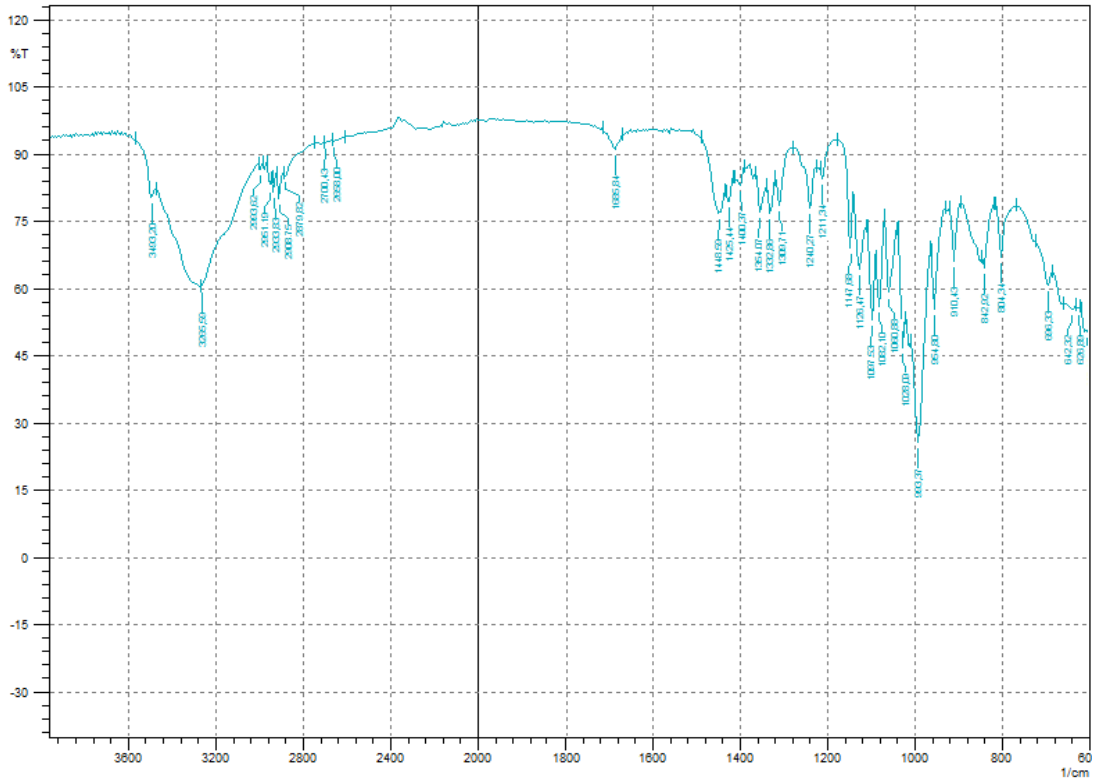

IR-Trehalose

Appendix

D1- SANS profile for DOPC-Amphotericin D (contrast variation)

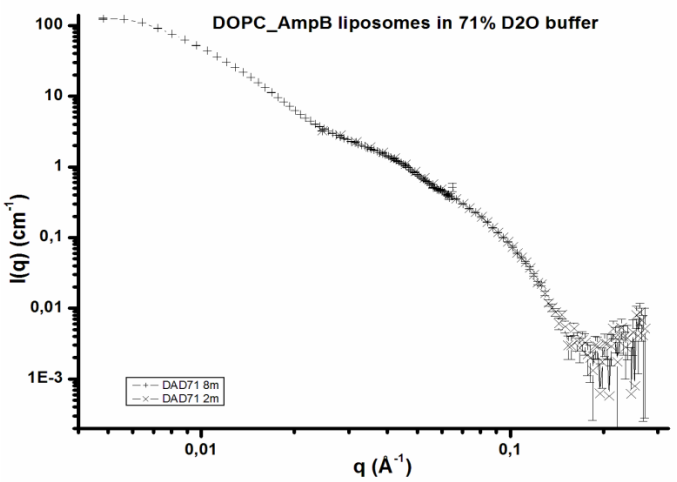

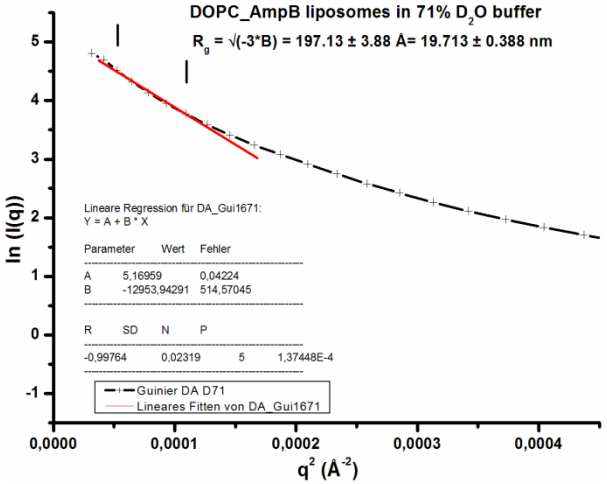

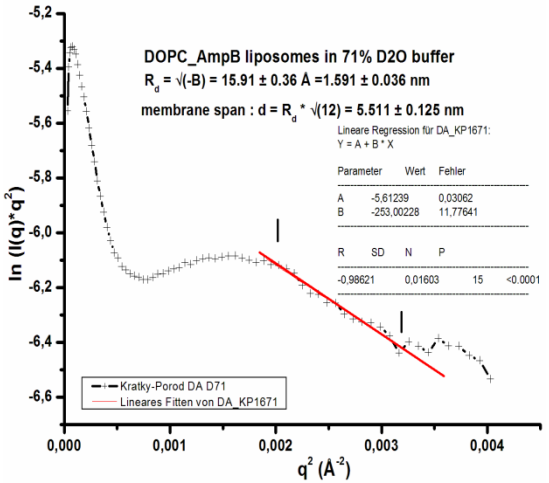

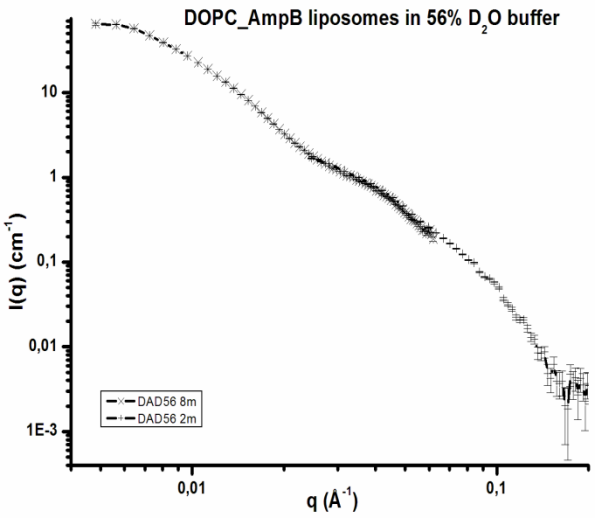

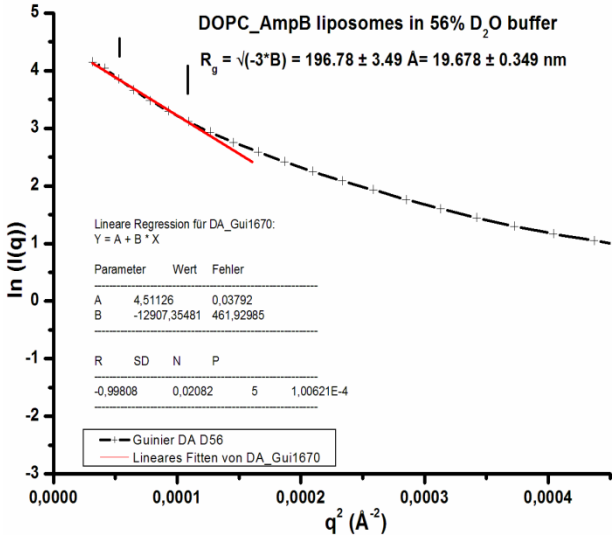

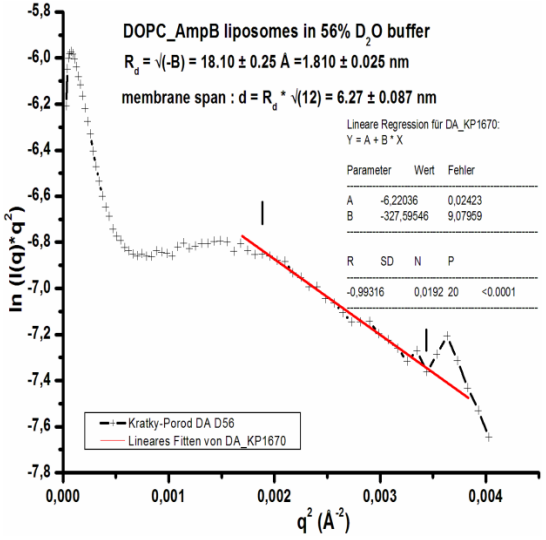

Appendix

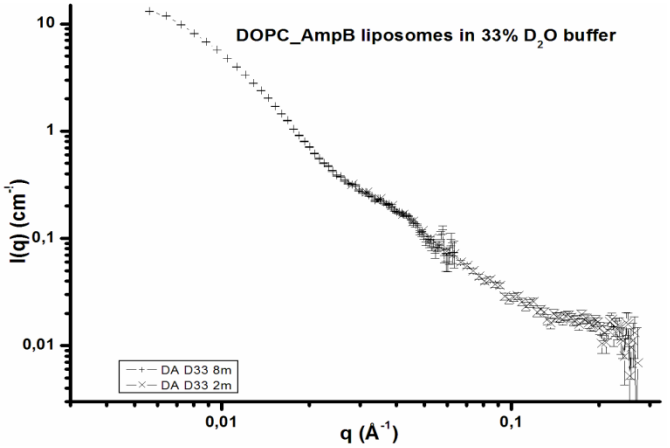

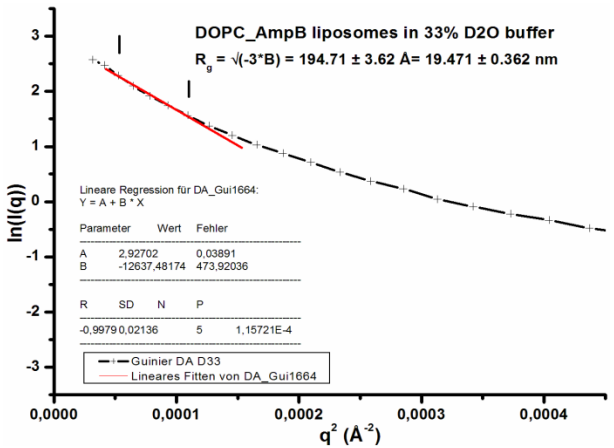

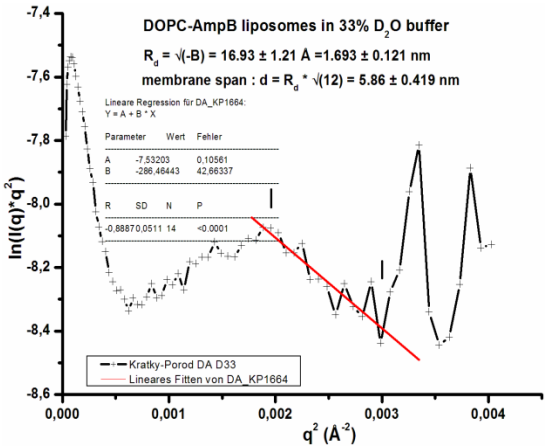

D2-SANS profile for DOPC-Cholesterol-Amphotericin B (contrast variation)

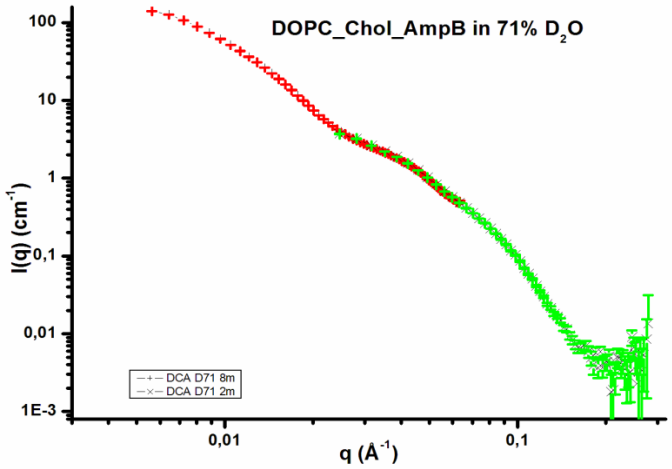

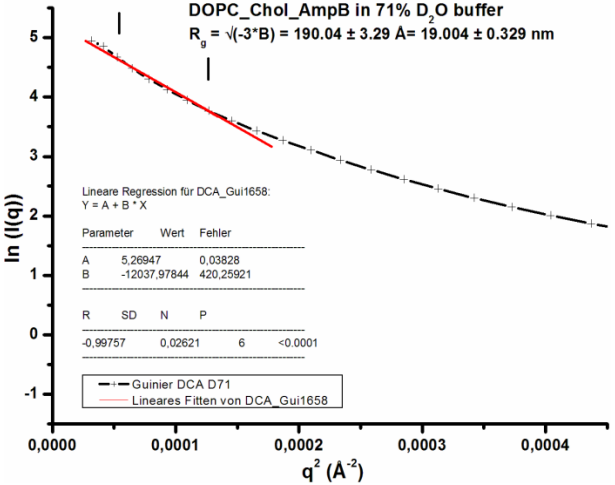

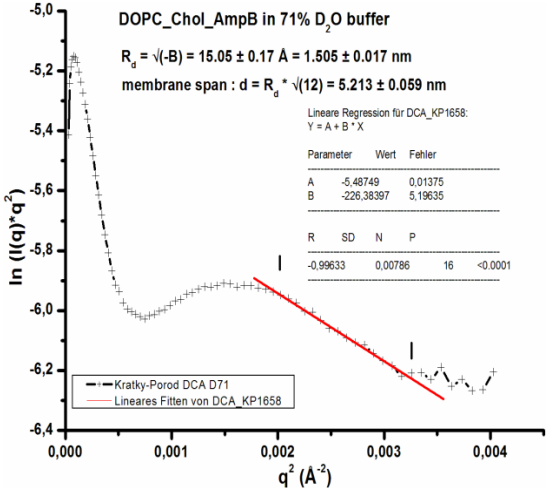

Appendix

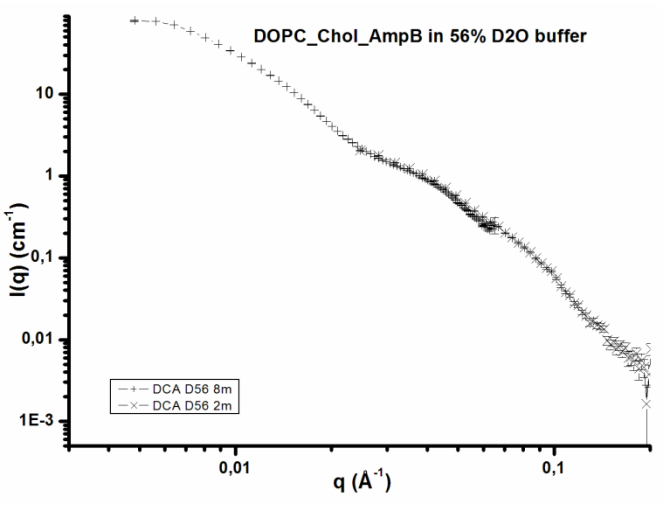
DOPC_Chol_AmpB in 56% D2O buffer
I(q) (cm-1)
q (Å-1)
DCA D56 8m
DCA D56 2m

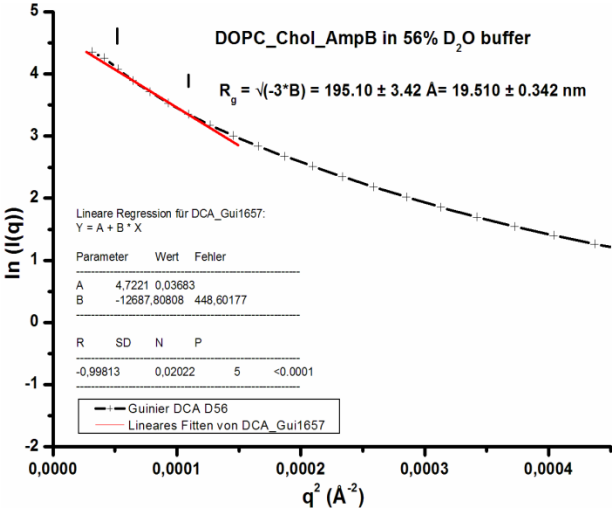
DOPC_Chol_AmpB in 56% D2O buffer
Rg = √(-3*B) = 195.10 ± 3.42 Å= 19.510 ± 0.342 nm
ln (I(q))
q2 (Å-2)
Lineare Regression für DCA_Gui1657:
Y = A + B * X
Parameter Wert Fehler
A 4,7221 0,03683
B -12687,80808 448,60177
R SD N P
-0,99813 0,02022 5 <0.0001
Guinier DCA D56
Lineares Fitten von DCA_Gui1657

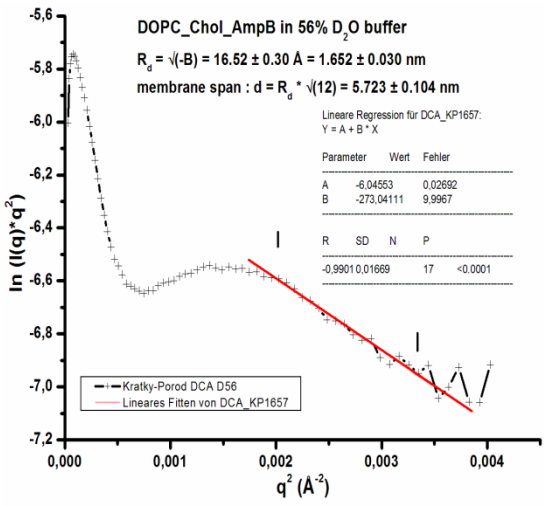
DOPC_Chol_AmpB in 56% D2O buffer
Rd = √(-B) = 16.52 ± 0.30 Å = 1.652 ± 0.030 nm
membrane span : d = Rd * √(12) = 5.723 ± 0.104 nm
ln (I(q)*q2)
q2 (Å-2)
Lineare Regression für DCA_KP1657:
Y = A + B * X
Parameter Wert Fehler
A -6,04553 0,02692
B -273,04111 9,9967
R SD N P
-0,9901 0,01669 17 <0.0001
Kratky-Porod DCA D56
Lineares Fitten von DCA_KP1657

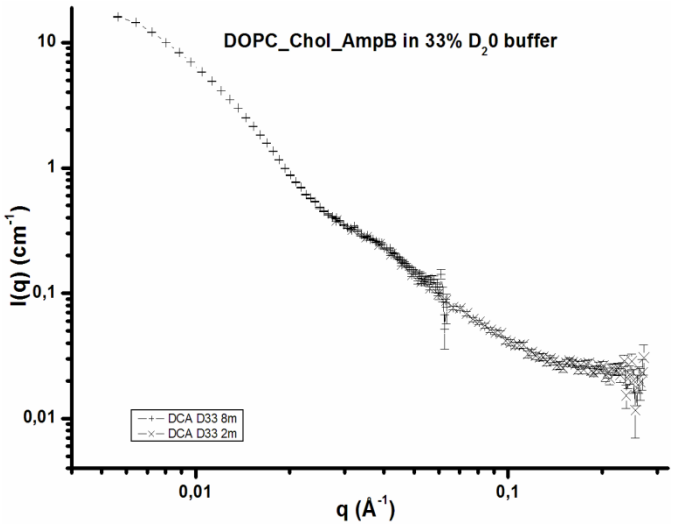
DOPC_Chol_AmpB in 33% D20 buffer
I(q) (cm-1)
q (Å-1)
DCA D33 8m
DCA D33 2m

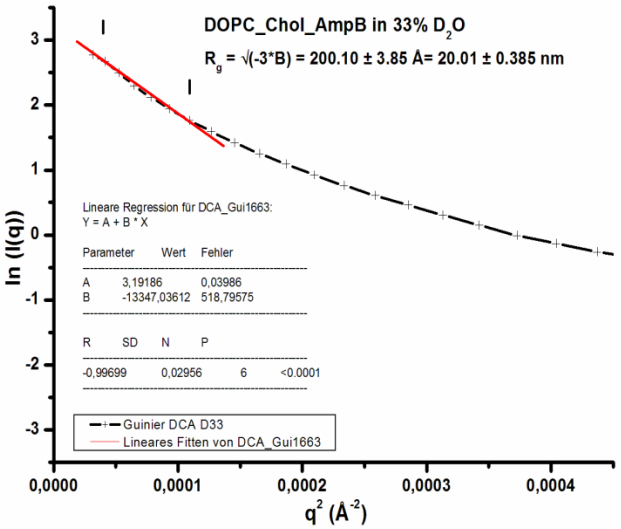
DOPC_Chol_AmpB in 33% D2O
Rg = √(-3*B) = 200.10 ± 3.85 Å= 20.01 ± 0.385 nm
ln (I(q))
q2 (Å-2)
Lineare Regression für DCA_Gui1663:
Y = A + B * X
Parameter Wert Fehler
A 3,19186 0,03986
B -13347,03612 518,79575
R SD N P
-0,99699 0,02956 6 <0.0001
Guinier DCA D33
Lineares Fitten von DCA_Gui1663

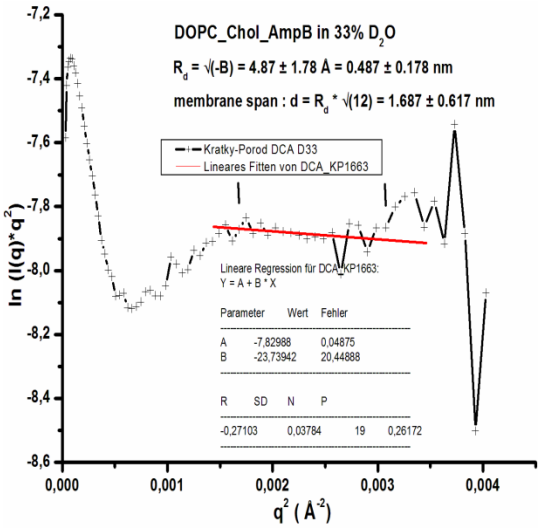
DOPC_Chol_AmpB in 33% D2O
Rd = √(-B) = 4.87 ± 1.78 Å = 0.487 ± 0.178 nm
membrane span : d = Rd * √(12) = 1.687 ± 0.617 nm
ln (I(q)*q2)
q2 (Å-2)
Kratky-Porod DCA D33
Lineares Fitten von DCA_KP1663
Lineare Regression für DCA_KP1663:
Y = A + B * X
Parameter Wert Fehler
A -7,82988 0,04875
B -23,73942 20,44888
R SD N P
-0,27103 0,03784 19 0,26172

Appendix

D3- SANS profile of AmB-HST (contrast variation)

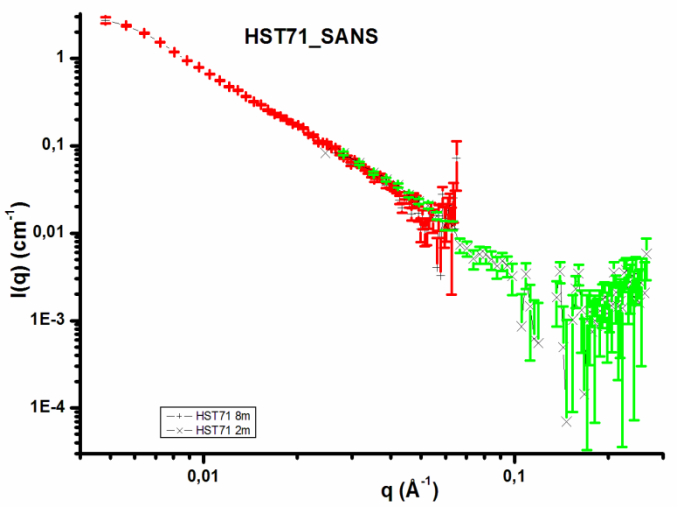

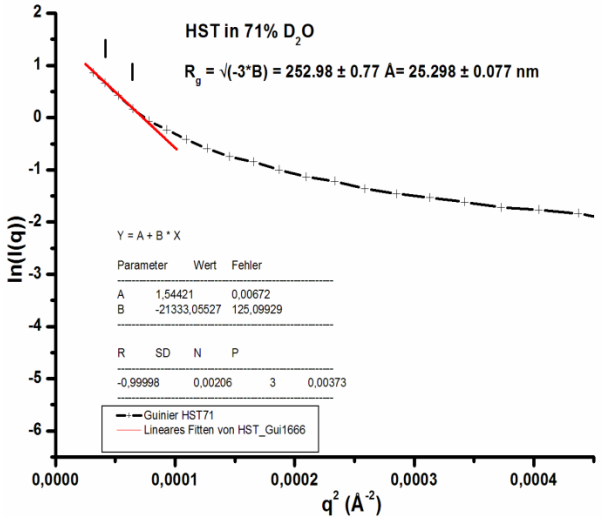

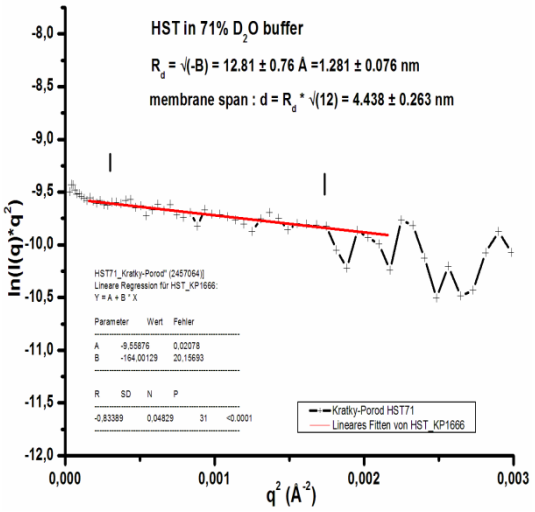

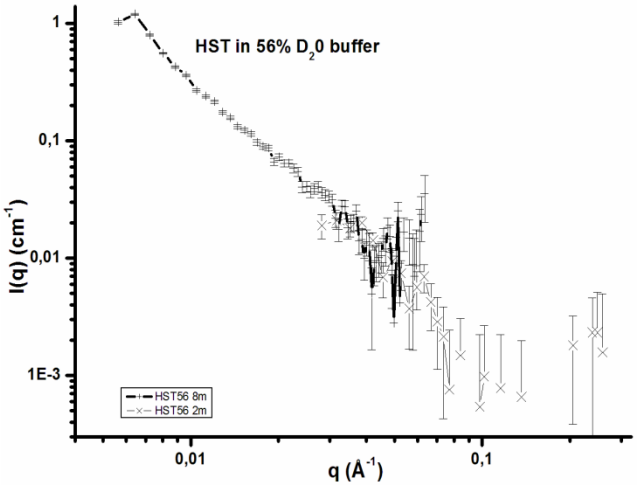

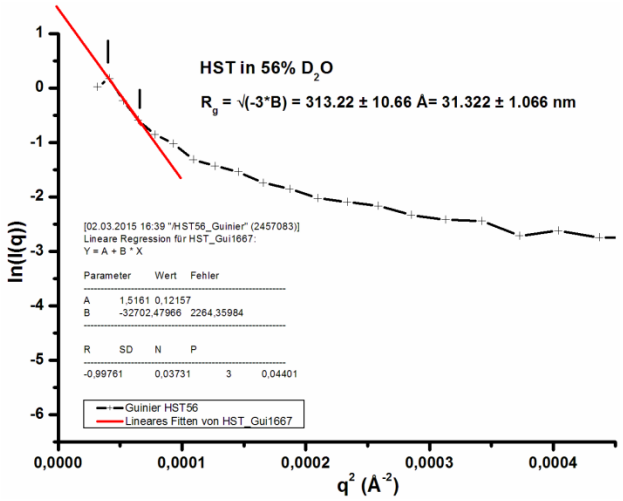

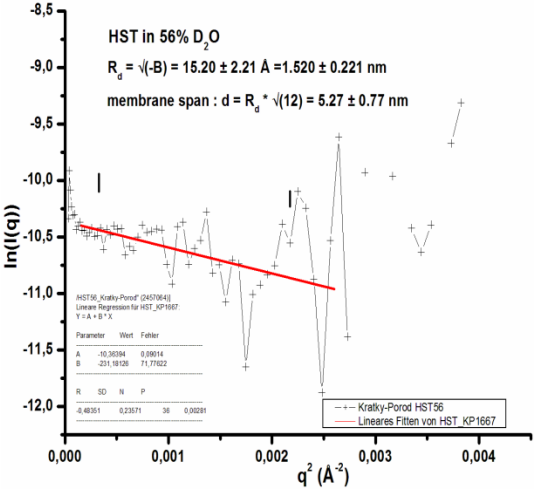

Appendix

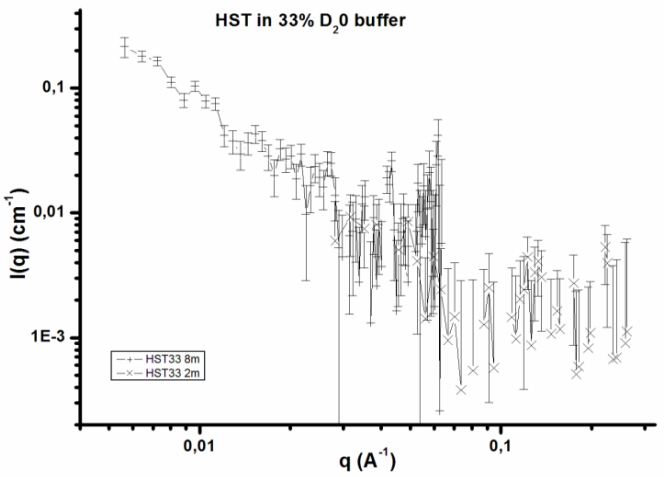

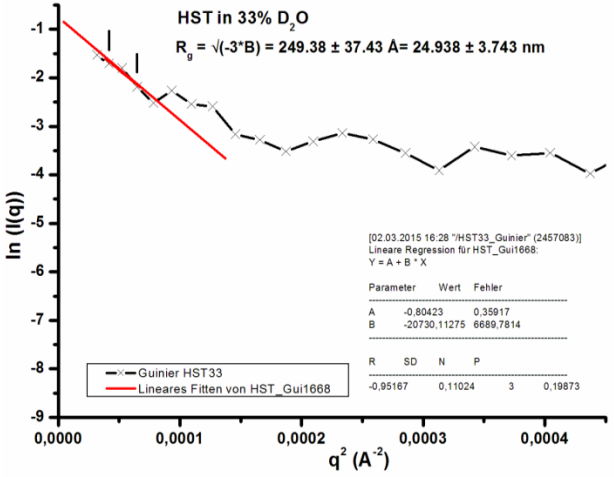

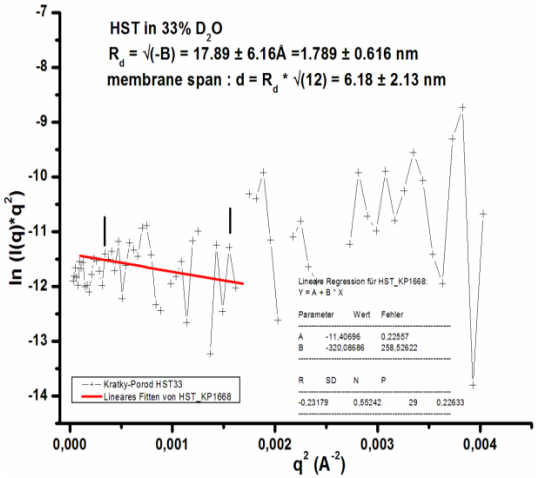

D4- SANS profile of DOPC in 33% D_20

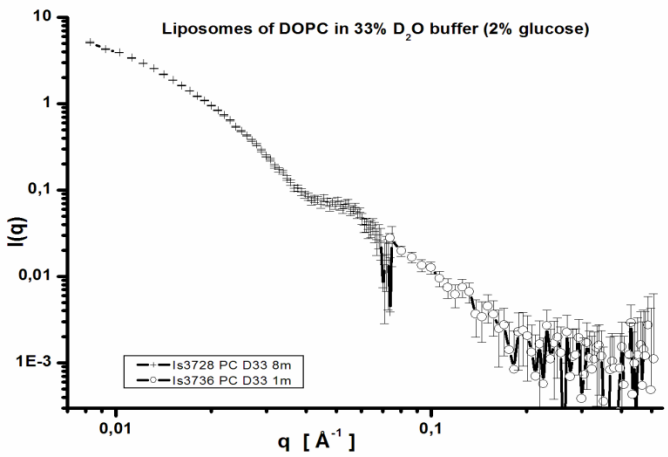

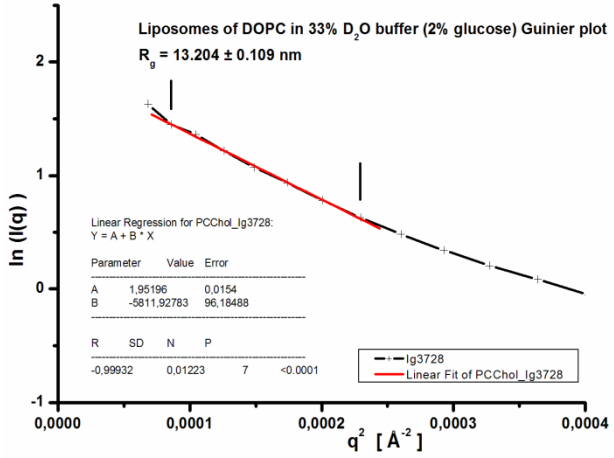

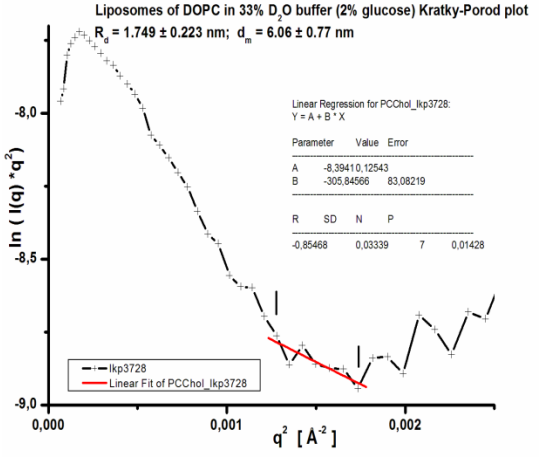

Appendix

D5- SANS profile of DOPC-Cholesterol in 33% D_2O

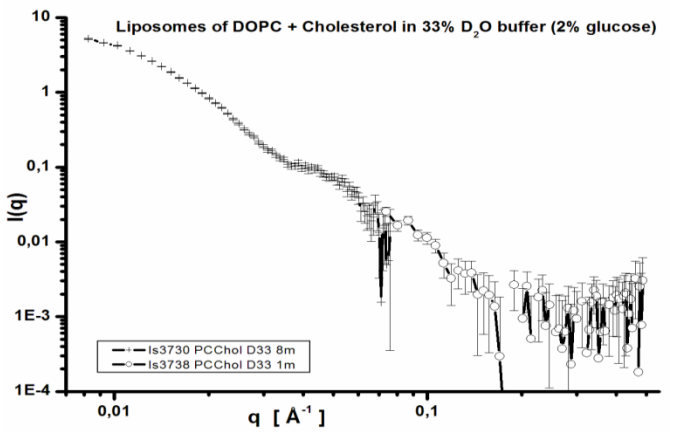

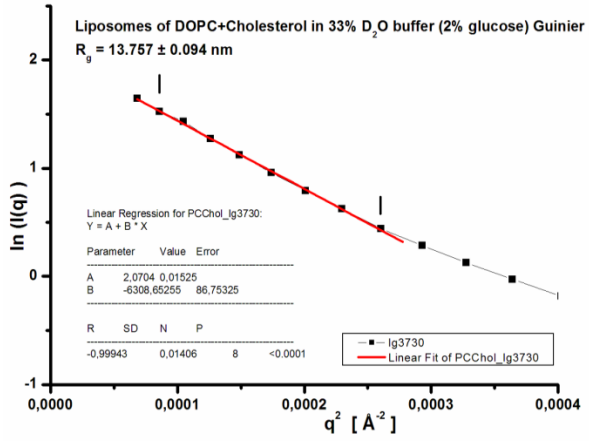

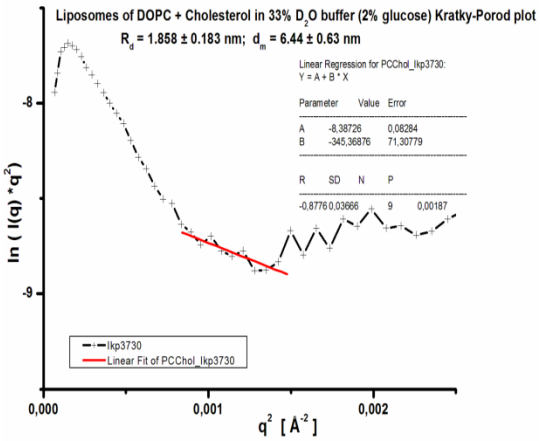

D6-Scattering curves of contrast variation of 85:10:5 DOPC-Cholesterol-Amphotericin B (SUV1)

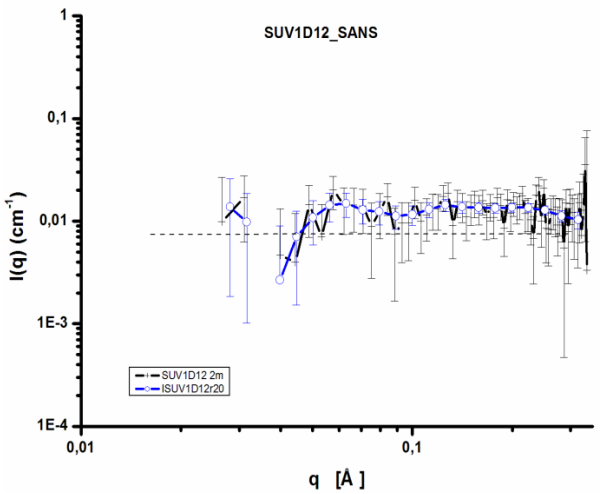

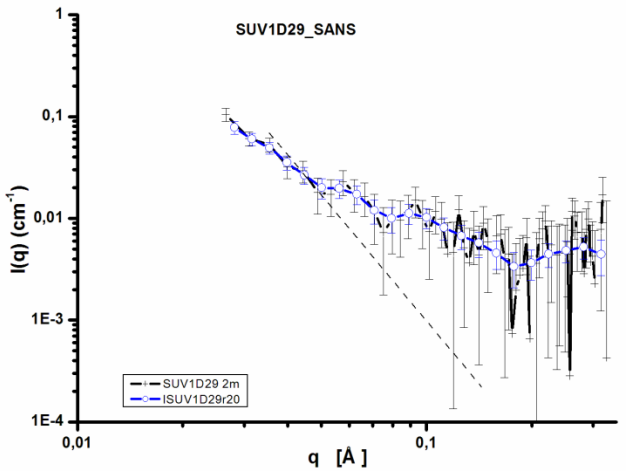

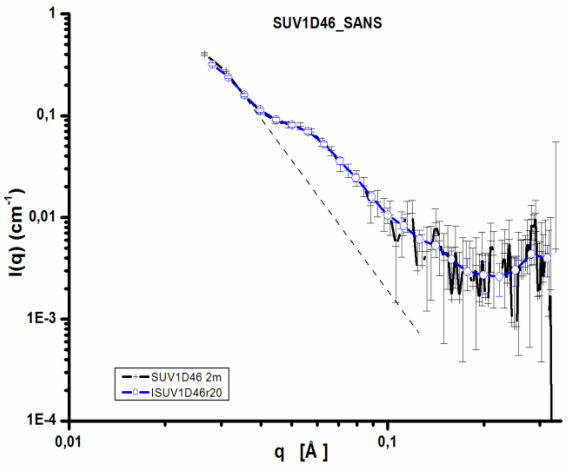

Appendix

D7-Scattering curves of contrast variation of 70:20:10 DOPC-Cholesterol-Amphotericin B (SUV2)

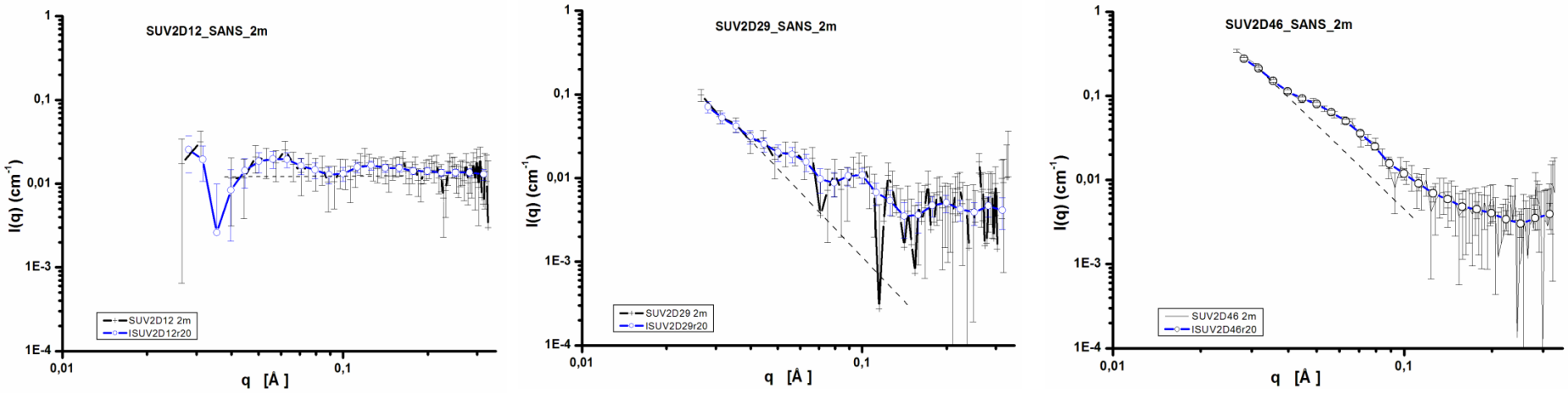

D8- Scattering curve of contrast variation of 60:30:10 DOPC-Cholesterol-Amphotericin B (SUV3) at 12% D_2O

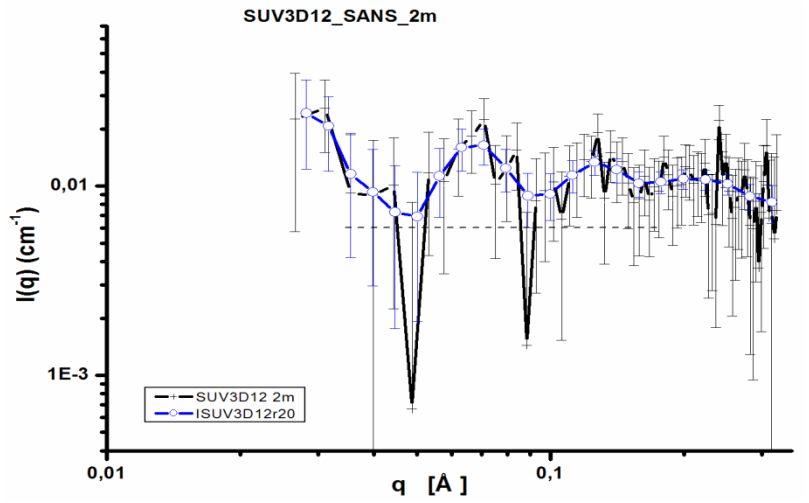

Appendix

E- UV-Visible spectra of some selected nanoemulsions

E1- Propylene glycol Nanoemulsion

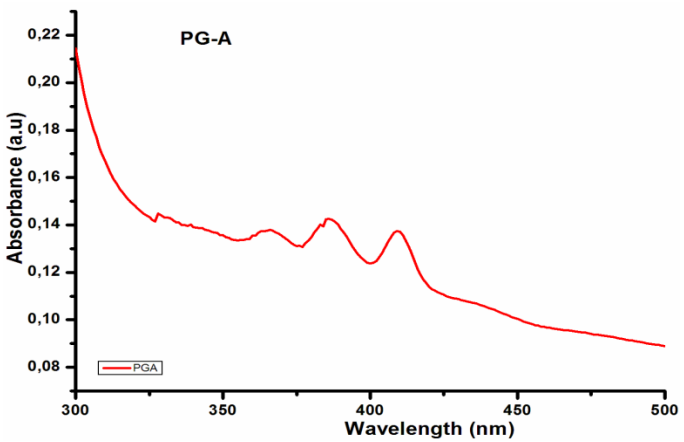

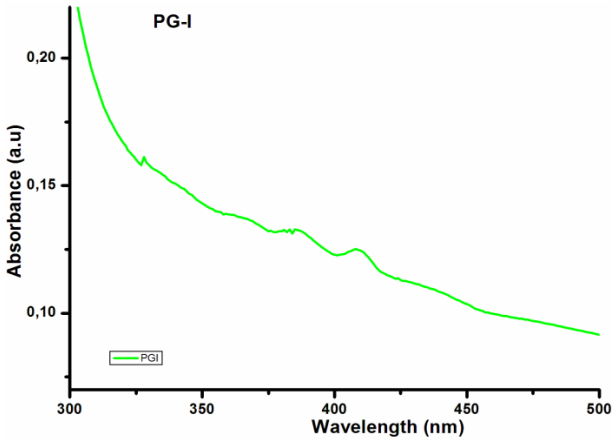

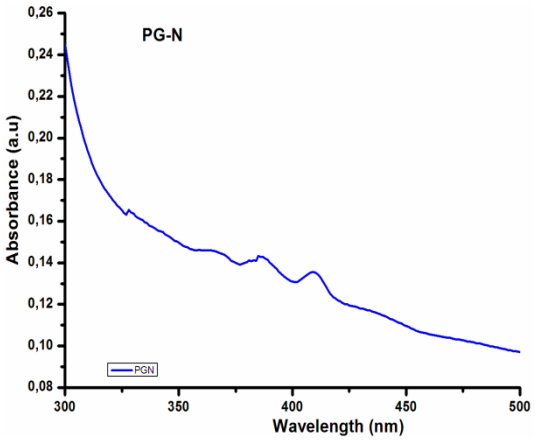

E2- Transcutol®P Nanoemulsion

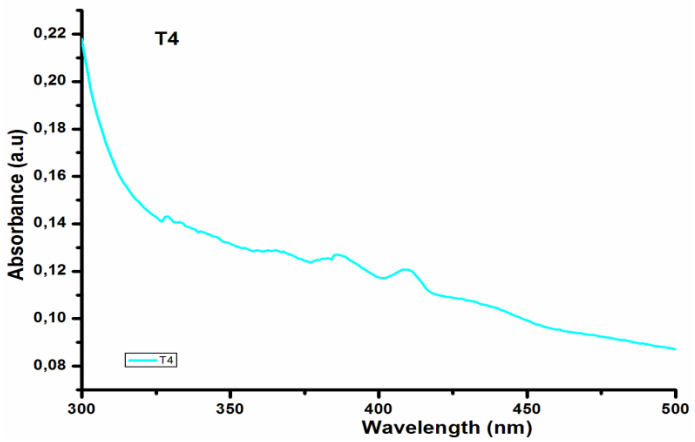

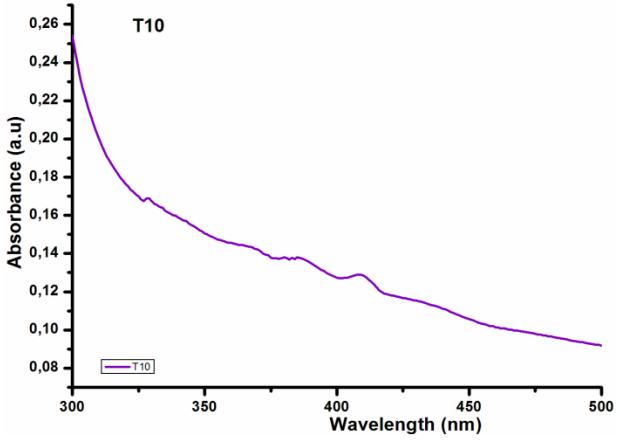

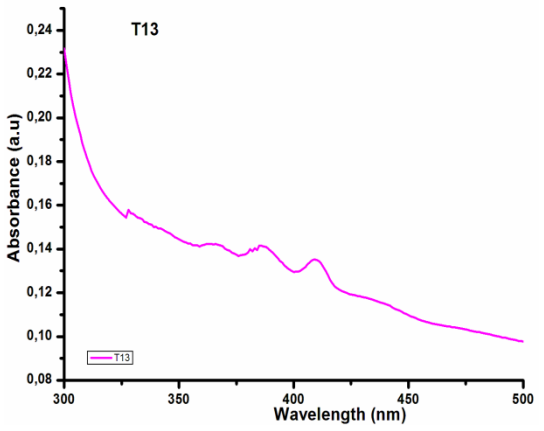

9. LIST OF PUBLICATIONS AND POSTER PRESENTATIONS

Publications

Johnson R., Khoshakhlagh P, Nawroth T, Langguth P, Schmueser L, Decker H, Hellmann N, Szekely N. 2014. Amphotericin B microparticles 'AmbiShell' from phospholipid and gelatin: Development and investigation by combined DLS and SANS resolves the core-shell structure. Eur. J. Lipid Sci. Technol., Vol 116, pp 1167 – 1173.

Khoshakhlagh P., **Johnson R.**, Nawroth T., Langguth P., Schmueser L., Decker H., Hellmann N., Szekely N. 2014. Nanoparticle structure development in the gastrointestinal model fluid FaSSIFmod6.5 from several phospholipids at various water content relevant for oral administration. Eur. J. Lipid Sci. Technol., Vol 166, pp 1155 – 1166.

Khoshakhlagh P., **Johnson R.**, Nawroth T., Langguth P., Schmueser L., Decker H., Hellmann N., Szekely N. 2015. Fasted-state simulated intestinal fluid "FaSSIF-C", a cholesterol containing intestinal model medium for in vitro drug delivery development. J. Pharm. Sci. Vol. 104, Issue 7, pp 2213–2224.

Thomas Nawroth, Pooneh Khoshakhlagh, Philipp Buch, **Raphael Johnson**, Peter Langguth, Lars Schmueser, Nadja Hellmann, Heinz Decker, Noemi Kinga Szekely. Bifurcation of the Nanoparticle-Excipient mediated Drug Solubilization Pathways of oral Formulations in the Gastro-Intestinal model Fluid $FaSSIF_{mod6.5.}$" International Journal of Pharmaceutics, submitted.

Pooneh Khoshakhlagh, Philipp Buch, **Raphael Johnson**, Peter Langguth, Thomas Nawroth, Lars Schmueser, Nadja Hellmann, Heinz Decker, Noemi Kinga Szekely.Excipient effect on the colloidal structure and drug solubility in cholesterol containing biorelevant intestinal medium (FaSSIF-7C) with Fenofibrate" J. Pharmaceutical Sciences, submitted.

Thomas Nawroth, **Raphael Johnson**, Pooneh Khoshakhlagh, Lidija Krebs, Karl Buch, Peter Langguth, Guenther Goerigk, Peter Boesecke, Alberto Bravin, Géraldine Le Duc, Noemi Szekely, Ralf Schweins. Target Nanoparticles for Therapy – SANS and DLS of Drug Carrier Liposomes and Polymer Nanoparticles. Journal of Physics: Conferences (JPCS). ECNS 2015-620. In process.

Poster presentation

Raphael Johnson, Pooneh Khoshakhlagh, Thomas Nawroth, Peter Langguth, Lidija Krebs, Heinz Decker, Nadja Hellmann, Noemi Szekely., Development and structure evaluation of lipid nanoformulations of Amphotericin B for oral administration. Phospholipids in Pharmaceutical Research, Heidelberg, Germany, 21st -22nd September, 2015.

Thomas Nawroth, **Raphael Johnson**, Pooneh Khoshakhlagh, Lidija Krebs, Karl Buch, Peter Langguth, Guenther Goerigk, Peter Boesecke, Alberto Bravin, Géraldine Le Duc, Noemi Szekely, Ralf Schweins. Target Nanoparticles for Therapy – SANS and DLS of Drug Carrier

Publications and presentations

Liposomes and Polymer. Proceedings of 6th European conference on Neutron science, Zaragoza, Spain, 30th Aug – 4th September, 2015

Nawroth Thomas, Pooneh Khoshakhlagh, **Raphael Johnson**, Lidija Krebs, Peter Langguth, Noemi Szekely, Patrick Augustijns. Human intestinal fluids HIF, and FaSSIF-C, a cholesterol containing intestinal model fluid: Comparison and nano-structure by dynamic light scattering DLS and neutron scattering SANS. OrBiTo open science day, Chilly-Mazarin, France, 1st July, 2015.

Nawroth Thomas, Pooneh Khoshakhlagh, **Raphael Johnson**, Lidija Krebs, Sarah Kindgen, Regine Rach, Peter Langguth, Lars Schmueser, Nadja Hellmann, Heinz Decker, Tobias Schrader, Noemi Szekely. Nano-structure dynamics in gastro-intestinal models for drug delivery. International Conference on Surfaces and Colloid Science (IACIS), Mainz, Germany, 24th – 29th May, 2015

Johnson R, Khoshakhlagh P, Nawroth T, Langguth P, Schmueser L, Decker H, Hellmann N, Szekely N., Structural Dynamics of Liposomal Amphotericin B in FaSSIF by combined SANS and DLS. Trends in Neutron Science – MLZ User Meeting, Ismaning, Munich, Germany, 23rd – 24th February, 2015.

Johnson R, Khoshakhlagh P, Nawroth T, Langguth P, Schmueser L, Decker H, Hellmann N, Szekely N., Structural Dynamics of Liposomal Amphotericin B in FaSSIF by combined SANS and DLS. Deutsche Pharmazeutische Gesellschaft Annual meeting, Frankfurt, Germany, 24th – 26th September, 2014.

T. Nawroth, P. Khoshakhlagh, S. Kindgen, L. Krebs, **R. Johnson**, P. Langguth, N. Szekely and R. Schweins., Gastro-Intestinal Simulator for in vitro Drug and Nanoparticle Tracing in Oral Drug Development. Deutsche Pharmazeutische Gesellschaft Annual meeting, Frankfurt, Germany, 24th – 26th September, 2014.

Khoshakhlagh P., **Johnson R.**, Nawroth T., Langguth P., Schmueser L., Decker H., Hellmann N., Szekely N., Structural Dynamics of Novel Gastrointestinal Model Fluids by combined SANS and DLS . Deutsche Pharmazeutische Gesellschaft Annual meeting, Frankfurt, Germany, 24th – 26th September, 2014.

Johnson R., Khoshakhlagh P, Nawroth T, Langguth P, Schmueser L, Decker H, Hellmann N, Szekely N., Oral Amphotericin B Nano-Formulations: Structure and Development in Gastrointestinal Fluids. ORBITO Workshop, Mainz, Germany, 17th – 19th September, 2014.

T. Nawroth, P. Khoshakhlagh, **R. Johnson**, P. Buch, P. Langguth, L. Schmueser, N. Hellmann, H. Decker, N. Szekely and R. Schweins., Nanoparticles in the human Gastro-Intestinal System and Drug Uptake – Modelling and Investigation by Time Resolved Neutron Scattering. Neutrons in Biology and BioTechnology, Grenoble, France, 19th-21st February 2014.

Publications and presentations

Raphael Johnson, Pooneh Khoshakhlagh, Thomas Nawroth, Peter Langguth, Lars Schmueser, Heinz Decker, Nadja Hellmann, Noemi Szekely., Amphotericin B lipid Nanoparticles for oral administration. Deutsche Pharmazeutische Gesellschaft Annual meeting, Freiburg, Germany, 9th – 11th October, 2013.

Khoshakhlagh P., Nawroth T., **Johnson R.**, Langguth P., Schmueser L., Decker H., Hellmann N., Szekely N., Gastrointestinal BCS 2-drug resolution in intestinal model fluids containing physiological lipids-drug dissolution and intestinal nanoparticle structure estimated by DLS and neutron scattering. Deutsche Pharmazeutische Gesellschaft Annual meeting, Freiburg, Germany, 9th – 11th October, 2013.

Raphael Johnson, Pooneh Khoshakhlagh, Thomas Nawroth, Peter Langguth, Lars Schmueser, Heinz Decker, Nadja Hellmann, Noemi Szekely., Structural dynamics of lipid complexes of Amphotericin B. Phospholipids in Pharmaceutical Research, Heidelberg, Germany, 16th -17th September, 2013.

T. Nawroth, P. Khoshakhlagh, **R. Johnson**, P. Buch, P. Langguth, L. Schmueser, N. Hellmann, H. Decker, N. Szekely and R. Schweins., Drug-uptake by Nanostructures in the GI-System: Simulator with DLS-SANS. Innovative Tools for Oral Biopharmaceutics OrBiTo, Uppsala, Sweden, 26th-27th June 2013.

Curriculum vitae

Curriculum Vitae